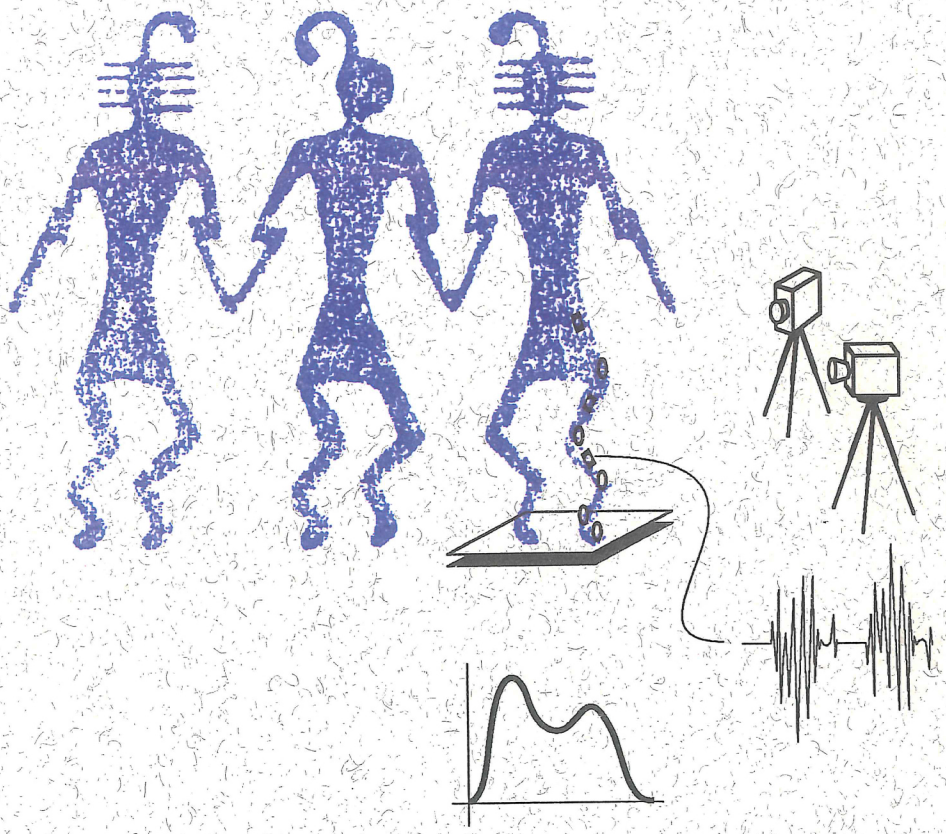
Proceedings of the

American Society of Biomechanics

The 15th Annual Meeting



October 16-18, 1991

Arizona State University
Tempe, Arizona

AMERICAN SOCIETY OF BIOMECHANICS

PROCEEDINGS
FOR THE
15TH ANNUAL MEETING

Arizona State University
Tempe, Arizona

October 16-18, 1991

SPONSORS

American Society of Biomechanics

Arizona State University

College of Liberal Arts and Sciences

College of Engineering

Department of Exercise Science and Physical Education

Department of Chemical, Bio and Materials Engineering

Interdisciplinary Ph.D. Program in Exercise Science

Table of Contents

American Society of Biomechanics/Executive Board iv

Sustaining Members of the American Society of Biomechanics v

Conference Program vi

Abstracts:

Keynote Symposia
- Biomechanics at the Cellular Level 1
- Biomechanics and Olympic Sports: Farther, Higher, Faster 7

ASB Young Scientist Awards 19
Session 1--Human Gait 27
Session 2--Thoraco-Lumbar Spine 43
Session 3--Pathological Gait 59
Session 4--Cartilage, Ligaments, and Bone 71
Session 5--Footwear 83
Session 6--Cervical Spine 95
Session 7--Knee Joint 107
Session 8--Sports 119
Session 9--Material Properties of Bone 131
Session 10--Running 145
Session 11--Artificial Implants 159
Session 12--EMG and Muscle Mechanics 171

Poster Presentations:
- Anatomical Joints 185
- Posture 201
- Cycling 209
- Jumping and Landing 221
- Ergonomics 237
- Fluid Mechanics 247
- Quantitative Techniques 251
- Gait 261
- Bone 271
- Spine 281
- Muscle Mechanics 295

Author Index 302

AMERICAN SOCIETY OF BIOMECHANICS

The American Society of Biomechanics was formed in 1977 to foster interaction among individuals in various disciplines in biomechanics research, such as anthropology, biology, engineering, ergonomics, exercise and sport science, orthopaedics, physiology, rehabilitation, speech and hearing, sports medicine, and zoology. In brief, Society members are persons applying principles of mechanics to the study of biological systems. The Annual Meeting provides an opportunity to exchange information and to broaden perspectives on biomechanics in both formal and informal settings.

The Executive Board that has governed the Society during the past year is represented by the following individuals:

President:
George T. Rab
University of California, Davis

Past-President
Nominating Committee Chair
Awards Committee Chair:
Roger M. Enoka
University of Arizona

President-Elect:
Thomas P. Andriacchi
Rush-Presbyterian-St. Luke's Medical Center

Secretary-Treasurer:
Melissa G. Hoy
University Of Michigan

Meeting Chair:
Philip E. Martin
Arizona State University

Program Chair:
Christopher L. Vaughan
University of Virginia

Program Chair-Elect:
Joan E. Bechtold
Hennepin County Medical Center
Metropolitan-Mt. Sinai Medical Center

Membership Committee Chair:
Thomas D. Brown
University of Iowa

Education Committee Chair:
Mary M. Rodgers
Wright State University

SUSTAINING MEMBERS OF THE AMERICAN SOCIETY OF BIOMECHANICS

The Society would like to thank the following organizations for their support as Sustaining Members:

Aircast, Inc.

DePuy, Inc.

DonJoy, Inc.

Electro-Biology, Inc. (EBI)

Howmedica, Inc.

Human Kinetics Publishers

Interpore Orthopaedics, Inc.

Kistler Instrument Corporation

Motion Analysis Corporation

Orthofix, S.R.L.

Protek, Inc.

Zimmer, Inc.

CONFERENCE PROGRAM

Wednesday, October 16

11:00 am-1:00 pm **Executive Board Meeting**
Colonade Room

1:00-5:00 pm **Registration**
Outside Palm Ballroom

1:00-3:00 pm **Tutorial: Primer on 3-D Kinematics**
Cavetto Room

3:00-5:00 pm **Tutorial: Neurobiology of Muscle Fatigue**
Cavetto Room

1:00-3:00 pm / 3:00-5:00 pm **Laboratory Tours**

* Exercise and Sport Research Institute / ASU Bioengineering Instructional Laboratories
* ASU Bioengineering Research Laboratories
* Harrington Arthritis Research Center

6:30-8:30 pm **Opening Reception / Cash Bar**
Fountain Courtyard

Thursday, October 17

6:30 am-5:00 pm **Registration**
Outside Palm Ballroom

6:30-7:50 am **Posters/Exhibits Set-Up**
Palm Ballroom, Rooms II & III

9:45 am-6:00 pm **Posters and Exhibits open for viewing**
Palm Ballroom, Rooms II & III

7:50-8:00 am **Welcome**
Palm Ballroom, Room I

8:00-9:45 am **Keynote Symposium**

Biomechanics at the Cellular Level

Christopher L. Vaughan, University of Virginia, Session Chair
Scot C. Kuo and Michael P. Sheetz, Duke University
Mechanics at the Molecular Level: Measuring the Isometric Force of Single Kinesin Molecules Using the Laser Optical Trap
Stephen Alexander and C.L. Reider, Wadsworth Center, Albany, NY
Chromosome Movement and Force Production in Mitosis
Robert Hard, S.U.N.Y. at Buffalo
Mechanical Aspects of Respiratory Cilia

9:45-10:00 am **Refreshment Break**
Outside Palm Ballroom

10:00-11:45 am **Session 1--Human Gait**
Chair: Melissa Hoy
Xavier Room

10:00
Biomechanics of Successful Recovery from a Stumble
M.D. Grabiner, T.J. Koh, L. Schaller, D.W. Jahnigen

10:15
Kinematics of Heel Strike During Walking and Carrying: Implications for Slips and Falls
M. Redfern, M.A. Holbein, D. Gottesman, D.B. Chaffin

10:30
Relationship Between Economy and Jerk-Cost During Walking
A.P. Hreljac, P.E. Martin

10:45
Application of the Integrated Kinematic Segment to the Study of Human Locomotion II, Joint Dynamics
Z. Ladin, G. Wu

11:00
The Evaluation of Coupled Dynamics in Observed Locomotion
D. Meglan, N. Berme, S.R. Simon

11:15
A Comparison Between Kinematic and Kinetic Methods of Segmental Power Calculation in Normal Walking
A.W. Smith

11:30
Mechanical Work and the Time Course of Energy Transfer in the Swing Phase of Gait
G.E. Caldwell, L.W. Forrester

10:00-11:45 am **Session 2--Thoraco-Lumbar Spine**
Chair: Jack Winters
Augustine Room

10:00
Comparative Study of Noninvasive Scoliotic Measuring Techniques
D.J. Pearsall, J.G. Reid, D.M. Hedden

10:15
Measurement of Forces by Boston Brace in the Treatment of Scoliotic Deformities
J. Dansereau, B. Cote, H. Labelle, C.E. Aubin

10:30
A Comparison of Torso Muscle Centroid Line Inclination Angles Relative to the L3-L4 Interspace
P.J. Moga, M. Erig, D.B. Chaffin, M.A. Nussbaum

10:45
In-Vivo Measurement of Intervertebral Creep: A Preliminary Report
A.M. Kaigle, M. Magnusson, M. Pope, H. Broman, T. Hansson

11:00
Effects of Anterior Vertebral Grafting on the Kinematics of the Traumatized Lumbar Spine Following Pedicle Screw-Plate Fixation
F. Pintar, D. Maiman, N. Yoganandan, J. Reinartz

11:15
Torque-Rotation Response of Lumbar Motion Segments in Flexion
J.J. Triano, R. Gudavalli

11:30
Relationship Between Functional Lifting Mechanics and Lumbar Extension Strength
D.L. Wheeler, G.J. Miller, P. O'Connor, R. Hubbard

11:45 am-1:45 pm **Lunch - Borelli Lecture**
Palm Ballroom, Room I

Van C. Mow, Ph.D., Orthopaedic Research Laboratory, Columbia University

Reminiscences of a Middle-Age Biomechanician

1:45-2:45 pm **Poster Presentations by Authors**
Palm Ballroom, Rooms II & III

2:45-4:00 pm **Session 3--Pathological Gait**
Chair: Mary Rodgers
Xavier Room

2:45
The Relationship Between Static and Dynamic Mechanical Factors and Tissue Degeneration Patterns: A Case Study of Primary Osteoarthritis of the Knee Joint
L. Kamibayashi, U.P. Wyss, T.D.V. Cooke, P. Costigan

3:00
Motion of the Normal and Anterior Cruciate Ligament Deficient Canine Knee During the Walk and Trot
D.L. Korvick, G.J. Pijanowski, D.J. Schaeffer

3:15
Gait Analysis Assessment of THR Patients Operated with PCA Prosthesis
F. Catani, A. Leardini, A. Battistini, M. DeZerbi, A. Ahdieh, S. Giannini

3:30
Velocity Dependent Characteristics of the Involved and Uninvolved Limbs of Hemiplegics During Overground Locomotion
K.L Perrell, R.G. Gregor, E.G. Fowler, B. Dobkin

3:45
Below-Knee Child Amputee Gait: Dynamics of an Energy Storing Prosthesis
T.J. Hart, K. Schneider, R.F. Zernicke, Y. Setoguchi, W. Oppenheim

2:45-4:00 pm **Session 4--Cartilage, Ligaments, and Bone**
Chair: Ted Gross
Augustine Room

2:45
Biphasic Creep Indentation Studies of Bovine Growth Plate Cartilage
L.R. Alberts, W.A. Abdul-Shafi

3:00
Biomechanical Properties of Hip Cartilage Using a Biphasic Finite Element/Optimization Procedure -- An Interspecies Study
K. Anthanasiou, A. Muffoletto, F.J. Dzida, G. Constantinides

3:15
Ligamentous Contributions to Pelvic Stability
M. Vrahas, T. Hern, D. DiAngelo, M. Tile, J.F. Kellam

3:30
Effects of Increased Tension of Medial Collateral Ligaments: A Biomechanical, Biochemical, and Histological Assessment
M. Gomez, S. Woo, D. Amiel, F. Harwood, L. Kitabayashi, J. Matyas

3:45
Mechanical Properties of Cellular Materials
M. Zhu, T.S. Keller

4:00-4:15 pm **Refreshment Break**
Outside Palm Ballroom

4:15-5:00 pm **ASB Young Scientist Awards**
Chair: Roger Enoka
Palm Ballroom, Room I

Pre-Doctoral: Joseph E. Hale, Orthopaedic Biomechanics Laboratory, University of Iowa

Alterations of Contact Stress and Tissue Histomorphometry in Size-Dependent Osteochondral Defect Repair
J.E. Hale, T.D. Brown, M.J. Rudert, C.G. Mohler, R.A. Brand, J.A. Buckwalter

Post-Doctoral: Scott L. Delp, Sensory Motor Performance Program, Rehabilitation Institute of Chicago

Effect of the Hip Center of Location on Muscle Strength

Post-Doctoral: Gregory S. Berns, School of Medicine, University of California, San Diego

The Effect of Roofplasty and Tibial Hole Placement on Impingement of Anterior Cruciate Ligament Reconstructions
G.S. Berns, S.M. Howell

5:00-6:15 pm **Session 5--Footwear**
Chair: Irene McClay
Xavier Room

5:00
The Effects of Footwear and Technique on Race Walking Mechanics
R.E. Snow, R.V. Bowen

5:15
Modelling of the Effect of Footwear on the Dynamic Loading on the Human Musculoskeletal System
W. Kim, A. Voloshin

5:30
Time Domain Modelling for the Assessment of Shock Absorbing Insoles
G. Lowet, L. Peeraer, K. Colpaert, G. Wallaeys, G. Van der Perre

5:45
Validation of a Mathematical Model of the Effect of Sole Elasticity Distribution of Pronation
P. Li, Z. Ladin

6:00
The Importance of Thermo-Mechanical Properties in the Selection of Athletic Foam Cushioning Foams
J. Poliner, S. White, M. Fenton

5:00-6:15 pm **Session 6--Cervical Spine**
Chair: Gary Yamaguchi
Augustine Room

5:00
Verification of Analytical Models Applicable to Motion Analysis in the Cervical Spine
P. Roozmon, S.A. Gracovetsky, G. Gouw, N. Newman

5:15
Bone Graft Translation of Four Cervical Spine Fixation Techniques in a Cadaveric Model
J.J. Crisco III, M. Panjabi, T. Oda, D. Grob, J. Dvorak

5:30
Estimation of Cervical Disk Pressures Induced by Muscle Actuator Forces in an Anthropomorphic Model Affixed by a Halo
W.A. Peterson, J.M. Winters

5:45
An Instrumented, Physical Spinal Cord Model For In situ Pressure Measurement
M.B. Schlick, F. Pintar, N. Yoganandan, D.J. Maiman, A. Sances Jr.

6:00
The Onset and Progression of Spinal Injury in a Porcine Flexion-Compression Trauma Model
T.R. Oxland, M.M. Panjabi

6:30-10:00 pm **Banquet**

6:30 pm Meet in hotel lobby to board buses
6:40 pm Buses depart for Pinnacle Peak Patio
10:00 pm Buses return to hotel

FRIDAY, OCTOBER 18

7:30 am-12:00 pm **Registration**
Outside Palm Ballroom

8:00 am-3:15 pm **Posters and Exhibits open for viewing**

8:00-10:00 am **Keynote Symposium**
Palm Ballroom, Room I

Biomechanics and Olympic Sports: Farther, Higher, Faster

Jesus Dapena, Indiana University
High Jumping

Ralph Mann, CompuSport, Orlando, FL
TAC Scientific Support Service Program: Sprints and Hurdles

Keith Williams, University of California, Davis
Biomechanical Analyses of Running Mechanics in Elite Distance Runners

Peter McGinnis, S.U.N.Y at Cortland
Biomechanics and Pole Vaulting: Run Fast and Hold High

10:00-10:15 am **Refreshment Break**
Outside Palm Ballroom

10:15-11:30 am **Session 7--Knee Joint**
Chair: Manssour Moeinzadeh
Xavier Room

10:15
Basic Mechanical Structure of the Knee: A Kinematically Unconstrained Biomechanical Gear System with Force Locked Stability
D. Kubein-Meesenburg, H. Nagerl, J. Fanghanel

10:30
Dynamic Analysis of a Functional Knee Brace and A Previous ACL Injury
P. DeVita, P. Hunter, W.A. Skelly

10:45
Forces and Moments on the Leg During Skiing Jump Maneuvers
A.G. Yee, C.C. Mote Jr.

11:00
The Axes of Rotation of the Knee
A.M. Hollister, S. Jatana, A.K. Singh, W.W. Sullivan

11:15
In vivo Tracking of the Human Patella
T.J. Koh, M.D. Grabiner, R.J. de Swart

10:15-11:30 am **Session 8--Sports**
Chair: Jill McNitt-Gray
Augustine Room

10:15
The Relationship between Body Roll and Hand Relative Motion during the Pull Phase in Freestyle Swimming
Q. Liu, J.G. Hay, J.G. Andrews

10:30
A Springboard Response System for Feedback on Diving Performance
D.I. Miller, M.A. Pizzimenti, I.C. Jones

10:45
Three-Dimensional Kinematic Analysis of the Throwing Motion in Four Elite College Football Quarterbacks
G. Rash, R. Shapiro

11:00
Factors Accounting for Variability in Distal End Speed in Kicking
C. Putnam

11:15
A 3-D Simulation of a Soccer Kick; The Effect of Varying Hip and Knee Torques
J.K. DeWitt, R.N. Hinrichs, G.T. Yamaguchi

11:30 am-12:30 pm **Presidential Address/Business Meeting**
George T. Rab
University of California, Davis
Palm Ballroom, Room I

12:30-1:30 pm **Lunch on your own**

12:30-1:30 pm **Executive Board Meeting**
Colonade Room

1:30-3:00 pm **Session 9--Material Properties of Bone**
Chair: Joseph E. Hale
Xavier Room

1:30
Correlation Between Mechanical Environment and Collagen Cross-Linking in Bone: An Example from the Deer Calcaneus
S. Gunasekaran, B. Constanz, J. Skedros

1:45
The Effects of Demineralization Protocols on the Mechanical Properties of Bovine Bone Collagen
W.R. Walsh, N. Guzelsu

2:00
Association Between Mechanical Stability, Cortical Strains and Histology, of Femurs Retrieved with Uncemented Femoral Prostheses
J.L. Comadoll, P.T. Bianco, J.E. Bechtold, R.B. Gustilo

2:15
Reproducibility of Finite Element Stress Distributions in MRI-Delineated Femoral Head Osteonecrosis
K.J. Baker, T.D. Brown, R.A. Brand

2:30
Atlas of Mechanical Properties of Human Cortical and Cancellous Bone
M.-C. Hobatho, J.Y. Rho, R.B. Ashman

2:45
Site Specific Adaptation of the Growing Skeleton to Altered Mechanical Stimuli
T.S. Gross, C.T. Rubin

1:30-3:00 pm **Session 10--Running**
Chair: Carol Putnam
Augustine Room

1:30
3-Dimensional Kinematics of the Patellofemoral Joint During Running
I.S. McClay, P.R. Cavanagh, A. Kalenak, H.J. Sommer III

1:45
The Effect of Orthotics on Ankle Pronation and Knee Rotation
K. Kozak, Z. Ladin, J.M. Giurini

2:00
Temporal Relationships Between Knee Flexion and Pronation in Running: Assessment of Pronation Event Selection
B.L. Caster, T.R. Derrick, B.T. Bates

2:15
Timing of the Knee and Sub-Talar Joint Actions During Treadmill Running
J. Hamill, B.T. Bates, K.G. Holt

2:30
Velocity and Ground Reaction Force Relationships During Walking and Running
J.L. Ray, A.M. Weisberger, T.S. Keller, S.S. Hassan, R. Shiavi, D.M. Spengler

2:45
Center of Pressure Estimation During Running Without a Force Platform
D. Andrews, J.J. Dowling

3:00-3:15 pm **Refreshment Break**
Outside Palm Ballroom

3:15-4:30 pm **Session 11--Artificial Implants**
Chair: Joan Bechtold
Xavier Room

3:15
Torsional Stability of Revision Hip Stems
J.A. Longo, T. McTighe, J.B. Koeneman

3:30
A Finite Element Analysis of the Effect of Coating Poisson's Ratio on Interface Conditions in Porous Coated Hip Endoprostheses
E.A. Friis, F.W. Cooke, S.J. Hooper

3:45
A Finite Element Analysis of the Simmons and Steffee Bone Bolts
M. Harbaugh

4:00

Glenoid Implant Technology - Part I: Development of a Three-Dimensional Finite Element Model
C.M. Smith, U.P. Wyss, D.R. Pichora, H.L. Ploeg

4:15

A Three Dimensional Finite Element Analysis in the Development of a Total Joint Replacement for the Great Toe
H.L. Ploeg, T.D.V. Cooke, A.R. Dujovne, C.M. Smith, U.P. Wyss

---

3:15-4:30 pm **Session 12--EMG and Muscle Mechanics**
Chair: Mark Grabiner
Augustine Room

3:15

Ligament Force Feedback and the Regulation of Joint Stability
T.S. Buchanan, S. Beckman, W.Z. Rymer

3:30

Torque and Muscle Activity in Various Isometric Elbow Tasks
J.C. Jamison, G.E. Caldwell

3:45

Assessment of the Double Differential Technique at Identifying and Eliminating EMG Crosstalk
C.V. Portfors, J.J. Dowling

4:00

Older Human Subjects Experience Less of a Change in EMG Frequency Content During a Fatigue Contraction
R.M. Enoka, A.J. Fuglevand, P.M. Barreto

4:15

Single Muscle Contractions Can Produce Muscle-Tendon Injury
J.W. Feuerbach, J.G. Hay, W.G. Darling

POSTERS: **Poster Presentations by Authors**
Thursday, 1:45-2:45 pm
Palm Ballroom, Rooms II & III

Anatomical Joints

Factors Affecting Elastic Energy Recovery in Stretch-Shortening Movements
M. Mungiole, J. Winters

High Pressure Planar and Spatial Measurements Between a Talar Bone Vector and the Malleolus-Metatarsal Vector During the Movements of Dorsiflexion and Plantar Flexion for the Foot
N. Murphy, P. Allard, R. Aissaoui

Kinematics of the Ankle: A Hinge Axis Model
A.K. Singh, K.D. Starkweather, S. Jatana

Intra-and Interday Assessment of Bilateral Symmetry in Isokinetic Knee Extension Moments
S.T. McCaw

Effects of Cold and Modified PNF Stretching on Acute ROM
W. Cornelius

Quantifying Two-Dimensional Joint Incongruity in the Osteoarthritic Hip
J.A. Miller Jr., J.G. Andrews, R.A. Brand, P.G.J. Marquet

In Vivo Euler Buckling at the Elbow
J.J. Crisco III, M. Panjabi, K. Rath

Posture

Optimization as Applied to Large-Scale 3-D Human Postural Systems: A Synthesis of Concepts and Approaches
J.M. Winters

Analysis of Human Standing Posture: Constraints and Objectives
A.D. Kuo, F.E. Zajac

Predicting Torso Muscle Activity During Asymmetric Loading: A Comparison of Three Optimization Models
M.A. Nussbaum, S.A. Lavender, R.E. Hughes

Cycling

Measurement of the Dynamic Forces During Manual Wheelchair Propulsion
M.G. Strauss, J. Maloney, F. Ngo, M. Phillips

A Comparison of Torque Production of Clip-In Pedals and Conventional Toe-Clips and Cleats
M.E. Cooper, R.A. Cooper, I.E. Faria

A 3-D Model of the Lower Limb in a Cycling Movement
T. Marsh, G.T. Yamaguchi

A Novel Propulsion System for a Human Powered Water Vehicle
A.D. Aswad

Influence of Orthotics on Lower Extremity Function in Cycling
T.G. Joganich, P.E. Martin

Jumping and Landing

A New Model for the Computer Simulation of Pole Vaulting
Wang Qin, Wei Wen-Yi

Individual Joint Contributions to Shock Absorption During Vertical Drop Landings
P.K. Schot, J.S. Dufek, B.T. Bates

Evaluation of Position Constraints on Landing Performance
J.S. Dufek, B.L. Caster, B.T. Bates

Differences in Reaction Forces Experienced by Gymnasts During Landing of Front and Back Saltos
J. McNitt-Gray, C.A. Barbieri, D.D. Anderson, D.M.E. Irvine

The Effect of Landing Surface on Muscle Activity in Preparation for Landing
J. McNitt-Gray, D.M.E. Irvine, C.A. Barbieri, D.D. Anderson

Arm Swing and Toe-Touch Movement Effects on Vertical Jump Performance
B.A. Munkasy, R.N. Hinrichs

Kinetic Evaluation of a Sports Tile System with a Horizontal Displacement
A. Bagley

Ergonomics

Thoracic Crush Injuries in a Tractor Wheel Rollover: Estimation of 3-D Forces
N. Yoganandan, K. Liu, J. Winterbottom, A. Sances Jr.

An Application of the Biomechanical Simulation of Human Movement to the Evaluation of Dwelling Space Design
T. Yokoi

Assessment of Risk Factors for Cumulative Trauma Disorders (CTD) Using A Video/Computer Graphics Approach
R. Wells, A. Moore

Resonance Behavior of the Human Exposed to Whole-Body Vibration
S.D. Smith, L.E. Kazarian

Fluid Mechanics

Flow Dynamics and Turbulence Measurements Past Mitral Valve Prostheses in a Model Left Ventricle: Experimental and Numerical Results
R.T. Schoephoerster, K.B. Chandran

Quantitative Techniques

Endpoint Problems in Smoothing Raw Kinematic Data: An Evaluation of Four Popular Smoothing Techniques
R.N. Hinrichs

A Comparison of DLT With and Without Extrapolation and NLT 3-D Cinematography Methods
S.P. McLean, R.N. Hinrichs, J.K. DeWitt, G.D. Heise, A.P. Hreljac, T.G. Joganich, T.P. Marsh, B.A. Munkasy

The Application of the Integrated Kinematic Segment to the Study of Human Locomotion, I - Kinematics
Ge Wu, Z. Ladin

Optical Scanner Calibration by Object-Image Planar Mapping and 3-D Object-Shape Reconstruction Accuracy
J. Kofman, B. Lindstrom, A. Karlsson, K. Oberg

Gait

Variant and Invariant Characteristics of the Human Step Cycle During Speed and Grade Perturbations
P. Hannon, D. Fukumoto, S. Fleming, R. Long, A. Pappas

Effects of Music and Rhythm on Gait Characteristics of Normal Individuals
S. Prassas, M. Thaut

New Stride Phases and the Development of Sport Shoe Prototype to Assist the Calf Muscles During Heel-Off
M.R. Pitkin

Gait Analysis in Patients After Van Nes Rotationplasty
F. Catani, R,. Capanna, M.G. Benedetti, A. Battistini, A. Leardini, G. Cinque, S. Giannini

Bone

Structural Transformations Indistinguishable By Point-Count Stereology
D.P. Fyhrie, S.J. Hollister, M.B. Schaffler, J. Kimura

Contact Stress Distributions in Malreduced Intra-articular Distal Radius Fractures
D.D. Anderson, A.L. Bell, M.B. Gaffney, J.E. Imbriglia

Normal and Shear Strain Distributions of the Equine Third Metacarpal During Locomotion: Characterizing Bone's Functional Milieu
T.S. Gross, K.J. McLeod, C.T. Rubin

Modal Analysis of the Human Tibia in vivo: Determination of the Resonant Frequencies and Mode Shapes
G. Lowet, M.C. Hobatho, M. Cornelissen, J.L. Cunningham, G. Van der Perre

Spine

Articulations Zygapophysiales and Intervertebral Disk: A Biomechanical Gear System with Positive Drive
H. Nagerl, D. Kubein-Meesenburg, J. Fanghanel

The Effect of a Football Helmet Accessory on Impact Characteristics and Moments of Force at the Neck
G.D. Heise, R.C. Nelson

Simulation of Back Motion
A.V. Komattu, C.D. Crane, D.L. Wheeler, G.J. Miller

Biomechanics of Human Thoracic Spine Laminectomy
N. Yoganandan, F. Pintar, D. Maiman, G. Bennet

A Personalized Finite Element Model for the Study of Boston Brace Correction in Idiopathic Scoliosis
C.E. Aubin, J. Dansereau, H. Labelle

Effects of Pedicle Screw Instrumentation and Disk Removal on 3-D Motion of Lumbar Spinal Columns Subjected to Various Loads
A.G.U. Sawa, J.M. Winters, J.B. Koeneman, J.K. Mayfield

Muscle Mechanics

Relative Cross-Sectional Areas of Upper and Lower Extremity Muscles in Humans
J.J. Dowling, N. Cardone

Morphology of the Psoas Muscle as Determined by Magnetic Resonance Imaging
J.G. Reid, L.A. Livingston, D.J. Pearsall

The Effect of Stretch Rate on Muscle Failure In Vitro
J. Crisco III, R. Gellman, M. Panjabi, P. Jokl

KEYNOTE SYMPOSIUM 1

BIOMECHANICS AT THE CELLULAR LEVEL

MECHANICS AT THE MOLECULAR LEVEL: MEASURING THE ISOMETRIC FORCE OF SINGLE KINESIN MOLECULES USING THE LASER OPTICAL TRAP

Scot C. Kuo and Michael P. Sheetz
Department of Cell Biology, Box 3709, Duke University Medical Center, Durham, NC 27710

INTRODUCTION

Microtubules translocated by a single kinesin molecule can be reversibly stalled using a novel instrument, the single-beam optical trap (also called laser optical tweezers). Preliminary measurements indicate that the maximum force (i.e. isometric force) of a single kinesin attachment is 2 pN (10^{-7} dyne). Future experiments would address the cooperativity of additional kinesin molecules driving the same microtubule filament.

REVIEW and THEORY

The characterization of molecular motors, such as the microtubule-dependent motor, kinesin[1], and the development of novel technology have permitted new approaches to elucidating the mechanism of biological force generation. These "molecular" motors, working as an ensemble of a few molecules, can exert force against filamentous polymers within the cell. The obvious structural and functional similarities to conventional muscle myosin have guided research. However, recent work with an *in vitro* motility system indicate that kinesin motility differs from the *in vitro* motility for conventional muscle myosin in that a single molecule of kinesin can translocate a microtubule many micrometers[2]. The recent development of the single-beam optical gradient trap[3] (laser optical tweezers) provides the requisite technology for fine and precise "micromanipulation" in our studies. The optical trap uses the momentum of light (radiation pressure) to trap microscopic particles, and the force of the trap, which is linear with laser power, can be calibrated by viscous drag on latex spheres. We have developed procedures to apply this technology to measuring the isometric force of a single kinesin molecule.

PROCEDURES

Details about the configuration of our optical trap, video-enhanced differential interference microscopy, and particle-tracking algorithms have been described elsewhere[4]. Procedures for biotinylating tubulin have also been described elsehere[5].

RESULTS

The general strategy for measuring the force of single kinesin motors is schematized in Fig. 1. Limiting dilutions of squid kinesin (2-12 molecules/μm^2)

were adsorbed to glass in the presence of carrier protein, such as cytochrome *c*, so that motility by single kinesin motors could be observed. Biotinylated microtubules could be translocated by this immobilized kinesin, and streptavidin-coated beads attached to these microtubules provided "handles" to stall its translocation. Once translocation has been stalled with the laser optical trap, the power of the laser was reduced. When the force of kinesin exceeded the trapping force, the bead would be pulled from the trap. This threshold of force operationally defines the isometric force of kinesin. Customized video overlays allowed simultaneous recording of the laser power while recording the bead position. Preliminary data from these experiments indicate that the isometric force of a single kinesin molecule is 2 piconewtons.

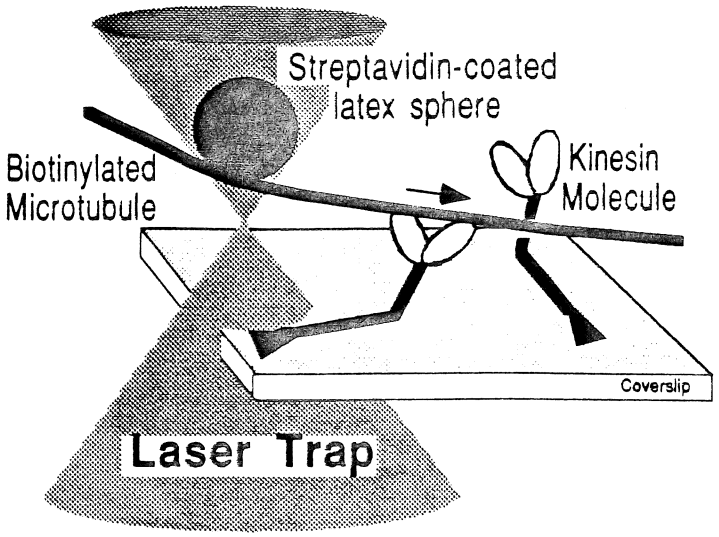


Fig. 1: Experimental Design

DISCUSSION

The paradigm for force generation and motility derived for conventional muscle myosin is being pushed to molecular dimensions by *in vitro* assay systems. Many groups have measured the forces generated by a handful of myosin crossbridges[6], however these studies were hampered by the low precision in estimating the exact number of crossbridges involved. Despite these difficulties, myosin has been estimated to generate 1-10 piconewtons of force per crossbridge. Albeit a different motor, our studies provide a better measure of the force of a single "crossbridge" and will address the cooperativity of force generation as more crossbridges are formed.

---

[1] R. D. Vale *et al. Cell* 42, 39 (1985)

[2] J. Howard *et al. Nature* 342, 154 (1989); S.M. Block *et al. Nature 348*, 348 (1990)

[3] A. Ashkin *et al. Science* 235, 1517 (1987); *Nature* 330, 769 (1987)

[4] S.C. Kuo *et al. J. Cell Sci Suppl 14*, 135 (1991); D.F. Kucik *et al. J Cell Biol 114, in press* (1991); J. Gelles *et al. Nature* 331, 6155 (1988)

[5] T.J. Mitchison & M.W. Kirschner *J.Cell Biol 101*, 755 (1985)

[6] S. Chaen *et al. PNAS USA 86*, 1510(1989); A. Kishino & T. Yanagida *Nature* 334, 76 (1988)

CHROMOSOME MOVEMENT AND FORCE PRODUCTION IN MITOSIS

Stephen P. Alexander & C.L. Rieder.
Wadsworth Center for Laboratories & Research, Empire Plaza, Albany, NY 12201. USA.

The fundamental cellular process of mitosis is one which has intrigued scientists for over a century. Exactly what drives chromosome movement, how the force is produced, controlled and applied, are questions which are still pondered by the majority of mitosis scholars. On the subject of forces during mitosis, E. B. Wilson (1911) remarks that there is "... so wide a divergence of opinion as to compel the admission that we have thus far accomplished little more than to clear the ground for a precise investigation of the subject; and the mechanism of mitosis still lies before us as one of the most fascinating problems of cytology". Although today there is a wealth of information about mitosis, we are still a long way from understanding chromosome movement at the molecular level. This talk will deal with 3 basic questions: How do chromosomes attach to the mitotic spindle? How do they move toward a spindle pole? What forces are generated in order to accomplish this movement?

To investigate these problems we have focused our attention on the pneumocytes of the newt *Taricha granulosa*. In primary culture, these cells are optimally suited for high resolution video-enhanced light microscopy and correlative electron microscopy, since they are extremely large (often >200 μm), they remain flat throughout cell division, and the chromosomes reside in a clear area of cytoplasm after nuclear envelope breakdown (Rieder and Hard, 1990). These features permit an unhindered view of the initial attachment of chromosomes to spindle microtubules (MTs) and allow us to track the subsequent poleward movement with a high degree of precision. Furthermore, Brownian movement of small particles residing in the clear area surrounding the chromosomes, can be used to estimate the apparent viscosity of the cytoplasm in the immediate vicinity of the chromosomes. Using these data we were able to observe chromosome attachment, characterize the initial chromosome movement, and calculate the forces involved.

Explants of lung tissue from *T. granulosa* were cultured in Rose chambers (See Rieder and Hard, 1990). After screening, coverslips with mitotic cells were mounted in microperfusion chambers (McGee-Russel and Allen, 1971) and observed with Nikon Microphot or Zeiss IM 35 microscopes, equipped with differential interference contrast (DIC) optics. Illumination was passed through heat, UV-cut and 546-nm interference filters and shuttered to minimize specimen irradiation (Alexander and Rieder, 1991). Video images were enhanced by grey-scale transformation and recorded with an optical memory disk recorder. These video recordings were then re-processed digitally and analyzed on a frame by frame basis for particle and chromosome motion. Selected cells were fixed by perfusion during recording and processed for immunofluorescence microscopy and correlative transmission electron microscopy (Rieder and Alexander, 1990).

How chromosomes attach to the array of MTs spanning the two spindle poles (i.e., the spindle), has been a subject of much debate. Since Schrader (1953) many investigators have believed that the kinetochores are responsible for "seeding" the growth of MTs. Our fluorescence microscopy of newt pneumocytes located in the clear zone and in close proximity to spindle MTs, show that kinetochores do not nucleate MTs (Rieder and Alexander, 1990). By chemically fixing cells as the chromosomes become initially attached, and then processing them for anti-tubulin immunofluorescence and serial thin-section TEM, we demonstrated that a single MT permits chromosome movement, and that this MT originates from the spindle pole, not the kinetochore. Furthermore, computer-generated 3-dimensional reconstructions showed that the MT passes through the outer layer of the kinetochore (the corona) indicating that the chromosome moves by sliding along the surface of an MT, and not

by disassembly of an MT which terminates at the kinetochore (the "pac-man" models, for reviews see Forer, 1988; Nicklas, 1988; Salmon, 1988).

The capture of a single MT growing out from a spindle pole and the immediate poleward acceleration of the chromosome was observed directly by Hayden et. al, (1990). Our high-resolution motion analysis demonstrated a close similarity between particle saltations on spindle MTs and the movement of chromosomes on the spindle (Alexander and Rieder, 1991). Such a similarity could be explained by a similar force-generating mechanism. Indeed, retrograde translocations of particles along MTs are very likely produced by the action of the force producing molecule dynein (Schnapp and Reese, 1989), which has also been localized at kinetochores (Pfar et al, 1990; Steuer et al, 1990) and even in the outer corona material (Wordeman et al, 1991).

In order to calculate the force produced by the interaction of a molecular motor with a single MT at the kinetochore, we first estimated the apparent viscosity of the cytoplasm in the immediate vicinity of the chromosomes. By recording the Brownian displacements of cytoplasmic inclusions in the spindle clear area and applying the data to the Einstein-Stokes equation (Alexander and Rieder, 1991), we obtained a range of viscosities from 57 cP to 772 cP with a mean of 282 cP. Then using the equation:

$$F = \eta SV$$

(where η is viscosity, S is a factor accounting for size and shape of the chromosome, and V is chromosome velocity; Nicklas, 1965) we calculated force production per MT for newt pneumocytes. This was estimated to be in the range 0.8 to 7.4 X 10^{-6} dyn, values within an order of magnitude of those calculated by Nicklas (1983) for grasshoppers.

To put such forces into perspective, Nicklas (1983) compared power output per unit engine volume for a variety of biological and man-made engines. The spindle's power output is some 300,000 times less than that of striated muscle, which in turn is 2 orders of magnitude less than that of the bacterial flagellum. Since the primary function of the spindle is the precise and controlled positioning of chromosomes during division, only sufficient power is required to overcome frictional resistance of the cytoplasm, since any excess power would need to be offset by a governor if controlled movement is to be maintained. Thus the cell has evolved an efficient and accurate machine for the movement and positioning of chromosomes during mitosis.

References:

Alexander, S.P., & C.L. Rieder. 1991. J. Cell Biol. 113:805-815.

Forer, A. 1988. J. Cell Sci. 91:449-453.

Hayden, J., et al., 1990. J. Cell Biol. 111:1039-1045.

McGee-Russel & R.D. Allen. 1971. Adv. Cell Mol. Biol. 1:153-184.

Nicklas, R.B. 1983. J. Cell Biol. 97:542-548.

Nicklas, R.B. 1988. Biophys. Chem. 17:431-449.

Pfarr, et al., 1990. Nature (Lond.). 345:263-265.

Rieder, C.L., & S.P. Alexander. 1990. J. Cell Biol. 110:81-96.

Rieder, C.L. & R. Hard. 1990. Int. Rev. Cytol. 122:153-220.

Salmon, E.D. 1989. In Mitosis: Molecules and Mechanisms. J.H. Axams, and B. R. Brinkley, eds. Acad. Press NY. 118-181.

Schnapp, B.J., & T.S. Reese. 1989. Proc. Natl. Acad. Sci. USA. 86:1548-1552.

Schrader, F. 1953. Mitosis. Columbia Univ. Press, NY. 170 pp.

Steuer, E.R. et al., 1990. Nature (Lond.). 345:266-268.

Wilson, E.B. 1911. The Cell.. Macmillan, NY, Lond. 483 pp.

Wordeman, L., et al., 1991. J. Cell Biol. 114:285-294.

KEYNOTE SYMPOSIUM 2

BIOMECHANICS AND OLYMPIC SPORTS: FARTHER, HIGHER, FASTER

HIGH JUMPING

Jesús Dapena
Department of Kinesiology
Indiana University, Bloomington, IN 47405

Biomechanical research directed to the improvement of sport results through the alteration of technique may be separated into two main forms: (a) basic research, which strives to achieve a better understanding of the mechanisms involved in a sport event and to identify advantageous technique elements; and (b) applied research, which attempts to identify and correct the technique deficiencies of individual athletes. For maximum effectiveness, the information gathered from both forms of research should be combined. Our laboratory has been involved since 1982 in a long-term applied research project on the Fosbury-flop style of high jumping sponsored by the U.S. Olympic Committee and The Athletics Congress. This paper will outline the most relevant aspects of the project.

The basic research stage started with a critical examination of the available literature. Most of the published work was concerned with the achievement of a clearer understanding of the Fosbury-flop, but usually with little or no quantitative information to support the theories proposed. The few quantitative studies were based on two-dimensional analysis, a major limitation for the study of the markedly three-dimensional motions of the Fosbury-flop. In the next step of the basic research stage, several studies were carried out. Their immediate objective was not the improvement of the performances of the high jumpers involved, but the acquisition of quantitative information that would permit a better understanding of the Fosbury-flop technique. The results permitted an evaluation of the theoretical literature, and led to a more comprehensive mechanical interpretation of the Fosbury-flop style.

Two paths were followed after this: further basic research, and applied research. In the applied research, high jumpers were filmed in official competitions. Computer analysis was used to calculate three-dimensional body landmark coordinates throughout the last strides of the approach run, the takeoff and the bar clearance, to calculate other kinematic and kinetic parameters of the jumps, and to produce computer plots that showed sequences of the jumps viewed from diverse directions. These data were then used to produce reports that explained to the athletes the advantages and disadvantages of their present techniques and gave recommendations on how to correct some of their technique problems.

The evaluation of the technique of each athlete started with an examination of the rotation over the bar and an analysis of the possible mechanisms that might have led to any problems observed in it. Following this, the factors that may have had an influence on the maximum height reached by the center of mass were scrutinized.

What follows is a brief account of the mechanical interpretation of the Fosbury-flop style which served as a basis for the evaluation of the technique of each athlete.

A high jump can be divided into three parts: run-up, takeoff and bar clearance. The run-up serves as a preparation for the takeoff phase, the most important part of the jump; the bar clearance is less important, because most of the motion is determined by the end of the takeoff phase.

Most high jumpers use a curved run-up. One of the main purposes of the curve is to make the jumper lean away from the bar at the start of the takeoff phase. In the last two or three strides, the athlete should gradually lower the hips without a significant loss of running speed. The takeoff phase determines the maximum height that the center of mass (c.m.) will reach, and the angular momentum that the body will have during the bar clearance. During the takeoff phase, the takeoff leg pushes down on the ground. In reaction, the ground pushes the body up with an equal and opposite force which changes the vertical velocity of the c.m. from near zero to a large upward vertical velocity. To obtain a large vertical velocity at the end of the takeoff, the vertical force made on the ground should be as large as possible, and it should be exerted for as long as possible. A fast run-up helps the athlete to make a larger vertical force on the ground during the takeoff phase. When the takeoff leg is planted ahead of the body at the end of the run-up, the knee extensor muscles resist against the flexion of the leg, but the leg is forced to flex anyway because of the forward momentum of the jumper. The knee extensor muscles are stretched, and the eccentric conditions that result help the jumper to exert a large force on the ground. To maximize the time during which the vertical force is exerted on the body, the center of mass has to travel through a long vertical range of motion during the takeoff phase. This can be achieved by having the c.m. in a low position in the last strides of the run-up and at the start of the takeoff phase. However, this is difficult to do without losing running speed. It is possible to achieve a run-up that is fast and low in the last strides, but this requires a considerable amount of effort and training. The run-up should not be excessively fast and low either: If the takeoff leg is not strong enough, it will be forced to flex too much, and will not be able to make a forceful extension. In other words, it may "buckle" under the stress, and the result will be an aborted jump. There is an optimum combination of run-up speed and c.m. height. This optimum will be a faster and/or lower run-up in more powerful jumpers. The arms are accelerated upward during the takeoff phase. This helps the takeoff leg to exert a larger force on the ground.

For a proper layout over the bar, the jumper needs to make a twisting somersault in the air. The twist makes the athlete turn the back toward the bar during the ascending part of the flight. The somersault makes the shoulders go down while the knees go up, and it can be broken down into forward and lateral somersaulting components. The angular momentum necessary for these rotations is generated during the takeoff phase.

Although the rotations of the athlete are determined primarily by the angular momentum, they can also be affected by other factors. By slowing down the rotations of some parts of the body, other parts will speed up as a compensation. Rotation can also be altered by changing the moment of inertia.

Since full understanding of high jumping technique has not yet been achieved, any recommendations to the athletes have to be adopted with reservations. However, these reservations will ease as more information becomes available through the process of basic research.

TAC SCIENTIFIC SUPPORT SERVICE PROGRAM: SPRINTS AND HURDLES

Ralph V. Mann, CompuSport at Grand Cypress
Orlando, Florida

INTRODUCTION

The evolution of study on elite sprint and hurdle athletes has progressed from simple kinematic description within the group, to more advanced kinematic as well as kinetic comparisons between the elite group and a group of proficient, but non-elite caliber athletes. These efforts have provided a profile of the significant stochastic performance criteria necessary for elite level sprint and hurdle performance. These criteria have now been integrated into dynamic sprint and hurdle models by first incorporating all performance data of the elite performers, then enhancing the models by emphasizing the significant performance parameters in each event.

Since the ultimate goal is to compare the dynamic sprint or hurdle model to the performance of any selected elite athlete, the models must be adaptable to the varying body dimensions of individual performers. Toward this end, it is currently possible to alter the enhanced elite performance model to match the inputted dimensions of any performer. To allow visual analysis by the elite coaches, the graphic model is overlaid on the actual video performance of the elite athlete.

REVIEW AND THEORY

Prior to the 1984 Olympics, the biomechanical analysis efforts of the Elite Athlete Project (EAP) Sprint and Hurdle Events focused upon gathering individual kinematic data on those few individuals that were obviously of elite performance caliber. Results of these analysis efforts were directed toward improving the performance of the individual by providing both the coach and athlete comparison data indicating strengths and weakness in selected biomechanical parameters (1).

Between 1983 and 1986, the kinematic results of the sprinters and hurdlers involved in the EAP were statistically compared with similar results produced by a group of non-elite collegiate sprinters (2) and hurdlers (3) to determine those factors critical to the production of an elite athlete performance in each event. This effort served to confirm, correct, and expand the specific variables that were presented in subsequent EAP analysis efforts (4,6).

In 1988 and 1989, the large collection of significant stochastic performance variables were integrated into standardized dynamic sprint (5) and hurdle (7) performance models. Each performance model was then used to make direct comparisons between the elite athlete and the model performance.

PROCEDURES

Results were generated in the EAP projects using film and force platform devices. Standard biomechanical data collection procedures were used in all cases. The modeling approach utilized the mean values for all EAP athletes for the basic model, then enhanced performance by maximizing those variables that have been deemed significant performance effectors.

RESULTS AND DISCUSSION

The results of the EAP project are contained in an interactive software program that runs on a computerized videographic system. The sprint and hurdle models are altered to match the body dimensions of the individual athlete, with the specifics of the performance altered accordingly. The resulting model performance is then overlaid on the actual video performance of the athlete. Visual comparisons can then readily be made. In addition, quantitative kinematic results can also be directly measured.

The final project results were applied at the 1989 and 90 Elite Sprint and Hurdle Seminars. The success of the comparative application was verified by comparing several performers using the current method and the past hardcopy approach. In addition, the ability of the software to adapt to the individual performer was verified in the same manner.

REFERENCES

1. Mann, R. V., Herman, J., Johnson, B., Schultz, C., & Kotmel, J. The Elite Athlete Project: Sprints and Hurdles. USOC Technical Reports 1-13, USOC Training Center, Colorado Springs, Co., 1982-83.

2. Mann, R. V., Herman, J., & J. Kotmel. "Kinematic Factors That Dictate Success in Sprinting: A Biomechanical Comparison Between Elite and Collegiate Class Sprinters." USOC EAP Research Report, USOC Training Center, Colorado Springs, Co., 1983, 84, 85.

3. Mann, R. V. & J. Herman. "Kinematic Factors That Dictate Success in Hurdling: A Biomechanical Comparison Between Elite and Collegiate Class Hurdlers." USOC EAP Research Report, USOC Training Center, Colorado Springs, Co., 1985, 86.

4. Mann, R. V. and D. Hayes. The Elite Athlete Project: Sprints and Hurdles. USOC Technical Reports 14-15, USOC Training Center, Colorado Springs, Co., 1987.

5. Mann, R. V. "Development of a Dynamic Model of Elite Sprint Performance." USOC EAP Research Report, USOC Training Center, Colorado Springs, Co., 1988.

6. Mann, R. V., The Elite Athlete Project: Sprints and Hurdles. USOC Technical Reports 16-18, USOC Training Center, Colorado Springs, Co., 1989-90.

7. Mann, R. V. "Development of a Dynamic Model of Elite Hurdle Performance." USOC EAP Research Report, USOC Training Center, Colorado Springs, Co., 1989.

BIOMECHANICAL ANALYSIS OF RUNNING MECHANICS IN ELITE DISTANCE RUNNERS

Keith R. Williams, Physical Education Department, University of California, Davis, Davis, CA 95616

While a primary goal of competitive distance running is to improve running performance and win races, performance measures are usually not appropriate dependent variables in distance running experimental studies and alternative criteria are needed. A maximal performance cannot be repeated frequently and there are many motivational factors that have the potential to confound performance measures. Some track and field events have underlying principles of mechanics that can be used to define performance and training objectives. For example in javelin throwing there are clearly definable mechanical objectives in terms of release conditions involving velocity, angle of attack, and angle of release. The role of mechanical principles in relation to distance running mechanics is more abstract and less clear. Physiological constraints are of major importance to distance running success, and mechanical factors are important in that they can affect the energy cost of running at a given speed or the levels of stress in the muscles and other tissues of the body. The primary focus of research with elite runners has been to gain a better perspective on how injury susceptibility and running economy are affected by the running mechanics, anatomical structure, and the functional capabilities of runners. Indirectly these factors will influence performance.

Analyses of elite distance runners has occurred over the last six years in cooperation with The Athletics Congress and the United States Olympic Training Center. Relationships involving measures of running mechanics have been examined using groups of runners and on a case-study basis. Data has been collected in three different experimental situations, including during elite level competition, as a part of a multi-disciplinary scientific evaluation involving groups of elite distance runners, and on an individual basis where a more involved set of biomechanical data have been collected. The outcome of these investigations has been the compilation of a substantial database of information concerning elite runners' mechanics and individual reports to athletes discussing potential relationships with injury and economy. Data has been analyzed for both male and female runners in events from 800m to the marathon. Many of the athletes have been tested on repeat occasions providing some information concerning longitudinal persistence of specific features of running mechanics.

Data collected in competitive situations has been limited to side view kinematics, with approximately 80 athletes involved during several different national championship competitions. Since some coaches were concerned that analyses of running mechanics in a laboratory during treadmill running are too far removed from the competitive world and result in inappropriate data, comparisons between competitive and laboratory conditions have been made. Data available for athletes analyzed in both the competitive and laboratory situations suggest that while some differences do exist, in most cases striking features of running mechanics for a given individual are present in the data for both environments. While data obtained in competitive situations has the advantage of describing the athlete's mechanics directly in relation to performance objectives, the limited amount of information that can be obtained and the influence of psychological competitive factors limit the applicability of the resulting data. While such information can provide descriptive information related to acute factors affecting performance, it does not necessarily reflect the more general mechanical influences that are present during training. Since most injuries are training related, rather than racing induced, there are some advantages to assessing runners in situations that emulate training conditions and training speeds.

The major emphasis in this work has involved analyzing running mechanics in a non-competitive environment under the assumption that the measures obtained are reflective of general features of running mechanics present during competition and that the measures obtained in laboratory situations are valid descriptors of aspects of running style that affect economy and injury susceptibility. Work evaluating distance running mechanics for groups of individuals has occurred over a five year period as part of an interdisciplinary evaluation sponsored by the United States Olympic Training Center. Twice each year 12-20 elite distance runners have been brought to the Olympic Training Center in Colorado Springs for six days of testing and evaluation. Data has been collected for more than 100 male and female elite runners. Testing has included: an anthropometric profile; biomechanical analyses of running mechanics; assessment of running economy and lactate profile across speeds; maximal aerobic capacity; pulmonary function; nutritional analysis; lower extremity strength assessment; podiatric evaluation; blood analysis; psychological evaluation and counseling; and, on occasion, bone scans. Each athlete received a verbal and written report of results before they left the camp in a multi-disciplinary feedback session where specific information from each area was discussed on its own merits and in relation to data from other disciplines.

Biomechanical measurements were limited to analyses of bilateral ground reaction forces and center of pressure patterns, stride length, bilateral rearfoot pronation analysis, and measures of sagittal plane kinematics for one side of the body. Anthropometrical measures of lower extremity structure and a functional foot examination were also included, and a history of injuries was recorded. The various mechanical and anthropometrical measures were evaluated for individuals in comparison to group data and in relation to injury history and measured running economy. Statistically significant relationships between various measures of running mechanics and economy have been found, but the relationships have generally been weak to moderate and have not remained consistent as the subject database has grown. More success has been found in relating some of the measures of mechanics to specific injury histories of individuals. For example, relatively high maximal ground reaction force values have been present in a number of runners with a history of impact related injuries, particularly if they use a midfoot-forefoot striking pattern.

The third experimental situation involving analysis of elite distance runners has involved a case-study approach were a more complete set of biomechanical data has been obtained. Only a small number of subjects have been involved in this relatively new program. Bilateral data has been collected for ground reaction forces, rearfoot pronation, sagittal plane kinematics, lower extremity anthropometry, lower extremity strength and muscular endurance, lower extremity flexibility, and foot function. A complete injury history is obtained from the runner, and physiological measures of running economy, lactate accumulation across speeds, and maximal aerobic capacity are also included. One advantage to this approach is being able to tailor the data collected to fit the needs and desires of the athlete and coach. Varying speeds might be investigated, or the use of different shoes or orthotics can be evaluated and compared to other conditions. Ideally this type of analysis will be longitudinal in nature with the same athletes evaluated periodically so that data can be put in reference to previous periods of training or racing. While not as scientifically rigorous, due to the case-study nature of the program, data for individuals can be compared to the database of information developed from the studies of the larger groups of elite runners. This approach has the advantage of providing more detailed information to the runner and the opportunity to discuss results thoroughly with the athlete, particularly with respect to their injury history, strength, flexibility, and training methods.

BIOMECHANICS AND POLE VAULTING: RUN FAST AND HOLD HIGH

Peter M. McGinnis
Physical Education Department, SUNY College at Cortland, Cortland, New York 13045

INTRODUCTION

Three decades have passed since a world record was first set on a fiberglass vaulting pole. In those three decades, the world pole vault record has risen more than four feet. After an initial frenzy of record breaking vaults in the 1960's, the rate of increase in the record slowed to about a foot per decade. In March of 1991, the first 20 foot vault was recorded. Appropriately, the first 21 foot vault will most likely occur in the early years of the 21st century. Equipment advances have obviously been responsible for much of the increase in the pole vault record, but advances in technique must also account for some of the rise in record heights as well. Have any of these equipment or technique advances been influenced by biomechanics? An organized program of biomechanics research and service has operated in the United States for the past decade with the primary goal of improving performances by American pole vaulters. The purpose of this paper is to describe and evaluate the scientific research and services provided by this program from 1983 through 1991.

SCIENTIFIC SERVICES

The scientific services provided to elite pole vaulters and their coaches consisted primarily of quantitative descriptions of competitive vaults, and in some cases diagnoses of possible errors in technique observed in these vaults. Typically, two dimensional high speed film records of vaults were recorded at two competitions each year: one competition in the early part of the outdoor season and one competition (usually the national championship) in the middle of the outdoor season. The successful vaults recorded on these films were digitized and the mechanical parameters which described these vaults were then derived from the digitized film data. The mechanical description and diagnosis of each vault were presented to the vaulters and coaches in personal reports. These reports were sent to the top vaulters and their coaches 30 to 90 days following each filmed competition. Videocassette copies of the analysis film also accompanied the reports. The coaches, vaulters, and biomechanist met once a year in the fall to discuss the reports and how to interpret the results.

The initial reports were not as useful to the athletes and coaches as subsequent reports since only a limited number of vaults were quantitatively described. This limited the comparisons which could be made. It was not known what was fast or slow, long or short, large or small, etc. In addition, the amount of data presented to quantitatively describe a single vault was somewhat overwhelming. More than 70 variables were measured and reported. The data contained in the reports were also "old". By the time the athletes and coaches received the reports, up to three months had passed since the performance of the vaults described in the reports. As the vaulters received more feedback in reports from season to season and as more vaults were analyzed, the reports became more useful. The more important variables were identified and comparisons could be made with other vaults and vaulters. The timeliness of reporting results was still slow, but the reports were useful in planning and preparing for the next competitive season.

In 1988, videocameras replaced film cameras as the data collection tool. The loss of resolution required the use of two cameras rather than one to record a two dimensional view of the vault. A high speed (200 hz) videocamera was used to obtain a panned sagittal view of the approach run and vault as well. A quick but accurate method of measuring the approach run velocities from this videorecord, so these velocity data were presented to the athletes and coaches in a report within one week after the competition rather than one to three months after the competition. This more immediate feedback was valuable for evaluating technique and training modifications in the current season as well as the next competitive season. In 1991, three dimensional video techniques were employed to record the takeoff phase of the vaults at the national championship. The data reported to the athletes and coaches this year will include not only planar descriptions of the vaults but three dimensional descriptions as well.

SCIENTIFIC RESEARCH

In the initial years of the Elite Athlete Project, not enough vaults had been filmed and digitized, so a finite element based computer model was developed to investigate the pole vault (McGinnis & Bergman, 1983). Parameters investigated with this model included initial dynamic conditions, resultant vaulter joint torque histories, and pole design. According to the model, faster takeoff velocities and higher takeoff angles led

to improved performances. In addition, the model was used to investigate several pole designs. The research results basically agreed with what the coaches and pole manufacturers already knew. The most enlightening outcome of the simulations was the indication of how sensitive a pole vault performance was to changes in any parameter (initial condition, pole stiffness, joint torque histories, etc.). This may explain why world class vaulters can vault 5.80 m easily on one day yet miss three attempts at 5.35 m on another day. If only the meet promoters and track and field fans understood this better.

An inverse dynamic analysis of the vault was completed in conjunction with the simulation of the vault in order to provide realistic resultant joint torque histories for the computer model (McGinnis, 1983; McGinnis & Bergman, 1986). Although only a limited number of vaults were examined, this study provided some indication of the role the left arm and hand played in the vault. Coaches had questioned: did the left hand push against the pole to assist with bending it and if it did, how long did it continue to push? Results from this study indicated that the left hand did push against the pole to produce a pole buckling moment but only briefly, for 0.20 s after takeoff.

By 1987, enough vaults by enough different vaulters had been filmed and digitized to develop some conclusions about factors related to pole vaulting success (McGinnis, 1987). Thirty two vaults by thirty two different vaulters were studied. The results indicated that horizontal velocity at take off and vaulter height were were significantly related to performance. Better vaulters ran faster and held higher on stiffer poles. This confirmed the coaches' admonition to "Run fast and hold high." But, in addition, this research revealed that the timing of the pole plant relative to the duration of support of the takeoff foot was important. Higher vaults occurred when the pole struck the back of the vault box closer to the instant of takeoff rather than touchdown. This timing was affected by the horizontal position of takeoff foot relative to the vaulter's top handgrip.

The importance of the vaulter's velocity, position, and timing at takeoff led to the investigation of the approach run. How did vaulters achieve fast takeoff velocities with an accurate placement of their takeoff foot? An investigation of the variability of step lengths and footstep positions during the approach run indicated that most vaulters adopted a visual control strategy during the last three to five steps of their approach run (McGinnis & Abendroth-Smith, 1989).

CONCLUSIONS

Although the Elite Athlete Project and subsequent programs have provided pole vaulters and coaches with information previously unavailable to them, the effect of these programs on the performances of American vaulters is difficult to assess. In the pole vault competition at the 1988 Olympic Games the highest placing by an American vaulter was fourth. This was the first time a medal was not won by an American pole vaulter in an Olympic Games in which the United States participated. This is not an indication of the failure of this program, but it is an indication of the success of the Soviet Union's pole vaulting program. Rather than leading the way in discovering new techniques, the research program has primarily just confirmed what many coaches believed or suspected. But, some research has settled disagreements concerning specific aspects of technique or has produced new insights into pole vaulting technique. More research leading to these types of results is needed for the continued success of the Elite Athlete Project.

REFERENCES

McGINNIS, P. M. (1983). The inverse dynamics problem in pole vaulting. *Medicine and Science in Sports and Exercise*, 15: 112 (abstract).

McGINNIS, P. M. (1987). Performance limiting factors in the pole vault. *Medicine and Science in Sports and Exercise*, 19: S18 (abstract).

McGINNIS, P. M., & ABENDROTH-SMITH, J. (1989). Approach run variability in the pole vault. In C. J. Dillman, R. C. Nelson, B. M. Nigg, R. O. Voy, & M. M. Newsom (Eds.), *Proceedings of the First IOC Congress on Sport Sciences*, (pp. 340-341). Colorado Springs, CO: U.S. Olympic Committee.

McGINNIS, P. M., & BERGMAN, L. A. (1983). A dynamic finite element model of pole vaulting. *Journal of Biomechanics*, 16: 287-288 (abstract).

McGINNIS, P. M., & BERGMAN, L. A. (1986). An inverse dynamic analysis of the pole vault. *International Journal of Sport Biomechanics*, 2: 186-201.

ASB YOUNG SCIENTIST AWARDS

ALTERATIONS OF CONTACT STRESS AND TISSUE HISTOMORPHOMETRY IN SIZE-DEPENDENT OSTEOCHONDRAL DEFECT REPAIR

J E Hale, T D Brown, M J Rudert, C G Mohler, R A Brand, and J A Buckwalter
Biomechanics Laboratory, Department of Orthopaedic Surgery
The University of Iowa, Iowa City, IA 52242

INTRODUCTION: Articular cartilage possesses limited capacity for repair. The extent to which repair does occur following injury appears to be dependent upon the size of defect present. Clinically, smaller defects tend to yield better outcomes than do larger defects. However, the local biomechanical factors responsible for altered cartilage repair have not yet been clearly elucidated. The aim of this study was to measure contact stress distribution changes and assess concurrent biological changes associated with the natural course of repair of osteochondral defects.

METHODS: Full-thickness osteochondral defects were created intra-operatively in the weight-bearing region of each femoral condyle in 15 adult mongrel dogs, using a trephine and drill. Defect sizes of 1, 3, and 5 mm were chosen based on in vitro data [1]. Dogs were allowed on runs for a period of 10 months prior to sacrafice. Mechanical testing was performed with the harvested knees locked in flexion and subjected to a 600 N (approximately 3 times body weight) compressive load. Cartilage contact stress distributions were recorded using Fuji Pressensor pressure sensitive film. Flexion angles were chosen such that the recorded contact patch maximally surrounded the defect. Contact stress distributions were quantified using digital image analysis. Contact stress values were read at regular radial increments along computationally constructed rays emanating from the defect center (Figure 1). Circumferential mean contact stress distributions were evaluated across the specimen population as a function of defect size. The integrity of repair tissue within the defect, as well as degeneration of the adjacent tissue, was characterized mechanically by indentation testing and histomorphometrically using a standardized grading index.

RESULTS: Series averaged (over 48 condyles) circumferential mean contact stress distributions were evaluated as a function of radial distance from the defect center for the three defect sizes (Figure 2). The intact case, based on in vitro results, is represented by the heavy solid line. Compared to an intact articular surface, contact stress within the defect per se diminished for all three defect sizes, while peak contact stress magnitudes in the surrounding cartilage were mildly elevated. With increasing defect size, peak contact stress occurred at increasing radial distance from the defect rim. The capacity of the repair tissue and adjacent cartilage to resist indentation was initially characterized by the secant slope of load-deformation plots from the indentation tests. In all cases, there was statistically significant compromise of the indentation resistance of repair tissue ($p<0.01$), compared to the adjacent cartilage. The resistance to indentation of the 1 mm defect repair tissue was significantly superior to that of the 3 mm ($p<0.02$) and 5 mm ($p<0.01$) defects (Table 1). Gross examination of the defects showed full repair of 1 mm defects, while 3 mm and 5 mm defects were irregularly filled with fibrous-appearing material. Histomorphometric grading further differentiated the quality of repair by defect size [Table 2].

DISCUSSION: There was only a loose relationship between defect diameter and the degree of contact stress increase in the adjacent cartilage. After ten months of repair, this relation was in fact even less distinct than its surprisingly weak acute/in vitro counterpart [1]. Nonetheless, relative differences in the measured contact stress distribution and in resistance to indentation corresponded to histologically apparent differences in the repair response. The decreased resistance to indentation of repair tissue for the 3 mm and 5 mm defects is consistent with its failure to contribute effectively to contact stress uptake as measured by Pressensor film. Although the resistance to indentation of the adjacent cartilage was not significantly different for the larger defects, decreased peak contact stress for the 3 mm and 5 mm defects relative to the 1 mm defect and in vitro results suggests peripheral degeneration and/or diminished capacity of this region to bear load.

REFERENCES: [1] Brown, TD et al.: Effect of osteochondral defect size on cartilage contact stresses. J Orthop Res, in press, 1991.

Acknowledgement: NIH grant AR38916.

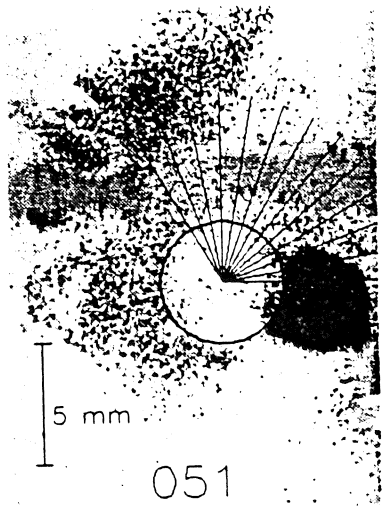


Figure 1

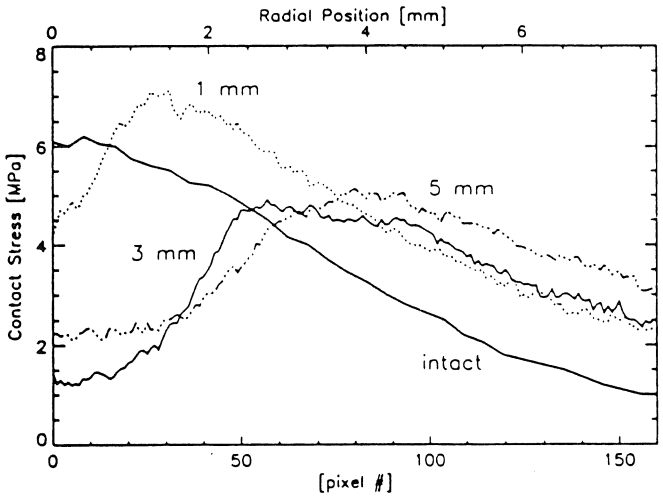


Figure 2

Table 1
Resistance to Indentation

g/mm³ (std.dev., n)

Defect Size (mm)	Adjacent (Normal?)	Repair Tissue	Percent of Normal
1	201.9 (86.1, 18)	63.7 (46.8, 13)	32*
3	203.2 (117.0, 26)	31.6 (28.0, 18)	16*¤
5	181.3 (85.6, 24)	21.9 (22.1, 21)	12*♦

* $p < 0.01$ vs normal
¤ $p < 0.02$ vs 1 mm repair
♦ $p < 0.01$ vs 1 mm repair

Table 2
Histomorphometric Mean Scores

Defect Size (mm)	Mankin Index♦ (0 - 14)	Buckwalter Index* (0 - 45)
1	4.35	35.87
3	6.63	31.75
5	6.50	32.32

♦ increasing score denotes more severe degeneration
* increasing score denotes less severe degeneration

EFFECT OF THE HIP CENTER LOCATION ON MUSCLE STRENGTH

Scott L. Delp

Departments of Biomedical Engineering and Rehabilitation Medicine, Northwestern University, and Sensory Motor Performance Program, Rehabilitation Institute of Chicago

INTRODUCTION

The functional result of an otherwise satisfactory hip reconstruction may be compromised if the capacity of the hip musculature to generate forces and moments is greatly reduced. For example, if the hip abductors are unable to generate the moments needed to stabilize the pelvis during single-leg stance, a limp is likely to result. If the hip extensors are weak, they may not be able to generate the moments needed to climb stairs or rise from a chair. Since surgical technique, prosthesis design, and joint pathology affect the position of the hip center, it is important to understand how variations in the location of the hip center affect muscle strength. The following results show that the position of the hip center can have large effects on the moment-generating capacity of the muscles (i.e., muscle strength).

REVIEW AND THEORY

The capacity of a muscle group to generate moment about a joint depends on the force and moment arm of each muscle in the group. Since the force-length relationship and moment arm of each muscle crossing the hip is affected by the position of the hip joint center, this study examined how the force- and moment-generating capacity of the hip muscles are affected by alterations in the position of the hip center. The specific objective was to quantify the effect of anterior-posterior, superior-inferior, and medial-lateral displacement of the hip center on muscle force, moment arm, and joint moment for four muscle groups (abductors, adductors, flexors, extensors).

PROCEDURES

A computer graphics model of the human lower extremity (Delp et al., 1990) was used to study the effects of displacing the hip center on the moment-generating capacity of the muscles. This model specifies the line of action, peak isometric force, optimal fiber length, tendon slack length, and pennation angle of 27 muscles crossing the hip. Thus, the maximum isometric force each muscle develops (i.e., the force developed when muscle is fully activated and held isometric) and the resulting joint moments can be computed at any combination of hip and knee angles. Moments from all the muscles in a group were summed to calculate the joint moment generated by the muscle group over a range of joint angles. Joint moments calculated for the muscle group were then compared with isometric joint moments that have been measured during maximum voluntary contractions at a variety of hip and knee angles (e.g., Cahalan et al., 1989). Calculated and measured moments corresponded closely.

The hip center was displaced along one of three axes (anterior-posterior, superior-inferior, and medial-lateral) while the position along the other two axes was maintained at the anatomical hip center. At each position along an axis, the average force, moment arm, and moment were computed for each muscle group. The *force* of a muscle group was computed as the sum of the maximum isometric forces developed by all the muscles in the group. The *moment arm* of a muscle group was computed as the sum of the moment arm of each muscle times its physiologic cross-sectional area (PCSA) divided by the total PCSA of all the muscles in the group. This represents a weighted average moment arm of the muscle group. The *moment* of a muscle force about the hip was computed by multiplying its moment arm and maximum isometric force. The moments generated by all the muscles in a group were then summed, yielding joint moment of the muscle group. The force, moment arm, and joint moment generated by a particular muscle group were first averaged over the range of hip angles used in walking, stair climbing, and rising from a chair. These average values were then plotted vs. the displacement of the hip center along each axis. From these plots the percent change in force, moment arm, and moment that result from displacement of the hip center along each axis could be determined for each muscle group.

RESULTS AND DISCUSSION

Table 1 shows the change in force, moment arm, and moment that results from displacing the hip center 2 cm in each direction (while the other displacements are set to zero) for each of four muscle groups. *Superior-inferior* displacement has a significant effect on all the muscle groups. For example, 2 cm of superior displacement decreases abduction force (33%), moment arm (12%) and moment (49%). This is the greatest effect that any displacement has on any muscle group. The forces and moment arms of both the adductors and extensors are significantly affected by superior-inferior displacement. However, since force and moment arm are changed oppositely in each case (e.g., force increases but moment arm decreases), adduction and extension moments are not affected very much. Superior displacement decreases flexion force, moment arm, and moment, while inferior displacement increases all three variables.

Anterior-posterior (AP) displacement has almost no effect on abduction or adduction moments. In contrast, both flexion and extension moments are affected significantly by AP displacement. For the extensors, anterior displacement increases average force, moment arm, and moment. Posterior displacement has the opposite effect. For the flexors, anterior displacement slightly increases the average force, but greatly decreases moment arm; thus, flexion moment is decreased with anterior displacement. Posterior displacement has exactly the opposite effect; it decreases force slightly, but increases moment arm greatly, so flexion moment increases.

Medial-lateral (ML) displacement has a large effect on adduction moment only. Lateral displacement increases adductor force (9%), moment arm (24%), and moment (40%). Medial displacement has the opposite effect. It is interesting to note that ML displacement has only a small effect on the abduction moment. Lateral displacement increases abduction force, but decreases moment arm; thus moment changes only 2%. Medial displacement decreases abduction force (16%), but increases moment arm (13%), so again, abduction moment is hardly affected.

Table 1. Percent Change in Average Force, Moment Arm, and Moment Resulting from Displacing the Hip Center 2cm in Each Direction

	superior	inferior	anterior	posterior	lateral	medial
Abduction						
muscle force	-33	+10	0	-3	+5	-16
moment arm	-12	+7	0	-3	-13	+13
moment	-49	+26	0	0	-2	-9
Adduction						
muscle force	-24	+21	0	0	+9	-18
moment arm	+15	-12	0	0	+24	-25
moment	-17	+10	+2	0	+40	-40
Extension						
muscle force	-20	+22	+14	-19	+5	-5
moment arm	+23	-22	+17	-22	0	0
moment	0	-5	+34	-36	+2	-2
Flexion						
muscle force	-28	+5	+6	-6	+4	-5
moment arm	-9	+10	-36	+35	-4	0
moment	-24	+17	-30	+23	-3	-3

S. L. Delp et al. *IEEE Trans. Biomed. Eng.*, vol. 37, pp. 757-767, 1990.
T. D. Cahalan et al. *Clin. Orthop. Rel. Res.*, vol. 246, pp. 136-145, 1989.
Supported by the Rehabilitation R&D Service, Department of Veterans Affairs and the Baxter Foundation

THE EFFECT OF ROOFPLASTY AND TIBIAL HOLE PLACEMENT ON IMPINGEMENT OF ANTERIOR CRUCIATE LIGAMENT RECONSTRUCTIONS

Gregory S. Berns* and Stephen M. Howell†
*School of Medicine, M-006, University of California, San Diego, La Jolla, CA 92093
†Department of Orthopedics, University of California, Davis, CA 95616

INTRODUCTION

The problem of ACL graft impingement by the intercondylar roof is an aspect of reconstructive surgery that has not been adequately studied. Impingement can be defined as any pathologic contact between a graft and the intercondylar roof. The purpose of this study was to determine the precision and the amount of bone removal from the intercondylar roof necessary to prevent impingement with different sagittal placements of the tibial tunnel. In human cadaveric knees we found that anterior tibial tunnels required more bone removal from the roof than did posterior tibial tunnels. With an incomplete roofplasty, contact between the roof and the graft occurred at large flexion angles. This suggests that the amount of roofplasty should be matched to the sagittal location of the tibial tunnel.

REVIEW AND THEORY

The role of impingement in ACL reconstruction is likely a complex one. The intra-articular path of the graft, which is determined by the location of both the tibial and femoral holes, obviously affects the amount of impingement. The size of the graft has also been positively correlated to impingement [3]. The factors substantially under the control of the surgeon are: 1) size and type of graft; 2) femoral hole placement, although this is rather tightly constrained to be near the average center of rotation; 3) tibial hole placement; and 4) amount of roofplasty.

Previous studies have suggested that the consequences of graft impingement are serious. MRI scans of impinged knees often appear edematous [2], suggesting less than ideal healing. More compelling is evidence for significant extension deficits in impinged knees [1]. Based on these prior findings, we hypothesized that the deleterious effects of impingement result from the generation of a pathologic pressure on the graft, thus impairing healing and leading to extension deficits. Our goal in this study was to determine both the flexion angle at which grafts contacted the roof and the effects of tibial hole position and roofplasty on the contact angle.

PROCEDURES

The perpendicular force of the intercondylar roof against an ACL graft was measured in 7 fresh-frozen cadaver knees. Two tibial hole placements were evaluated: an anterior hole (27%±3% of sagittal depth) and a posterior hole (42%±3%). A transducer which measured the contact force with the graft was implanted perpendicularly through the roof, emerging in the center of the distal end of the intercondylar notch. The sensor was advanced into the joint so that it just contacted the intact ACL with an extension torque of 2.5 Nm. This defined 0° flexion. The intact ACL was then excised and the center of the two tibial positions were located with 2.4 mm k-wires. A femoral pin was placed so that isometric testing of both tibial holes through this common femoral hole resulted in 2 mm or less excursion from 0°-120° flexion. A 9 mm diameter cotton rope was used as a graft material and was attached to a tension sensor at the tibial end. An extensive roofplasty was performed so that the sensor would bear all the roof force. With the graft first in the posterior hole, flexion/extension cycles were applied to a maximum of 20 Nm extension with a 6 degree-of-freedom load application system. Roof force, graft tension, and extension angle were continuously recorded. Load cycles were repeated with the roof force sensor backed out in 0.8 mm increments, which represented corresponding amounts of roofplasty. After backfilling the posterior hole with methylmethacrylate, the protocol was repeated for the anterior tibial hole.

RESULTS

Typical force profiles for both anterior and posterior tibial holes are shown in Figure 1. It can be seen that the anterior hole resulted in graft contact at a larger flexion angle, and the force at maximum extension was significantly higher. Flexion angle at graft contact as a function of sensor backout is shown in Figure 2. With the anterior hole, the roof sensor (no backout) contacted the graft at $13^{\circ}\pm7^{\circ}$ flexion, whereas the posterior hole contacted the graft at $4^{\circ}\pm4^{\circ}$ ($p=0.020$). With zero impingement defined as no contact between the roof and the graft with the knee in maximum extension (20 Nm torque), the anterior hole required 4.6 ± 1.0 mm of sensor backout, and the posterior hole required 1.3 ± 1.1 mm sensor backout ($p\leq0.0001$). Allowing the transducer to extend into the notch 0.8 mm resulted in elevated forces between the graft and the roof. In this configuration, graft contact always occurred before the knee reached terminal extension.

DISCUSSION

Although the graft material used in this study was substantially different from those used in surgery, we believe the results pertaining to the flexion angle at roof-graft contact are valid. The cotton graft may have had a larger transverse stiffness than a tendonous graft. This difference manifests itself as the rapid rise in force seen in Figure 1. Regardless of the graft material, the flexion angle at which the roof contacts the graft should be the same. We have assumed that the sensor backout corresponds to millimeters of roofplasty; however, the correspondance is obviously not exact. Given these cautions, a relationship appears to exist between the sagittal placement of the tibial tunnel and the amount of roofplasty required to prevent impingement. The flexion angle at graft contact was significantly greater for the anterior tunnel. The use of an anterior tunnel with an insufficient roofplasty may result in flexion contractures and repetitive trauma to the graft. Our results suggest that these problems can be avoided by moving the tibial tunnel posterior, allowing a more conservative roofplasty. However, retaining an extra 0.8 mm of bone can still result in elevated pressures to the graft. The extent of the roofplasty should be precisely matched for the sagittal location of the tibial tunnel.

REFERENCES

1. Howell SM, Berns GS, Farley TE: Signal intensity measurements of unimpinged and impinged anterior cruciate ligament grafts. *Radiology* 179:0-0, 1991 (in press).
2. Howell SM, Clark JA, Farley TA: A rationale for predicting anterior cruciate graft impingement by the intercondylar roof: an MRI study. *Am. J. Sports Med.*, in press.
3. Tanzer M, Lenczner E: The relationship of intercondylar notch size and content to notchplasty requirement in anterior cruciate ligament surgery. *Arthroscopy* 6:89-93, 1990.

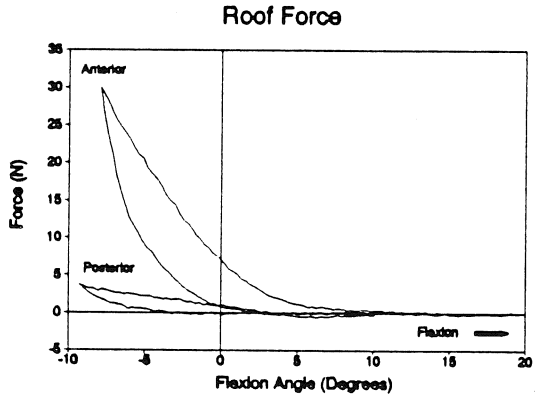


Figure 1. Typical force vs. angle data.

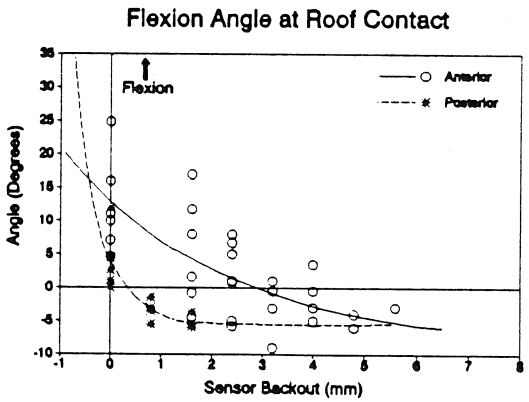


Figure 2. Contact angle dependence on backout.

SESSION 1

HUMAN GAIT

BIOMECHANICS OF SUCCESSFUL RECOVERY FROM A STUMBLE.

M.D. Grabiner[1], T.J. Koh[1], L. Schaller[1], T. Lundin[1], D.W. Jahnigen[2]
Departments of [1]Biomedical Engineering & Applied Therapeutics, and [2]Geriatric Medicine
The Cleveland Clinic Foundation

Introduction: Falls account for the majority of accidental injuries, the sixth leading cause of morbidity for individuals over age 65. Notably, women fall more often than men until age 75, after which the frequency is similar[1]. Falling has been reported to be related to dorsiflexion weakness[2], hip muscle weakness[3], impaired gait[4,5], decreased proprioception[6], increased reaction time[7], and postural instability[8,9]. However, there is presently no consensus regarding the mechanisms underlying the male-female difference in falling behavior, the age-related exponential increase in falling behavior, or factors predisposing an individual to falling. The purpose of this study was to determine the change in selected kinematic gait variables as a result of an induced-stumble. This study is part of a larger effort intended to construct a model which includes neuromotor and biomechanical variables that could be used to characterize predisposition to falling and direct clinical intervention.

Methods: Seven healthy, recreationally active males participated in the study. The body was represented by an eleven segment model marked by nine pairs of bilateral, passive reflective markers, the motions of which were recorded using four video cameras at 60 Hz. Six control walking trials were performed prior to walking trials during which induced stumbles were randomly administered. Stumbles were induced by a mechanical device, three inches high, that could be raised from its position flush with the floor surface. Equal numbers of stumbles were induced on the right and left legs. Based upon qualitative observations of laboratory-induced stumbles, five variables were extracted for analysis: maximum values of trunk flexion angle, knee flexion angle, hip flexion angle, knee extension velocity and hip flexion velocity.

Results and Discussion: Between-trials differences were not found and the data were subsequently pooled. Subsequent analysis using a 2 by 2 (Stumble-No Stumble Condition by Left-Right Feet) repeated measures analysis of covariance (ANCOVA) was performed using preperturbation horizontal velocity of the center of gravity as the covariate. The stumble may be divided into two phases: perturbation and recovery. The perturbation phase is dominated by trunk flexion. Maximum trunk flexion angle increased from a mean of 4.3 degrees (control) to 18.3 degrees following a perturbation ($p=0.057$). The perturbation phase was defined to include recovery leg knee flexion up to the instant of maximum value. This knee flexion motion assists the recovery by (a) increasing the distance between the foot and floor/obstacle thereby decreasing the likelihood of a second perturbation during recovery and (b) reducing the lower extremity moment of inertia thereby increasing the velocity with which the hip can be subsequently flexed. The maximum knee flexion angle increased from 60 (control) to 89 degrees during perturbation trials ($p=0.009$).

The recovery phase may be further divided into the (a) positioning, and (b) support phases. The positioning phase includes recovery leg motion up to the instant of recovery foot touchdown which begins the support phase. Recovery requires that the recovery foot be placed anteriorly to the center of gravity (COG) to regain dynamic balance. Since the maximum knee extension for both the control and induced stumble conditions approached full extension, the hip flexion excursion influences the distance that the foot may be placed anteriorly to the COG. The maximum hip flexion angle increased from 26 (control) to 47 degrees during the induced stumble trials ($p=0.039$). Although maximum hip flexion velocity increased 79 percent during the induced stumble trials compared to the control trials the increase was not significant ($p>0.05$). The maximum knee extension velocity increased 36 percent during the induced stumble compared to the control trials but was not

statistically significant ($p>0.05$). Notably, the results of the analysis of covariance revealed that of all the variables, only the trunk flexion angle was significantly related to the preperturbation walking velocity ($p=0.036$).

Conclusions: The large trunk flexion amplitude resulting from the perturbation suggests that the ability to regain control of the trunk is a crucial element underlying recovery. Control of the trunk must be restored by a fairly rapid generation of an eccentric trunk-hip extension moment. The generally high incidence of low back disfunction in conjunction with the significant relationship between trunk flexion amplitude and prepertubation walking velocity offers a tempting hypothesis that age-related decreases in walking velocity are related to decreased trunk function. The significant increases in hip and knee range of motion, and large increases in the joint velocity parameters point toward possible relationships between ability to recover from a stumble and muscular strength/power at these joints. Further kinetic analysis of the repositioning and support phases will elucidate the joint moment/power requirements and aid in the application of more clinically viable methods to determine recovery ability.

TABLE 1

Summary of Kinematic Changes Associated with an Induced Stumble

	Trunk Flexion (deg)	Knee Flexion (deg)	Hip Flexion (deg)	Knee Extension Velocity (deg/s)	Hip Flexion Velocity (deg/s)
Control	4.3	60.1	25.9	412.6	187.4
	p=.057	p=.009	p=.039		
Induced Stumble	18.3	89	47.3	561.2	334.9

1. Tinetti ME, Speechley M: The New England Journal of Medicine, 320:1055-1059, 1989.
2. Whipple RH et al: Journal of the American Geriatric Society, 35: 13-20, 1987.
3. Robbins AS et al: Archives of Physical Medicine, 149:1628-1633, 1989.
4. Morse JM et al: The Gerontologist, 27:516-522, 1987.
5. Wolfson L et al:Journal of Gerontology, 45:M12-M19, 1990.
6. Kaplan FS et al: Acta Orthopedica Scandinavica, 56:71-74, 1985.
7. Adelsberg S et al: Archives of Physical Medicine and Rehabilitation, 70:737-739, 1989.
8. Crosbie WJ et al: Archives of Physical Medicine and Rehabilitation, 70:751-754, 1989.
9. Heitmann DK et al: Physical Therapy, 69:923-931, 1989.

KINEMATICS OF HEELSTRIKE DURING WALKING AND CARRYING: IMPLICATIONS FOR SLIPS AND FALLS

Mark S. Redfern[1, 2], Mary Ann Holbein[2], Dan Gottesman[3], and Don B. Chaffin[3]

1. Dept. of Otolaryngology at the The Eye & Ear Institute, Univ. of Pittsburgh
2. Dept. of Industrial Engineering, Univ. of Pittsburgh.
3. Center for Ergonomics, Dept. of Industrial Engineering, Univ. of Michigan.

INTRODUCTION

Slips and falls are a major cause of injury throughout the world. Mosts slips occur at heel strike, therefore the dynamics of the heel at floor contact are an important factor in determining slip potential. The goal of this study was to quantify heel motion during the heel strike event while free walking and carrying boxes of varying weights at three different cadences. The kinematics of the heel during heel strike were evaluated for six subjects using a SELSPOT movement detection system. Parameters of interest were velocity of the heel at and 100 ms before heelstrike, heel deceleration, heel slip after heelstrike, foot angle at heelstrike, and time from heelstrike to foot flat. The results showed that small amounts of heel movement usually occur after heelstrike and the velocity of the heel before and at heelstrike are highly dependent upon subject differences and cadence, but not on the load carried.

REVIEW AND THEORY

Slips are directly related to the frictional properties of the shoe-floor interface and the kinematics of the shoe during activities such as walking, carrying, and pushing (Strandberg, 1983). Slip usually begin at heel strike, causing the floor reaction forces to be extended beyond the center of mass of the body, potentially creating a fall (Strandberg, 1983). Thus, the *dynamic* frictional characteristics of the shoe/floor interface and the kinematics of the heel are of critical importance. In fact, dynamic friction is dependent on the sliding velocity of the shoe, the vertical force applied, contact area, and the angle of the shoe (Redfern, et al., 1990; Strandberg, 1983; Perkins and Wilson, 1983). Levels for these parameters used in dynamic slip testing should therefore be based on the biomechanics of the activity performed to acquire appropriate measures.

The primary purpose of this study was to experimentally determine the kinematics of the foot just before and during heelstrike under various load carrying conditions and walking speeds with the long term goal of reducing slips and falls.

PROCEDURES

An assessment of the heel dynamics before and immediately after heelstrike was performed. Six subjects were tested with ages ranging from 22 to 37 years. All subjects wore the same brand of steel-toed work shoes given to them specifically for the study. A two dimensional SELSPOT motion detection system was used to track movement of the foot and shank during the trials. Infrared Light Emitting Diodes (IREDs) were placed on the foot and leg at the following landmarks: heel of the shoe; shoe sole below the fifth metatarsal joint; ankle (lateral malleous); and the knee (lateral femoral epicondyle). Foot force data was also recorded using a Kistler force plate to determine when heel strike occurred. Heelstrike was defined as time zero (0.0 s) with negative time being swing phase and positive time being stance phase. All data was synchronously sampled using an HP-1000 minicomputer at a sampling rate of 100 Hz. The IRED data were then used to calculate the six dependent variables of interest described in the Introduction. Velocities were determined by band limited numerical differentiation of the position data of the heel. The amount of slip after heel strike (microslip) was defined as the horizontal distance traveled by the heel IRED after heelstrike.

The two independent variables tested in this experiment were cadence of walking and load carrying. The levels of cadence were 70, 90 and 110 steps/minute. Five load carrying conditions were used: free walking without carrying a box, and carry with loads of 0, 4.5, 9.0, and 13.5 Kg. The box was 30 cm x 33 cm with a depth of 28 cm. and handles on the sides near the top of the box.

RESULTS

The effects of the independent variables (subjects, cadence and load carrying) were determined by ANOVA analysis with separate analyses for each of the six dependent variables. The results showed subject and cadence effects were significant for all measures and the subject*cadence interaction was significant for al but one variable. Load carry conditions, however, affected only the microslip and heel angle variable. Further investigation found that cadence accounted for about 90 % of the variance for variables before heelstrike (velocity and acceleration before heelstrike); and subject differences was the predominating factor for those variables at heel strike (microslip, foot angle, and velocity).

Table 1 shows the mean values of each variable grouped by cadence along with values found in the literature. The results of this study agree to those of Strandberg and Lanshammer (1985), but were different from those presented by Leamon and Son (1989).

DISCUSSION

The biomechanics of heelstrike are primarily affected by cadence and subject variabilities. The ANOVA results indicate that people have similar foot trajectory patterns at the end of swing phase with cadence being the overriding factor. As the heel contacts the floor, however, subject variability becomes increasingly important. One surprising finding was that load carry conditions tested were found to have minimal impact on the kinematic variables. Thus some compensation during walking may be taking place to adjust to changes in posture created by the carrying task.

The results of this study have direct implications towards testing of floor surfaces for slip resistance characteristics. First, the finding that the heel slips after heelstrike before coming to a complete stop indicates that dynamics slip resistance testing is more relevant than static testing. Second, establishing velocity levels is critical since slip resistance measurements have been shown to be highly dependent upon velocity (James, 1983; Perkins and Wilson, 1983; Redfern, 1990). This study establishes a range of velocities for normal walking and load carrying. This range takes into consideration walking speed (as shown by the cadence effects) and variations due to individual differences (as shown by the subject effects).

Table 1: Mean values of measured variables and comparison of previously published results.

	RESULTS (by cadence)				Strandberg & Lanshammar (1981)	Leamon & Son (1989)
Steps/min.	70	90	110	Avg.	90,100,110,120	
Microslip (cm)	1.13	1.34	1.56	1.34	1.2 (mini)	
	(.34)	(.39)	(.55)	(.47)	(0.4)	
Angle at heelstrike (deg)	17.9	19.4	20.3	19.2	22.0 (grips)	32.0
	(3.5)	(3.3)	(4.2)	(3.8)	(5.3)	
Velocity at heelstrike (cm/s)	13.9	19.0	24.1	19.1	28.2 (grips)	90.0 (slow) 180.0 (fast)
	(9.9)	(15.1)	(20.8)	(16.4)		

REFERENCES

Leamon TB and Son, DH, *Adv. Ind. Erg.* ed. Mital, 1989.

Perkins, PJ and Wilson, MP, *Ergonomics*, 26(1): 73-82, 1983

Redfern, MS, et al. *J. Safety Res.*, 21:61-65, 1990.

Strandberg, L, *Ergonomics* 26(1):11-31, 1983.

Strandberg, L, and Lanshammer *J. Occup. Accidents* 3, 153-162.

Szymusiac, SM, Ryan JP, *Occup. Health Safety*, June, 1982.

RELATIONSHIP BETWEEN ECONOMY AND JERK-COST DURING WALKING

Alan P. Hreljac and Philip. E. Martin
Exercise and Sport Research Institute
Arizona State University, Tempe, AZ., 85287-0404

INTRODUCTION

Many performance criteria (PC) have been hypothesized to be important during human movement. One PC shown to be important in walking at a given speed, is metabolic energy consumption ($\dot{V}O_2$). A kinematic PC linked to minimizing $\dot{V}O_2$ in a mathematical model, is jerk-cost (J_c), given by the equation:

$$J_c = \int_0^T \left(\frac{d^3 \mathbf{r}}{dt^3} \right)^2 dt \quad (1)$$

where **r** is a position vector, and T is the total movement time. The theoretical model suggesting that these two performance criteria are related was experimentally tested in this study, using walking as the movement task. Very low correlation was found between these variables as stride length (SL) was varied by ±10% and ±20% of freely chosen (FC), indicating that $\dot{V}O_2$ and J_c are not compatible performance criteria during walking.

REVIEW AND THEORY

It has been demonstrated (Flash & Hogan, 1985) that for motions of the hand, a major goal of motor coordination is the production of the smoothest possible movement. This requires that the function given in (1) be minimized, and that jerk is measured in the coordinate frame in which motion is planned. The two coordinate frames most often referred to are angular and endpoint (Cartesian) coordinates. It has been suggested (Hogan, 1984) that this model has "considerable generality". Stein, Oğuztöreli, and Capaday (1986) have shown that minimizing energy consumption is related to minimizing jerk over a range of conditions. It has been demonstrated by several authors (Cavanagh & Williams, 1982; Kaneko et al., 1987; Morgan & Martin, 1986) that $\dot{V}O_2$ increases curvilinearly as SL is varied from FC in both walking and running. If the theory of maximum smoothness could be generalized to walking, and if J_c is related to $\dot{V}O_2$, then it could be postulated that J_c would show a response similar to that shown by $\dot{V}O_2$ as SL is varied during walking. The purposes of this study were to test the hypothesis that J_c is related to $\dot{V}O_2$ at a given walking speed, and to determine whether the choice of coordinate frame used to calculate jerk is important during a treadmill walking task.

PROCEDURES

Twenty-four well trained subjects walked on a treadmill (1.75 $m \cdot s^{-1}$) until steady-state $\dot{V}O_2$ was attained for each of 5 SL conditions (FC, ±10%, and ±20% of FC). Filming (60 Hz) in the sagittal plane and subsequent digitizing of three strides produced position coordinates of relevant points which were

smoothed using a 2nd order Butterworth filter. These data were normalized in distance and time before finding the 3rd derivative with finite difference equations. 2D normalized J_c values were calculated using the method described by Schneider and Zernicke (1989). Endpoint J_c (EJ_c), calculated at the heel and angular J_c (AJ_c), calculated at the ankle are presented in $J_c \cdot s^{-1}$. A repeated measures MANOVA tested for differences between levels of the independent variable (SL) for each of the three dependent variables. Correlation coefficients were calculated across and between SL conditions.

RESULTS AND DISCUSSION

$\dot{V}O_2$ exhibited somewhat of the expected response (minimum at FC and -10%), whereas the two measures of jerk were lower for the shorter SL conditions (Figure 1). Across SL conditions, weak, but statistically significant negative correlations (-0.20 and -0.27) were found between $\dot{V}O_2$ and each of the two measures of jerk, suggesting that $\dot{V}O_2$ is not positively related to jerk during walking. Within SL conditions, correlation coefficients between $\dot{V}O_2$ and jerk-cost measures ranged from -0.36 to -0.67, indicating that a moderate amount of variance (up to 44%) in $\dot{V}O_2$ could be explained by differences in J_c. However, these correlations are opposite in direction to that expected. The two jerk measures were highly correlated (0.72), implying that the coordinate frame used in the J_c computation was not important for a well-learned task such as walking. Since jerk is also postulated to be related to a constant muscular stiffness (Nelson, 1983), low J_c and high metabolic costs at shorter strides may be due to a relatively greater duration of cocontraction. For short SL conditions, it is likely that sensory feedback cannot be utilized to a large extent due to transmission delays. We may chose to walk at a SL which allows feedback control, yet does not require larger active forces needed for longer strides.

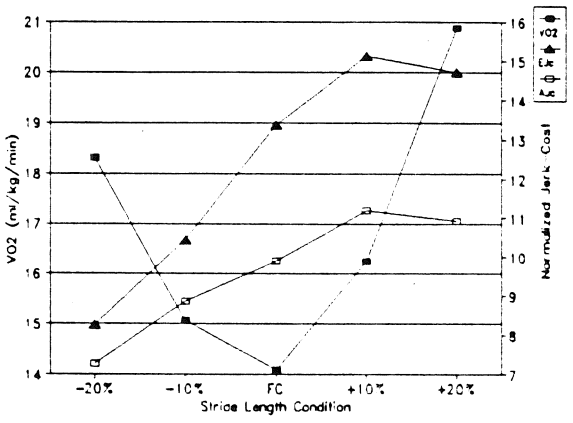


Figure 1. $\dot{V}O_2$ and Jerk-cost

Cavanagh P, Williams K: Med Sci Sports Exer. 14:30-35, 1982.
Flash T, Hogan N: J. Neurosci. 5:1688-1703, 1985.
Hogan N: J. of Neurosci. 4:2745-2754, 1984.
Kaneko et al: In Jonsson (Ed.) Biomech. X-B, pp.803-807, 1987.
Morgan D, Martin PE: Can. J. App. Sports Sci. 11, 211-217, 1986.
Nelson WL: Biol. Cybern. 46:135-147, 1983.
Schneider K, Zernicke RF: Biol. Cybern. 60:221-230, 1989.
Stein et al: Human Muscle Power, pp.131-150, 1986.

THE APPLICATION OF THE INTEGRATED KINEMATIC SEGMENT TO THE STUDY OF HUMAN LOCOMOTION, II - JOINT DYNAMICS

Zvi Ladin and Ge Wu
Biomedical Engineering Department and NeuroMuscular Research Center
Boston University, Boston, MA 02215

Introduction

The calculation of human joint forces and moments during locomotion is usually based on the non-invasive measurements of the kinematics of a given body segment, and the solution of the 'inverse dynamics problem'. The kinematic information is usually obtained by either direct position measurement or direct acceleration measurement. A new approach, called the Integrated Kinematic Segment (IKS) approach is applied to the study of the three dimensional kinetics of human lower limb during normal walking and running. The knee joint forces and moments are presented in this paper.

Methodology

Three healthy young male subjects were tested. The WATSMART optoelectronic system with two cameras was utilized. Three IKSs were attached to the foot, shank, and thigh of right lower limb, respectively (for detailed experimental set up, refer to Part I). The inertial properties of lower limb were estimated according to the regression equations by Zatsiorsky and Seluyanov [1]. All the experiments were done with bare foot. The average speed for normal walking was $4.7km/h$, and for running was $13.84km/h$.

Results and Discussion

Figures 1 through 3 show the foot-floor reaction force, and knee joint force and moment for normal walking and running. All the joint loads are described as being applied to the distal link of the joint. The forces are normalized by the subject's body weight (BW), and the moments are normalized by the subject's body weight times body height (referred to as body moment, BM). The results are presented in three orthogonal axes in the lab coordinate system.

The ground reaction forces of both walking and running showed typical shapes as seen in the literatures. The maximum forces were in the vertical direction (about 1.25 times of BW for walking and three times of BW for running). Also, the forces in both the M-L and A-P directions for running increased as compared to normal walking. The most significant difference between the two tasks is at HS (heel strike) where there were larger, more rapid changes in running than in walking.

Although the maximum force component at the knee joint was in the vertical direction, there were distinct M-L peaks at HS in both tasks. Clearly, the maximum knee forces of all the components were higher in running than in walking. Comparing the knee forces to the ground reaction forces, the overall shapes were similar except the high frequency spikes at HS not existed in the reaction forces. These spikes were due to the inertial forces of the distal body segments and they became more significant in running than in walking.

The major knee moments for both walking and running were in the stance phase. In walking, only the M-L component was dominant. In contrast, the maximum moments of all three components in running were comparable which suggested that the torsional moment at knee was an important component that need to be taken into account. Also, the moments of all the components increased as the speed of the tasks increased.

Conclusion

The IKS approach is able to increase substantially the frequency range in the human joint load estimates, especially at the transients occurring during fast activities. It is able to provide high quality estimates of joint force and moment in three anatomical directions and at any time or location during locomotion.

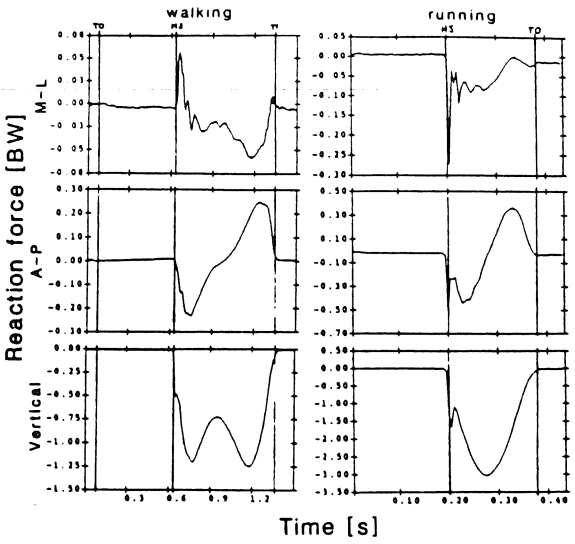


Fig. 1. Foot-floor reaction forces in normal walking and running

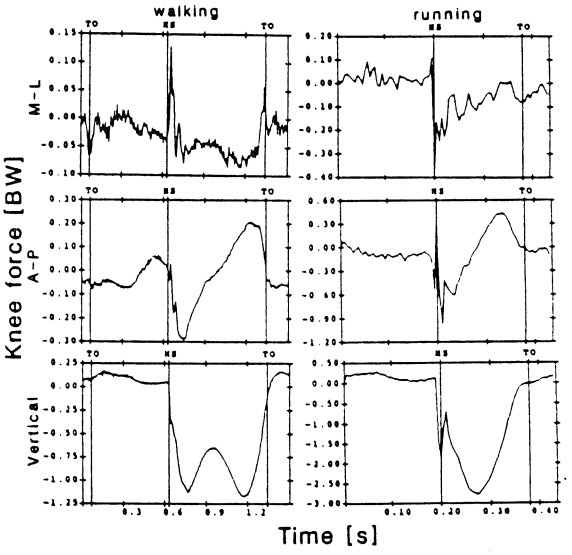


Fig. 2. Knee joint forces in normal walking and running

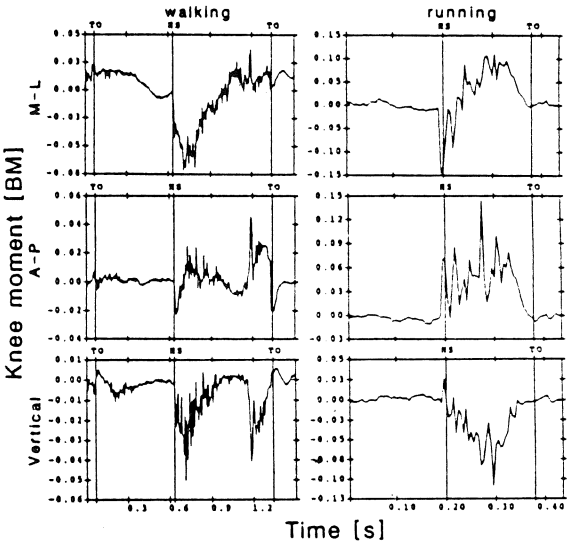


Fig. 3. Knee joint moments in normal walking and running

Reference

[1] Zatsiorsky, V.M. and Seluyanov, V.N. (1983): *The mass and inertia characteristics of the main segments of the human body.* Biomechanics VIII-B

Acknowledgement: This work was supported by a National Science Foundation Grant No. EET-8809060 and by a grant from the Whitaker Foundation.

EVALUATION OF COUPLED DYNAMICS IN OBSERVED LOCOMOTION

Dwight Meglan, Necip Berme, and Sheldon R. Simon
Departments of Mechanical Engineering and Orthopaedic Surgery
The Ohio State University, Columbus, OH 43210 USA

INTRODUCTION

Many quantitative clinical gait analysis studies do not consider how resultant loads in joints (JRL) in other parts of the body influence the motion of a specific joint during locomotion. If this is considered, the evaluation focuses upon the qualitative description of compensation behavior where the interpreter of the data infers that the behavior at another joint of the body is influencing a particular characteristic of the joint of interest. The knowledge to make such inferences is based primarily upon experience and therefore conclusions can only be justified by qualitative arguments. At present, there is no commonly used tool on hand to validate such interpretations quantitatively. Inverse dynamics provides information about causative factors of motion but it does not describe the quantitative link between these and the observed motions. A quantitative method of evaluating these interrelations, which are the result of the human body being a system of interconnected links in which the dynamic behavior of each link is coupled to the behavior of all other links, would be valuable for this purpose. The exact contribution of each joint's moments to the a given joint's observed motion would provide conclusive information about whether a joint has a significant influence upon another joint's motion. To accomplish this, a general method has been developed to evaluate full body dynamic interrelationships during observed spatial locomotion and applied to human gait.

REVIEW AND THEORY

Some recent studies have used the evaluation of the interrelationships of joint dynamics, referred to as induced accelerations or coupled dynamics, in specific applications. Khang [1] used the method in a theoretical study of the control of functional electrical stimulation in the maintenance of standing. Zajac [6] described some general aspects of evaluating the coupled dynamics of the body with the specific example of a theoretical 2D standing balance case. The method was applied to understanding the relative significance of muscles in controlling a computer simulation of a simplified gait [5]. That study is an excellent example of the usefulness of coupled dynamics evaluation, for if it had not been used countless trial and error simulations would have been required to produce a successful gait.

The existence of coupled dynamics in body motions can be seen in the general form of the body's dynamics equations.

$$\mathbf{M}\vec{\mathbf{a}} = \vec{\mathbf{T}} + \vec{\mathbf{C}} \quad \Rightarrow \quad \vec{\mathbf{a}} = \mathbf{M}^{-1}\left(\vec{\mathbf{T}} + \vec{\mathbf{C}}\right)$$

Here, M is the mass matrix, a is the vector of body accelerations, T is the joint moments and C is the combined coriolis, gravity, and ground reaction load (GRL) factors. M has dimension *nxn* while the vectors are *nx1* where there are *n* body degrees of freedom (DOF). The second form shows that if $\mathbf{M}^{-1}$ is fully populated then each element in T, which represents the resultant moment about a joint DOF, produces an acceleration in every joint.

PROCEDURES

A numerically based technique derived from the Newton-Euler multibody dynamic simulation method [3] was used to compute the governing dynamic equations of the full human body. The body was modeled by 13 segments connected by spherical joints having a total of 34 DOF with 28 DOF that sustain controlled JRL's from muscles, joint contact, and capsule/ligaments. A

motion measurement system was used to obtain the spatial segment kinematic trajectories and collect GRL data for a normal subject's gait. This information combined with anthropometric information was used to compute JRL's at each time frame. The M, T, and C components of the dynamics equations were computed and the full set of body accelerations resulting from all the sources in the model (each element of T plus gravity, coriolis, and GRL) was calculated in the measured data. In the present model there were 31 possible contributors (28 + gravity, coriolis, and GRL) to a given DOF's acceleration. Thus, there were a total of 1054 acceleration components calculated in each time frame. An algorithmic technique was used to scan this large number of acceleration components at each time frame to determine the significant contributors to a joint's kinematic behavior. The individual accelerations from these contributors were then isolated for evaluation.

RESULTS AND DISCUSSION

The coupled dynamics for each of the DOF's in the 12 joints in the body as modeled were computed over a full gait cycle. The significant contributors to a joint's motion varied across the cycle, though in general the relative contributions were consistent during mid-single stance in the stance leg and mid-swing in the swing leg. In all DOF's, the magnitudes of the acceleration contributors were much larger than the summation acceleration. This summation is the same as the observed, or measured, acceleration. In general, the sagittal plane JRL's in the stance leg served to balance the GRL induced acceleration in the sagittal plane of that leg in single stance. During swing, the swing and stance leg's nonsagittal JRL's and coriolis load had significant influence upon the swing leg sagittal accelerations. Specific joint DOF result characteristics were numerous. Stance ankle flexion acceleration resulted primarily from the components due to the GRL and the ankle's flexion moment– both of these components being much larger than the observed acceleration and of opposite signs. The stance knee flexion during single stance was driven almost entirely by the stance leg ankle and hip flexion moments. During late swing, however, the swing leg knee flexion moment contributes significantly to that knee's flexion motion, as would be expected since knee extension is normally braked by the knee flexors at this point. Another interesting result is that the shoulder flexion motion was found to be almost entirely driven by the trunk vertical twisting moment which agrees with previous research [2].

The large magnitude of the acceleration contributors of the joints in comparison to the summed accelerations confirmed the commonly accepted viewpoint that locomotion is a finely balanced activity dependent upon the interplay of numerous factors. From these results, it is apparent that small, simultaneous changes in several acceleration components could easily yield the same summed, or observed, acceleration. This is the same as causative factors of a gait varying while the measured motion remains unchanged as has been described by [4].

1. Khang, G., Zajac, F.E. (1988) *Model Control Biomech Systems*, ASME, 45-54.
2. Townsend, M.A. (1981) *J Biomech* 14, 727-738.
3. Walker, M.W., Orin, D.E. (1982) *J Dynam Sys Meas Cont* 104, 205-211.
4. Winter, D.A. (1989) *J Motor Behav* 21, 337- 355.
5. Yamaguchi, G.T., Zajac, F.E. (1989) *XII Int Cong Biomech*, 166.
6. Zajac, F.E., Gordon, M.E. (1989) *Exer Sport Sci Rev* 17, 187-230.

A COMPARISON BETWEEN KINEMATIC AND KINETIC METHODS OF SEGMENTAL POWER CALCULATION IN NORMAL WALKING*

Andrew W. Smith, PhD, School of Physical and Health Education,
University of Toronto, Toronto ONT Canada, M5S 1A1

INTRODUCTION

The purpose of the present study was to quantify differences in segmental power calculations using (a) direct measurement based on kinetic data and (b) differentiation of segmental energy values. Findings support that of a previous study (3) and have implications for mechanical energy investigations which utilise kinematic data only.

REVIEW AND THEORY

Methods used for the calculation of segmental power were first presented by Elftman (1,2) and formed part of a study by Robertson et al. (3). The total power for a segment can be calculated by adding together the segment's joint power with its muscle power. The determination of these quantities in gait requires a force platform and the calculation of joint reaction forces and velocities, joint reaction moments of force and segmental angular velocities (3).

Segmental power can also be determined by calculating the time rate of change of energy of the segment. This involves knowledge of the segment's mass, mass centre location (CM) and moment of inertia, along with the linear velocity of the CM and the segmental angular velocity. These quantities can be obtained in the absence of a force platform. In theory, the two methods should yield the same results. In practice, however, differences do occur and these need to be taken into account.

METHODOLOGY

The four subjects used in the present study were college students who volunteered to participate. The subjects were screened for any neuromuscular dysfunctions and were informed of the purpose of the study. Informed consent was obtained prior to testing. The subjects, one female and three males, each made one visit to the laboratory and had four trials of data recorded. These were obtained from both sides of the body (two trials from each side).

Specific details of the methodology used appear in the literature (4). In summary, kinematic data were collected using a video camera. Video has been shown to be sufficiently fast for walking studies (5). These data were synchronised with force platform data collected during each stride of walking. Analysis of the data included calculating segmental energy components along with joint and muscle powers for each segment.

RESULTS AND DISCUSSION

All stride-based data were time-normalised to 100% of stride and ensemble averaged at each 2% of stride (4). The four trials from each subject were ensemble averaged to obtain intra-subject (ITS) mean and standard deviation curves. Inter-subject (IRS) mean and standard deviation time-histories were calculated by ensemble averaging the ITS mean values. The IRS mean values for each of the two methods of power calculation were compared using a Pearson product moment correlation (**r**). The **r** values were

calculated on data from the entire stride (0-100%), and stance (0-60%) and swing (60-100%) phases respectively. These data can be found in Table 1.

TABLE 1
Correlation Coefficients: Kinematic versus Kinetic Methods

Segment	Stride[1]	Stance[2]	Swing[3]
Foot	0.537	0.085	0.999
Leg	0.936	0.834	0.999
Thigh	0.850	0.822	0.965

[1] 0 to 100% of stride
[2] 0 to 60% of stride
[3] 60 to 100% of stride

As can be seen in Table 1, the two methods of segmental power calculation yielded similar values, especially during swing phase where 93.1-99.8% of the variance of one method is explained by the other across the three segments. The data for the entire stride, however, contain more unexplained variance, due to differences between methods during the stance phase. This is particularly noticeable for the foot segment. These findings are consistent with previous studies (1,3).

In reporting similar discrepancies for the foot segment, Robertson et al. (3) attributed these to the determination of either joint or muscle powers during stance, particularly during weight acceptance and push-off. The pattern in this segment of large joint and muscle powers which were of near equal magnitude but opposite polarity seen by these authors during push-off was also clearly evident in the present study.

Robertson et al. (3) attributed the differences in foot segment powers from the two methods to errors in the kinetic methodology as it was applied to the foot segment. The authors point out that the location of the instantaneous centre of rotation at the ankle might be necessary since the muscle power calculation appears to be sensitive to errors in joint centre location. The relatively slow motion of the foot is also cited as evidence of the possibly more accurate kinematic method for the foot segment. This may not be the case, as the following illustrates: if a subject was cycling on an ergometer at a constant pedal rate of 60 rev·min^{-1}, the kinematic method of calculating segmental powers would produce the same data regardless of the external power demands placed on the subject by the ergometer. Thus, 140 W work rate would appear kinematically identical to 280 W (or any other value one might choose). Clearly, the kinematic method, while precise, would not be accurate in this situation.

The results of the present study reinforce the strong phasic relationship between kinematic and kinetic methods of segmental power calculation first reported by Robertson et al. (3). Caution is advised, however, in interpreting segmental power data based solely on kinematic inputs.

REFERENCES

1. Elftman, H. **Am J Physiol 125**, 339-356, 1939a.
2. Elftman, H. **Am J Physiol 125**, 357-366, 1939b.
3. Robertson, D. et al. **J Biomech 13**, 845-834.
4. Smith, A.W. **Int J Sport Biomech 6(3)**, 262-282, 1990.
5. Winter, D.A. **J Biomech 13**, 923-927, 1980.

* The author wishes to acknowledge the assistance of *Paul Donovan* in the collection of these data. This study was partially supported by a *Cumberland College of Health Sciences (Sydney, Australia) Research Grant.*

MECHANICAL WORK AND THE TIME COURSE OF ENERGY TRANSFER IN THE SWING PHASE OF GAIT

G.E. Caldwell and L.W. Forrester
Department of Kinesiology, University of Maryland
College Park, MD, USA 20742

INTRODUCTION

Estimates of muscular mechanical work and the time course of energy transfers within and between the segments of the leg were examined for the swing phase of walking and running. Mechanical work as calculated from energy changes (W_{WB}) underestimates the muscular cost calculated from power models by 34% in walking and 64% in running. Values of energy transfer within and between segments are higher for walking than running when expressed as a percentage of the muscular cost. Further, the time course of these transfers differs between the two gait modes.

REVIEW AND THEORY

The concept of energy transfer within and between body segments has been considered in attempts to quantify the mechanical work performed by muscles during movement (e.g. Winter, 1979). Transfers are assumed to indicate work performed with low (or no) metabolic cost. In many studies work and transfers have been calculated from changes in segmental energies. However, energy models yield incorrect muscular work estimates (W_{WB}), and transfer values which have multiple power sources, some of which are muscular in nature (Chapman *et al.*, 1987; Aleshinsky, 1986). Using power equations one may calculate a more valid muscular work cost (TBW), and specific types of within-segment (*whip* and *pendulum*) and between-segment (*tendon* and *joint*) transfers. Furthermore, the power approach provides a means of viewing these transfers as functions of time throughout a motion. The purpose of the present study was to examine muscular cost estimates, and energy transfers as a function of time, in the recovery leg for walking and running.

PROCEDURES

Standard 2D film techniques were used to collect sagittal plane kinematic data from one male subject (185 cm; 76.5 kg) during 4 trials each of walking (2.3 m/s) and running (5.0 m/s). The data were used to calculate time histories of the energies of each leg segment during swing phase, along with the underlying power sources (Aleshinsky,1986). These power sources permitted the calculation of exchange of kinetic and potential energies (*pendulum* transfer [TP]) and of kinetic and rotational energies (*whip* transfer [TWh]) for each segment. Transfers of energy between adjacent segments were attributed to *joint* (TJ) or *tendon* (TT) sources as in Robertson *et al* (1980) and Elftman (1939). Muscular cost was assessed using both W_{WB} and TBW. All data presented are means or ensemble averages for either walking or running.

RESULTS AND DISCUSSION

Mechanical work estimates for the recovery leg in walking illustrate the underestimation involved in the use of W_{WB} (39.3 ± 4.2 joules) as compared to TBW (59.0 ± 11.2 J). This work underestimation is magnified in running (W_{WB}: 91.0 ± 6.2 J; TBW: 250.5 ± 35.5 J). Mechanical energy changes are also brought about by the transfer mechanisms. For walking, these values were 17.8 joules (30% of TWB) for TP, 53.8 J (91%) for TWh, 7.9 J (13%) for TT and 108.0 J (183%) for TJ. In running the energy changes due to transfers were substantially higher, although not if viewed as a proportion of TBW (TP 42.0 J [17%]; TWh 178.5 J [71%]; TT 20.8 J [8%]; TJ 407.8 J [163%]). The TWh and TJ mechanisms redistribute large amounts of energy during the gait cycle, but are dynamic consequences of a multi-segmented body and not necessarily 'energy saving' mechanisms. In contrast, TP and TT may be more directly implicated in metabolic savings. Differences between walking and running are evident in the time histories of these transfers. The thigh segment displays differences in both magnitude and phasing of TP in walking versus running (fig. 1).

Another difference between the gait modes occurs at the knee, in which the power profiles are similar while the energy effects on the thigh and shank segments differ (fig. 2a & b). This results in TT at different times and in different directions during recovery (fig. 2c & d). These energy transfers are more valid indicators of energy distribution than those reported from mechanical energy models (e.g. Norman *et al.*, 1985). 1987).

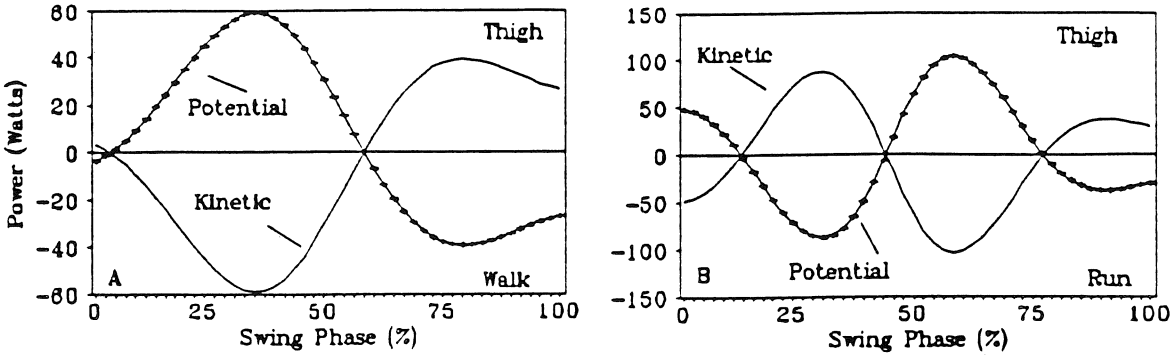


Fig. 1: Pendulum transfer in the thigh: a) walk; b) run.

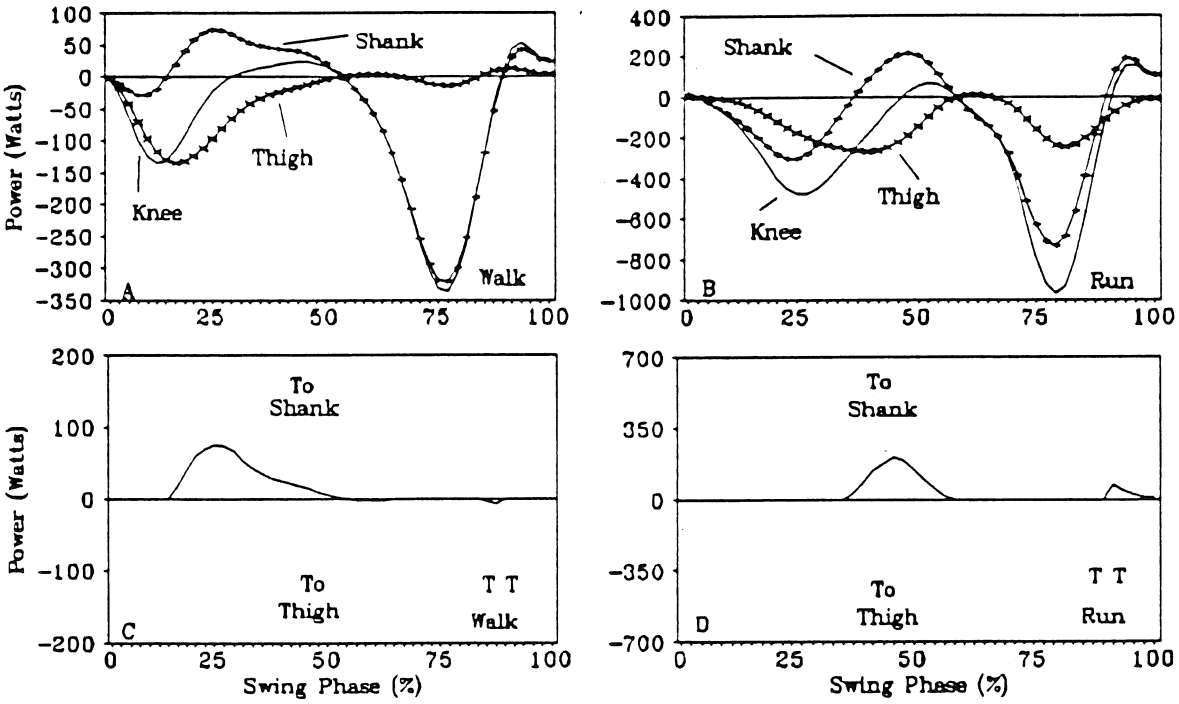


Fig. 2: Knee power for a) walk; b) run; and tendon transfer for c) walk; d) run.

References

Aleshinsky, S.Y. *J. Biomech.* 19:307-309, 1986.
Chapman, A.E. *et al. Biom. X* pp. 875-879, 1987.
Elftman, H. *Am. J. Physiol.* 125:357-366, 1939.
Norman, R.W. *et al. Int. J. Sp. Biom.* 1:253-262, 1985.
Robertson, D.G.E. *et al. J. Biomech.* 13:845-854, 1980.
Winter, D.A. *J. Appl. Physiol.* 46:79-83, 1979.

SESSION 2

THORACO-LUMBAR SPINE

COMPARATIVE STUDY OF NONINVASIVE SCOLIOTIC MEASURING TECHNIQUES

DJ Pearsall, *MSc, Dept of Anatomy, Faculty of Medicine, Queen's University, Kingston, Canada.*
JG Reid, *PhD, School of Physical and Health Education and Dept of Anatomy, Queen's University.*
DM Hedden, *MD, Dept of Surgery, Faculty of Medicine, Queen's University.*

INTRODUCTION

Three techniques for the noninvasive prediction of scoliotic curvature were compared and validated. These included the Scoliometer (SCOL)[1,2], Back-Contour Device (BCD)[2,3] and Moiré topographic imaging (MTI)[5,6]. Axial trunk rotation (ATR) values were obtained using the above methods for 14 subjects (10 female, 4 male) with idiopathic adolescent scoliosis and were compared to Cobb angles derived from antero-posterior radiographs. Correlation of ATR measures were significant for the SCOL and BCD ($r=.87$, $p<.005$) but not for the MTI. The observed discrepancy probably arose due to posture variation between techniques; that is, the forward-bending position was used for the SCOL and BCD while an upright posture was assumed in the MTI. Low ATR/Cobb correlations were observed for the back in general; however, significant correlation was observed when comparison was isolated to the thoracic region ($r= .59, .70, .80$, for SCOL, BCD and MTI, respectively) but not within the lumbar region. The poor accuracy of these techniques for estimation of scoliotic curvature represents a major weakness for their use in the clinical setting.

REVIEW AND THEORY

Several noninvasive techniques have evolved to assess scoliosis, a pathological lateral curvature of the spine; yet, the clinical success of these in diagnosing scoliotic conditions has been variable. Furthermore, the measurement variation between these techniques is not clear. Therefore, the focus of this study was to compare and evaluate the validity of the three different methods for prediction of the scoliotic lateral curves.

PROCEDURE

Three noninvasive scoliotic measuring methods (SCOL, BCD, MTI) were utilized following clinical examination while Cobb angle measurements were derived from antero-posterior (AP) radiographs. For the SCOL and BCD, a forward-bending posture was required while an upright stance was assumed for the MTI and radiographs. To enable a comparison between techniques, ATR was chosen as a common variable. The values obtained from the SCOL were taken as ATR measures. For the BCD and MTI, however, the ATR values were calculated from the transverse trunk profiles following the method employed by Hefti et al.[7] The maximum ATR measures from the thoracic and lumbar regions were recorded for each of the three techniques.

RESULTS AND DISCUSSION

Comparison of ATR measures revealed that both the SCOL and BCD were in close agreement, particularly when correlation was restricted to the thoracic region ($r=.91, p<.005$). However, the relation between the MTI and the other techniques was not substantial. Only when comparison of ATR measures was focused to the thoracic region were the three techniques significantly correlated ($r=.58-.91$, $p<.025$). These results indicated that ATR calculations by BCD and ATR measurement by SCOL were of equivalent sensitivity. As well, the data revealed that ATR as measured in the forward-bending posture were different from those in the upright position,

particularly for the lumbar region which is in agreement with previous findings[8]. These observations suggest that the measurement techniques cannot be used interchangeably in clinical recording.

The accuracy of the three techniques for prediction of lateral curvature was specific to the region of the back (Table 1a-c). The Cobb/ATR correlation for the combined thoracic and lumbar regions was low in general. Only the MTI revealed a significant relationship ($r=0.58, p<0.005$). When comparison was limited to the thoracic segment of the back, the relationship was observed to improve substantially. The Cobb/ATR correlations were $r=0.59$ ($p<0.025$), $r=0.70$ and $r=0.80$ ($p<0.005$) for the SCOL, BCD and MTI, respectively. Conversely, when limiting analysis to the lumbar segment, no significant correlations with Cobb angles were shown. These findings agree with Daruwalla et al.[5] The poor lumbar Cobb/ATR correlation represents a major deficiency of these noninvasive techniques. Therefore, the noninvasive techniques examined may function best for objective screening of scoliosis; however, they do not possess the accuracy necessary for clinical diagnosis.

Table 1.
Pearson Correlation Coefficients for Cobb angle measures to ATR values of the SCOL, BCD and MTI from (a) the thoracic and lumbar regions (n=24), (b) the thoracic region only (n=12), and (c) the lumbar region only (n=12).

Cobb angle:	*(a)*	*(b)*	*(c)*
ATR values:			
SCOL	*0.18*	*0.59*[a]	*0.20*
BCD	*0.31*	*0.70*[b]	*0.17*
MTI	*0.58*[b]	*0.80*[b]	*0.42*

[a] $p<0.025$ [b] $p<0.005$

REFERENCES

1. *Bunnell WP. J Bone Joint Surg 66:1381-1387, 1984*
2. *Amendt LE et al. Phys Ther 70:108-117, 1990*
3. *Burwell RG et al. J Bone Joint Surg 65:452-463, 1983*
4. *Thulbourne T et al. J Bone Joint Surg 58B(10):64-71, 1976*
5. *Daruwalla JS et al. J Bone Joint Surg 67:211-213, 1985*
6. *Stokes IAF et al. Automedica 5:71-83, 1985*
7. *Hefti FL et al. Surface Topography and Spinal Deformity. Stuttgart: Gustave Fischer Verlag. 189-198, 1983*
8. *Stokes IAF et al. J Bone Joint Surg 69A(2):203-211, 1987*

MEASUREMENT OF FORCES GENERATED BY BOSTON BRACE IN THE TREATMENT OF SCOLIOTIC DEFORMITIES

Dansereau, J.[1-2], Côté, B.[1], Labelle, H.[2], Aubin, C.-É.[1]

1- Dept. of Mech. Eng., École Polytechnique, P.O. Box 6079, Station "A", Montréal, QC, Canada, H3C 3A7
2- Hôpital Sainte-Justine, 3175, Côte Sainte-Catherine, Montréal, QC, H3T 1C4

INTRODUCTION: The biomechanical action of the Boston brace on three-dimensional (3-D) scoliotic deformities is not well-known. Only few clinical studies using 3-D reconstruction techniques (Asher et al., 1987, Shinoto et al., 1987) have been made to evaluate the 3-D spinal morphological changes due to Boston brace wear. A recent stereoradiographic study, made by the authors on 26 idiopathic scoliosis patients (Dansereau et al., 1990), reveals that the Boston brace does not really correct 3-D deformities because, although it reduces the Cobb angle in the frontal plane, it aggravates the deformity by increasing the thoracic hypokyphosis without having a real effect on the derotation of the spine and rib cage. To complete our understanding of these clinical results, it was decided to measure the mechanical action of the Boston brace by finding the location and amplitude of its different pressure points. Studies carried out by Cochran and Waugh (1969) with standard mechanical sensors and by Chase et al. (1989) with pneumatic sensors allowed to measure locally on the lateral pad of the brace mean forces of 23 N and 58 N ± 18 N, respectively. This paper presents a new method to measure and graphically represent the amplitude and distribution of forces at any location between the patient skin and the interior surface of the Boston brace.

METHODS: Forces generated by Boston brace were measured by means of new very thin polymeric Force Resisting Sensors (FRS) developed by the Interlink Electronics Company (California). These sensors are not sensible to temperature fluctuations and their optimal force measurements vary between 0.1 N to 200 N. Thirty of these sensors (1.3 cm x 1.3 cm) were mounted individually in a very flexible tissue matrix (5 rows and 6 columns forming a 28 cm x 36 cm matrix) in order to fit perfectly the different interior curved surfaces of the brace. All sensor cells were connected to a micro-computer by means of multiplexors and output signals were then translated into pressure values (in mm of Hg). Measurements were made on two female twins of 13 years old with almost identical idiopathic scoliosis curves (right thoracic Cobb of 32° and 27° and left lumbar curve of 37° and 37°, respectively). Spinous process locations were determined by palpation on each patient and marked. The sensor matrix was then put horizontally on the right side, afterwards on the left side and finally on the anterior part of the brace. Each time the corresponding vertebral level was noted. Using this method, 90 force measurements allow a complete description of the pressure pattern at the "skin-brace" interface. From previous 3-D spinal and rib cage reconstructions of the patients and from the relative positions of the sensor matrix with respect to the spinous processes, a computer program, running on a Personal Iris workstation, was developed to graphically represent the reconstructed bony structure inside a modelled brace (shown as an elliptical cylinder) on which the 90 force amplitudes were represented by associations to a color code. The positioning error of the modelled brace on the reconstructed geometry was evaluated as being ± one anatomical level.

RESULTS: Graphical representations of force distribution and amplitudes are represented on Figure 1. Pressure measurements vary between 0 to 65 mm of Hg. These results indicate that the brace has regions of no contact between the skin and its interior surface. The mechanical action of the brace is rather associated to specific points or regions of pressure. For both patients, points of pressure were found: 1) on both sides of the pelvis; 2) on the lower part of the abdomen; 3) on the buttocks (more on the right side); 4) latero-posteriorly on the right side of the rib cage (ribs T9 to T11) and 5) posteriorly on the lower part of the rib cage, but on the opposite side of the rib hump. These observations are in agreement with our clinical results concerning the study of the immediate 3-D morphological changes due to Boston brace and may explain the fact that no significant difference was found in vertebral axial rotation and rib hump angulation.

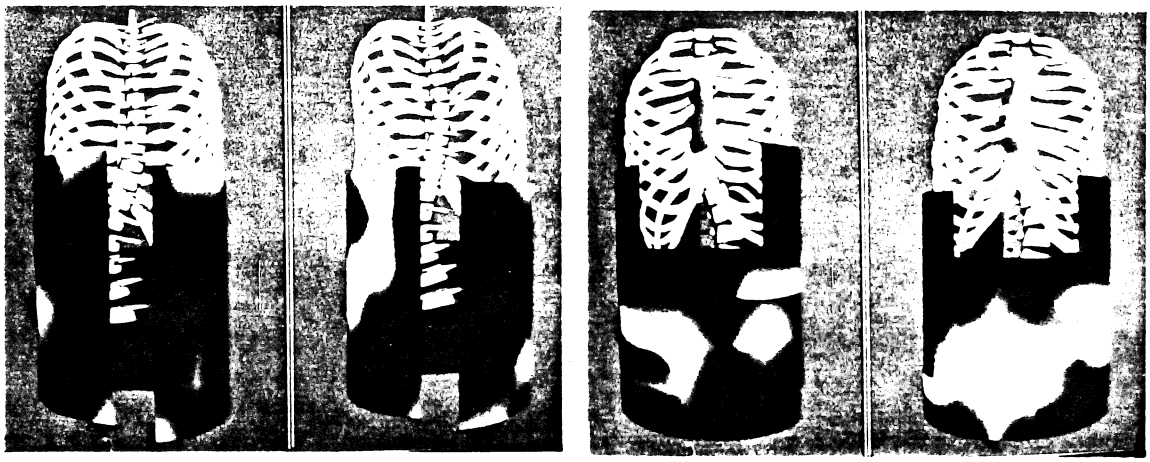


Figure 1 - Pressure distribution for both female twins (white regions represent higher pressures); a) postero-anterior view of pressure points on the pelvis, the buttocks, right ribs T9 to T11 and on the opposite side of the rib hump; b) antero-posterior view of pressure distribution on the abdomen

CONCLUSION: This study reveals that the Boston brace does not generate a uniform distribution of forces, but acts mechanically based on regional pressure points. Negative effects were observed posteriorly on the opposite side of the rib hump. However, it is not possible to conclude that this effect can be generalized for all treated cases because it was observed that some patients had an immediate improvement of their rib hump with Boston brace wear. This lets suppose that the quality of the custom manufacturing of each individual brace is of great importance for a "good" biomechanical action of the orthotic treatment.

REFERENCES: 1) Asher, M. et al., Orthop. Trans. 11:105-106, 1987; 2) Chase, A.P. et al., Spine 14:636-642, 1989; 3) Cochran, G.V.B. and Wangh, T.R., J. Bone Joint Surg. 51A:201, 1969; 4) Dansereau, J. et al., 37th Annual Meeting, Orthopaedic Research Society, Anaheim, California, USA, p. 639, 1991; 5) Shinoto, A. et al., Proc. of the 4th International Symposium on Surface Topography and Spinal Deformity, Gustav Fisher Verlag, New York, p. 113-130, 1987.

ACKNOWLEDGEMENTS: This research was funded by PNRDS, CRSNG and FCAR. Special acknowledgements to Steven Reinecke from University of Vermont.

A COMPARISON OF TORSO MUSCLE CENTROID-LINE INCLINATION ANGLES RELATIVE TO THE L3-L4 INTERSPACE

Moga, P.J.*, Erig, M., Chaffin, D.B., and Nussbaum, M.A.
Center for Ergonomics and *Division of Kinesiology
University of Michigan, Ann Arbor, MI 48109

INTRODUCTION

In constructing torso biomechanical models, it is desirable to incorporate muscle line-of-action and reference plane intersection angle information into the data set. This knowledge is integral to the quantification of muscle forces and moments about the spine. The application of two techniques for measuring these angles is described in this paper and the resulting values are compared to those of two other groups.

REVIEW AND THEORY

Jensen and Davy (1975) illustrated a technique to represent skeletal muscle actions, in which they determined thigh muscle centroid paths by linking centroids calculated from each muscle's cross-sectional area obtained from CT scans. Rab, et al.(1977) used this method to study torso muscles by circumscribing the sectioned muscles' perimeters and analyzing them to yield centroid values. Dumas, et al.(1988 & 1991) dissected unsectioned cadavers to track trunk muscle lines-of-action. Muscle fiber bundles were traced from origin to insertion, giving a "linear or curvilinear path" depending upon the bundle complexity. Subsequent geometric analysis gave the spinal level intersection angles.

PROCEDURES

The two approaches taken to investigate muscle centroid-line intersection angles were based upon the centroid data from a recent torso CT scan moment arm study. As in the manner of Jensen and Davy (1975) and Rab, et al.(1977), individual CT sections were superimposed to yield centroid-line paths, with the L3-L4 cutting plane as a reference. The first method used the trigonometric relations between the centroids of two adjacent, parallel CT sections, to yield the intersection angle (Fig. 1a). The second technique involved the direct goniometric measurement of antero-posterior (A-P) and lateral (lat.) figures from six representative anatomic texts. Here, one arm of the goniometer was aligned with the L3-L4 plane and the other was oriented to the muscle fiber direction as it intersected this plane at the centroid. Comparison of these legs then gave the angle of inclination (Fig. 1b).

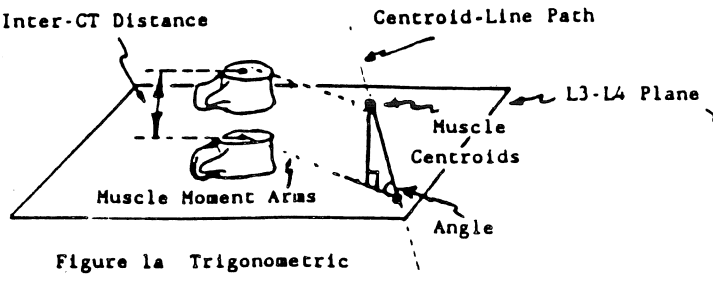


Figure 1a Trigonometric

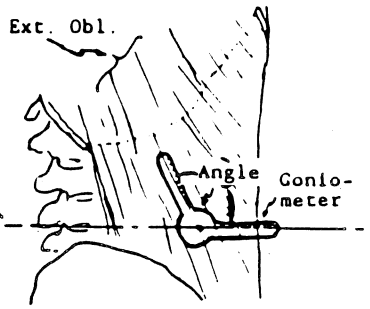


Figure 1b Goniometric

The data of Rab, et al.(1977), N=2, was converted to degrees with a goniometer measuring the visually smoothed centroid-line paths at the L3-L4 level. Fiber bundle values from Dumas, et al.(1991), N=5

were chosen based upon the path, origin, and insertion that approximated that of the CT centroids. Iliocostalis Lumborum and Longissimus Dorsi angles were averaged, as these are "usually referred to as the erectores spinae" (Dumas, et al.1988). The results are displayed in Figure 2.

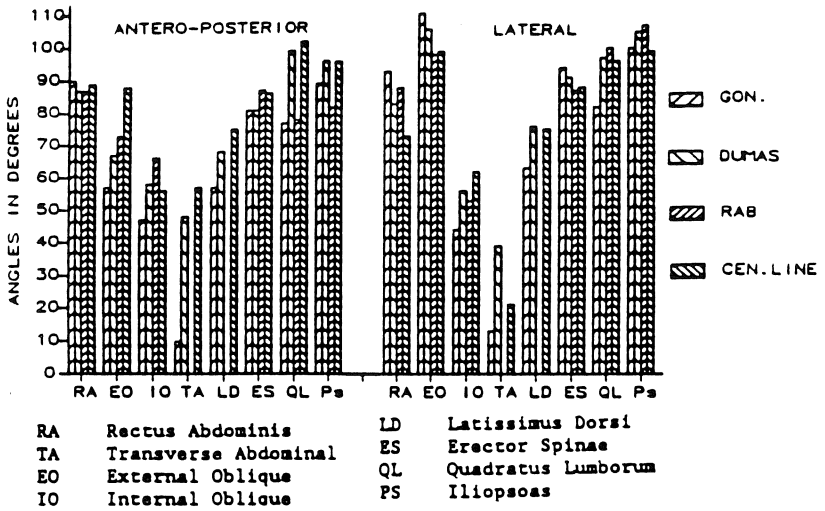


Figure 2 Torso Muscle Fiber Intersection Angles at L3-L4 Plane

RESULTS

The angle data variations based upon the work of different anatomical illustrators ranged from 0^{o} to 2^{o} for the Rectus Abdominus and Erector Spinae muscles to 17^{o} for the External Oblique. The goniometer data, when compared to other authors, varied from 3^{o} to 6^{o} with the former muscle group (A-P) to 31^{o} with the later muscle, with an average of 15^{o}, excluding the Transverse Abdominal. Rab, et al.(1977) did not measure this muscle, feeling it to "run horizontally and therefore make no contribution to the flexion moment". Exclusion of the centroid-line data changed the cross-study differences to variations of 15^{o} in the Ext. Oblique muscle, 7^{o} in the Latis. Dorsi comparisons (A-P view), 10^{o} in Rectus Abd., and 9^{o} in the Int. Oblique (lat. view), with an average of 12.5^{o}.

DISCUSSION & CONCLUSIONS

The large differences from the abdominal muscles were probably related to their curvilinear, multi-directional nature, as well as subject position and anthropometry. The changes noted with the centroid-line technique were likely due, especially from lateral data, to difficulty in reconstructing the proper lumbar lordosis, as the original CT's had only A-P reference x-rays. Despite such discrepancies, these comparisons are remarkably similar and may help augment both torso muscle line-of-action, muscle force, and moment calculations.

REFERENCES

Dumas, et al. (1991) Spine, 16(3):293-303.
Dumas, et al. (1988) Spine, 13(5):532-541.
Jensen, et al. (1975) J. Biomech. 8:103-110, 1975.
Rab, et al. (1977) Ortho. Clin. of N. Amer. 8(1):193-199.

IN-VIVO MEASUREMENT OF INTERVERTEBRAL CREEP: A PRELIMINARY REPORT

Allison M. Kaigle[1], Marianne Magnusson[2], Malcolm H. Pope[1], Holger Broman[3], Tommy Hansson[2]
[1]McClure Musculoskeletal Research Center, Dept. of Orthopaedics, University of Vermont, Burlington, Vermont, USA; [2]Dept. of Orthopaedics, Sahlgren Hospital, University of Göteborg; [3]Dept. of Applied Electronics, Chalmers University of Technology, Göteborg, Sweden.

INTRODUCTION

The viscoelastic creep behavior was studied in human lumbar motion segments using a novel in-vivo technique. The intervertebral sagittal plane rotation, axial translation, and anterior-posterior shear translation were continuously measured over a 5 minute period in 2 healthy female subjects free of low back pain. During the test period, each subject maintained a comfortable controlled upright sitting posture. A mechano-electrical transducer rigidly fixed to the L4-L5 motion segment via intraosseous pins measured the relative motion. Coupled relative sagittal rotation and anterior-posterior shear translation did not accompany axial translation. The axial creep magnitudes at the end of the 5 minute test period for each subject were the following: 0.2mm (subject 1), 1.1mm (subject 2), and 0.9mm (subject 2 repeat). Distinct modulating effects of respiration were observed superimposed on the axial creep curves. Differences in adopted postures between the subjects influenced the creep response.

REVIEW AND THEORY

The viscoelastic phenomenon known as creep is defined as the time-dependent strain under constant stress. The creep behavior of the intervertebral disc has primarily been studied using cadaveric specimens. Keller et al.[1] has shown in porcine intervertebral discs that the viscoelastic behavior of a motion segment can be quite different in the absence of the normal physiological environment. The IMD technique, as described by Kaigle et al.[2], is a mechano-electrical linkage system capable of measuring mid-sagittal plane motion of a spinal motion segment. Unlike previous methods, it is an in-vivo technique which allows for continuous measurement of quasi-static or dynamic rigid body motion. The objective of this study was to examine, for the first time, the in-vivo creep response of a human lumbar motion segment during physiologic loading.

PROCEDURES

The L4-L5 motion segment was studied in 2 female subjects (subject 1 - 1 trial, subject 2 - 2 trials). With the subject lying on her side in the operating room and under local anesthesia, 2 pins (2.4mm diameter) were inserted approximately 10mm into the spinous processes of the motion segment then the IMD was fixed onto the pins. The subject remained lying for a duration of 20 minutes before the test period so as to minimize any preloading effects. The subject was then positioned on the sitting platform equipped with posture control rods and the 5 minute recording period begun. The IMD linkage employed 3 strain-gaged extensometers. When intervertebral translation and/or rotation occurred, the extensometers either compressed or extended, thereby changing their output voltages. Knowing the geometry of the IMD and the output voltages of the extensometers, a computer algorithm calculated the intervertebral motion occurring at the anterior aspect of the superior vertebra.

RESULTS AND DISCUSSION

Deformation-versus-time curves of the relative axial translation for each subject are displayed in Fig. 1. The curves are deficient of the initial creep because time was needed to position the subject and adjust the posture control rods accordingly. Negligible sagittal rotation and anterior-posterior shear translation were measured. Subject 2 (1.1mm and 0.9mm) crept much more than subject 1 (0.22mm). Keeping in mind human variability between subjects, the large discrepancy in overall creep magnitudes could be attributed to differences in adopted postures. Different sitting postures have been shown to affect the intradiscal pressure; the disc pressure during relaxed (slouched) sitting is greater than during upright sitting[3]. During the experiment it was observed that subject 1 had a distinctly less lordotic lumbar curvature than subject 2. Since the compression is computed at the anterior aspect of the superior vertebra, it is believed that the anterior part of the disc of subject 1 was initially compressed to a greater extent than subject 2, thus resulting in less overall creep. The higher frequency modulations seen superimposed on the curves were due to respiratory effects (15-16 breaths/minute) whereas the lower frequency components could be attribute to slight postural shifts. Keller et al.[1] also observed respiratory effects on porcine intervertebral motion and found 20 to 30 percent greater in-vivo creep response as compared to in-situ and in-vitro.

CONCLUSIONS

A method for measuring interspinous kinematics of human lumbar motion segments in the sagittal plane has been applied for the first time. The L4-L5 intervertebral motion during quasi-static sitting was continuously quantified over a 5 minute period in 2 subjects. Axial creep was the predominant motion: 0.2mm (subject 1), 1.1mm and 0.9mm (subject 2). Coupled sagittal rotation and anterior-posterior translation did not accompany axial translation. In-vivo physiologic factors such as respiration and differences in adopted postures appear to have influenced both the creep magnitudes and patterns of motion.

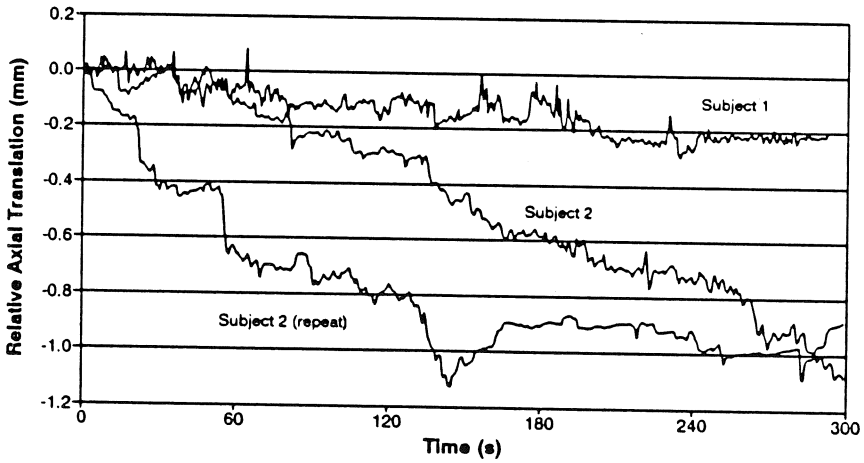


Fig. 1 Deformation vs. time curves for subjects 1 and 2

REFERENCES

1 Keller et al., J Spinal Disorders 1:267-278, 1989.
2 Kaigle et al., ASB, Miami, Florida. November 15-16, 1990.
3 Andersson et al., Orthop Clin North Am 6:105-120, 1975.

EFFECTS OF ANTERIOR VERTEBRAL GRAFTING ON THE KINEMATICS OF THE TRAUMATIZED LUMBAR SPINE FOLLOWING PEDICLE SCREW-PLATE FIXATION

Frank A. Pintar, PhD, Dennis J. Maiman, MD, PhD,
Narayan Yoganandan, PhD, and John Reinartz, MS

Department of Neurosurgery, Medical College of Wisconsin, Milwaukee, WI 53226
Department of Veterans Affairs Medical Center, Milwaukee, WI 53295

ABSTRACT

To examine the effect of osteotomy and strut grafting on the stability of the fixated spine, retroreflective targets were placed into the vertebral bodies, facets, and spinous processes of eight lumbar columns. Spines were loaded until fracture at 2.5 mm/sec (initial cycle); then reloaded to the same deformation (injury cycle). Following transpedicular fixation, spines were again reloaded (fixation cycle). Partial osteotomy of the fractured body and anterior strut grafting using bicortical iliac crest was accomplished, the spine again loaded (graft cycle), and biomechanical and kinematic parameters analyzed. The stiffness of the stabilized spine was decreased by osteotomy and grafting ($p < .05$). However, kinematic data showed reduced motion at the posterior vertebral region between the fixated levels ($p < .05$). Anterior grafting does not appear to add acute stability to the fixated spine; however, the importance of grafting on long-term alignment and stability will require in-vivo studies.

INTRODUCTION

The purpose of the present study was to investigate the effects of anterior bone strut placement on the biomechanical characteristics of the traumatized lumbar spine. Localized kinematics of the spinal column at various levels were analyzed to determine the role of anterior strut grafting on early stabilization.

MATERIALS AND METHODS

Thoracolumbar spines (T10 to sacrum) from eight fresh human cadavers were used in the study. Both ends of the spinal column were rigidly fixed into 10 cm diameter steel rings and held in place with 7 mm steel pins. Retroreflective targets were placed at each level into the anterior and posterior aspects of the vertebral body at the superior and inferior endplates, in the facet column, and in the posterior spinous process. The continuity of the anterior cortex of the vertebra in the middle of the spinal column was disrupted to insure fracture at an appropriate level. Spinal columns were positioned in the MTS electro-hydraulic servo system with a slight flexion bending moment. A lateral radiograph was obtained. The piston of the MTS was instrumented with a force gauge to measure the amount of load delivered, and a built-in linear variable differential transformer (LVDT) measured displacement. Loads were delivered at 2.5 cm/sec until failure, defined as the point after which forces decrease with additional deformation ("intact cycle"). This coincides with wedge fracture of the vertebral body and disruption of the posterior elements. After failure, radiographs were taken with the specimen still under load. The specimens were then reloaded ("injury cycle") to the maximum deflection achieved during the initial injury cycle, and radiography repeated.

The specimens were unloaded and Steffee plates inserted one level proximal and distal to the fractured segment. Repeat loading was carried out to the injury deflection value ("fixation cycle"), biomechanical parameters recorded, and the specimens then radiographed under load. Following the fixation trial, partial vertebrectomy at the fractured level was performed, resecting the posterior half of the vertebra. A tricortical iliac crest graft, taken from that cadaver, was introduced into troughs made in the vertebral bodies cephalad and caudad to the fractured bodies. The specimens were then reloaded ("graft cycle").

BIOMECHANICAL DATA

Biomechanical information was gathered digitally using a modular data acquisition system. The six-axis

generalized force (and moment) histories were gathered from a Denton load cell fixed at the distal end of the specimen. All the data were transferred to a 386 system computer for analysis. Force, deformation, stiffness, and energy were used to assess the strength characteristics of the specimen under the different configurations. The localized kinematics of the specimens were obtained by documenting the motion of the retroreflective targets using a video based motion analysis system. The digital information was transferred to a computer to evaluate the changes in localized movement at levels proximal and distal to the fixation device, as well as between the fixated levels, and compare these results to the intact specimen, to determine changes in localized flexibility/rigidity imparted to the spinal column. Paired student t-tests were conducted to determine the significance levels.

RESULTS

During the initial loading cycle failure occurred with compressive fractures at the midpoint of the column. Forces required to cause biomechanical failure initially averaged 3229 N (range 2096-4501 N, ± 359). Deformation averaged 13.3 mm (range 10.9-17.1 mm, ± .868). Initial stiffness values averaged 313 (±39.6) N/mm. The mean failure load for the injury run was 1142 (± 191) N. The difference from the initial run was significant ($p < .001$). Initial stiffness values ranged from 25.37 to 84.88 N/mm (mean 49.78 ± 8.61), and average final stiffness was 92.3 (± 26.6) N/mm. Post fixation mean forces increased to 1767.9 N (± 279.1). These values were significantly lower than the initial failure loads ($p < .05$), but higher than those obtained for the injury run ($p < .05$). Deformations recorded for all runs were similar to those from the initial run. Final stiffness for the intact column was higher than that for any conditions ($p < .05$). Final stiffness values for the injury run were significantly lower than those for the fixated spine ($p < .05$). Initial and final stiffness values for the instrumentation run were 75.70 (± 12.3) N/mm and 184.21 (± 34.9) N/mm, respectively. For the graft run, stiffnesses were 82.37 (± 19.90) N/mm and 136.15 (± 25.75) N/mm. The instrumented spine had a greater final stiffness than the instrumented spine with the strut graft ($p <.05$).

Relative motions for the injured spines and stabilized spines were evaluated. As compared to the injured (destabilized) specimen, the fixated specimen showed a statistically significant decreased motion at the fixated posterior element targets ($p < .01$). Decreases in anterior vertebral target motion were also significant at the $p < .05$ level. Motion of vertebral bodies proximal and distal to injury (but within the fixation) were not significantly altered. Outside the fixation, posterior vertebral motion increased ($p < .05$). Similar phenomena were observed in the fixated/grafted specimens, with increases proximal and distal to the screws. Also, motion was significantly lower ($p < .05$) across the fracture than in the injury runs. Anterior motion was minimally affected, when compared to the fixated spine.

DISCUSSION

The impetus for the present study was the recognition that (clinically), severe fractures often require anterior grafting as well as posterior instrumentation to retain alignment. Whitecloud et al reported poor results in four of five patients with thoracolumbar fractures, using only pedicle screw/plate fixation. In spite of initially satisfactory alignment, some patients suffered screw breakage, with recurrence of their deformities. However, several have suggested that pedicle screw/plate fixation provides "three-column" fixation, presumably because the screw penetrates the vertebral body over at least 50% of its AP diameter.

In the present study, osteotomy and anterior strut grafting decreased the stiffness of the fixated spine. However, stiffness is only one measure of instability: kinematic data is required as well. Motion decreased at the anterior and posterior vertebral body. An increase in motion would have been expected in light of our observation that the graft tended to compress into the vertebral bodies above and below the osteotomy. If this did not occur, it would be likely that decreased motion would be observed. It can be inferred that this decrease will occur as the graft begins to incorporate into the spine, and therefore actively stabilize the spine.

ACKNOWLEDGMENT

This research was supported in part by PHS CDC Grants R49CCR703640, R49CCR502508 and Department of Veterans Affairs Medical Center Research Funds.

TORQUE-ROTATION RESPONSE OF LUMBAR MOTION SEGMENTS IN FLEXION

John J. Triano, M.A.,D.C.,Ram Gudavalli, Ph.D.
National College of Chiropractic, Lombard, Illinois.

INTRODUCTION

Manipulation treatment of lumbar complaints produces torsional loads where intersegmental flexion is an initial condition (1,2,3). A number of studies have examined the mechanics of rotation in motion segments for neutral and extension postures. Three reports(4,5,6) have suggested that degeneration and flexion conditions put the posterolateral motion segment components at risk. Occasional disc injury from manipulation has been clinically reported. This study examined the effect of rotation loads like those in a manipulation on a kineto-elasto-static computer model of the lumbar spine. Healthy and degenerative discs under flexion initial conditions were included. Motion limits from stop-action of the facets were exceeded by a factor of 3. The resulting axial rotation was nearly identical to grade 4 disc response to axial load reported by Adams & Hutton(7).

REVIEW AND THEORY

Torsion of the spine as a possible risk for disc degeneration and prolapse was an early concern of Farfan(8). Subsequent studies of tissue properties and motion characteristics de-emphasized this consideration because of the strong limiting action of the facets on axial rotation and conflicting reports of stiffness properties (See 7,9,10,11 for example). Several factors prevent the feasibility of risk from being settled. For both healthy and degenerative discs, the flattened lumbar lordosis imposed by the treatment procedure may result in substantially disengaging the facets (Figure 1) minimizing or preventing their stop-action. A wide range of material properties derived from cadaver studies are available. Keller et al(12) have recently shown that they are likely to over-estimate the relevant stiffnesses In-Vivo by as much as 30%. Finally, a number of reports of load-motion data contain cases where axial rotations occurred that were substantially beyond the mean value limit of 2° (see 7,13,14). For example, axial rotations grouped according to grade of degeneration reported by (7) ranged up to 7°. This project hypothesized that degenerative discs in flexion that undergo torsional load could experience large axial rotations.

PROCEDURES

A kineto-elasto-static computer model of a lumbar spine motion segment was constructed(15). Properties of the ligaments were held constant while various disc stiffnesses (1.44 N-m/deg to 5 N-m/deg) taken from the literature were tested. The motion segment was pre-loaded in flexion to achieve intersegmental

positions of 2.5, 5 and 10 degrees. A 10.6 N-m twisting moment was applied in each position and the relative displacements and ligament loads and stretching were obtained.

RESULTS

Figure 2 displays the comparison of displacements for healthy (3 N-m/deg) and degenerative disc (1.44 N-m/deg) properties. The first three bars for each cluster represent healthy disc and the last three represent degenerative disc motions. If the degenerative properties are decremented 30% to represent hypothetical In-Vivo conditions, the resulting displacements (7°) match Grade 4 disc responses reported in (7).

DISCUSSION

The data reported here indicates that large displacements might occur under torsional load and flexion conditions. While few cases of injury result clinically, it would seem beneficial to continue study of this issue in effort to minimize potential risk even further.

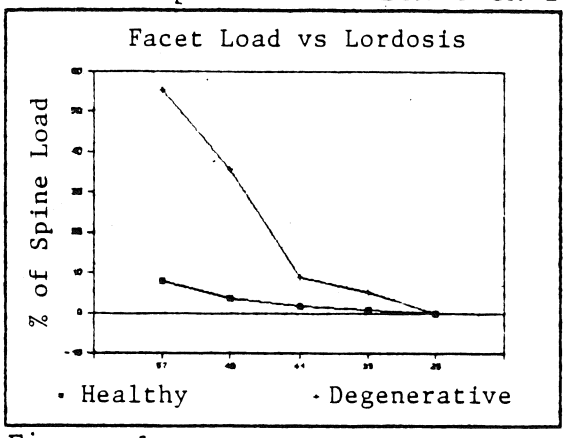


Figure 1:

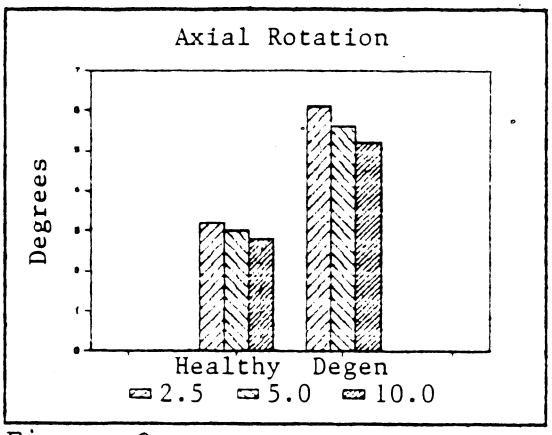


Figure 2

References

1. Kirkaldy-Willis W, Cassidy J: Can Fam Phys 535-540,1985
2. Rogoff J:Manipulation, Traction and Massage. 1971
3. Wilson J, Ilfeld F: Am J Surg, 173-175, Feb 1952
4. Tencer A, et al: J Biomech Eng 104, 193-201,1982
5. Adams M, Hutton W: JBJS 62B #3,358-362,1980
6. Shirazi-adl A, et al: Spine 11 #9, 914-927, 1986
7. Adams M, Hutton W: Spine 6 #3, 241-247, 1981
8. Farfan, H: JBJS 52A, 468-497, 1970.
9. Ahmed A, et al: Spine 15 #5, 391-401, 1990
10. McFadden K, Taylor J: Spine 15 #4, 295-299, 1990
11. Nachemson A, et al: Spine 4 #1, 1-8,1979
12. Keller T, et al: Spine 15 #8, 751-761, 1990
13. Yamamoto I, et al: Spine 14 #11, 1256-1260, 1989
14. Cyron B, Hutton W: Spine 5 #2, 168-172, 1980
15. Gudavalli R, Triano J: Adv Bioengin BED-17,231-234, 1990

RELATIONSHIP BETWEEN FUNCTIONAL LIFTING MECHANICS AND LUMBAR EXTENSION STRENGTH

Wheeler, DL*; Miller, GJ*, O'Connor, P†; Hubbard, R†
* Department of Orthopaedics, University of Florida
† Department of Physical Therapy, Shands Hospital
Box J246, JHMHC, Gainesville, FL 32610

Introduction

Workers engaged in lifting tasks often injure or strain their lower back musculature either acutely by attempting to lift too much or chronically due to muscle fatigue. These injuries lead to loss of productive work days to the employer as well as pain and inconvenience to the worker. In order to circumvent these injuries, preliminary research has been conducted to determine the relationship between an individual's maximum lumbar extension strength and the torque at the lumbosacral joint (L5S1 torque) predicted through kinetic analysis during lifting. The strength and lifting mechanics of 6 healthy individuals were evaluated. This assessment provided the basis for prediction and subsequent verification of the maximum weight the subjects could lift for a simple task. A very high correlation ($r=0.995$) was found between maximum lumbar extension strength and predicted maximum L5S1 torque during lifting for this preliminary study. This correlation provides a means to quantify limitations in lifting capacity for normal or injured workers.

Literature Review and Theory

The MedX lumbar extension machine (MedX, Inc; Ocala, FL) has been used by several researchers to accurately and consistently measure the strength of the musculature used to extend the trunk (1). The MedX machine was designed to isolate the lumbar extensor muscles and measure the maximum L5S1 torque an individual can generate. This machine has been used for both clinical assessment as well as rehabilitation. Kinematic and kinetic analyses have also been used to estimate the load across the lumbar extensor muscles during work tasks (2,3). Kinetic software is available to predict the L5S1 torque necessary to perform simple two-dimensional (2-D) lifting tasks. However, little information is available which directly combines the results of these assessments (strength and kinetic) for the same individual under controlled conditions. This study will provide assessment and comparison of lift task requirements and strength capabilities to better document functional lifting capacity.

Materials and Methods

Subjects ($n=6$) between the ages of 18 and 21 were recruited from the student body of the University of Florida. The protocol and risks were explained to all subjects and appropriate consent was obtained under the institutional research guidelines. The subjects completed three phases of testing, Phase I and II on one day and Phase III on a subsequent day. Each testing phase as well as statistical analyses are described below:

Phase I. Maximum isometric strength for each subject was measured at 7 angles of trunk flexion using the MedX lumbar extension machine. Strength at each angle was defined as the average of two trials.

Phase II. Functional lifting mechanics were determined through sagittal plane 2-D kinetics (LiftTraK software, Motion Analysis, Inc.; Santa Rosa, CA) using a Motion Analysis Kinematic System (Motion Analysis, Inc.; Santa Rosa, CA). Subjects were asked to squat and lift a light load (5-15 lbs) within a 18"x18" box with side mounted handles. This lift was repeated 5 consecutive times to ensure consistency and proper lifting techniques. The mean torque value calculated by LiftTrak kinetic software for this light load lift was then extrapolated to develop a L5S1 torque versus "load lifted" relationship. This torque/load relationship reflects the individual's lifting mechanics. This relationship was then used to predict the maximum possible load the individual could lift based on the maximum torque generated in Phase I (MedX).

Phase III. The subjects were then asked to attempt to lift as much weight as possible 5 consecutive times using proper body mechanics. The first load attempted by the subjects was calculated as 80% of their predicted maximum load (Phase II). The weight of the lift was incrementally increased until the subject felt as if they could not lift anymore weight or their lifting mechanics were deemed improper by the physical therapist.

Statistical Analyses. Pearson correlation coefficients were calculated between the maximum load the subjects actually lifted and the predicted lift based on their MedX isometric lumbar extension strength at each of the 7 angles of trunk flexion.

Results

A very high correlation ($r = 0.995$) was found between the subjects' maximum isometric lumbar extension strength and the associated maximum predicted lift using kinetic analysis and the load the subjects were able to lift with proper form.

Discussion

The high correlation between predicted and actual weight lifted in this preliminary study may offer a new and promising means to combine strength testing and kinetic analysis for an optimal functional assessment of lifting tasks. Additional subjects are currently being tested to further validate this hypothesis. This combined analysis could potentially allow workers to be assigned to tasks compatible with their strength and, therefore, obviate injuries or expedite the worker's return to work in a limited capacity following injury.

References

1. Graves, JE et al. Spine 15(4):289-294. 1990.
2. Chaffin, DB et al. J. Biomech. 2:429-441. 1969.
3. Freivalds A et al. J. Biomech. 17(4):251-262.

Acknowledgement: CDC/NIOSH grant #1-R03-OH02684-01

SESSION 3

PATHOLOGICAL GAIT

The Relationship Between Static and Dynamic Mechanical Factors and Tissue Degeneration Patterns: A Case Study of Primary Osteoarthritis of the Knee Joint

Kamibayashi,L., Wyss,U.P., Cooke,T.D.V., Costigan,P.
Department of Anatomy/Clinical Mechanics Group, Queen's University, Kingston ,Ontario, Canada, K7L 3N6.

Introduction

Primary osteoarthritis (OA) is a progressive disease of unknown etiology which leads to the degeneration of articular hyaline cartilage and changes to the underlying subchondral bone within a joint. While OA may ultimately be the result of an interplay of many different factors, understanding the stresses within a joint during static and dynamic loading conditions may explain the distribution of tissue degeneration within a joint (1,2,3). We hypothesize that limb malalignment and geometric changes of the articular surfaces contribute to changes in compressive and shear stress distribution which may encourage localized joint degeneration.

Procedure

A pilot study was undertaken to test the experimental protocol. Our subjects were elderly individuals, 55 years and over with a diagnosis of primary OA of the knee joint requiring knee arthroplasty and possessing the ability to walk unassisted without the use of a walker or cane. This paper will illustrate one typical case, a 74 year old male (height-171 cm, weight-90 kg) presenting with bilateral OA with the right knee more severely affected than the left. The analysis involved both a mechanical assessment and a histopathological assessment:

(1) Mechanical Assessment (i) QPR (static assessment)
(ii) QGAIT (dynamic assessment)

(2) Histopathological Assessment (i) gross assessment
(ii) histomorphometry

Mechanical Assessment

Static and dynamic mechanical assessments of the subjects were made one week pre-operatively using QPR (Questor Precision Radiography) and QGAIT (Questor Gait Analysis in Three Dimensions) respectively. QPR is a standardized method of radiological assessment of knee alignment with respect to the hip and ankle in a static weight-bearing position. Linear and angular alignment measurements can be derived from the QPR. QGAIT is a method of gait analysis based on a optoelectric tracking system which along with computer algorithms calculates net forces, net muscle moments and knee angles using a fixed body coordinate system during a walking trial along a level walkway across a force platform. EMG was also collected from relevant muscles influencing knee motion.

Histopathological Assessment

Post-operative confirmation of the diagnosis and assessment of articular surface was performed using a semi-automatic image analysis system. Each tibial plateau was sectioned coronally parallel to the maximum transcondylar width (MTW). Bone volume fraction was sampled from three regions: anterior (30% of anterior distance from the MTW), middle adjacent to the MTW and posterior (30% of the posterior distance from the MTW). Each

section was embedded in epoxy resin and surface stained with a modified von Kossa method. A 5mm x 5mm grid was placed at the midpoint of each medial and lateral condylar surface parallel to the resected surface (ie. perpendicular to the mechanical axis of bone calculated through QPR) with the top of the grid at the chondro-osseous junction. Up to three levels below the chondro-osseous junction were investigated depending on the availability of tissue.

Results

QPR: The QPR of this patient indicated bilateral genu varus deformities with mild lateral subluxation of the tibiae and narrowing of the medial joint space of both knees. There was evidence of minimal patellar spurring.

QGAIT: During gait analysis, the patient demonstrated an antalgic gait where loading of the painful right limb was decreased to avoid discomfort. There was a decrease in peak force, peak moment and maximum flexion angles compared to our previous study of normal, asymptomatic adults (unpublished).

Surgical Intervention: A left hemi-arthroplasty of the medial joint compartment and a right total knee arthroplasty were performed replacing the distal femoral and proximal tibial articular surfaces. Both patellae were left intact.

Gross Assessment: The left knee demonstrated erosion of the medial distal femoral condyle and the central portion of the medial tibial plateau. The medial meniscus was found in two pieces. On the right knee, the medial and lateral femoral condyles were both eroded as well as the medial tibial plateau.

Histomorphometry: The pathology report confirmed osteoarthritis with visible articular cartilage fibrillation, fragmentation and chondrocyte clumping. Since varus deformity is associated with medial compartment damage we investigated the distribution of damage within the joint. Bone volume fraction was highest in the middle region of each condyle. This corresponds to the maximum load-bearing region within the joint. Progressing outward from this middle region the bone volume fraction decreased both anterior and posterior. On the right knee, the medial condylar bone volume fraction is overall higher than on the lateral side possibly indicative of higher load-bearing on the medial than the lateral side as a consequence of the varus deformity.

Conclusions

While this has been only a preliminary investigation, this case illustrates that knee joint pain associated with varus malalignment deformity produced changes in the gait patterns that indicated that the patient was trying to minimize loading the affected limb. The subchondral bone particularly in the medial compartment of the joint demonstrated that one of the consequences of this malalignment may be a compensatory increase in the bone volume fraction with an absence of articular cartilage in the central region of the medial tibial condyle where there is increased load-bearing.

References

(1) Hutton,C.W. (1989) Annals of Rheumatic Diseases, 48,958-961.
(2) Radin,E.L. et al. (1972) The Lancet, March 4.
(3) Cooke,T.D.V. (1985) Clinics in Rheumatic Diseases,11,2.

MOTION OF THE NORMAL AND ANTERIOR CRUCIATE LIGAMENT DEFICIENT CANINE KNEE DURING THE WALK AND TROT

Donna L. Korvick, V.M.D., Ph.D
Gerald J. Pijanowski, D.V.M., Ph.D.
David J. Schaeffer, Ph.D.

Department of Veterinary Biosciences
College of Veterinary Medicine
University of Illinois
Urbana, Illinois 61801

INTRODUCTION

Rupture of the anterior cruciate ligament (ACL) is a common orthopedic problem in dogs. Despite over 40 years of clinical and research experience with ACL rupture, we do not yet fully understand the dynamic function of the canine ACL. An instrumented spatial linkage (ISL) was used to measure the three-dimensional joint motion of the normal and ACL deficient canine knee joint during the walk and trot. Motion data was presented in terms of a clinical coordinate system. Loss of the ACL altered joint motion during the entire gait cycle but the changes were most severe during the stance phase. At the swing to stance transition, the ACL deficient knee demonstrated an abrupt anterior subluxation of the tibia which was sustained throughout stance.

REVIEW

Shiavi (1987) used a six degree of freedom linkage to study knee kinematics in the normal and ACL deficient human patient. He found that the ACL deficient knee flexed less and adducted more than normal during the stance phase. The injured knees also showed a medial displacement during swing. Arnoczky (1977) described the range of motion of the normal and ACL deficient canine cadaver knee. He concluded that the function of the ACL was to limit anterior drawer and internal rotation. There are no reported studies of the three dimensional kinematics of the canine knee during walking and trotting. The objectives of this investigation were to: 1. record the three-dimensional motion of the normal and ACL deficient canine knee during the walk and trot; 2. characterize the motion in a clinical coordinate system.

PROCEDURES

Joint motion was recorded for the normal and ACL deficient knee joint of five dogs during the walk and trot using a six degree of freedom ISL (Kinzel, 1972) attached to the femur and tibia with a modification of the system of Scherrer (1979). A bone fixed coordinate system was established in the femur and tibia

by implanting three 0.8 mm tungsten spheres into each bone. The evaluation of ground reaction forces was used to determine that the surgical interventions had minimal effect on the use of the limb. Radiophotogrammetry, based on the direct linear transformation photogrammetric method (Abdel-Aziz, 1971), was used to determine the transformation from the ISL coordinate system to the bone coordinate system. Joint motion was described by a set of three clinically relevant translations and three rotations about the "Joint Coordinate System" described by Grood and Suntay (1983).

RESULTS

The kinematic data was highly reproducible for a given dog. Loss of the ACL altered joint kinematics over the entire cycle but the changes were most severe during the stance phase. At the swing to stance transition, the ACL deficient knee demonstrated an abrupt anterior subluxation of the tibia which was sustained throughout stance. Internal rotation and abduction were also noted during stance. The transition to the swing phase was characterized by an abrupt return of the femoral and tibial surfaces to their normal relative position. The dog dramatically reduced the external forces placed on the ACL deficient limb and carried it in greater flexion thoughout the gait cycle.

DISCUSSION

The canine knee was demonstrated to be ACL dependent during the stance phase. It is clear that loss of the ACL results in a mechanical derangement of the joint which the dog cannot compensate for by reducing the external forces on the limb or by changing the carrying angle of the knee. We infer that the dog could not prevent the joint from subluxating by altering the muscle forces across the joint. Surgical reconstruction should be designed to control the anterior laxity in the range of 40 to 60 degrees of flexion which is the functional range over which the knee is ACL dependent.

REFERENCES

Abdel-Aziz YI, et al. Prod Symp Close-Range Photogram. 1971.
Arnoczky SP, et al. Am J Vet Res 38:1807-1814. 1977.
Grood ES, et al. J Biomech Eng 105:136-144. 1983.
Kinzel GL, et al. J Biomech 5:283-293. 1972.
Scherrer PK, et al. J Biomech Eng 101:271-278. 1979.
Shiavi R, et al. J Biomech 20:653-665. 1987.

GAIT ANALYSIS ASSESSMENT OF THR PATIENTS OPERATED with PCA prosthesis.

Catani F., Leardini A., Battistini A., DeZerbi M., Binazzi R., Ahdieh A., Giannini S.
Dept. of Orthopaedic Surgery, Biomechenics Laboratory, Istituto Ortopedico Rizzoli, Bologna, Italy

INTRODUCTION

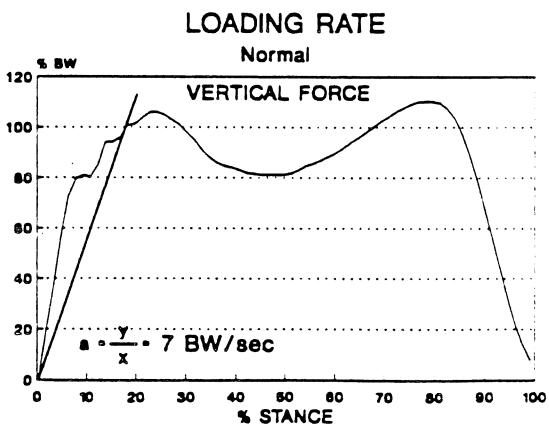
The purpose of this study is to describe the clinical and biomechanical gait evaluation of a group of abnormal subject after PCA total hip replacement due to congenital hip dislocation primary osteoarthritis. We will report data gained from a brief clinical evaluation according to the "PCA score" obtained by questionnare and various measurements on A-P X-Ray, of functional status such as kinematic, kinetic and temporal and distal factors during "free-speed" walking trials. All these pathological data have been compared to a "normal" population (Group A) created at our lab in the last year.

REVIEW AND THEORY

We do believe that while subjective clinical information is important, biomechanical gait analysis provides an objective method of gait evaluation. Our research goals have been to study the functional status, the treatment technique, allowing comparison of different implantation technical errors such as vertical cup, varus stem, lateral or medial or superior displacement of the joint center, and the eventually causes of X-ray signs of bone remodelling due to stresses bone changes (cortical hyperthrophy, stress shielding, bone osteosclerosis) and of high wear causing implant debritis.

PROCEDURES

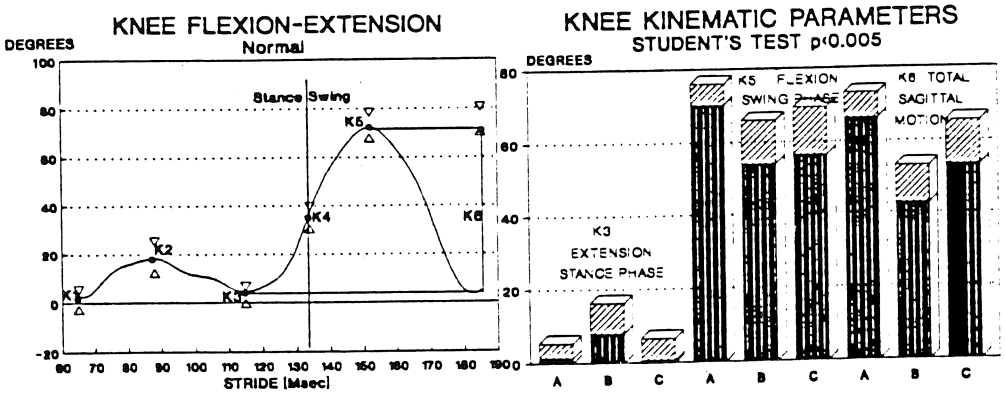
Twenty patients were evaluated; the diagnostic category was 10 patients with displastic arthrosis (Group B) and 10 patients with primary osteoarthrosis (Group C). The patients were studied in the biomechanic laboratory of the Istituto Ortopedico Rizzoli , as they walked on a walk-way containing a forceplate. Kinematics in the sagittal, coronal and trasversal plane of lower limb joints was measured by ELITE stereophotogrammetric system. Temporal and distance factors such as velocity, cadence, stride length were calculated. A forceplate KISTLER incorporated in the walk-way was used to determine the vertical, fore-aft and medio-lateral components of floor reaction force generated during the stance phase of gait. Moreover force data synchronized with kinematic data allowed to calculate sagittal, coronal and trasverse external joint moments. We gained 65 overall parameters for statistical analysis for each patient. Parameters were appropriately normalized by subject weight, height and lower limb lenght.



According to Collins ('89) we also calculate the loading rate as important parameter to study joint load during the first period (20-30%) of the stance phase; loading rate is defined and showed as the slope of the best fit line drawn to the first peak of the vertical component force. The biomechanical gait parameters that we will only discuss for both group A, B and C have been choosen by Scheffe Procedure an Ranges for the .050, by one-way and t-student's test with $p<0.005$.

RESULT

The biomechanical gait parameters statistically significant were 25. An example of data discussed are presented in figure: on the left the evalueted knee angles parameters and on the



right the comparison of the significantly parameters for the 3 population.

Measuring the A-P pelvis X-Ray we gained some parameters defining the location of the joint center and the abductor lever arm; the data were compared with the controlateral side. We calculated: A medial-lateral off set; B lowering of the joint center (JC) with respect to the tear drop; C anatomical lever arm; D abductor muscle length.

CONCLUSION

1) We did not find joint moment or loading rate increase due to joint center location changes or implantation technical errors. Surprisely at what we thoght we found decreased hip join moment also when the joint center location was altered. Than we believe that is more reasonable a stable implant also with modificated joint center location than a instable implant in the primitive joint center location.

2) We fill that there is, as also documented by other author in the literature, a positive correlation between walking velocity, loading rate and joint moment.

So patients with a high rate of limb loading because of a fast walking velocity and a relatively unguarded hip because of weak muscle function would seem to be at a higher risk of failure.

REFERENCES

1 - R.Gore, P.Murray, M.Gardner, A.Millinger, "Comparison of Function Two Years After Revision of Failed Total Hip Arthroplasty and Primary Hip Arthroplasty", Clin.Orthop.,208:168-173, July 1986.

2 - N.Stauffer, L.Smidt, B.Wadsworth, "Clinical and Biomechanical Analysis of Gait Following Charnley Total Hip Replacement", Clin.Orthop., 99:70-77, March-April, 1974.

3 - T.Perrin, D.Dorr, J.Perry, J.Gronley, B.Hull, "Functional Evaluation of Total Hip Arthroplasty with Five- to Ten-year Follow-up Evaluation", Clin.Orthop., 195:252-260, May 1985.

4 - J.J.Collins, M.W.Whittle, "Influence of gait parameters on the loading of the lower limb", J.Biomed.Eng. 1989, Vol 11, September, 409-412.

5 -S.B.Goodman, S.J.Adler, D.P.Fyhrie, D.J.Shurman, "The Acetabular Teardrop and Its Relevance to Acetabular Migration", Clin.Orthop., 236:199-204, November 1988.

6 - S.A.Yoder, R.A.Brand, D.R.Pedersen, T.W.O'Gorman, "Total Hip Acetabular Component Position Affects Component Loosening Rates", Clin.Orthop., 228:79-87, March 1988.

VELOCITY-DEPENDENT CHARACTERISTICS OF THE INVOLVED AND NONINVOLVED LIMBS OF HEMIPLEGICS DURING OVERGROUND LOCOMOTION

K.L. Perell, R.J. Gregor, E.G. Fowler, and B. Dobkin
Department of Kinesiology and Rehabilitation Services, UCLA, Los Angeles, CA 90024

INTRODUCTION: Temporal asymmetries in gait such as prolonged stance and shortened swing phases for the noninvolved (nonparetic) leg characterize hemiplegic gait . These are compensatory responses to a limited range of motion and weight bearing capabilities observed in the involved leg. Symmetry, however, has been demonstrated in the timecourse patterns of joint angle profiles as well as in work and power analyses (Olney et al., *Arch. Phys. Med. Rehabil.* 72: 309-314, 1991), hip-knee angle/angle patterns (Chin, et al., *Advances in Stroke Therapy*, ed. F.C. Rose, 197-201, 1982), and joint loading curves (Marks, *Arch. Phys. Med. Rehabil.* 9-20, 1953) in both legs. The discrepancy between asymmetrical temporal characteristics and symmetrical kinematic and kinetic patterns may reflect disrupted control mechanisms in both legs. Winstein and Garfinkel (*J. Motor Behavior*. 21:373-391, 1989) used dynamical systems theories in a qualitative analysis of the involved leg of three hemiplegics. Their findings indicated differences in coordination and control features between the involved leg and profiles in normal subjects. The effect of these abnormal control mechanisms may have adverse effects on the noninvolved leg as well. The purpose of this study was to evaluate the coordination and control of both legs as a basis for understanding the compensatory mechanisms in hemiplegic gait.

METHODS: Two male hemiplegics (R.R., age 59, J.W., age 68) from the UCLA Department of Rehabilitation Services outpatient therapy program served as subjects. Both patients suffered a cerebrovascular accident (CVA), with primary involvement of either the right (J.W.) or left (R.R.) cerebral hemisphere resulting in hemiparetic movement deficits on the contralateral side. Both were at least one year post CVA at the time of data collection.

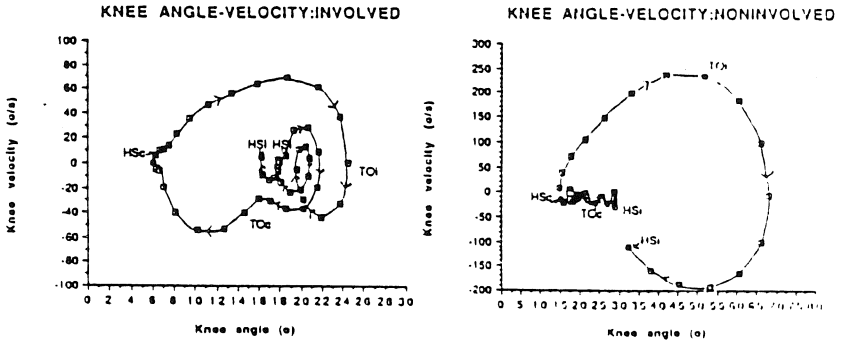
Reflective markers were placed on the iliac crest, greater trochanter, knee joint center; lateral malleolus, and 5th metatarsophalangeal joint of each subject. Two video cameras were employed for 3D kinematic analysis. Trials were filmed at 30 fields/sec. Subjects were instructed to walk at a comfortable speed down a walkway using whatever stabilizing devices they normally use (R.R., quad cane, J.W., hemicane) and a therapist's hand for extra guidance. Two trials were collected from each side of the body and contained at least two strides (heel strike to ipsilateral heel strike). Videos were digitized using the ARIEL Life System and coordinate data smoothed at 4 Hz. Phase-plane diagrams were constructed using angles derived according to the Grieve convention and velocities obtained using a 5 point moving average.

RESULTS: Exemplar data from one subject (R.R.) are presented in Figure 1. The knee and hip phase-plane diagrams were obtained from the same trials for each leg. Positive values denote flexion while negative values denote extension. Nomenclature includes: HSi: heel strike, ipsilateral; TOi: toe off, ipsilateral; HSc: heel strike, contralateral; and TOc: toe off, contralateral. Contralateral and ipsilateral refer to side closest to the camera. The involved leg is ipsilateral in Involved phase plane diagrams and contralateral in Noninvolved phase plane diagrams.

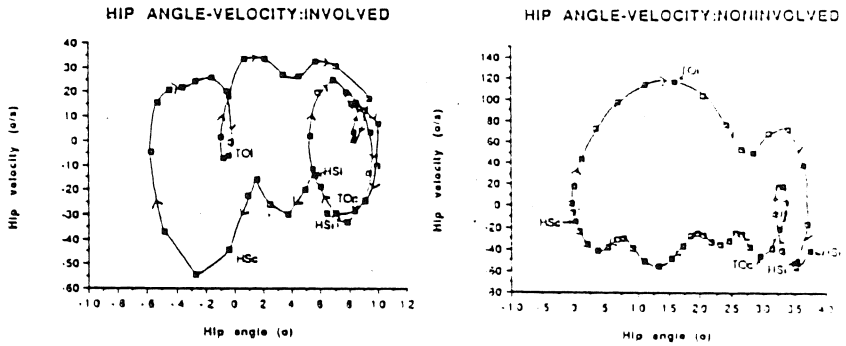
As presented in Figure 1, the patterns for both legs seem to lack the squareness associated with normal knee phase-plane diagrams as reported in Winstein and Garfinkel (*J. Motor Behavior*. 21:373-391, 1989) during mid phase. This results from accelerations (non-constant velocities) during mid swing and stance. In particular, the involved leg displayed large velocity changes during early stance. The involved leg displayed cusps (indicative of oppositions to intended

movement direction that are abruptly terminated) that became loops (movement reversals) during swing, while the noninvolved leg showed cusps during single limb support. Cusps always pointed inward toward the zero line for both legs. The trajectory of the involved leg showed range of motion and velocity deficits as the overall size of the trajetory was smaller than that of the noninvolved leg. The noninvolved leg showed velocity deficits when compared to normal curves.

Figure 1. Knee Phase-Plane Diagram



Hip Phase-Plane Diagram



Hip range of motion and angular velocity show large decrements as demonstrated by the small involved leg trajectory, especially in the flexor direction. Large velocity changes (vertical lines) occurred in late stance in the involved leg and during late swing in both legs. Both legs show cusps during single limb support, but loops occurred in the involved leg during double support. The noninvolved leg, otherwise, showed a relatively smooth trajectory throughout most of the rest of the cycle characteristic of normal.

DICUSSION: These data suggest that both legs show abnormal control mechanisms at the hip and knee. A lack of constant velocity phases inferred the use of ballistic movements. At the knee, this is demonstrated during the loading phase as the involved leg locked into full extension. The noninvolved knee and hip showed oscillations during single support reflective of compensatory responses to clonus during swing-through of the involved leg. The movement oppositions (cusps) show an invariant pattern of pointing inward or forming loops inward for either joint and either leg. This implied that the opposition to extension was similar to the opposition to flexion (Winstein and Garfinkel, 1989), suggestive of symmetric motor deficits. Range of motion and velocity magnitudes and patterns were most affected in the involved hip. Abnormal control mechanisms may be reflective of abnormal phasic firing patterns in the muscles of both legs during hemiparetic gait (Carlsoo et al., *Scand. J. Rehab. Med.* 6:166-179, 1974) and ground reaction forces and knee moments (Marks, *Arch. Phys. Med. Rehabil.* 9-20, 1953). These data suggest the need to study compensatory mechanisms in the noninvolved leg as both are adversely affected during hemiplegic gait.

BELOW-KNEE CHILD AMPUTEE GAIT: DYNAMICS OF AN ENERGY-STORING PROSTHESIS.

T.J. Hart, K. Schneider, R.F. Zernicke, Y. Setoguchi, and W. Oppenheim
Departments of Kinesiology, Pediatrics, and Surgery,
University of California, Los Angeles, Los Angeles, CA 90024-1568

INTRODUCTION

For the young child, stable and independent gait represents a significant milestone in motor skill development. The ability to locomote freely requires careful coordination of many body segments. For the child with amputation, the development of walking is more challenging, as the child must adopt movement strategies to compensate for the residual limb and prosthesis. With the development of "energy-storing" prostheses, the conventional functional requirements of prosthetics are being reassessed, but few studies have examined the benefits of this new generation of prostheses, and no investigation to date has addressed their benefits for children. Thus, we analyzed the kinematic and kinetic profiles of below-knee amputee children as they walked at normal and fast speeds wearing either a conventional prosthetic foot (SACH foot) or a new energy-storing foot (Flex-Foot).

REVIEW

Although the gait mechanics of adult below-knee amputees have been analyzed by various researchers (3,4,5,7,10,11), only very limited data are available on the gait mechanics of child amputee—either above-knee (8,12) or below-knee child (6). Furthermore, the new generation of "energy-storing" prostheses (*e.g.*, VA Seattle foot, Flex Foot), have only been evaluated for adult locomotion (3,4,5,10). Thus, it remained to be determined whether these energy-storing prostheses would be effective for children amputees.

PROCEDURES

Seven girls and five boys (mean(SD) age was 10.9(3.2)yr, height 150.2(16.0)cm, and mass 43.4(17.0)kg) participated in the study. All subjects were physically active and in good health. Each child had worn the SACH prosthesis for a minimum of 2 yr prior to beginning the present study. The average SACH foot component (including pylon and socket) mass was 1.17(0.4)kg. The subjects were tested by having each subject walk at normal (0.9m/s) and fast (1.3m/s) cadences while their movements and ground reaction forces were recorded. After this initial test, each subject was fit with the Flex-Foot. The Flex-Foot component averaged 1.24(0.4)kg. After a two-month habituation period, each child was retested while wearing the Flex-Foot prosthesis. The motion of each child amputee was recorded (200 Hz) using a motion-analysis system (WATSMART, Waterloo, Ontario, Canada) as the children walked along a 9-m walkway that contained a force plate (40 x 60 cm, Kistler Instruments, Winterthur, Switzerland). At least 80 trials were collected for each of the 12 children (10 trials x 2 speeds of locomotion x 2 prostheses x 2 limbs—prosthetic limb vs noninvolved limb). Standard kinematic and kinetic analyses (1,2,8,11,12) were performed.

RESULTS AND INTERPRETATION

A primary distinction between the SACH and the Flex-Foot was in the fore-aft (F–A) reaction force patterns. The transition from normal to fast walking resulted in a significant increase in the retarding force for the SACH and Flex-Foot, but the Flex-Foot produced significantly less retarding force than the SACH at the faster speed of walking. While the SACH foot showed no change in propulsive force with change in speed, the Flex-Foot generated significantly more force when the child walked at the fast speed. The propulsive force generated by the Flex-Foot was also significantly greater than the SACH foot at the faster walking speed. The maximal F-A propulsive force for the Flex-Foot not only was greater than the SACH foot values, but the difference between SACH and Flex-Foot increased with walking speed. Thus, the Flex-Foot adapted to changing demands brought about by changes in speed, and with the Flex-Foot the children amputees had greater hip excursion during stance to increase the range through which force could be applied.

On the prosthetic limb, the CP excursions were different for the SACH and the Flex-Foot (Fig. 1). Across speeds, the SACH foot had a more rapid transition out of the rearfoot region than did the Flex-Foot. The SACH-foot's cushioned heel permitted a rapid lowering of the SACH foot to the flat-foot position. The Flex-Foot, however, had a relatively stiff heel. The stiffness of the heel contributed to the slower lowering of the Flex-Foot to the foot-flat position and, thus, a slower CP transition. CP direction (F–A) reversals were frequently observed with the SACH foot.

The amount of energy absorbed by the SACH foot increased by more than twofold at the faster walking speed, but, power generation stayed the same as in normal walking. In contrast, the Flex-Foot absorption/generation percentage increased with increased walking speed. The Flex-Foot absorbed and generated significantly more energy than the SACH foot at normal and fast speeds and returned a significantly greater percentage of the energy originally absorbed (cf. 5). As with adults (5,10), these children amputees were able to exploit the energy-return features of the Flex-Foot to generate increased reaction forces, increased range of hip joint motion, and greater lower extremity joint moments. Nonetheless, it remains to be determined whether these greater forces will have long-term detrimental effects on lower extremity joint structures.

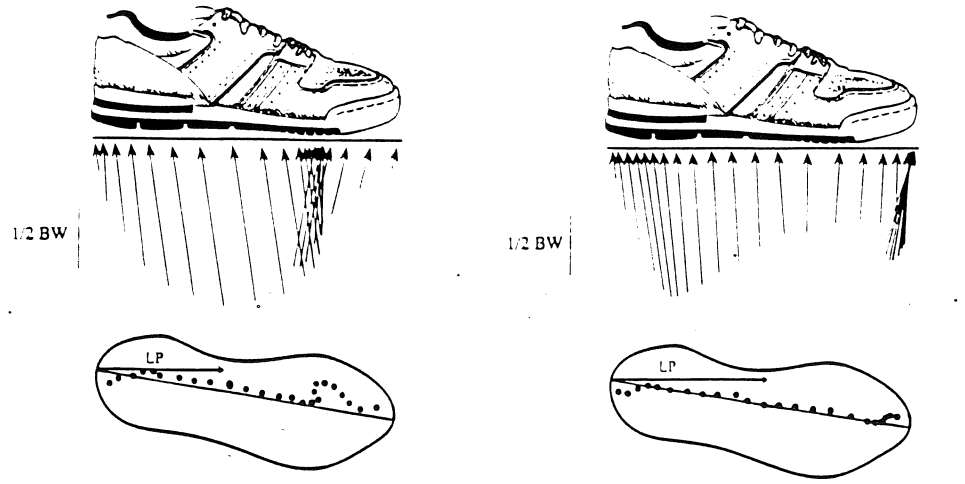


Fig. 1. Exemplar reaction-force vectors and center of pressure excursions for fast walking with the SACH (left) vs Flex-Foot (right) for the same subject. LP is the line of progression.

REFERENCES

1. Andriacchi, T. P. *et al.* (1977) *J. Biomech.* **10,** 261-268.
2. Bresler, B. *et al.* (1950) *Trans. ASME* **72,** 27-36.
3. Burgess, E. M. *et al.* (1985) *J. Rehab. Res. Dev.* **22,** 75-84.
4. Burgess, E. M. *et al.* (1983) *J. Orthot. Prosthet.* **37,** 25-31.
5. Czerniecki, J. M. *et al.* (1991) *J. Biomech.* **24,** 63-75.
6. Engsberg, J. R. *et al.* (1990) *Pediatr. Exerc. Sci.* **2,** 255-262.
7. Enoka, R. M. *et al.* (1982) *Am. J. Phys. Med.* **61,** 66-84.
8. Hoy, M. G. *et al.* (1982) *Arch. Phys. Med. Rehabil.* **63,** 74-82.
9. Miller, D. I. *et al.* (1981) *Biomechanics, VIII*: 443-449.
10. Smith, A. (1990) *Int. J. Sport Biomech.* **6,** 262-282.
11. Winter, D. A. *et al.* (1988) *J. Biomech.* **21,** 361-367.
12. Zernicke, R. F. *et al.* (1985) *Arch. Phys. Med. Rehabil.* **66,** 736-741.

Supported in part by a grant from the Shriners Hospitals for Crippled Children (15952).

SESSION 4

CARTILAGE, LIGAMENTS, AND BONE

BIPHASIC CREEP INDENTATION STUDIES OF BOVINE GROWTH PLATE CARTILAGE

L. R. Alberts and W. Abdul-Shafi
University of Nebraska-Lincoln
Lincoln, Nebraska 68588-0347

INTRODUCTION

Indentation creep tests were performed on growth plate cartilage from the proximal femoral bovine growth plate. We used a creep indentation apparatus with porous tip indentor that was developed by Mow, *et al.* (1). We found values of the shear modulus and aggregate modulus similar to those found for bovine articular cartilage, but the permeability was roughly twice that of bovine patellar cartilage.

REVIEW AND THEORY

Knowledge of the mechanical properties of the growth plate cartilage has particular relevance to diseases of slipped femoral capital epiphysis and various forms of dwarfism. It is also important for an understanding of how mechanical forces interact with osteogenesis, and with the growth and development of the bone. Fracture studies of the growth plate in rabbits by Guse (2) indicate that their may be changes in the mechanical properties of growth plate cartilage as the animal ages. Good values of the mechanical properties are also needed for analytical models.

PROCEDURES

Fresh bone samples were taken from the distal femur of Holstein cows about four years old. At this age, the growth plates were still intact in some of these animals while in others it was at various stages of mineralization. Within twenty four hours after slaughter, samples from the distal and proximal femurs were removed. They were then wrapped in gauze impregnated with normal saline solution (0.15 M NaCl) and containing enzymatic inhibitors (EDTA, 2mM; benzamidine HCl, 5 mM; N-ethyl malemide, 10mM and PMSF, 1 mM). Some of the sample were frozen in a deep freeze, while others were examined fresh.

A low speed diamond saw was used to cut sections about 2.5 mm thick through the capital of the femur. From these sections we removed parallelepiped segments about 2.5 mm x 2.5 mm and 10 mm to 20 mm long and containing a layer of growth plate cartilage about 0.5 to 1.5 mm thick. Segments were selected that contained fairly flat segments of growth plate cartilage. A razor blade was then used to cut through the proximal end of the growth plate and remove the cancellous bone proximal to the plate.

For indentation studies, the testing procedure of Mow *et al.* (1) for articular cartilage

was followed. We affixed the samples to the holder with cyanoacrylate cement, and aligned them perpendicular to the indenter. A tare load of 3 grams (.0294 Newtons force) was applied to the tissue, and allowed to creep for 15 minutes before application of a 5 gram (0.049 Newton force) test load. The samples were then allowed to creep for 90 minutes (5,400 s) and to recover for an equal amount of time. After recovery, the thickness of the indentation site was measured using a penetrating thickness probe. Three thickness readings were taken and averaged. Samples were saved for later histological examination.

After each test run, the creep data was saved on a file on a floppy disk. These files were then transferred to a VAX 8800 for input into a FORTRAN program developed by Mow *et al.* (1). This program applies the theory developed by Mak *et al.* (3) to determine the aggregate modulus, the shear modulus, the Poisson's ratio, and the permeability.

RESULTS

Based on five measurements that followed the above described procedure, we found the aggregate modulus (average ± standard deviation) of the solid matrix to be H_a = 1.02±.31 MPa, the Poisson's ratio to be μ_s = .34±.09, and the permeability to be k = .19±.11 x 10^{-14} m^4/Ns with an average cartilage thickness of 0.86±.22 mm.

DISCUSSION

These results indicate values of bovine growth plate cartilage for the aggregate modulus and the shear modulus are similar to those values for bovine articular cartilage. However the value of the permeability is roughly twice that of bovine patellar cartilage (1).

Values need to be taken from different ages of animals to determine if there are indeed age related changes in the mechanical properties of growth plate cartilage as was suggest by Guse (2). Also, more work needed to determine if the small size of the samples can significantly effect the results.

REFERENCES

1. V. C. Mow, *et al. J. Biomechanics 22*:853-861, 1989.
2. Guse, R., *et al. J. Orthopedic Research 7*:667-673, 1989.
3. A. F. Mak, *et al. J. Biomechanics 20*:703-714, 1987.

ACKNOWLEDGEMENTS

This work was supported by a grant from the National Science Foundation, award number 8907235. We would like to thank Dr. Van Mow and his staff for their helpful assistance.

BIOMECHANICAL PROPERTIES OF HIP CARTILAGE USING A BIPHASIC FINITE ELEMENT/OPTIMIZATION PROCEDURE -- AN INTERSPECIES STUDY

K. Athanasiou, A. Muffoletto, F.J. Dzida, G. Constantinides

Orthopaedic Biomechanics Laboratory, Department of Orthopaedics
University of Texas Health Science Center, San Antonio, Texas 78284

INTRODUCTION:

Utilizing the linear KLM biphasic theory for soft hydrated tissues [5], the material properties of normal adult articular cartilage were determined in the femoral head (FH) and acetabulum (AC) of baboons, mongrel dogs, and bovines, and compared to those of normal human hip cartilage [2]. *In situ* creep and recovery indentation experiments [1, 6] were performed using a new, automated indentation apparatus. In order to curvefit the entire creep curve, we developed a numerical algorithm based on biphasic finite element (FE) methods [8] and nonlinear optimization. This effort represents the first successful use of 100% of the creep indentation curve to obtain the mechanical properties of normal articular cartilage. Our results show that material properties of articular cartilage exhibit significant topographical variations in the FH and AC, and between these two anatomical structures. Furthermore, significant differences exist in the mechanical properties of hip cartilage among the four species. Specifically, in all species the smallest aggregate modulus is found in the inferior aspect of the FH. Among all species, human hip cartilage is the stiffest in all test sites; bovine tissue is the softest. The compressive modulus of human hip cartilage is closely resembled by that of baboon hip cartilage. Human tissue has the smallest ν_s and k in all test sites. Based on our data, the baboon represents the most appropriate animal model of normal human hip articular cartilage.

REVIEW AND THEORY:

Experimental animal models have been used extensively in orthopaedic research to develop implants for replacement of the human hip joint [4] and to study normal and diseased human hip articular cartilage [3, 7]. In this study, our objective was to perform intra-articular and interspecies comparisons of the in situ biomechanical properties of articular cartilage in the hip joint. The goal is to determine which of three animal models has hip articular cartilage with material properties that most closely resemble those of the human hip cartilage.

PROCEDURES:

Materials & Methods: We performed in situ creep indentation experiments in 3 sites in each AC and 4 sites in each FH of 6 baboons, 6 mongrel dogs, and 5 bovines. The mechanical properties were then compared to those of normal human hip articular cartilage, obtained in a different study [2]. The animal hip joints were harvested within 8 hours of death and were stored at -80°C. We tested the central portions of the anterior (A), superior (S), posterior (P), and inferior (I) segments of the FH, and the central portions of the A, S and P segments of the AC. These were labeled in a manner representing the human anatomic position in which the S portions of the FH and AC are in contact.

Fully-Automated Indentation Apparatus: The osteochondral specimens were tested using a new automated indentation apparatus to obtain the creep and recovery behavior of articular cartilage on the joint surface *in situ* [2]. At time of testing, a fiber-optic positioning system was used to align the loading shaft normal to the cartilage surface. Perpendicularity was achieved within 20s, even for 'small' specimens. Tare and test loads varied from 0.029N to 0.069N and 0.163N-0.302N respectively. Loads were applied via 1.2mm-2.0 mm dia. rigid, porous tips. The slope of the tare creep was monitored and when it became smaller than $1x10^{-6}$ mm/s, the test load was automatically released onto the cartilage, and the tissue's deformation was measured with an LVDT. When the slope of the creep curve was smaller than $1x10^{-6}$ mm/s the load was automatically removed, the tissue recovered, and data acquisition ceased automatically. Air bearings decreased frictional resistance to less than $9.81x10^{-4}$N. The air supplied to the bearings was passed through a chiller/warmer/filter system for complete moisture removal. Once recovery equilibrium was achieved, thickness measurement was performed with a needle probe system. All data acquisition and control software was written using the Labview icon environment.

FE Modeling: The tissue is modeled as an axisymmetric cylinder of uniform depth of a material described by the linear biphasic theory [5], with unknown properties $\mathbf{K_1}$, where, $\mathbf{K_i} = [H_A^i, \nu_s^i, k^i]^T$. The central region of the cartilage layer is subjected to a step load $P(t)=P_oH(t)$ through a frictional, rigid, porous, cylindrical indenter with material properties $\mathbf{K_2} = [3x10^{36}\text{MPa}, 0.25, 2.30x10^{-10}\text{m}^4/\text{Ns}]^T$. Subchondral bone is modeled as rigid and impervious to fluid flow. Each FE mesh is automatically generated for each specimen by specifying the tip radius, specimen thickness, and test load. The creep experiment yields the solid axial displacement (U_e) as a

function of time. This creep problem is solved using a FE formulation [8]. Numerical curvefit is provided by an optimization technique. The objective of the optimization technique is to obtain the unknown vector $\mathbf{K_1}$. Our code consists of the main program, the FE subroutine and the optimization subprograms -- obtained from the ADS library [9]. In the main program, we read U_e, decide on an initial guess ($\mathbf{K_1}^0$), apply the FE solution, postprocess the solid axial displacement (U_t), set up and calculate the objective function $F(\mathbf{K_1})=\Sigma (U_e - U_t)^2$, and apply the optimization procedure to minimize $F(\mathbf{K_1})$. Function $F(\mathbf{K_1})$ is to be minimized subject to side constraints $X_j^l \le X_j \le X_j^u$ (j=1,2,3), which define the feasible space of search for $\mathbf{K_1}$. Once $F(\mathbf{K_1})$ is calculated, a search direction ($\mathbf{S}^p$) is established using the 1st order BFGS variable metric method for unconstrained minimization. The design vector is then updated via $X^p = X^{p-1} + \alpha^p S^p$, where α^p indicates the amount of move in search direction $\mathbf{S}^p$. The scalar parameter α^p is obtained through an interpolation scheme using polynomial approximations. Thus, the problem is reduced to minimization of a function of one variable (α^p). This iterative procedure is executed on the Cray supercomputer.

RESULTS AND DISCUSSION:

Results are shown in table 1 (mean±SD). Statistically, these results were examined using one-way analysis of variance (ANOVA), two-way ANOVA, and Fisher least significant difference multiple comparisons test ($p<0.05$). In all species, the I aspect of FH has the smallest H_A in the joint. Among all species, human hip cartilage is the stiffest and bovine tissue is the softest. The compressive modulus of human hip cartilage is closely resembled by that of baboon hip cartilage. Human tissue is the least permeable (smallest k) and most compressible (smallest ν_s) in all test sites. Based on cartilage material properties, baboon is the most acceptable model of human normal hip cartilage; bovine is the least acceptable model. This biomechanical methodology, based on biphasic FE analysis and optimization techniques, allows the determination of all 3 intrinsic material properties of normal hip cartilage *in situ* in the joint, using the entire creep indentation curve.

REFERENCES:

1) Athanasiou et al., J Orthop Res 9(3):330-340, 1991. 2) Athanasiou et al., submitted, WAM ASME, 1991. 3) Bentley, JBJS 53B(2):324-337,1971. 4) Cook et al., JBJS 71B(2):189-197, 1989. 5) Mow et al., J Biomech Eng 102:73-84, 1980. 6) Mow et al., J Biomech 22:853-861,1989. 7) Scheck & Sakovich, CORR 86:115-120, 1972. 8) Spilker & Suh, Comp & Struc 35:425-439, 1990. 9) Vanderplaats, Eng Des Opt, 1981

Table 1: Material properties obtained from the biphasic FE/optimization procedure. AC, acetabulum; FH, femoral head; A, anterior; P, posterior; S, superior; I, inferior; H_A, aggregate modulus; ν_s, Poisson's ratio; k, permeability.

BABOON	H_A (MPa)	ν_s	$kx10^{15}$ (m^4/Ns)	h (mm)
AC A n=12	0.95±0.26	.26±.09	4.19±2.11	0.70±0.12
AC P n=12	1.03±0.43	.26±.09	3.80±2.57	0.96±0.59
AC S n=12	1.21±0.41	.28±.06	3.70±1.06	0.85±0.25
FH A n=12	1.06±0.58	.30±.04	4.10±0.88	0.53±0.18
FH I n=12	0.71±0.34	.29±.09	3.31±1.98	0.48±0.22
FH P n=12	1.10±0.66	.29±.08	3.92±2.06	0.54±0.20
FH S n=12	1.11±0.36	.28±.08	3.90±0.96	0.68±0.26

DOG	H_A (MPa)	ν_s	$kx10^{15}$ (m^4/Ns)	h (mm)
AC A n=12	0.89±0.33	.31±.07	4.08±1.02	0.47±0.16
AC P n=12	0.90±0.24	.31±.06	3.36±0.98	0.42±0.08
AC S n=12	0.76±0.26	.31±.06	4.08±1.26	0.38±0.15
FH A n=12	0.97±0.36	.29±.05	4.20±0.78	0.51±0.13
FH I n=12	0.48±0.23	.22±.10	2.96±0.96	0.52±0.26
FH P n=12	1.05±0.31	.27±.06	3.61±0.86	0.60±0.15
FH S n=12	0.79±0.22	.31±.06	3.62±0.82	0.47±0.14

BOVINE	H_A (MPa)	ν_s	$kx10^{15}$ (m^4/Ns)	h (mm)
AC A n=10	0.30±0.12	.25±.13	4.01±1.59	1.51±0.58
AC P n=10	0.28±0.12	.27±.06	4.57±1.13	1.54±0.42
AC S n=10	0.42±0.12	.34±.04	4.47±1.29	1.58±0.28
FH A n=10	0.51±0.13	.30±.06	4.56±1.98	1.07±0.31
FH I n=10	0.23±0.07	.16±.07	3.38±0.36	0.83±0.21
FH P n=10	0.39±0.22	.24±.09	3.33±0.72	0.92±0.25
FH S n=10	0.47±0.19	.29±.09	4.45±0.94	1.29±0.15

HUMAN	H_A (MPa)	ν_s	$kx10^{15}$ (m^4/Ns)	h (mm)
AC A n=10	1.24±0.61	.04±.04	0.91±0.44	1.24±0.15
AC P n=10	1.32±0.45	.06±.04	0.76±0.33	1.04±0.22
AC S n=10	1.18±0.56	.03±.04	1.06±0.77	1.60±0.43
FH A n=10	1.36±0.82	.05±.05	0.92±0.35	1.55±0.20
FH I n=10	0.82±0.18	.05±.04	0.91±0.31	1.23±0.22
FH P n=10	1.36±0.52	.03±.04	0.94±0.48	1.45±0.18
FH S n=10	1.44±0.08	.06±.06	0.91±0.35	1.39±0.16

LIGAMENTOUS CONTRIBUTIONS TO PELVIC STABILITY

M. Vrahas, T.L. Hern, D. DiAngelo, M. Tile, J.F. Kellam
Division of Orthopaedics, College of Medicine,
The Pennsylvania State University
Hershey, Pa. 17033
Sunnybrook Health Science Center, Devision of Orthopaedics
The University of Toronto

Distinguishing stable and unstable traumatic pelvic disruptions can be difficult, yet this distinction forms the basis for major treatment decisions. Despite this clinical importance, little is known about the biomechanics of pelvic stability, and an improved understanding could aid in the treatment of these difficult injuries. The purpose of this project was to estimate the relative contributions of major ligamentous structures to the composite stability of the pelvic ring during double leg stance.

We tested 14 fresh cadaver specimens comprised of pelvis, L4 and L5 vertebrae. All specimens had intact pubic symphysis (PS), anterior sacroiliac ligaments (ASI), and posterior sacroiliac ligaments (PSI). A majority of pelves had intact sacrotuberous (ST), and sacrospinous (SS) ligaments.

For testing, the potted L4 vertebrae was loaded with the Ram of a hydraulic MTS through a freely moving ball and socket articulation. Positioning of the pelvis simulated double leg stance with femoral protheses transmitting load through the acetabula. Mounting the femoral prostheses on roller plates allowed free motion in the coronal plane, and partially constrained anterior - posterior motion.

Each specimen was cyclicly loaded to 600N using a haver sine function at 1 hz, and load displacement curves were recorded at stable hysteresis. The specimen was then loaded to 600n under displacement control, and one of the major ligaments was cut while recording the resultant drop in load. This sequence was repeated until all ligaments had been cut. Numerous ligamentous combinations were tested by varying the order of sectioning. Where we suspected the pelvis would fail at 600N we choose smaller peak loads. Average stabilities were calculated from load displacement curves between 200 and 400N in all but 7 cases where a lower range was used.

A ligaments affect on pelvic stability depended not only on the ligament cut, but also on the other ligaments remaining intact. Cutting the PSI, ASI, or PS first caused respective reductions in stability compared to intact pelves of 24%(+-24), 12%(+-11.4), and 31%(+-5.3). Conversely, when these ligaments were the only ligaments remaining, they maintained respective stabilities of 60%(+-17.6), 36%(+- 36%), and 69%(+-16.5%) of the intact pelves (figure 1). Cut first, the ST, and SS ligaments caused negligible reduction in pelvic stability.

However, when the SS, ST, and PSI were the only ligaments remaining, cutting the SS and ST caused a %10 reduction in stability. Similarly, cutting the ASI first reduced stability 12%(+-11.4), yet when the PS was cut first, cutting the ASI caused a 36%(+-6) reduction stability. At the loads used, no displacements greater then 1cm were noted at the sacroiliac joint, and no estimation was made of the loads necessary for failure.

Measurements of global pelvic stability do not necessarily correlate with stability at the clinically important sacroiliac (SI) joint, yet our measurements elucidate mechanisms for ligamentous contributions to this stability. A ligaments contribution to SI stability depends not only on the ligament, but also on its interaction with other remaining structures, and with the bony pelvis. From previous internal fixation studies one would expect SI stability to be affected greatest by the PSI and least by the PS. In these tests, the PSI alone maintained 60%(+- 17%) of intact pelvic stiffness, while the PS alone maintained 67%(+-16.5%). Ultimately, the PSI may better resist failure, but it is important to understand the contribution of the PS. One might consider the pelvis loaded in a position simulating double leg stance to approximate a three point bend test. Loading the pelvis with the PS alone intact would be analogous to loading a beam in a three point bend configuration with the beam partially sectioned at its mid point. The PS would be analogous to the inferior intact portion of the beam, and the disrupted SI joint would be analogous to the superior disrupted portion of the beam. Loading the beam would result in tensile stresses at the inferior portion of the beam (in our tests tensile forces at the PS), and compressive forces at the superior portion of the beam (in our tests the disrupted SI joint). The compressive forces would generate frictional forces which would help to resist vertical shear. Clinical observations suggest the pelvis can remain relatively stable (no tendency to displace) with only the pelvic floor, SS, and ST intact. Given their anatomic orientations, these ligaments could not directly resist vertical SI displacements, but they could increase stability by promoting SI joint compression. Moreover, all pelvic ligaments may contribute to SI stability by directly resisting vertically sheer, allowing compression at the SI joint, or both.

THE EFFECTS OF INCREASED TENSION ON MEDIAL COLLATERAL LIGAMENTS: A BIOMECHANICAL, BIOCHEMICAL AND HISTOLOGICAL ASSESSMENT

[1]Mark A. Gomez, [2]Savio L-Y. Woo, [3]David Amiel, [3]Frederick L. Harwood, [3]Linda Kitabayashi and [4]John R. Matyas

[1]Orthopaedic Bioengineering Laboratory, University of Colorado Health Sciences Center, Denver, CO. 80262, [2]University of Pittsburgh, PA. 15261, [3]University of California, San Diego, CA. 92093, [4]University of Calgary Health Sciences Center, Alberta, Canada T2N-4N1

INTRODUCTION

Both experimental and theoretical techniques were utilized to examine the question of how increased tension affects the biomechanical, biochemical and histological properties of medial collateral ligaments (MCL). This is an important area of research as it would provide knowledge on the effects of exercise on ligament properties. The results of this study demonstrated a significant improvement in the stress-strain properties of the ligament material after twelve weeks of increased tension. The histologic appearance of the ligament revealed increased cellularity at this same time period while the biochemical analyses showed that active remodelling of collagen was still ongoing.

REVIEW

Studies have shown the positive effects of increased stress on the biomechanical properties of ligament tissues (Tipton, et al., 1970; and Woo, et al., 1979). However, there is a need to quantitate the increased stresses and strains that occur in ligament tissue during a particular training regimen in order to establish correlations between these parameters and the changes observed in the material or structural properties of the ligament. These changes may then be correlated to joint function as well as any biochemical and histological differences that may occur.

Therefore, the hypotheses to be tested in this study are 1): that the biomechanical, biochemical and morphological properties of normal ligament depend on the level of in-situ stress and 2): these same properties depend on the time increased stress levels are applied.

PROCEDURES

Medial collateral ligaments (MCL) in the left hindlimb of rabbits were subjected to increased tension by placing a 1.6mm diameter stainless steel pin perpendicularly underneath the distal end of the ligament. At six or twelve weeks post-operation, quantitative measurements of varus-valgus joint function were performed. Next, cyclic biomechanical testing of the ligament was done and the stress-strain results were described by the following constitutive equation:

$$\sigma_{33} = Ce_{33}\exp(ae_{33} + be_{33}^2) \qquad (1)$$

This equation was derived using a pseudo-strain energy function proposed by

Fung (1973). The material constants "C", "a" and "b" were determined by curve fitting Eqn. (1) to the experimental data. In-situ strains measured prior to testing were combined with this data to define in-situ loads. Tested samples were analyzed for the amounts of both the total collagen and the Schiff base collagen cross links, DHLNL and HLNL. An independent set of samples provided histologic data.

RESULTS

At 6 weeks post-operation, the in-situ load for MCL with the tension pin was 6.6 $\pm$ 2.0 N compared to 6.3 $\pm$ 2.0 N for the contralateral side. At 12 weeks, this higher load was maintained in the exp. MCL. The increase in MCL tension did not change the joint laxity relative to the control at either time period. However, a statistical analysis of the derived material constants showed that the stress-strain curves of MCL with increased tension at six weeks defined a lower stress for a given strain compared to that seen for the normal ligament. At twelve weeks, though, this trend had reversed showing a significant improvement in stress-strain properties (Fig. 1). At both time periods, the total collagen levels remained the same, but there were increased ratios of DHLNL to HLNL indicating the presence of immature collagen. Histologically, the experimental MCLs had increased cellularity.

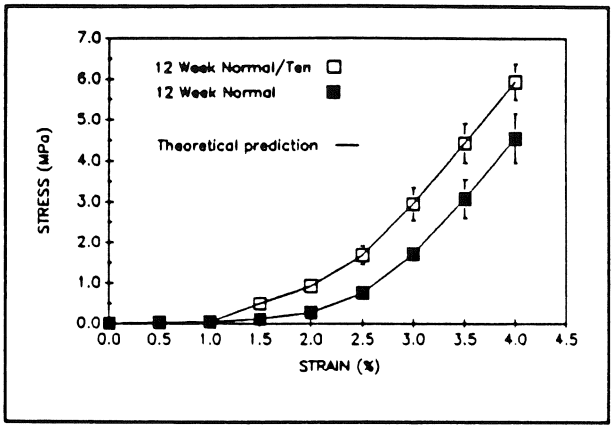


Fig. 1 - Stress-strain curves for MCL with and without tension at 12 wks. post-op. Symbols indicate exp. values.

DISCUSSION

At six weeks, the pin causes a significantly reduced stress for a given strain compared to normal MCL. The etiology of this change is attributed to a possible inflammatory response due to the proximity of the pin. This is consistent with the observed increase in MCL cellularity and the slight drop in total collagen levels along with increased amounts of Schiff base cross-links. At 12 weeks post-operation, the increase in MCL stress due to the pin provides for a positive increase in stress relative to strain compared to the normal side. Thus, all inflammatory responses are diminished by this time, but increased cellularity and continued higher cross-link levels would indicate that the MCL is still actively remodelling. In conclusion, one can accept the hypothesis that the aforementioned properties of ligament depend on the level of stress the ligament substance experiences. One may further conclude that the observed changes are time-dependent.

REFERENCES:

Fung, Y-C., Biorheology, 10:139-155, 1973; Tipton, C.M., et al., Am. J. Physiol., 218(3):894-902, Mar. 1970; Woo, S.L-Y., et al., ASME/AMD, 32:67-70, 1979.

MECHANICAL PROPERTIES OF CELLULAR MATERIALS

Mengke Zhu and Tony S. Keller
Dept. of Orthopaedics and Rehabilitation
Vanderbilt University, Nashville, TN 37232-2550

INTRODUCTION

The mechanical properties of cellular materials are dependent upon numerous factors including specimen density, structure, geometry and test conditions. In order to understand the effects of specimen size on as-measured mechanical properties of cellular materials such as human cancellous bone, nondestructive compression tests were performed on rectangular specimens of polymeric foams and human cancellous bone with 3 height-to-width h/w ratios. The elastic modulus E of these specimens was found to decrease with decreasing h/w ratios. This height effect, however, decreased with increasing sample density becoming negligible for specimen E>1.0 GPa. A formula was derived to characterize this height effect, and predicted differences in the measured modulus associated with different h/w ratios were verified by regional strain measurements of the samples using a microscope.

REVIEW AND THEORY

Specimen size is an important factor to be considered in investigations of the mechanical properties of cellular materials. For instance, the elastic modulus of cancellous bone from the human tibia was recently reported to decrease by a factor of 5 with decreasing specimen height-to-width ratio from 2 to 0.5 [1]. Morphologically uniform, rigid polyurethane foams (PU) were chosen to conduct an investigation of the height effect because PU's are cellular materials with a density range similar to that of trabecular bone, and also because they have a very uniform structure so that the effect of specimen height alone can be investigated.

Because cellular materials have rough contacting surfaces and sub-layers consisting of many open or broken cells, much higher strains may occur in the surface layer than the bulk. This is described by the formula:

$$E/E_b = \frac{Y}{Y(1-t)+t} \qquad (1)$$

where E/E_b is the ratio of measured to bulk modulus; $Y = E_s/E_b$ is the ratio of surface layer to bulk modulus; and $t = h_s/h$ is the ratio of surface layer height to specimen height. Assuming $Y = E_s/E_b = \varepsilon_b/\varepsilon_s$, Y can be determined by microscopic examination of the regional strains in the surface layer and the bulk of a sample for a given total strain. This formula is proposed to evaluate the influence of surface compliance on the measured elastic modulus of cellular materials.

PROCEDURES

Bulk Strain Evaluation: 275 rectangular specimens with a cross section area of 10 mm x 10 mm and 3 height-to-width ratios (h/w = 2, 1, and 0.5, respectively) were prepared from 5 density groups (ρ=0.06-0.64 g/cm^3) of PU (LAST-A-FOAM^R, GPMC, Tacoma, WA). 123 specimens of cancellous bone (ρ=0.04-0.3 g/cm^3) with a cross section area of 9 mm x 9 mm and h/w ratios similar to PU were prepared from 5 human lumbar spines. Nondestructive compressive tests of these specimens were conducted using an MTS 858 Bionix^R test machine. Each specimen was loaded along its primary axial direction at a strain rate of 1%/s (ε_{max}=1.6% for foams, ε_{max}=1% for bone). The elastic modulus E was determined as the slope of the stress-strain curves in the range 0.5-1.3% ε and 0.1-0.8% ε for the PU and bone specimens, respectively.

Regional Strain Evaluation: A specially modified micrometer was also used to apply a static compressive strain (≈1.6%) to several samples of polyurethane foams and bone with varying density and h/w ratio. In order to use Eq. (1), the ratio $t = h_s/h$ and the surface layer and bulk strains, ε_s and ε_b, were measured from photomicrographs of the surface layer of cells and the bulk, respectively, of each specimen.

RESULTS AND DISCUSSION

In Figure 1, as the specimen height decreased, E decreased significantly in all density groups except for the highest PU density group (ρ=0.64 g/cm^3). The percent change in E with respect to the tall samples (h/w=2) in each group increased with decreasing density (Figure 2), suggesting that a more porous structure contributes more to the height influence than a denser structure. For the bone specimens, the mean E of the short specimens (h=5 mm, ρ_{mean}=0.19 g/cm^3) was 42% lower than that of the tall specimens (h=16 mm, ρ_{mean}=0.21 g/cm^3). This height effect in PU and bone was further evaluated using Eq. (1), and the calculated differences are shown in Figure 2 (dashed lines and starred circle, respectively). Based on the measured Y and t values, the ratio E/E_b was calculated and is plotted in Figure 3. Experimentally determined $\varepsilon_b/\varepsilon_s$ ratios (solid circles in Figure 3) approached 1 with increasing foam density (Y=1 for ρ=0.64), which is consistent with the decreased difference in E measured between the short and tall samples. As the specimen height increases, $t=h_s/h$ decreases, and thus the influence of the surface compliance decreases, as shown by both Eq. (1) and the experimental data (Figures 1 and 2). Similar results are also predicted for cancellous bone, but the relation of E/E_b vs. ρ could not be precisely evaluated due to structural differences among the bone specimens.

CONCLUSIONS

The decrease in E with decreasing h/w ratio found in this study corroborates, but was much less dramatic than that reported previously [1]. These variations are hypothesized to be the influence of surface compliance and, therefore, this effect is most dramatic in short and low density specimens of cellular materials. Hence, very short specimens should be avoided, although the error in E caused by specimen height can be evaluated using Eq. (1). Since bulk density variations in both polymeric foams and cancellous bone have been associated with architectural features (open and closed cell, asymmetric and columnar structures) [2], this relation is further complicated, and structural indices are needed to fully characterize the mechanical behavior of cellular materials.

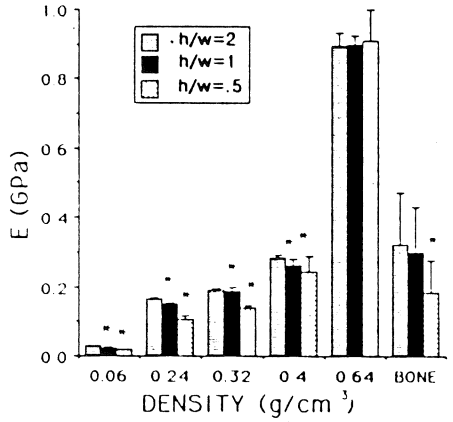


Figure 1. Mean E vs. Density and Height for PU and Bone. Asterisks indicate a significant difference (ANOVA, p<.05) in comparison to h/w=2. E values for BONE represent averages for all densities.

REFERENCES: 1. F. Linde et al., 7th Meeting of the European Society of Biomechanics, July, 1990 Aarhus, Denmark, A25. 2. L.J. Gibson, J. Biomechanics, 18: 317, 1985.

Research supported by the Department of Veterans Affairs Medical Center.

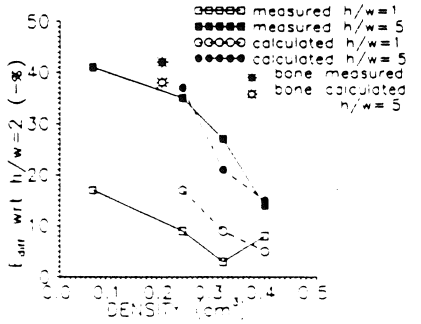


Figure 2. Effects of h/w and Density on Measured and Calculated Differences in E for PU and Bone

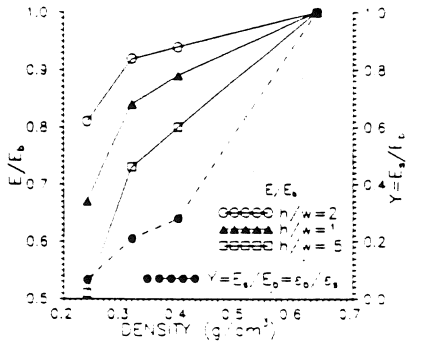


Figure 3. Effects of Density on Measured E_s/E_b Ratios for PU and the Corresponding E/E_b Values Calculated for Different h/w Ratios.

SESSION 5

FOOTWEAR

THE EFFECTS OF FOOTWEAR AND TECHNIQUE ON RACE WALKING MECHANICS

Rebecca E. Snow* and Rhys V. Bowen+
*United States Olympic Committee, Colorado Springs, CO
+University of California, Davis, CA

INTRODUCTION

Ten elite race walkers walked on a treadmill and across a Kistler force plate at 358 cm/s in each of four conditions to study the effect of shoes and technique on race walking mechanics. The four experimental conditions comprised two different types of shoes (running training flats and race walking shoes) and two race walking styles (international style and hiking style). There were no significant effects of shoe type on the kinematics or kinetics of the race walkers. Trunk angle at footstrike was significantly more flexed ($p < 0.0018$) in the international style than in the hiking style, but significantly less ($p < 0.0018$) thigh flexion at footstrike and less ankle dorsiflexion at footstrike were noted in the international style. Medial impulse through the entire cycle was significantly higher ($p < 0.0009$) for the international style than for the hiking style, but vertical impulse was significantly lower ($p< 0.0009$).

REVIEW AND THEORY

The U.S. National Race Walking team is undergoing an evolution in style to imitate the more successful Mexican and European race walkers. Hiking style, which is characterized by an upright trunk, was common among all race walkers in the 1960's and until recently was still used by U.S. walkers. International style is defined by an anterior trunk lean and is currently used by the Mexican and European race walkers. One purpose of this study was to compare the two styles of race walking from a kinematic and kinetic perspective so that a scientific analysis can contribute to the stylistic transition among U.S. walkers. Many race walkers are currently walking in shoes that were designed for running. However, the footwear needs of race walkers, as inferred from kinetic data, are very different from the needs of runners (Fenton, 1984). A second purpose of this study was to examine the effects of shoes on the mechanics of race walking.

PROCEDURES

Kinematic and kinetic variables were measured on ten elite race walkers walking on a treadmill and across a Kistler force plate at 358 cm/s. Each subject walked in two different types of shoes (running training flats and race walking shoes) and two race walking styles (hiking style and international style) in a crossed experimental design, giving a total of four conditions. Sideview kinematic data were collected on the treadmill to determine if there were differences between the four walking conditions in 28 angular and velocity variables. All data were collected at 200 fps from a sagittal view using a NAC HSV 400 camera and video recorder. The kinematic data were analyzed using Motion Analysis ExpertVision. Five walking cycles were averaged for each subject. The maximum ground reaction force peaks, impulses, and timing of the forces and impulses, for the vertical, anteroposterior, and mediolateral directions—a total of sixty-four dependent variables—were derived from the raw kinetic data. Five trials were averaged for each subject. A two-way repeated measures ANOVA with shoe and style as within-subject independent variables was used to analyze each kinematic and kinetic dependent variable. Because of the large number of dependent variables, separate Bonferroni adjustments were made on the alpha level for the kinematic and kinetic data. This adjustment resulted in significance levels of approximately 0.0018 and 0.0009 for the individual kinematic and kinetic variables, respectively.

RESULTS

There were no significant interactions between shoe type and style for any of the dependent variables. There were no significant effects of shoe type on kinematics or ground reaction forces in spite of significant differences between running and walking shoes in weight, heel flare angle, swing angle, and shock absorption. Trunk angle at footstrike was significantly more flexed ($p < 0.0018$) in the international style than in the hiking style. Significantly less ($p < 0.0018$) thigh flexion at footstrike and less ankle dorsiflexion at footstrike were noted in the international style compared to the hiking style (Table 1). Medial impulse through the entire cycle was significantly higher ($p < 0.0009$), but vertical impulse was significantly lower ($p< 0.0009$), for the international style than for the hiking style.

Table 1: Mean values (and standard deviations) of three kinematic variables under four walking conditions, comprised of two shoe types (race walking (walk) and running (run)) and two walking styles (hiking and international (int'l)) (n=10 subjects).

Variable	Walk-Hiking	Walk-Int'l	Run-Hiking	Run-Int'l
Trunk at Footstrike (deg)*	0.7 (2.6)	7.0 (3.1)	0.5 (2.6)	6.9 (5.2)
Thigh at Footstrike (deg)*	21.2 (2.3)	19.5 (2.4)	21.5 (2.2)	20.0 (2.0)
Ankle at Footstrike (deg)*	89.0 (3.1)	87.5 (2.5)	90.0 (4.0)	88.8 (3.7)

* Significant difference between styles ($p < 0.0018$)

DISCUSSION

Coaches define the international style of race walking by anterior trunk lean. It is not surprising, therefore, that there is a significant difference in the trunk flexion at footstrike between the international style and hiking style. The quantitative biomechanical data merely confirm the difference between the two styles that is visually apparent to coaches and walkers. Many coaches have asserted that an increase in trunk angle by race walkers alters anteroposterior ground reaction forces; specifically, the braking force should decrease and the propulsive force should increase as trunk angle increases. The results of this study do not confirm this theory. There was no significant effect of walking style on any of the anteroposterior forces. This lack of effect, however, may have been due to the shorter stride length ($p < 0.008$) that occurs in international style walking than in hiking style—if stride length were somehow to remain constant between styles, significant differences in anteroposterior forces might occur in association with the difference in trunk angle.

It is suggested that the decrease in thigh flexion and ankle flexion while walking in the international style, relative to the hiking style, is due to an anterior displacement of the body's center of mass caused by the anterior trunk flexion. The increase in medial impulse may be due to greater pronation in the international style, and the decrease in vertical impulse is due to the shorter contact time seen in the international style than in the hiking style.

References:
Fenton, R.M., Sports Biomechanics, Academic Publishers, pp. 61-70, 1984.

This study was supported by a grant from the Rockport Walking Institute.

MODELING OF THE EFFECT OF FOOTWEAR ON THE DYNAMIC LOADING ON HUMAN MUSCULOSKELETAL SYSTEM

Wangdo Kim and Arkady S. Voloshin
Department of Mechanical Engineering and Mechanics

Lehigh University
Bethlehem, PA 18015, USA

The goal of this study is to develop a mathematical tool which can explain the dissipation and attenuation during the impact of the foot striking the ground. The spring-damper-mass model was suggested to model the transient strain wave propagation through the lower extremity.

To understand the interaction between the effective vertical spring stiffness, damping, impact velocity, and the body mass, a three degree-of-freedom model was developed (Fig. 1), which represents a functional view of a runner (lumped in the masses m_1, m_2, m_3) striking a ground cushioning system represented by k_1 and c_1. The model will be used to predict the vertical impact transient during running. There are six system parameters to be identified (k_1, k_2, k_3, c_1, c_2, c_3) as shown in the suggested biomechanical model. Anthropomorphic data was used to represent the mass of each element, m_1, m_2, and m_3 are considered to represent the foot, tibia and the rest of the body. To identify the unknown parameters of the model, acceleration of m_2 (measured *in vivo* at the tibial tuberosity) was used. An eighteen year old male subject weighing 542 Newtons participated in this study. The subject's running velocity during the test was adjusted to approximately 0.75-0.80 sec/running cycle. The PCB piezoelectric accelerometer was mounted on the holder and attached to the subject's tibial tuberosity with an elastic velcro strip. In this work quasilinearization is used for system identification by using measurement data to formulate the problem as a multipoint boundary-value problems.

The analysis of the model using results from three consecutive heel strikes that were measured in the middle of the runway yielded the identification of the unknown parameters as shown in the Table 1.

Table 1.

k_1(N/m)	k_2	k_3	c_1(Nsec/m)	c_2	c_3
landing cushion	tibia and ankle	knee and above			
45.7	94100	40100	174	444	35.9

The model presented provides a way to explain the magnitude of shock waves transmitted in the body as direct functions of the landing cushion parameters k_1 and c_1. From the identified parameters, the landing cushioning properties are varied to investigate the change of the ground reaction forces. Fig. 2 and 3 show that the magnitude of the impact ground forces are proportional to the damping c_1, while the spring value k_1 does not significantly affect the ground reaction force. This can be explained by noting that the damping constant is the dominant factor in controlling the impact momentum because its magnitude has a large value compared to the spring value k_1. The small value of k_1 indicates that the energy storing

capacity of both the tissue beneath the heel and the surface of the ground is almost not present in terms of the physical interpretation of our model.

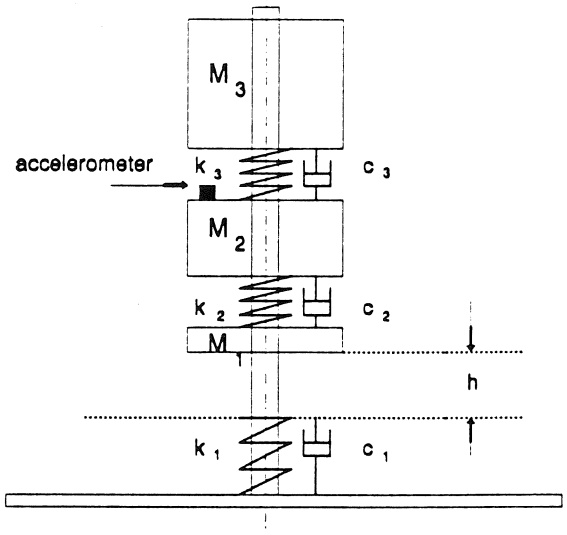


Figure 1. Landing model of running.

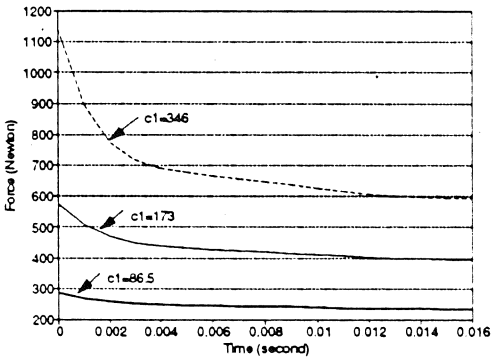


Figure 2. The ground reaction forces with three different landing properties of c's.

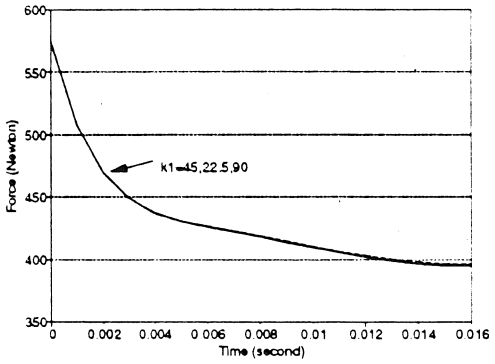


Figure 3. The ground force with three different landing properties of k's.

Since it is impossible to change the shock absorbing capacity of the subject, the only parameter which can be controlled in order to reduce the heel strike impact might be the landing cushions represented by k_1 and c_1. By reducing the damping properties of the foot-ground interaction, we can accomplish the major attenuation of the oncoming shock waves through the body. Since the properties (k_1 and c_1) represented were obtained from running with bare feet, those parameters can be affected by the runner's particular footwear. The method presented here may and should encourage designers to simulate and to develop biomechanically optimized running shoes that incorporate the best available designs and materials for the soles and insoles.

TIME DOMAIN MODELLING FOR THE ASSESSMENT OF SHOCK ABSORBING INSOLES

G. Lowet, L. Peeraer, K. Colpaert, G. Wallaeys, G. Van der Perre
Division of Biomechanics, K.U.Leuven, 3001 Leuven, BELGIUM

INTRODUCTION : In order to attenuate the shock at heel contact during running and walking, several insoles have been developed. A mathematical model was constructed, including nonlinear elements for the insole, which gave a good estimate of the real ground reaction forces and accelerations at the ankle at heel strike. This model allows the prediction of ground reaction force and acceleration, based on the elastic and damping properties of the insole.

REVIEW AND THEORY : Shock propagation during heel strike in walking and running is subject of a growing interest in the past years. In literature several pathological conditions are believed to be caused by these shocks (1). Research on the influence of shock attenuating insoles was mainly comparative, and the relation between the mechanical characteristics and the dynamic performance was never investigated. Also frequency analysis was used (2) in order to quantify the effect of the insoles. Earlier work done at our laboratory pointed out that frequency analysis was not adequate because of the nonlinear nature of the materials used for these insoles. In this work, we aimed at the construction of a model which takes into account the nonlinearity of the insole to predict the actual ground reaction forces and accelerations at the ankle.

PROCEDURES : The insole was modelled by a single mass, damper and spring system. Creep tests using different loads allowed to determine both stiffness and damping properties of the insole (brand : Viscolas), both were a function of the compression. It was observed that stiffness was related to compression by a third order polynomial, while damping could be modelled by a second order polynomial.
Two distinct models were constructed for a human body. The first model, the "body force model" (BFM), consists of three masses, three springs and three dampers. The input is the vertical velocity at heel strike. The output is the ground reaction force. The parameters of this model were determined by experiment. A young man kept himself hanging at two rings, which were mounted such that his feet were at a height of 15 cm above a force plate. An accelerometer was attached at the ankle by means of a close fitting lightweight cast. He let himself fall on the plate, keeping his body and legs straight and landing on the heels. Ground reaction force and acceleration were measured and showed to be highly repetitive. The values of the 9 elements of the force model were tuned until the measured and the modelled ground reaction force were identical.
The second model, the "ankle acceleration model" (AAM), aimed at simulating the acceleration at the ankle, given the

ground reaction force. The three masses, three dampers and three springs of the latter model were determined through fitting on the measured transfer function, which is the Fourier-transform of the ankle acceleration divided by the Fourier-transform of the ground force (exerted upon the heel).

RESULTS : The models are used as follows. Given the velocity at landing, easily calculated from the height of fall, the ground reaction force can be derived from the BFM. This force is now the input for the AAM which returns the ankle acceleration. In order to evaluate the insole, the insole model is inserted in the force model. This combined model gives, for the same landing velocity, another ground reaction force which leads consequently to an altered acceleration signal. These predicted signals were in very close agreement with the experimental results. Using a different insole, and thus a different insole model, we found the same correlation between modelled and measured ground reaction forces and acceleration signals.

DISCUSSION : In agreement with literature, a clear change in ground reaction force and in ankle acceleration due to the use of these insoles was observed. The presented models however allow to estimate the ground reaction forces and accelerations based on the mechanical properties of the insole. Figure 1 shows the acceleration and force maxima which are calculated with the established models for an insole, multiplying the polynomial characterising the spring with a factor ranging from 0.05 to 2, and the polynomial characterising the damper with a factor ranging from 0.0005 to 5. The two graphs in Fig. 1 in principle allow to find the optimal combination of damper and spring characteristics to minimize ground reaction force and acceleration.

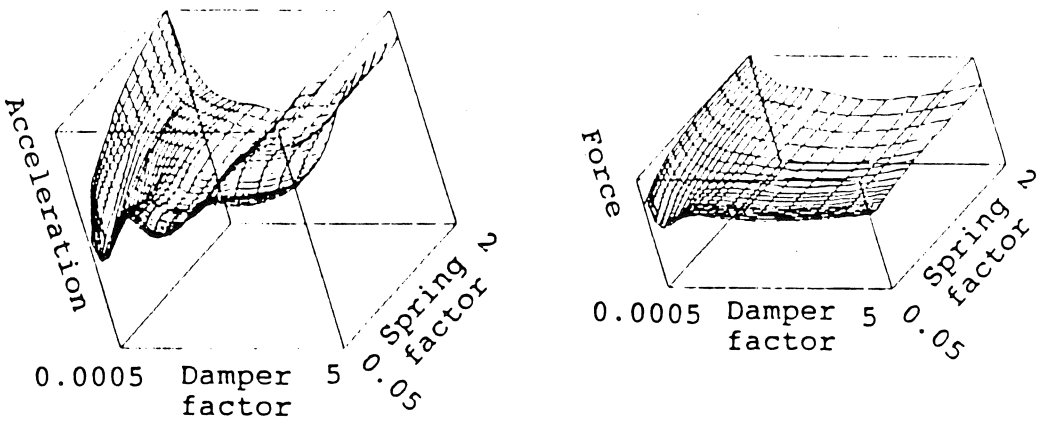


Fig. 1 : Acceleration (left) and force (right) as a function of spring and damper factor.

1. Wosk J. et al., J. Biomech., 15:21-27,1982
2. Johnson G.R., Eng in medicine, Vol 15 nr 3, 1986

Validation of a Mathematical Model of the Effect of Sole Elasticity Distribution on Pronation

Perry Y. Li [1] and Zvi Ladin
Biomedical Engineering Department and NeuroMuscular Research Center
Boston University, Boston, MA 02215

Introduction

Excessive pronation has been cited as a cause for many musculo-skeletal injuries. In order to properly address this issue in the design of elastic soles in running shoes, a mathematical model relating sole elasticity distribution and pronation is helpful. Li and Ladin (1989) presented a lumped parameter model of an elastic sole using an energy minimization approach. In that model the top surface of the sole was shown to behave like a rigid body mechanism supported by a vertical and a rotational spring (Fig. 1). The parameters of this model (2 spring constants, location of the pivot) can be computed from the coronal plane elastic distribution of the sole. Using this model together with a spring loaded rigid body model of the lower limb (Fig. 1), expressions for the pronation angle and the centre of pressure location can be derived (Fig. 2). Besides the system parameters, the inputs to the combined model are the vertical and horizontal forces and the absolute shank angle. In this abstract, we present a static validation experiment of these expressions in which the elastic distribution of the sole was systematically varied. Changes in pronation angles and in centre of pressure locations were predicted and compared with experimental measurements.

Methods

A composite foam was made by joining two pieces of foam of different stiffnesses side by side. By moving the binding line between the two materials medial-laterally under the foot of the subject, different elastic distributions were simulated. The subject stood still with one foot on the composite foam and the other, 2.5 ft away on a control foam. The rigid body kinematics of the shank and the foot were measured using the WATRACK system that is composed of the WATSMART optoelectronic system and the TRACK© software. Reaction forces and moments were measured by an AMTI force plate system. Measurements were averaged over a period of 5 s during which the subject was instructed to maintain a constant posture. The experiment was repeated with the binding line at 6 locations under the foot with the stiffer material on the medial side first and then on the lateral side. Pronation angles were inferred from the rotation of the foot relative to the shank and the centre of pressure locations were calculated from the force plate data. Model predictions were computed using expressions in Fig. 2.

Results and Discussion

Figs. 3 and 4 show the predicted (dotted lines) and the measured (solid lines) pronation angles and centre of pressure locations with the binding line at different locations under the foot. These figures clearly show that the predictions are accurate with respect to both the range and the presence of the various features in the curves. Moreover, the fact that both the pronation angle and the centre of pressure expressions in Fig. 2, (which can be shown to be mathematical duals), are accurate, further suggests that the structure of the model is consistent with reality. By expanding the model to include elasticity distribution along the sole, it could become a useful tool for footwear design.

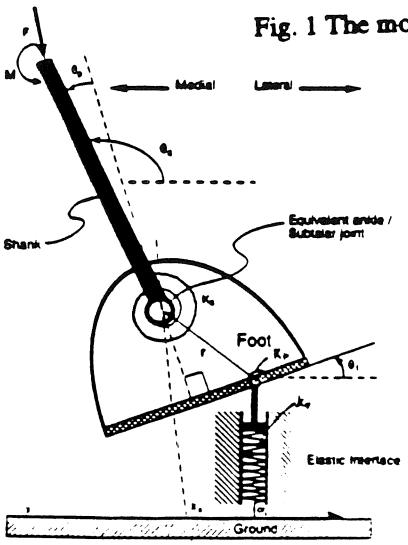
---

[1] Current address: Department of Mechanical Engineering, University of California, Berkeley, CA 94720

Acknowledgement
This work was supported by a grant from Reebok International Ltd.

Reference
P. Li and Z. Ladin, (1989), 'Energy Minimisation Approach to the Design of Sole Elasticity For Pronation', *Proc. of the 12th Ann. Meeting of the Amer. Soc. of Biomech.*, Burlington, VT.

Fig. 1 The model

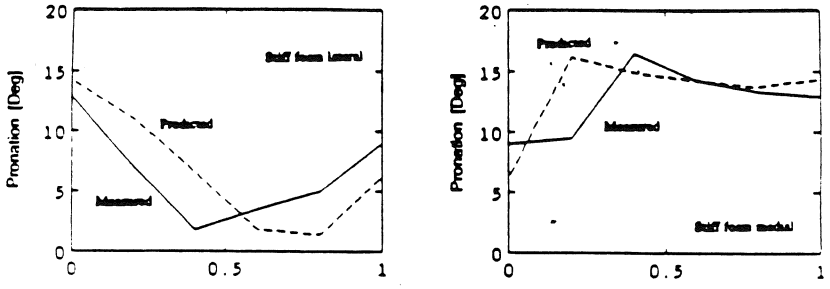


$$\theta_p = \frac{K_a\theta_p^0 + (K_r + \mathbf{r}\cdot\mathbf{F})(\theta_s - \pi/2)}{K_a + K_r + \mathbf{r}\cdot\mathbf{F}} + \frac{(X_a - CP_0)F_z}{K_a + K_r + \mathbf{r}\cdot\mathbf{F}} \quad (1)$$

$$CP = \frac{K_a CP_0 + (K_r + \mathbf{r}\cdot\mathbf{F})X_a}{(K_a + K_r + \mathbf{r}\cdot\mathbf{F})} - \frac{K_a(K_r + \mathbf{r}\cdot\mathbf{F})}{(K_a + K_r + \mathbf{r}\cdot\mathbf{F})F_z}(\theta_s - \frac{\pi}{2} - \theta_p^0) \quad (2)$$

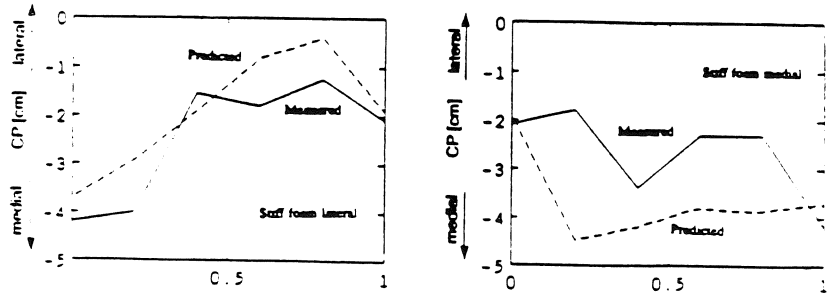
where K_r, CP_0 are the ankle stiffness, model rotational stiffness and pivot location (as defined in Li and Ladin (1989)), K_a is the ankle stiffness.

Fig. 2 Expressions for CP and Pronation angle



Distance of binding line from medial edge normalised to foot-width

Fig. 3 Predicted and Measured Pronation Angle



Distance of binding line from medial edge normalised to foot-width

Fig. 4 Predicted and Measured Pronation Angle

THE IMPORTANCE OF THERMO-MECHANICAL PROPERTIES IN THE SELECTION OF ATHLETIC SHOE CUSHIONING FOAMS

Jeff Poliner, Spencer White, and Mark Fenton
Reebok International, Ltd., Stoughton, MA 02072

INTRODUCTION

Material tests have demonstrated that the foams used for cushioning in athletic footwear exhibit a large amount of hysteresis energy loss during impact. Some of this energy is converted to heat, which can modify the stiffness characteristics of the foam. This study was designed to measure the temperature increase in running shoes, to examine its effect on material stiffness during the course of a single exercise bout, and to compare materials with high and low hysteresis.

PROCEDURES

Two pairs of running shoes were constructed, with the midsoles of one composed of Hytrel foam (HF), which exhibited approximately 20% hysteresis energy loss, and the other midsoles composed of EVA of similar stiffness, which exhibited almost twice the energy loss (approximately 40%). The shoes were instrumented with thermistors embedded in the heel and forefoot regions. Seven male subjects ran in the shoes at a self-selected pace for 7.25 km (4.5 mi), stopping briefly every 0.73 km so that the temperature of the foams could be recorded.

Blocks of HF and EVA were also tested on an hydraulically driven stroke-control impact machine. The materials were cyclically loaded at 1.2 Hz to a constant strain for 5,000 cycles. Each impact period was 100 msec, with maximum compression occurring after 25 msec. Peak loads were characteristic of those experienced by the midsoles of running shoes. Internal foam temperature was measured by a thermocouple embedded in the center of the foam block. Temperature, force and compression data were collected every 50'th cycle. Average stiffness was calculated as the ratio between the maximum load and total strain during each impact cycle.

RESULTS/DISCUSSION

Figure 1 shows a plot of midsole heel temperature as a function of distance run for a typical subject. At the end of the run, heel foam temperatures had increased an average of 11.7°C (±5.9°) in EVA and 9.0°C (±3.7°) in HF. Forefoot increases were 17.1°C and 16.8°C (±1.4 and 2.8°) in EVA and HF respectively.

To determine the effect of these temperature increases on foam stiffness, material tests were also conducted. The temperature changes in foam blocks during cyclic loading on an impact machine are shown in Figure 2. EVA heated 17.0°C and HF 14.0°C after 5,000 cycles. Average stiffness, normalized to the first impact cycle, as a function of number of impacts is displayed in Figure 3. EVA became 36% softer and HF 11% softer after 5,000 impacts. Clearly, the time course of the drop in stiffness closely matches the rise in temperature.

Figure 4 shows normalized average stiffness plotted against temperature. The slope of these curves, which represents the sensitivity of the material to changes in temperature, was 0.0199 $°C^{-1}$ for EVA and 0.0057 $°C^{-1}$ for HF. Thus, for a given change in temperature, EVA showed a greater change in stiffness.

The results from the material tests were combined with the data from the human subjects, to estimate changes in midsole stiffness over the course of a workout. The change in midsole temperature measured during the run was multiplied by the material sensitivity calculated from

the impact test data. Based on these calculations the foam in the rearfoot softened by 23% (±11.7%) in EVA and 5% (±2) in HF; the forefoot softened 34% (±3) in EVA and 10% (±2) in HF.

CONCLUSIONS

These results demonstrate that during a single bout of exercise there is a significant increase in temperature, and a concomitant decrease in stiffness, of foam materials used in running shoe midsoles. The increase in temperature appears to be related to mechanical energy losses during impact, since a material with lower hysteresis (Hytrel foam) demonstrated less temperature increase than one with higher hysteresis (EVA). Hytrel foam also demonstrated less sensitivity to temperature than EVA. The combined effect of lower heat production, and lower heat sensitivity resulted in significantly less softening of Hytrel foam during cyclic loading than EVA. These results indicate that energy efficiency and thermal characteristics should be considered when choosing cushioning materials for use in athletic footwear.

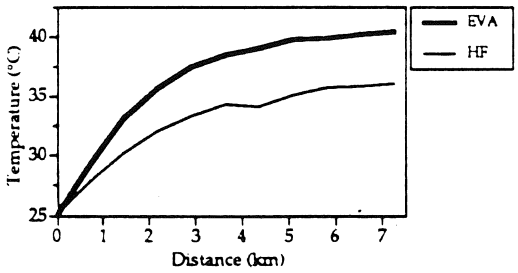


Figure 1: Plot of heel foam temperature vs. distance run for a typical subject.

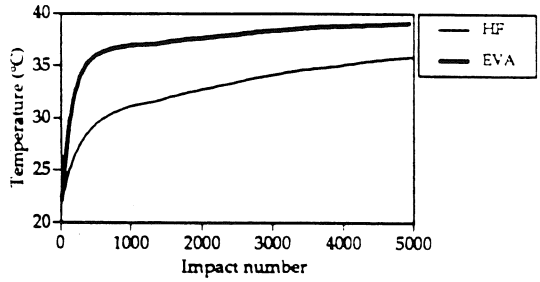


Figure 2: Increase in temperature during impacting of Hytrel foam and EVA.

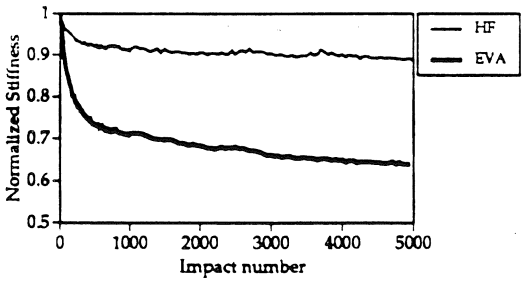


Figure 3: Decrease in stiffness during impacting of Hytrel foam and EVA.

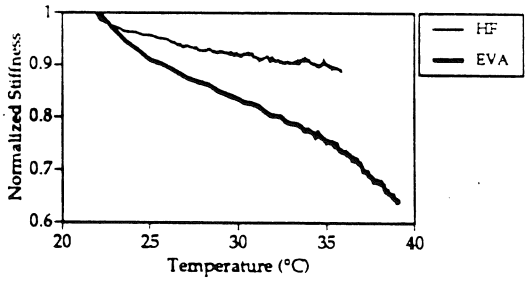


Figure 4: Foam temperature vs. average stiffness for Hytrel foam and EVA.

SESSION 6

CERVICAL SPINE

VERIFICATION OF ANALYTICAL MODELS APPLICABLE TO MOTION ANALYSIS IN THE CERVICAL SPINE.

P. Roozmon, SA Gracovetsky, GJ Gouw, N Newman. Diagnospine Research Inc, 1980 Sherbrooke West, Suite 1100. Montreal, Quebec, Canada H3H 1E8. Concordia University Departments of Electrical and Mechanical Engineering, Dept. of Orthopaedic Surgery, Hotel Dieu Hospital, Montreal.

INTRODUCTION

Several multi-disciplinary teams previously associated with low back pain research have now turned their attention to the neck. As a result, the previous dearth of experimental data on the cervical spine has been somewhat alleviated. Both in-vivo and in-vitro techniques have been employed to quantify the mobility of cervical motion segments. The consequence of this is that analytical models may now be tested using realistic data for simulations. Hence all of the parameters needed in a comprehensive model of the cervical spine can now be quantified. A new opto-electronic device has been developed which may be used to help verify such models in the upper spine. Our purpose is to consider the range of existing models and to evaluate the usefulness of this instrument in verifying them.

REVIEW AND THEORY

A number of models for various accelerations and loadings have been proposed during the past decade (figure 1).[1,2,3] Using the data available on the ultimate strengths of soft tissues and cervical vertebral bodies, these may now be verified.[4,5] Computer tomography and biplanar radiographs have been used in live subjects to determine limits of rotation for each joint.[6,7] Motion segment testing machines have yielded extensive data on coupled motion in cervical spines from cadavers.[8,9] However, models describing the upper portion of the spine appear to be less numerous than those for the lower back. They usually represent the head, neck and upper torso as a deformable collection of rigid bodies.[10,11,12] When considering the behaviour of the spinal cord in particular, verification of models requires a way to identify narrowed canals. Magnetic resonance imaging techniques have made this possible as well.[13,14] According to Panjabi and White (1988), there are currently no mathematical models that relate external loads to the internal stresses within the spinal cord.[13] This is area that will require considerable investigation before it can be incorporated into spinal models.

PROCEDURES

The motion analysis device used in our work is known as the Cerviscope and was developed by Spinex Medical Technologies of Montreal. In this instrument, two cameras are used to track a set of small infrared emitting diodes (IREDs) affixed to the subjects' skin. Discrete motion samples are recorded at a frequency of 180 frames per second. Kinematic data for the motion of the markers is processed automatically such that absolute coordinates for the location of each IRED at any time are tabulated and coordinated with EMG data (figure 2). Overall analysis includes displays assessing cervical lordosis, thoracic kyphosis, and inter-segmental mobility. Characterization of coupled motion has been treated as an addition to these, involving a series of plots illustrating principal vs secondary motion. Principal movements include flexion-extension, lateral bending, and axial rotation. Mobility is represented in terms of Euler angles corresponding to the relative motion of vectors normal to triangles defined by IREDs placed on the head and shoulders.

DISCUSSION

We considerthe role of analytical models in describing motion in the cervical spine. The models described here were all developed through analogous methodologies. Points of insertion for muscles or ligaments were digitized and the forces estimated. Approximations were generally used to render the systems of equations deterministic. The cerebrospinal fluid is accounted for by

considering flexible, liquid filled tubes. However, a biomechanical model for the spinal cord is not yet available. Physical models are used primarily to test their analytical counterparts. It appears that the physical models do not yet simulate head/neck motion adequately. Accurate predictive injury modelling is thus not possible, though normal and pathological motion can be approximated. A tool for analysing range of motion is expected be useful in verifying such approximations.

REFERENCES

1. Schuldt K, Harms-Ringdahl K: EMG/Moment Rel. in Neck.... Clin. Biomech. 3: 129-136,1988.
2. Helleur et al : Modelling of the ... Cervical Spine. Mathem. Modelling 6: 443-462, 1985.
3. Deng YC, Goldsmith W: Response ... Head/Neck ... II. J. Biomechanics 20: 487-497, 1987.
4. Yoganandan et al : Dynamic Response of Human Cervical Spine.... Spine 14: 1102-1110, 1989.
5. Myklebust et al : Tensile Strength of Spinal Ligaments. Spine 13: 526-531, 1988.
6. Penning L, Wilmink JT: Rotation of the Cervical Spine: A CT Study .... Spine 12: 732-738, 1987.
7. Dvorak et al : CT-Functional Diagn. ... Upper Cervical Spine, Part 2. Spine, 12: 726-731, 1987.
8. Mimura et al : 3D Motion Analysis of the Cervical Spine .... Spine 14: 1135-1139, 1989.
9. Panjabi et al : 3D Load-Displ. Curves ... Cervical Spine. J. Orthop. Res. 4: 152-161, 1986.
10. Merrill et al : 3D Response of a ... Head-Neck Model .... J. Biomechanics 17: 81-95, 1984.
11. Williams JL: comment on Deng and Goldsmith (1987b). J. Biomechanics 21: 687-692,1988.
12. Liu YK: Problems in the ... Modelling of Head and Neck Injury. Proceedings of Head and Neck Injury Criteria: A Consensus Workshop, Washington D.C., March 1981, pp 125-132.
13. Panjabi MM, White AA: Biomech. of ... Cervical Spinal Cord Trauma. Spine 13: 838-842, 1988.
14. Dvorak et al : Funct. Evaluation of Spinal Cord ... Cervical Spine. Spine 14: 1057-1064, 1989.

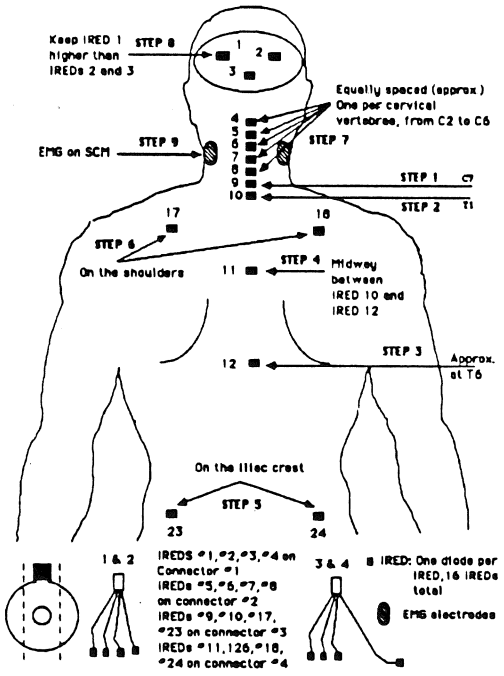


Fig 1(a): Cervicscope IRED and EMG placement.

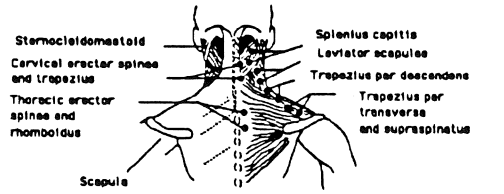


Fig 1(b): Suggested locations of EMG electrodes for measuring cervical muscle activity. Adapted from Schuldt and Harms-Ringdahl (1988). [1]

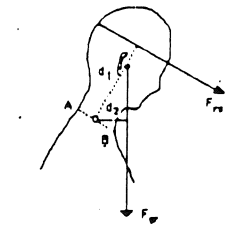


Fig 2(a): Moment calculations

F_{rs} = resistance force
F_g = gravitational force
d_1, d_2 = moment arms
M_m = muscle moment

$\therefore M_m = d_1 F_{rs} + d_2 F_g$

Adapted from Schuldt and Harms-Ringdahl (1988). [1]

Fig 2: Examples of moment calculations, determination of load distributions, and muscle insertions for models of the cervical spine.

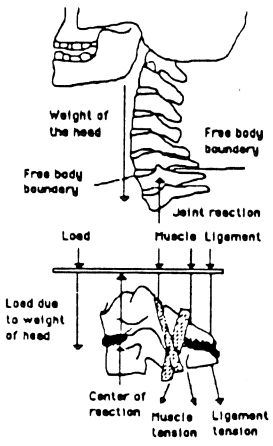
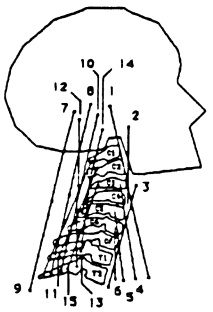


Fig 2(b): Free body analysis of an intervertebral joint in the lower cervical spine, showing load distribution. Adapted from Helleur et al. (1985). [3]



1 Sternocleidomastoid
2 Longus capitis
3 Longus colli
4 Scalenius anterior
5 Scalenus medius
6 Scalenus posterior
7 Trapezius
8 Splenius capitis
9 Splenius cervicis
10 Spinalis capitis
11 Spinalis cervicis
12 Semispinalis capitis
13 Semispanalis cervicis
14 Longissimus capitis
15 Longissimus cervicis

Fig 2(c): Three point muscle insertions for the head/neck model of Merrill, Deng, and Goldsmith. Adapted from Deng and Goldsmith (1987). [3]

BONE GRAFT TRANSLATION OF FOUR UPPER CERVICAL SPINE FIXATION TECHNIQUES IN A CADAVERIC MODEL

Joseph J. Crisco III, PhD, Manohar M. Panjabi, PhD, Takenori Oda, MD, Dieter Grob, MD, and Jiri Dvorak, MD. Biomechanics Laboratory, Department of Orthopaedics and Rehabilitation, Yale University School of Medicine, New Haven, Connecticut, 06510

INTRODUCTION AND REVIEW

The goal of spinal fixation is to promote bony fusion by restricting motion at the site of the bone graft. However, previous researchers have studied only motion at the point of load application and motion of the whole vertebral body in one, two, and three dimensions. In order to evaluate the efficiency of various cervical fixation techniques, which was the goal of this study, we determined translations at the posterior arch of C1 for four C1-C2 posterior techniques: Gallie (1938), Brooks (1978), Magerl (1986), and Halifax (Tucker, 1975). We assumed that translational laxity or micromotion was the critical motion parameter and evaluated this parameter, quantified herein as the neutral zone, at seven points along the graft site. We found that there was no significant difference with fixation technique in the average axial translation. In shear translation, the Magerl averaged 1 mm which was significantly less than the Gallie (2.1 mm). The Brooks and Halifax were not different from each other, Magerl, or Gallie.

METHODS

Ten fresh human cadaveric (avg. age 52 yrs.) cervical (C0-C3) specimens were obtained. We applied pure moments of flexion /extension (±Mx), left/right axial rotation (±My), and right/left lateral bending (±Mz) in each test. Moments were applied in three cycles of 0.5 Nm steps to a maximum of 1.5 Nm. Using stereophoto/radiography, the three-dimensional vertebral motion of C1, with respect to C2, was determined relative to the anatomical coordinate system of Figure 1. The load-displacement curve of the third cycle consisted of approximately two linear ranges or zones. The first zone was one of negligible stiffness (laxity), which we quantified as the neutral zone (NZ). From this data the translational NZ at the vertebral points A, B, C,D, E, F and G were calculated (Figure 2). The specimens were tested intact, injured, and after being instrumented with each fixation technique. The injury consisted of the transection of the tectorial membrane, transverse, alars, and left capsular ligaments of C1-C2.

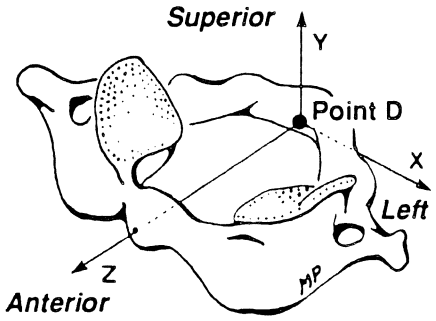


Figure 1. C1 coordinate system.

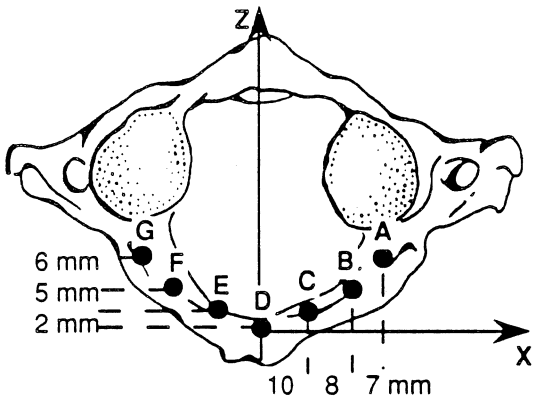


Figure 2. Translations were determined at these points along the bone graft.

RESULTS

The relative translation at each point reflected the structural design of the fixation technique. With Brooks and Magerl, the principal fixations were lateral grafts and lateral intra-articular screws, and we found that the translations decreased with lateral position. Whereas, the Gallie is a midsagittal technique, and the translations increased with lateral position. With the Halifax, which consisted of bilateral clamps, the translations were fairly constant across the seven points. We evaluated the statistically (ANOVA,Fischer LSD post-hoc) significant difference in the translations at each point. We

found no significant difference in the axial translations (Y direction) at any of the points. In the shear translation (XZ plane), however, there were significant differences. We found that the shear translation at the lateral Points A, B and G of the Magerl were significantly ($p<0.05$) less than those of Gallie. At Points C and F, Magerl allowed less motion than Gallie but at a significance of $p<0.1$. Brooks and Halifax were not significantly different from either Gallie or Magerl at any point. When comparing the average of the seven points, only the Magerl allowed significantly ($p<0.05$) less shear translation than the Gallie.

Table 1. The shear and axial translations (mm) averaged over Points A,B,C,D,E,F, and G. The values are the means and standard deviations of all specimens (n=10: Brooks Magerl, Gallie; n= 5: Halifax).

	BROOKS	MAGERL	GALLIE	HALIFAX
shear	1.60 [1.2]	1.17 [1.0]	2.09 [0.9]	0.99 [0.4]
axial	1.07 [0.9]	1.26 [1.0]	1.47 [0.7]	0.53 [0.2]

DISCUSSION

A commonly stated goal of any fixation technique is to provide stability. Although no clinical definition of stability is commonly accepted, fixation is generally deemed successful if fusion occurs. In long bones, the "maintenance" of "good approximation" of fragments, ie. the restriction of motion, has indicated successful fusion (Chao et al, 1989). The required "maintenance" and threshold of "good approximation" are, quantitatively, elusive parameters. Joint laxity (NZ), and not ROM, has been demonstrated to correlate with clinical instability of the knee (Markolf, 1976). We have applied this same philosophy to our study of fixation techniques by reporting the neutral zone translations, a quantitative measure of laxity or micromotion. Upon averaging the axial translation across the posterior arch (Table 1), we found that there was no significant difference with fixation technique. One may extrapolate this result to the clinical setting; with the assumption that axial micromotion is beneficial to healing, our results reflect the clinical experience that each technique has successfully promoted fusion.

Correlating the NZ measured *in vitro* with pseudoarthrosis in the spine is presently not possible because of the difficulty in measuring *in vivo* spinal motions. However, there appears to be a correlation between our experimental results and the clinical work on femur neck fractures by Rehnberg et al.(1989) - if we use their value of 1.3 mm as a threshold for shear translation. We found the Gallie had an average shear NZ translation of 2.1 mm, and clinically the largest number of nonunions: eight out of ten were reported by Fried (1973), and fourteen out of fifteen were reported by McGraw (1973). Much better clinical results, nonunion in one out of thirty patients (Griswold et al., 1978), have been reported with the Brooks technique which, in our study, had a translational neutral zone of 1.6 mm. To the best of our knowledge, there have been no reported nonunions with the Magerl or Halifax techniques. In our experiment, these were the only techniques that had average NZ translations less than 1.3 mm (1.17 and 0.99 mm, respectively).

In contrast to other testing philosophies, we believe the present concept has several advantages. The principal advantage is that the analysis at the graft site, rather than at the point of load application or an analysis of the whole vertebral body, may provide deeper insight into the mechanical environment provided by the fixation technique. We also believe that reporting results in terms of displacements (neutral zone, micromotion, etc.) is more comprehensive than reporting stiffness value, for example. It is also important to note that three-dimensional testing is essential for any complete study involving spinal fixation techniques.

REFERENCES

Brooks et al. *J Bone Joint Surg* 60-A:279-284, 1978
Chao et al. *Clin Orthop* 241:24-35, 1989
Fried *J Bone Joint Surg* 55-B:490-496, 1973
Gallie WE *Am J Surg* 46:495, 1939
Griswold et al. *J Bone Joint Surg* 60-A:285-292, 1978
Magerl et al. In: *Cervical Spine I*, ed by Kehr and Weidner, Springer Verlag, 1986, pp 322
Markolf et al. *J Bone Joint Surg* 58-A:583-593, 1976
McGraw et al. *J Bone Joint Surg* 55-B:482-489, 1973
Rehnberg et al. *J Bone Joint Surg* 71-B:173-177, 1989
Tucker *Can J Neurol Sci* 2:381-382, 1975

Acknowledgements: Research supported in part by NIH Grant AR30361 and SGO-Foundation, Switzerland.

ESTIMATION OF CERVICAL DISC PRESSURES INDUCED BY MUSCLE ACTUATOR FORCES IN AN ANTHROPOMORPHIC MODEL AFFIXED TO A HALO

William A. Peterson and Jack M. Winters
Bioengineering Program, Department of Chemical, Bio & Materials Engineering
Arizona State University, Tempe, AZ 85287-6006

INTRODUCTION

Very little is known about the influence of muscle activity on internal loading within the cervical spine. As the relative muscle activity between various neck muscles change, it would be expected that the internal loading distribution (e.g. disc pressures) would change as well. An injured spine would be expected to be especially sensitive to such muscle forces, which may function to create movement and/or serve as a splint to help stabilize a region of the spine. A common method for treating severe cervical injuries is to place the individual in a halo. Little is known about the interplay between the halo orthotic, the type of injury, muscle activity, and the effects of body posture. In this study a halo orthotic is placed on a carefully constructed anthropomorphic replica by a trained orthotist. The influence on measured disc pressures throughout the cervical spine due to various combinations of muscle contractions and body orientations within a gravitational field is investigated.

REVIEW AND THEORY

Since originally introduced in 1959 [1], the halo orthotic device has evolved into one of the primary modes of treatment for the severely injured spine. The halo orthotic device consists of a halo ring mechanically coupled to the skull via skull pins, a vest that is attached to the torso, and a mechanical bar linkage system that couples the ring to the vest. Typically the halo is mounted with traction while the individual is supine. In general, the halo has been a remarkably successful device with regards to rehabilitation, but there have been problems. One study [2] has shown that cervical spine motion while supported in a halo can be extensive and that often the neck is not in traction, but actually in compression for certain tasks. Additionally, the role of muscles is unknown.

The goal of our group has been to estimate internal loading within the neck by using several techniques, and then utilize this information to establish causal relationships between head orientation, the amount of traction, the type of injury, muscle activity, and various movement tasks. Here we present data from an anthropomorphic model that correlates muscle actuator activity to measured intervertebral disc pressures.

PROCEDURES

An anthropomorphic replica of the head-neck-torso-pelvis system was constructed that included 55 artificial bones, appropriate ligaments and discs, and 63 muscle actuators. Each tissue was fabricated to simulate the shape and mechanical properties of the actual biological tissues as closely as possible. The model was mounted at the pelvis to a linkage system that allowed the pelvis to be oriented in various postures. Calibrated pressure transducers (Precision Measurement, Sensym) were embedded into the superior surface of the cervical and upper thoracic vertebrae with the sensing element facing upward into the cavity representing the nucleus pulposus. After attachment of the vertebrae via a "disc" (annular meshes embedded with silicone rubber) and appropriate drying time, the disc interior was pressurized to 50 KPa using mineral oil and a syringe needle. The air was evacuated using a second syringe. Appropriate ligaments and muscles were also attached. The muscle actuators shortened when pressurized. These cylindrically-shaped units included an internal silicone rubber bladder surrounded by a braided nylon mesh. Under a given excitation pressure, they exhibited spring-like length-tension behavior reasonably similar to biological muscle. In all, there were 56 muscles of interest crossing the cervical region. Three-dimensional motion analysis of the cervical vertebrae was obtained using four markers attached to a small tree structure whose base was screwed into strategic bodies.

Upon completion of the model and some preliminary testing, a halo was affixed to the skull and torso by an experienced orthotist. The model was placed in three different positions: prone, supine, and sitting. For each position, a total of seven muscle contraction strategies were performed: flexion (two combinations), extension, shoulder shrug, right axial rotation (two combinations), and massive co-contraction. Each of these were conducted under two levels of muscle excitation pressures, 25 psi (172 KPa) and 50 psi (344 KPa). A total of 30 independent runs were made. Of primary interest here was how disc pressures change as a function of relative muscle activity and model orientation.

RESULTS AND DISCUSSION

For this paper, only two representative muscle strategies, extension and flexion (strategy 1), will be looked at while both supine and sitting. The extension strategy included the semispinalis capitis, splenius capitis, longissimus capitis, the semispinalis cervicis, splenius cervicis, and longissimus cervicis. Flexion strategy 1 includes the sternocleidomastoid, the logus coli muscles, and the longus capitis. Tables 1 and 2 list the observed disc pressure changes, with positive values representing a compressive strain while negative values indicate tension. The pressure values are not absolute pressures, but instead are the change in pressure from beginning to end for each muscle strategy. Notice that gravity has a large influence on disc pressures. In almost every instance, disc pressure changes are larger (in compression) while sitting verses supine. It should be noted that any change in disc pressure is a result of vertebral motion. The large values seen in the upper region are most likely due to the large number of muscle origin sites located close by. From a simple mechanical perspective these results suggest that the axis of rotation for each vertebra - in both flexion and extension - is located somewhat posteriorly from the center of the vertebral body. From our results it is clear that, even with a halo attached, changes in internal tissue loading occurs as a function of both muscle contraction levels and orientation within the gravitational field.

Table 1. Extension @ 50 psi

level	sitting	supine
C2-C3	14.3 KPa	2.8 KPa
C3-C4	10.5 KPa	3.3 KPa
C4-C5	1.7 KPa	-0.1 KPa
C5-C6	0.1 KPa	-0.3 KPa
C7-T1	0.9 KPa	1.6 KPa
T1-T2	0.5 KPa	-0.1 KPa
T2-T3	0.9 KPa	1.2 KPa

Table 2. Flexion @ 50 psi

level	sitting	supine
C2-C3	73.0 KPa	30.0 KPa
C3-C4	62.0 KPa	50.0 KPa
C4-C5	24.0 KPa	23.0 KPa
C5-C6	13.0 KPa	12.0 KPa
C7-T1	6.7 KPa	5.2 KPa
T1-T2	7.3 KPa	4.3 KPa
T2-T3	-0.9 Kpa	-2.1 KPa

ACKNOWLEDGEMENTS

This project was funded by grants from the U.S. Dept. of Education (Nat. Inst. of Disab. & Rehab. Res. #H133C90140-89) and from the Ace Medical Company. The collaborative assistance of Dr. Volker Sonntag, M.D. and George Mattingly, C.O., is gratefully acknowledged.

REFERENCES

1. Perry, J. and Nickel, V.L., "Total Cervical-Spine Fusion for Neck Paralysis", J. Bone & Joint Surgery, 41-A: 37-60, 1959.

2. Koch, R.A. and Nickel, V.L., "The Halo Vest. An Evaluation of Motion and Forces Across the Neck", Spine, 3: 103-107, 1978.

AN INSTRUMENTED, PHYSICAL SPINAL CORD MODEL FOR *In situ* PRESSURE MEASUREMENT

Michael B. Schlick, Frank A. Pintar, Narayan Yoganadan,
Dennis J. Maiman, Anthony Sances, Jr.

Department of Neurosurgery, The Medical College of Wisconsin, Milwaukee, WI 53226
Department of Veterans Affairs Medical Center, Milwaukee, WI 53295

INTRODUCTION

Spinal cord injury continues to be significant in terms of societal cost and impact on the individual. The differences in the patterns of cord and bony trauma range from severe vertebral fracture with no cord trauma to significant neurologic deficit with no associated vertebral fracture. The mechanisms of injury to the cord are still poorly understood. Recently, an experimental protocol developed in our laboratory was found to produce clinically relevant mid to lower cervical spine injuries in the cadaveric head-neck preparation under dynamic loading (Pintar, *et al*) The present research is aimed at developing an instrumented, artificial spinal cord that can be used to gather quantitative cord pressures while experimental injury is produced using the above protocol.

MATERIALS AND METHODS

The Collagen Encased Gelatine Cord Model (CEG)

The initial step in producing an instrumented spinal cord is to identify the mechanical properties of the cord tissue. As reported by Blight, a 12% gelatine mixture has the consistency and feel of spinal cord material. This was tested quantitatively in the laboratory by comparing the material properties of various gelatine mixtures to that of human as well as animal spinal cords. The gelatine was encased in collagen casings to simulate the sheathing properties of the dura mater without the typical qualities of other materials such as latex®, silastic®, etc. The gelatine's percentage was adjusted until the spinal cord material properties were reproduced, resulting in a range of the gelatine's firmness.

Drop tests similar to those first reported by Allen were used to compare the properties of the collagen encased gelatine cord model (CEG) to that of spinal cord tissues. The CEG was compared to human data from an adult male just hours *post mortem, in situ* at C-4. In order to acquire *in vivo* data, anesthetized cats were used with the vertebrae clamped superiorly and inferiorly at the lower-thoracic, mid-thoracic, and upper-thoracic levels. The CEG was tested in a plexiglass® tube with an approximately 2 cm transverse hole as a "laminectomy" while the tube sat rigidly on a table. The 150 gm drop mass assembly, used in all tests, had a circular impact surface area machined to 1 cm^2 and an affixed accelerometer. This mass was dropped from a 2 cm height onto the human cadaver cord, *in vivo* cat cord, and the CEG while the acceleration was measured. By integrating the acceleration-time curve twice, the displacement-time curve was obtained; by multiplying the acceleration-time curve by the mass, the force-time curve was obtained.

The Transducers

In order to instrument *in situ* a very thin, pressure sensitive transducer was developed utilizing 110 μm thick piezoelectric film. The Kynar® Piezo Film, is sensitive to pressures with a wide frequency range: from quasistatic to giga Hertz, and produces a proportional charge per area when a stress is applied. To measure discrete points and still have enough surface area for the film's signal to be effective, each sensor was cut in 1 cm square pieces and attached to identical pieces of stainless steel to prevent bending. The piezoelectric film was

fashioned into seven individual sensors, to obtain independent pressure data at each level along the length of the cord. The sensors were spaced 1.5 cm apart (the average distance between vertebral bodies as indicated through x-ray and cryosection analysis) held in place and sealed water-tight. Soaking the complete sensor array in normal saline for 5-6 hours tested the seal. The array then lays parallel on the outer surface of the CEG such that antero-posterior pressures are sensed. They were calibrated by placing them on a flat, smooth, rigid surface and dropping a flat, smooth impounder, fitted with an accelerometer, onto them. The force per unit area of the impounder was compared to the force per unit area of the transducers.

RESULTS AND DISCUSSION

In order to compare the force/displacement properties of the cat, the human, and the gel spinal cords, of different diameters, the force of the applied impounder was normalized with respect to the percentage of compression. A very firm gelatine mixture was seen to be the stiffest, next was the human data, followed by the cat data. Finally a soft mixture of the gelatine was observed as the least stiff of the materials tested. With the gel mixtures enveloping the real cords data, simply fine tuning the mixture reproduces the appropriate material characteristics. Neither the gel, the cat cord nor the human cord was seen to rise more than 5 N before they were compressed by more than 50%. It is not until they are compressed 60-80% that the force starts to increase appreciably. Recently the drop test apparatus was scaled down in mass and surface area as well as fitted with a linear potentiometer to give displacement more directly. The acceleration-time history was double integrated and compared to the displacement-time history and were found to correlate well.

The transducer array connects directly to seven separate Kistler® charge amplifiers, model 5004. Each of the sensors can be individually calibrated by independently adjusting the charge amplifiers' sensitivity setting according to the impounder data for a precise match. Before the final construction of the CEG with the instrumentation array each transducer is calibrated. After an experiment is conducted the transducers can be removed and recalibrated for consistency.

In vitro experiments with the CEG and the transducer array are used to further validate the sys-tem. Various drop tests on the *in vitro* system will determine the magnitude and propagation of traumatic forces on the cord. The CEG and transducer system has been used *in situ* during a testing protocol described by Pintar *et al* to examine its robustness and practicality of use. The system withstood the experimental environment and initial data demonstrated the pressures associated with the applied trauma were approximately ten times higher in magnitude than those produced before and after with simple physiologic flexion and extension motions.

An *in situ* measurement of the pressures directly on the spinal cord will greatly enhance cord injury study. The adjustability of this CEG model as well as its simplicity and availability of materials lend it to a wide range of uses.

ACKNOWLEDGMENT

This research was supported in part by PHS CDC Grants R49CCR703640, R49CCR502508 and Department of Veterans Affairs Medical Center Research Funds.

REFERENCES

Allen AR: JAMA 11; pp 878-880, 1911.
Blight A: Syp S C Inj Mods, pp 26-34, 1987.
Pintar FA, et al: SAE Paper #902309, pp 55-72, 1990.

THE ONSET AND PROGRESSION OF SPINAL INJURY IN A PORCINE FLEXION-COMPRESSION TRAUMA MODEL

T.R.Oxland and M.M.Panjabi
Biomechanics Lab, Dept. of Orthopaedics and Rehabilitation
Yale University School of Medicine
333 Cedar St., New Haven Ct. 06510

INTRODUCTION

Traumatic injuries to the spine are a significant problem in today's society. It is well recognized that most spinal injuries are not bony fractures [Allen et al 1982], and that many "subacute" injuries have potentially hazardous consequences [Herkowitz & Rothman 1984]. Improvements in the clinical diagnosis and treatment of spinal injuries can be made by a better understanding of the acute spinal injury mechanisms and the resultant instabilities. For spinal injury diagnosis, a critical question is what defines injury? Clinically, injury is probably described best by White and Panjabi [1990] where the spine is considered unstable if, under physiological loads, it results in abnormal motion patterns, neurologic deficit, excessive deformity and/or pain. The goal of this study was to document the onset and progression of spinal injury in a flexion-compression porcine trauma model. By defining spinal injury in terms of several different spinal flexibility parameters, the parameter which was the best measure of injury was determined.

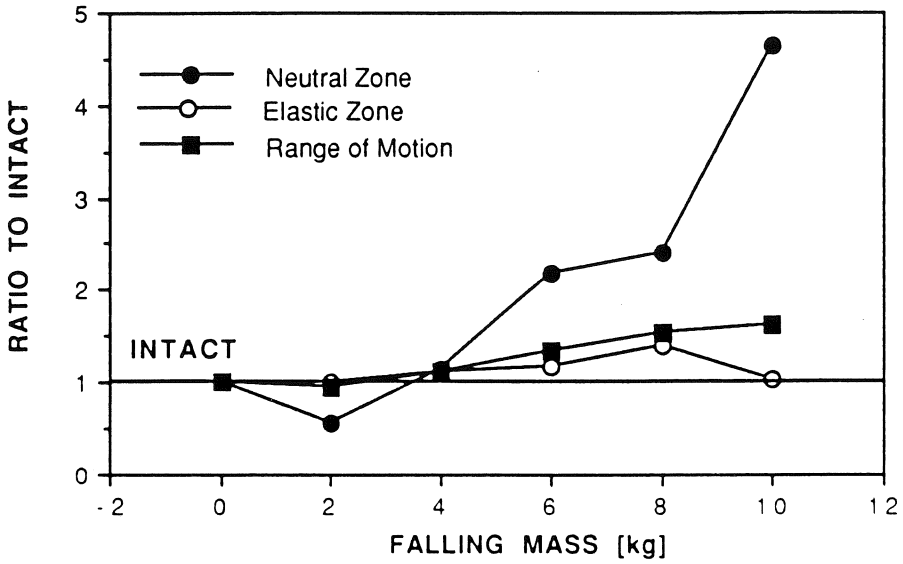
METHODS

Six lower cervical porcine spine specimens (C4-C6) were dissected of all nonligamentous soft tissue and mounted in polyester resin casts (Plastic Padding, Gothenburg, Sweden) such that their vertebral body centroids were aligned vertically. The porcine cervical region has vertically oriented facets and extensive posterior ligaments, similar to the human lumbar region [Oxland et al 1991]. Flexion-extension flexibility tests were performed on each intact specimen by the application of anterior and posterior shear forces to the top of the specimen. Maximum moments of 3.2 Nm were applied stepwise in three load cycles. Rotation of the top vertebra was measured by an Angular Displacement Transducer at each load step of the third load cycle. Flexibility parameters: Neutral Zone (NZ), Elastic Zone (EZ) and Range of Motion (ROM), were calculated in both flexion and extension for each test. The NZ was the displacement from the neutral position under zero load on the third load cycle. The EZ was the displacement from the zero load position to the position under the maximum load. The ROM was the total displacement, and therefore the sum of the NZ and EZ. Incremental impacts of increasing severity were performed, and after each impact the flexibility test was repeated. The testing for each specimen was completed when the injury was too severe for subsequent trauma. A specially-designed apparatus was used to perform the high-speed impacts. This apparatus consisted of a mass falling from a 1 m height through a Plexiglas tube onto an impounder placed on top of the specimen. The mass was variable from 2.3 kg to 10.3 kg in 2 kg increments. To define the point of load application, a cylindrical interface was placed on the top padding, directly below the impounder. To produce the flexion-compression loads for this study, the cylinder was placed 5 mm anterior to the balance point. Statistically significant changes in the flexibility parameters with increasing injury were tested using a Factorial Analysis of Variance and post-hoc Scheffe's F-test at a 95% significance level.

RESULTS

The flexibility parameters of flexion NZ, EZ and ROM relative to their intact values are plotted against increasing impact mass in the Figure. Note that with increasing impact mass, the relative increase in both ROM and EZ was very small compared to the dramatic increase in the

NZ. Upon closer investigation, the EZ actually decreased with the largest impact mass. The increases in the NZ from 4 to 6 kg and 8 to 10 kg were statistically significant. The ROM values at 8 and 10 kg were significantly different from its values at 0, 2 and 4 kg. None of the changes in the EZ were significant. There were no significant changes or trends in the extension flexibility parameters with increasing injury.



The anatomic lesions produced by these impacts were not grossly observable vertebral fractures, ligament ruptures or annulus tears. The only exception was at the largest impact energy (10 kg drop mass) where some externally observable ligaments (ie. interspinous and supraspinous, anterior longitudinal ligaments) were ruptured in some specimens.

DISCUSSION

An unconventional aspect of this study was the application of multiple impacts with sequentially larger energies to each specimen. Our philosophy in adopting such an approach was to objectively monitor the onset and progression of spinal injury in a high speed trauma model. The effects of increasing injury on the response of three flexibility parameters: NZ, EZ and ROM, were determined. The NZ was found to be the most sensitive parameter in detecting increases in spinal motion and therefore spinal injury. The ROM did detect a statistically significant increase in the spinal injury but at a higher load level than the NZ. The EZ did not change significantly after any impact load. Interestingly, after the 10 kg mass impacts, the EZ decreased. The variation in the NZ, EZ and ROM have some interesting ramifications for the pattern of injury to an intervertebral joint. The NZ is a measure of the laxity of the entire joint complex, while the EZ is a measure of stiffness of the intervertebral joint beyond the initial lax region. The different responses of these parameters to injury are due to the nonlinear characteristics of the materials comprising the intervertebral joint.

REFERENCES

Allen, Jr., B. L. et al. (1982) *Spine* 7:1-27.
Herkowitz, H. N. and Rothman, R. H. (1984) *Spine* 9(4):348-357.
Oxland, T. R. et al (1991) *J Orthop Res* 9:452-462.
White, A. A. and Panjabi, M. M. (1990) *Clinical Biomechanics of the Spine*. Second Edition.

SESSION 7

KNEE JOINT

BASIC MECHANICAL STRUCTURE OF THE KNEE: A KINEMATICALLY UNCONSTRAINED BIOMECHANICAL GEAR SYSTEM WITH FORCE LOCKED STABILITY.

D. KUBEIN-MEESENBURG Department of Orthodontics, Univ. of Göttingen
H. NÄGERL Department of Physics, Univ. of Göttingen.
J. FANGHÄNEL Institue of Anatomy, Univ. of Greifswald
Germany

In order to describe the mechanical structure of the knee one cannot merely look at the function of the tibiofemoral joint. The articulating function of the patellar tendon and the patellofemoral joint have to be taken into account at the same time because the biomechanical function of the knee is given by the static, kinematic, and dynamic interaction of *three* rigid bodies: tibia, patella, and femur.

We derive from the morphology of the mutual articulating surfaces the fact that in the sagittal plane interactions between patella and femur as well as between femur and tibia can be explained by an overlapped dimeric link chain (1). Overlapped dimeric link chains are only stable in the presence of compressive forces. The patellar tendon represents a stretched, therefore tensionally stable, dimeric link chain. These three chains are linked to each other, forming an unconstrainedly closed kinematic chain that consists of 6 links and 6 hinges (fig.). The chain is overly mobile: It possesses three degrees of freedom. Being influenced by forces (force locking) the system can become constrained (one degree of freedom) or rigid (no degree of freedom). In squat position e.g. the system turns into an octangle that consists of five dimeric and two tenary link chains due to the effect of the m. quadriceps and gravity. In this function the system is movable upwards but rigid downwards. The angle of squatting directly depends on the length of the m. quadriceps. This gear system is closely related to th constrained Stephenson-mechanism (which has been used by the gearing of the early steam locomotives).

The analysis of the acting forces and torques and of the kinematics of the system indicates that in every sqat position the interacting force between patella and femur is only horizontally aligned if the patellar tendon is of individually specific length.

The adaptability of the knee to diverse functions is rendered possible by the overly mobile link chain that takes on diverse guiding functions according to the geometrical structure of the applying force system.

In contrast to the link quadrangle of the crucial ligaments (as described in literature, e.g. 2,3) that neglects the guiding function of the force transferring articulating surfaces and of the tensional loaded patellar tendon, the presented system describes the diverse functional states of the entire knee.

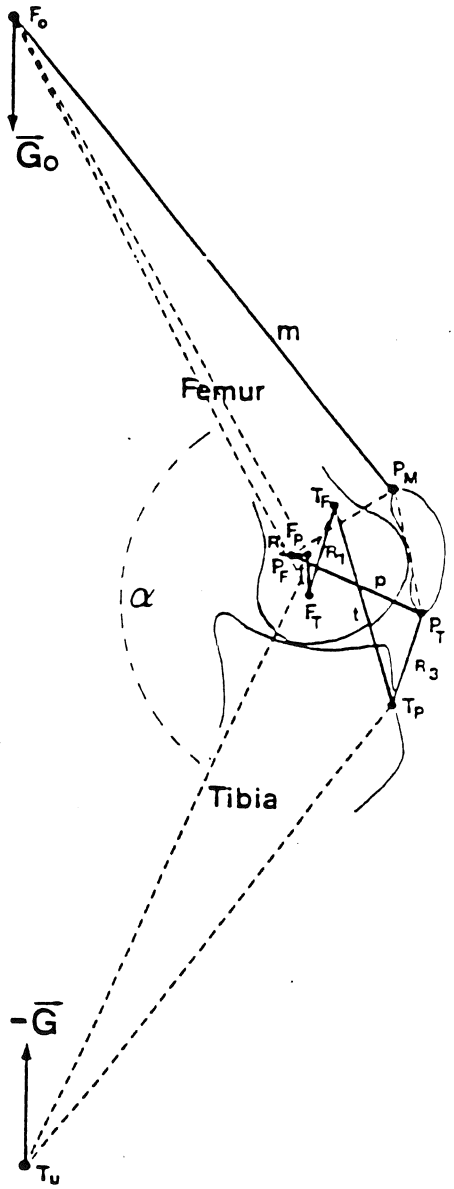
Computer simulations confirm these qualitative contemplations. The complex interaction between muscular forces, gravity, and gear system will be exemplified by means of experiments on models in the course of the lecture.

References.

(1) Kubein-Meesenburg, D., Nägerl, H. and Fanghänel, J.: Elements of a General Theory of Joints. 1. Basic Kinematic and Static Function of Diathroses. Anat. Anz., Jena, 170, 301-308 (1990).
(2) Huson, A.: The functional anatomy of the knee joint: the closed kinematic chain as a model of the knee joint. Proc. int.Congr.: The knee joint No. 324, p. 163-168 (1973).

(3) Menschik, A.: Mechanik des Kniegelenkes. 1. Teil. Z. Orthop. 112 (1974), S. 481 - 495.

Fig.: **The knee joint in squat position (sagittal function).**
The guiding function of the knee is given by a kinematically unconstrained sexangle ($P_T P_F F_P F_T T_F T_P$) consisting of three dimeric link chains: R_1 (femur-tibia), R_2 (femur-patella), R_3 (patella-tibia: patellar tendon). F_T and F_P are centers of curvature of the femoral articular surfaces; P_F = the center of curvature of the patella; T_F= center of curvature of the tibia. The external forces $\overline{G}_0$ and $\overline{G}$ produce the minimum bending angle α. Then the single links R_1, R_2, R_3, p,t,f of the chain are in mechanically stable locations compelled by the external forces. R_1 and R_2 are loaded by compressive forces, R_3 by tension. The bending angle α depends on the location of the point P_M that is given by the m. quadriceps. $\alpha = \alpha(m)$ is a function of the length m of this muscle. The entire system is in a mechanically stable equilibrium.



DYNAMIC ANALYSIS OF A FUNCTIONAL KNEE BRACE AND A PREVIOUS ACL INJURY

Paul DeVita, Pamela Hunter and William A. Skelly
Department of Physical Education, Southern Illinois University
Carbondale, Illinois 62901

INTRODUCTION

Effects of a functional knee brace (FKB) on lower extremity joint moments during the stance phase of running were examined in subjects with a previous Anterior Cruciate Ligament (ACL) injury. The moments from the ACL subjects were also compared with those from healthy runners. Results showed that the FKB had no effect on the moment patterns in the ACL subjects. Distinct differences between the healthy and ACL subjects were observed with the ACL group having greater extensor moments at the hip and ankle and a smaller extensor moment at the knee.

REVIEW AND THEORY

FKBs are often used by individuals who have had severe ACL injury to provide support for the limb. However, few analyses of FKB effects on lower extremity kinetics have been reported. One study identified larger ground reaction forces during the impact phase of running while wearing FKBs (4). To our knowledge there have been no investigations of FKB effects on internal limb kinetics during gait. Also, the adaptations used by ACL injured subjects are not well documented as only one study (2) has reported the internal lower limb kinetics for these subjects. The purposes of this study were to assess the effects of a FKB on joint moments in the lower extremity during the stance phase of running in subjects with a previous ACL injury and to compare these moments with those from healthy subjects.

METHODOLOGY

Five subjects (mean mass 80 kg, age 24 years) with a history of unilateral ACL injury and five healthy subjects (mean mass 68 kg, age 27 years) volunteered for the study. All ACL subjects were at least one year post-operative. Experimental setup consisted of a force platform, timing system to monitor running speed (3.83 m/s) and a 16 mm cine camera. ACL subjects were tested with and without a FKB. Healthy runners were tested without the FKB. Inverse dynamic analysis was used to calculate stance phase moments at ankle, knee and hip. 9 trials per subject/condition were analyzed. Extensor angular impulse values were calculated from each moment curve and entered into a mixed, two factor ANOVA to identify differences ($p<.05$) between the three experimental groups: ACL - no brace, ACL - brace, and healthy runners.

RESULTS AND DISCUSSION

Figure 1 shows the mean moment curves from all subjects and conditions. The moment curves were nearly identical between the brace and no brace conditions for the ACL subjects. The FKB therefore did not affect the kinetics of the lower extremity in the previously injured runners. In contrast, there were large differences between the healthy and ACL subjects. The extensor angular impulse, on average, was 49% and 32% larger (both $p<.05$) at the hip and ankle joints in the ACL group. Alternatively, the healthy runners had a 233% larger ($p<.05$) extensor angular impulse at the knee joint.

The similarity in the moment curves between conditions for the ACL group suggests that these subjects may have accommodated to their FKB during the rehabilitation period. During this time the subjects may have learned the observed moment patterns associated with the FKB and may now use these

patterns when running without the brace. During the early post-operative phase, differences between the brace and no brace conditions may have existed and further research into the learning effects due to wearing the FKB seems warranted.

The reduced knee moment in the ACL group was in agreement with results of Berchuck et al (2) who identified lower extensor moments at the knee in ACL injured subjects compared to healthy runners. Results were also in agreement with EMG studies on ACL injured subjects which showed increased hamstring (3,6) and decreased quadriceps activity (3) during gait and in isokinetic tests. ACL loads and anterior tibial displacement are related to moments produced by the quadriceps and hamstrings (1,5). Larger knee extensor moments place greater loads on the ACL and tibia while larger moments by the hamstrings reduce these loads. The observed gait adaptations of reducing the extensor torque at the knee and compensating by increasing the extensor torques at the hip and ankle therefore reduced the stress on the ACL and tibia while at the same time enabled the ACL subjects to run at the required speed.

REFERENCES

1 Arms, et al. American J. Sports Medicine, 12: 8-18, 1984.
2 Berchuck, et al. J. Bone and Joint Surgery, 72-a: 871-877, 1990.
3 Grabiner, et al. Proceed. 13th annual American S. Biomech: 140-141, 1989.
4 Knutzen, et al. Medicine & Science in Sports and Exer, 19: 303-309, 1987.
5 Renstrom, et al. American J. Sports Medicine, 14: 83-87, 1987.
6 Shiavi et al. Proceed. 5th biennial Canadian S. Biomech: 142-143, 1988.

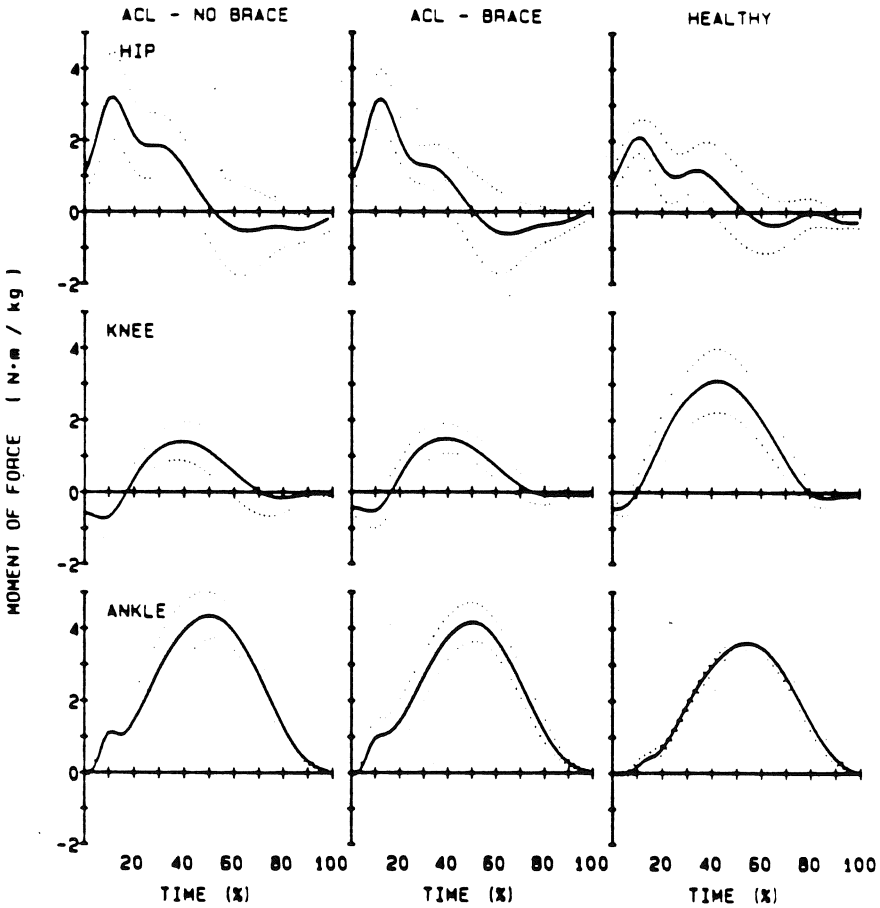


Figure 1. Mean joint moment curves for each experimental group averaged over all subjects and trials and normalized for body mass. Dotted lines are +/- 1 SD. Positive values are extensor or plantarflexor moments.

FORCES AND MOMENTS ON THE LEG DURING SKIING JUMP MANEUVERS

A. G. Yee and C. D. Mote, Jr.
Department of Mechanical Engineering
University of California, Berkeley
Berkeley, CA 94720

INTRODUCTION

The forces and moments on the leg at the boot top and knee during ski jumps are discussed. Time histories and maximum values of forces, moments, ankle flexion, and knee flexion are presented.

REVIEW AND THEORY

Severe (third-degree) knee sprains in skiing increased in frequency by 172% between 1972 and 1987 (Johnson et. al, 1989). These injuries usually involve rupture of the anterior cruciate ligament (ACL). One proposed mechanism of ACL disruption is anterior drawer, which is proposed to occur when a skier lands on the ski tails after a jump maneuver (McConkey, 1986). This proposed injury mechanism motivates study of forces and moments on the leg during jumps.

PROCEDURES

Skiing experiments with jumps were conducted at Donner Ski Ranch, California during April 20-22, 1991. Two 0.3 m high ramps made of snow were built 12 m apart down a 12 degree slope. Five subjects skied the course a total of 19 times; they jumped at the top of each ramp and landed on the ski tails. Figure 1 shows the experiment sensors. Two six degree of freedom dynamometers located under the toe and heel bindings of the left ski measured the complete force and moment at the boot toe and heel. Rotary potentiometers measured ankle and knee flexions. Three accelerometers measured linear acceleration of the boot, and three transducers measured angular velocity. Surface electromyogram signals from three muscle groups of the shank and thigh were also recorded, but are not used here. As the subject skis, the data are transmitted via telemetry to a ground station .

RESULTS

Force and moment components are defined to be acting on the boot/foot/shank system; see Figure 2 for force and moment directions.Typical time histories during a jump are shown in Figure 3. Table 1 shows the peak values of selected force and moment components that occur on landing. Duration of the peak is defined to be the time interval separating half the maximum force magnitudes.

DISCUSSION

Maximum values of the force and moment components at the knee and boot top are generally in the same range as those presented by Quinn and Mote (1991) for normal slalom skiing. However, maximum $-F_z$ on the tibia at the knee was 4340 N and maximum $-M_y$ on the tibia at the knee was 621 Nm; these values are 244% and 204% larger than their corresponding values reported by Quinn and Mote (1991). These maximum values are of short (≈ 20 ms) duration, and occur during landing.

Forces during take off can be larger than forces during landing. In one run, the maximum F_x force at the knee on take off was 873 N; maximum F_x force during landing for the same run was 731 N.

Jump landings in these tests produce large anterior force (F_x) on the tibia at the knee, but not large posterior force. The angle of the tibia relative to the direction of the impact force determines the direction of the F_x force. The largest anterior force on the tibia at the knee (F_x) was 1580 N; the largest posterior force on the tibia at the knee ($-F_x$) was 314 N. Normally, the posterior force was negligible. Because anterior drawer requires significant posterior force on the tibia at the knee, anterior drawer of the tibia is not an apparent injury mechanism of the ACL in these jumps.

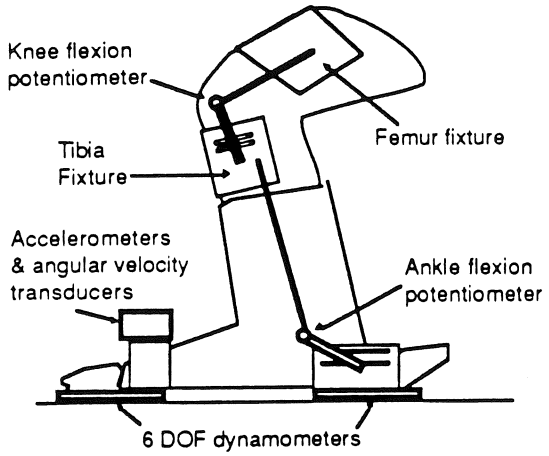


Figure 1: Sensors mounted on left leg, boot, and ski.

Table 1: Maximum values of selected force and moment components on the tibia at the knee and boot top.

Location	Loading Component	Peak Value	Duration (ms)
Knee	$+F_x^k$, N	1580	16
	$-F_x^k$	314	39
	$-F_z^k$	4340	20
	$+M_y^k$, Nm	289	39
	$-M_y^k$	621	20
Boot Top	$+M_y^b$	211	39
	$-M_y^b$	198	19

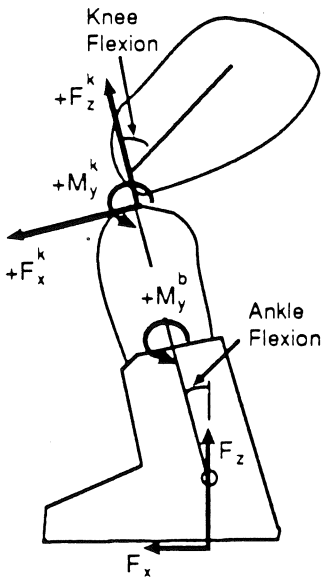


Figure 2: Angle, force and moment component definitions.

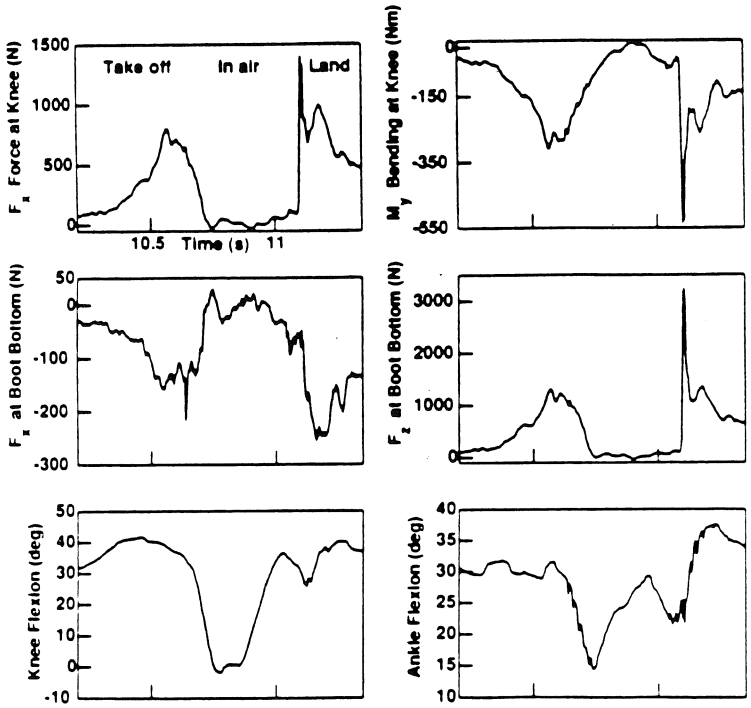


Figure 3: Typical time histories for selected force and moment components on the tibia at the knee and on the boot bottom during a ski jump.

REFERENCES

1. Johnson, R.J., Ettlinger, C.F., and Shealy, J.E., in *Skiing Trauma and Safety:Seventh International Symposium, ASTM STP 1022*, pp. 25 - 31, 1989.
2. McConkey, J.P., *Am. J. Sports Med.*, **14**(2): pp. 160-164, 1986.
3. Quinn, T.P., and Mote, C.D., Jr., *J. Biomech.*, in press, 1991.

THE AXES OF ROTATION OF THE KNEE

Anne M. Hollister, M.D., Sanjay Jatana, M.D., Anoop K. Singh, F.R.C.S.
William W. Sullivan, M.D., and Andrei G. Lupichuk, B.S.E.E.

INTRODUCTION

A mechanical device was used to locate the flexion-extension (FE) and the longitudinal rotation (LR) axes of six fresh cadaver knees. Kinematic investigation was performed with time lapse photography to record arcs about and perpendicular to the FE axis. Analysis using curve fitting techniques described a circular, planar paths, corresponding to two fixed axes. The tibia and femur were drilled along the axes demonstrated by the mechanical device. Anatomic correlations were determined by magnetic resonance imaging (MRI) and dissection. Mathematical analysis of MRI sections of the condyles perpendicular to the FE axis had a circular profile, consistent with a fixed FE axis. The FE axis of the knee is constant and directed from antero-superior on the medial side to postero-inferior on the lateral side passing through the origins of the medial and lateral collateral ligaments and superior to the crossing point of the cruciates. The LR axis is anterior and not perpendicular to the FE axis. The offset of the FE axis explains the valgus external rotation with extension and the varus internal rotation with flexion. Our investigation indicates that knee motion occurs about two fixed, non-orthagonal axes in contrast to the present variable FE center theory. In addition, this suggests that motion is pure rotation about these fixed axes.

REVIEW AND THEORY

Kinematics of the knee has been described as occurring about a variable flexion-extension (FE) axis located in the posterior femoral condyle and about an independent tibial rotation axis. This theory of knee kinematics is based on the works of several investigators [2,3,21] whose studies were later reviewed by Fick [5], Strasser [19], and Steindler [18]. This variable FE axis theory was derived from both anatomic and kinematic studies which were done in the sagittal plane. The Reuleaux method [15], a planar technique that determines the center of rotation, has been used to study knee motion [1, 6,16,17,21]. The purpose of this investigation is to locate the FE and the LR axis of the knee using a simple mechanical device; to evaluate the kinematics about these axes; and to demonstrate their anatomic correlation by MRI and dissection.

PROCEDURES

A mechanical device, the axis finder was used to locate the LR and the FE axis. This device has previously been used to demonstrate the axes of rotation of the knees of living subjects [10]. We found that this device can locate the axis of rotation of a hinge to within one mm and 1.5 degrees. Six fresh frozen cadaver knees were prepared, the skin and soft tissues around the knee being preserved. Three 5 mm external fixator pins were inserted into the femur, and the knee was then mounted on a firm platform to find the LR axis. Once the axis was found, the Steinman pin was drilled into the tibia. The knees were then mounted with three tibial pins, and the FE axis in the femur then found.Three flashing light emitting diodes (LED's) which spanned a 20 cm distance were placed on the tibial Steinman pin located on the LR axis. The knee was then moved passively from extension to full flexion in internal , neutral and external tibial rotation. The three arcs described by the three LED's were recorded by time lapse photography. The camera was then placed perpendicular to the axis with and end-on view of the femur and the same movements were repeated.

The femur was rigidly fixed and the specimen then drilled along the FE axis in the distal femur. Location of the axes was documented by plain radiography in three planes and by MRI. Measurements of the location of the axes were obtained from each view .The specimens were dissected and the relationship of the axes to the condyles and ligaments demonstrated.

Photographs of the LED paths and MR sections of both condyles were scanned into a computer and the images were processed . The LED paths were digitized, resulting in reference X and Y coordinates for each data point. The data set from each of the three arcs was entered into a non-linear optimization program [13] which determined the center of the concentric arcs by least squares fit. The optimization subroutine began with a user-supplied set of initial conditions for the three radii and their common center of rotation. These parameters were improved iteratively until a best fit to the data points was obtained. Data from concentric circular arcs would generate a common center and minimal residual error. Non-circular or non-concentric arcs would yield a higher residual error. The percentage error was calculated from the F value and the optimized mean R values. A low percentage error would indicate that the arcs are parts of three concentric circles.

Three MR sections of both the medial and lateral condyle were evaluated for circularity. The meniscal impression was the anterior margin of the condylar curve . The posterior limit of the curve was the posterior end of the bearing surface excluding on average a 1 cm distance. The curve from each MR section averaged 120 degrees of arc, but represented different portions of the femorotibial contact surface. The central sections included a more posterior and the outer sections, a more anterior area of tibial contact. Points were digitized from the center of the cartilaginous rim of the posterior condyle. The arc of each MR section was analyzed separately using a non-linear optimization routine similar to that above. The F and percentage error were calculated for each curve. The distance from the determined center and the drill hole center for the FE axis was measured with the Image program.

RESULTS

The three LED's produced arcs when knee motion was recorded with the camera aligned along the FE axis. Non-linear curve optimization for the three arcs for all six knees revealed low F and percentage error values indicating close fit to concentric circles. These values were similar to those obtained for a two fixed-axis model used to simulate knee motion [12]. Since the LED's were placed on the LR axis, the effect of tibial rotation during knee flexion was minimized. Tibial internal and external rotation during flexion and extension resulted in arc pathways with similar F and percentage error values (mean F value 0.01, $\pm$ sd 0.002, Mean percentage error value 0.70, $\pm$ sd 0.08). Statistical analysis of the results using the Sign test demonstrated no significant difference between the percentage error values obtained for the knees, the model and the arc test ($p>0.15$) knees.

The FE axis was aligned with the x-ray beam to produce the axial lateral x-rays.The tibial rotation axis averaged 47.5% of the width of the tibial plateau (W) from the medial side. On the axial lateral, the FE axis was 35.3 % of width of the distal femur. The radius of the medial posterior femoral condyle was 22.8 mm. The angle between the most distal aspect of the femoral condyles and the FE axis averaged 4.3 degrees on standard AP views with the knee in full extension. On plan views of the distal

femur, it averaged 3.3 degrees. This discrepancy is due to the superimposition of transition zone of the distal femur on the posterior femoral condyles. MR sections were made in a plane perpendicular to the FE axis. The contour of the posterior femoral condyles appeared circular. Curve fitting of 120 degrees of the posterior condylar surface of three sections gave percentage errors of 1.59 ± sd 0.38 and 1.42 ± sd 0.45 for the medial and lateral condyles respectively. This confirmed the circularity of the condylar surface. The optimized centers representing the location of the FE axes for all knees was found to differ from the drilled axes by a mean distance of 4.6 mm ± sd 0.14 mm. This represents primarily the errors associated with the drilling technique. The FE axis runs through the collateral ligament origins and superior to the intersection of the cruciate ligaments. The relationship of the axes to the collateral and cruciate ligaments demonstrated by the MRI sections was confirmed at dissection for all six knees. The FE axis passed through the origins of the medial collateral (MCL) and lateral collateral (LCL) ligaments in all knees dissected. The LR axis passed through the insertion of the anterior cruciate ligament (ACL) on the tibial plateau and was directed postero-medially in the proximity of the insertion of the posterior cruciate ligament (PCL) at the femoral notch. The length of the patellar groove ran perpendicular to the FE axis. When the FE axis was viewed end on, the posterior femoral condyles were superimposed and appeared circular.

DISCUSSION

Knee motion is felt to occur about a variable FE axis which is perpendicular to the sagittal plane and a tibial rotation axis which is perpendicular to the tibial plateau. This theory is based on kinematic and anatomic investigations done in the sagittal plane [1,2,3,5,6,8,16,17,18,19,20,21]. These investigators assumed that the axis(es) for knee flexion extension motion is/are perpendicular to the sagittal plane. Previous studies have not limited knee motion to a single plane [1,2,6,16,17,20,21]. The early workers [2,3,5,21] noted the obligatory tibial internal rotation and varus which occur with flexion, but did not realize that these motions could be conjoint rotations occurring because the FE axis is not perpendicular to the sagittal plane. They felt that the non-sagittal components of knee FE motion were not significant and analyzed only sagittal plane motion. These investigators did not correct for the independent tibial rotation in their analyses.

Plain radiographs of our knees gave an average radius of 22.8 mm for the posterior aspect of the medial condyle. Non-linear optimization found the arcs of knee motion to be circular with values in the same range as a model with fixed FE and LR axes [12]. Our results differ from those of previous kinematic studies [1,2,6,16,17,20,21] because we limited motion to the knee joint, located and then aligned our camera with the FE axis and minimized the effects of independent tibial rotation. The study adheres to Panjabi's guidelines [14].

The 1% error inherent in this planar technique can allow significant misalignment of the camera with the plane of motion. Our study is similar to Inman's work on the ankle [11], where a mechanical method demonstrated fixed, non-orthogonal axes for joints thought to have variable centers in sagittal plane kinematic studies. Classically, joint motion has been considered to occur about axes which lie in the anatomic planes, with separate perpendicular axes for FE, LR, and abduction-adduction (AA). If an axis of rotation is not perpendicular to the anatomic planes, the plane of motion will not be in an anatomic plane. Joint motion about an axis which is offset in two planes will include all three movements of FE, LR, and AA.

Our study indicates that motion of the human knee occurs about two fixed non-orthogonal axes. This suggests that knee motion is pure rotation about these fixed axes. The FE axis is not in the coronal plane, nor is the LR in the sagittal plane. Motion about each axis includes varus-valgus, flexion-extension and internal- external rotation. The major component of motion about the FE axis is flexion and extension, but conjoint varus and internal rotation occur with flexion because the axis is not perpendicular to the sagittal plane.This model with two fixed non-orthogonal axes can explain the shape of the condyles, the location of the ligaments, and the obligatory tibial varus and internal rotation that occur with flexion.

REFERENCES

1. Blacharski, P.A., and Somerset, J.H.: A Three-dimensional study of the kinematics of the human knee. J. Biomechanics, 8: 375-384, 1975.
2. Braune, W., and Fischer, O.: Classe der Konigl. Sach. Gesell. der Wissensch. 17: 75-150, 1891.
3. Bugnion, E.: Le Mechanisme du Genou. Recueil inaug. Univ. Lausanne. 1892.
4. Elias, S.G., Freeman, M.A.R., and Gokcay, E.I.: . Clin. Orth. and Rel. Res. 260:98-103, 1990.
5. Fick, R.: Handbuch der Anatomie und Mechanik der Gelenke. Vol.2:109-117,3:538-40,556-6,1911.
6. Frankel, V.H., and Burstein, A.H., and Brooks, D.B.: Biomechanics of Internal Derangement of the Knee. J. Bone and Joint Surg. 53-A: 945-962, 1971.
7. Freeman, M.A.R.: Proceedings of the Knee Society 1985-1986, Aspen Publication.
8. Goldberg, V.M., Davy, D., Figgie, H.E.III, Kraay, M.J., Shay, K., Singerman, R.: Kinematic Comparison of Posterior Cruciate Substituting and Posterior Cruciate Retaining Total Knee Arthroplasty. Presented at the AAOS Annual Meeting, Anahiem, Ca. 1991.
9. Grood, E.S., Stowers, S.F., Noyes, F.R.: Limits of Movement in the Human Knee: Effect of Sectioning the Posterior Cruciate Ligament and Posterolateral Structures. J. Bone and Joint Surg., 70A:88-97, 1988.
10. Hollister, A.M., Kester, M.A., Cook, S.D., Brunet, M.E., Haddad, R.J.: Knee Axes of Rotation: Determination and Implication. Trans. Orthop. Res. Soc., 11:383; 1986.
11. Inman, V.T.: The Joints of the Ankle. Williams & Wilkins Co., 1976.
12. Jatana, S., Singh, A.K., Sullivan, W.W., Hollister, A.M., Lupichuk, A.G.: Perspectives in Knee Motion. Submitted for publication.
13. Kahaner, D.; Moler, C.; and Nash, S. : Numerical Methods and Software. Prentice Hall, New Jersey, 9:1989.
14 Panjabi, M.M., Goel, V.K., and Walter, S.D.: J. Biomechanics. 15:537-44, 1982.
15. Reuleaux, F.: Theoretiische Kinematik: London, Macmillin, 1876.
16. Smidt, G.L.: Biomechanical analysis of Knee Flexion and Extension. J. Biomechanics. 6:79-92, 1973.
17. Soudan, K., and Auderkercke, R.V.: J. Biomechanics. 12: 27-33, 1979.
18. Steindler, A.: Kinesiology of the Human Body, Charles Thomas, Springfield, 1955.
19. Strasser, H.: Lehrbuch der Muskel und Gelenkmechanik, Vol III, Berlin, Springer, 1917.
20. Walker, P.S., Shoji, H., and Erkman, M.J.:.Clin. Orth. and Rel. Res. 89:160-170, 1972.
21. Zuppinger, H.: Die Aktive Flexion im unbelasten Kniegelenk, Med. Habil. Schift Zurich u. Anat. Hefte, 1904.

IN VIVO TRACKING OF THE HUMAN PATELLA

Timothy J. Koh[1] Mark D. Grabiner[1] Robert J. de Swart[2]
[1]Department of Biomedical Engineering and Applied Therapeutics
[2]Department of Orthopaedic Surgery
The Cleveland Clinic Foundation, Cleveland, OH 44196

INTRODUCTION Patellofemoral disorders, which are among the most common knee disorders, are often assumed to be related to abnormal tracking of the patella. However, little quantitative data on patellofemoral joint kinematics is available in the literature. The majority of the relevant studies have (a) used static experimental conditions, (b) not accounted for tibial rotation, which has been shown to influence patellar tracking, and (c) produced inconsistent results (1). Only Lafortune (2) has presented dynamic *in vivo* patellar tracking data. The purpose of the present study was to describe the dynamic, *in vivo*, three-dimensional tracking pattern of the patella during non-weight bearing and weight bearing knee flexion/extension for one male subject.

METHODS One male subject with no history of knee joint disorder volunteered for participation in this study. After a standard surgical preparation and application of local anesthetic, threaded intracortical pins (1.6 mm diameter) were inserted into the patella, the femur, and the tibia of the right lower limb. A triad of reflective markers (1.25 cm diameter spheres) was attached to each of the intracortical pins. Patellofemoral kinematics were analyzed during non-weight bearing (seated) and weight bearing (squatting) knee flexion/extension. Range of motion was limited approximately to the initial 60 degrees of flexion because of soft tissue impingement on the intracortical pins past 60 degrees flexion. The three-dimensional motions of the markers on the intracortical pins were recorded at 60 Hz with 4 video cameras and analyzed using a Motion Analysis system. The calculated error in determining the linear motions of the markers was less than 1 mm, and in determining the angular motions of the marker triads was less than 1 degree.

Axes of Cartesian reference systems for the patella, femur and tibia were defined to be parallel in full active knee extension and were directed medially (X-axis), superiorly along the long axis of the thigh (Y-axis), and anteriorly (Z-axis). These directions were determined from reflective markers placed on the skin of the thigh. The origin of the patellar reference system was located at the estimated center of the patella, and the origin of the femoral reference system was located at the midpoint between markers on the skin over the medial and lateral condyles of the femur. All motions were defined relative to the femoral reference system. Patellar and tibial rotations were defined as Cardan rotations with a XZY order of rotation. Patellar Cardan rotations were termed, in order (positive/negative), flexion/extension, medial/lateral rotation, and medial/lateral tilt. Tibial Cardan rotations were likewise termed flexion/extension, varus/valgus, and internal/external rotation. Patellar translation along the femoral X axis was termed medial/lateral shift.

RESULTS AND DISCUSSION Figure 1 shows plots of mean values of patellar Cardan rotations, patellar translation, and tibial Cardan rotations, versus knee flexion angle (averaged over 5 trials) for non-weight bearing (seated) flexion/extension. Only knee flexion data is shown in these plots; knee extension produced similar curves (with opposite trends). Internal/external rotation of the tibia was quite small. In their *in vitro* study of patellar tracking, van Kampen and Huiskes (1) showed that internal/external tibial rotation of up to 25 degrees strongly influenced patellar tracking. It is not considered likely that the small amount of internal/external rotation seen in the present study was an important determinant of patellar motion. The patella flexed with knee flexion, but patellar flexion lagged behind knee flexion. The patella also tilted laterally (rotated such that the front of the patella faced laterally) with knee flexion, and showed very little medial/lateral rotation (rotation about an axis perpendicular to the patellar plane). Finally, the patella shifted laterally with knee flexion.

Van Kampen and Huiskes (1) reported that, in 4 cadaveric specimens, the patella showed flexion, very little medial/lateral rotation and lateral shift within the range of knee flexion used in the present study. Their data were inconsistent with respect to tilt -- two specimens showed medial tilt, and two showed lateral tilt. The results of the present study show qualitative agreement with those of van Kampen and Huiskes. However, the results of the present study showed a greater flexion lag, and greater lateral tilt and shift than those of van Kampen and Huiskes. This may reflect larger quadriceps forces in the present study, and different relative loading of individual quadricep components between studies: large quadriceps forces would tend to resist patellar flexion, and a large vastus lateralis force (relative to vastus medialis oblique force) may tend to tilt and shift the patella laterally.

Figure 2 shows plots of mean values of patellar Cardan rotations, patellar translation, and tibial Cardan rotations, versus knee flexion angle (averaged over 3 trials) for weight bearing flexion/extension (squatting). The tibia externally rotated a small amount, and showed a relatively large varus rotation (compared to the non-weight bearing condition) as the knee flexed. Despite the difference in tibial rotations between the non-weight bearing and weight bearing conditions, and the assumed greater quadriceps activation in the weight bearing condition, the patellar rotations and translation were quite similar. The small differences present occurred predominantly during the initial degrees of knee flexion, when passive constraints to patellar motion (e.g. the intercondylar groove of the femur) are minimal.

The goal of many conservative and surgical interventions for patellofemoral disorders is to obtain normal tracking of the patella. However, little data exists that suggests the attainment of this goal. As only *in vivo* studies are likely to be useful in evaluating interventions which include rehabilitation exercises, further *in vivo* study seems warranted to reveal the mechanisms underlying success (or failure) of these interventions.

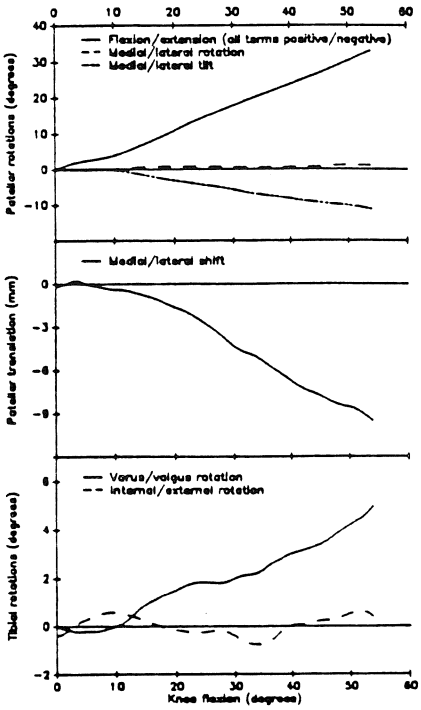


Figure 1. Average patellar and tibial motions during non-weight bearing knee flexion (n=5 trials)

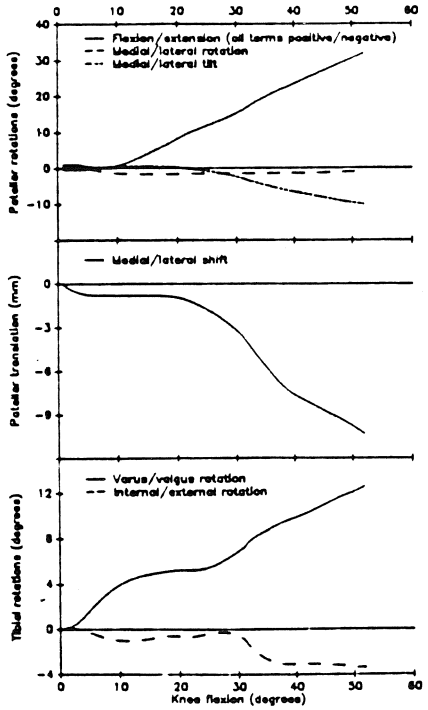


Figure 2. Average patellar and tibial motions during weight bearing knee flexion (n=3 trials)

REFERENCES

1. Kampen, A van *et al*: *J Orthop Res* 8, 372-382, 1990.
2. Lafortune, MA: Doctoral dissertation, Pennsylvania State University, 1984.

SESSION 8

SPORTS

Interactions between Body Roll, Hand Relative Motion, and Handpath during the Pull Phase in Freestyle Swimming

Qi Liu*, James G. Hay and James G. Andrews
Department of Exercise Science,The University of Iowa,Iowa City,IA 52242
MIKE Sport Research Laboratory, Beaverton, OR 97005-6453*

INTRODUCTION

Over the last twenty years, researchers studying the biomechanics of swimming have developed a theory of hand propulsion which emphasizes the role played by lift forces in generating hand propulsion. At the kinematic level, the fundamental patterns of hand motion used by competitive swimmers have been defined; and at the kinetic level, the contributions of lift forces to propulsion have been identified for the different competitive strokes.

Hay, Liu and Andrews(2) have suggested that the path followed by the hand of a swimmer might be attributed to motion of the arm relative to the trunk, to rolling of the trunk around the longitudinal axis, or to a combination of these two; and have conducted a computer simulation study to explore these possibilities. There appears, however, to have been no attempt to quantify the influence of body roll on the handpath in actual freestyle swimming. The purpose of this study was to determine the influence of body roll and motion of the arm relative to the trunk on the path followed by the hand during the pull phase in freestyle swimming.

PROCEDURES

Ten, male swimmers from a university swimming team were used as subjects. Each subject swam three 20 m-long trials at workout pace. Two periscope video systems were used to record each subject's performance in side view and front view. A balsa fin was mounted on the swimmer's back to permit body roll angle vs time histories to be obtained (1). The two video tapes were analyzed using a Peak 2D Motion Measurement System. The body roll angle vs time histories were found directly and the actual handpath was found by projection angle reconstruction. A 3D mathematical model was developed to determine the handpath that would have been recorded by each subject if there had been no medial-lateral motion of his hand relative to his body. A geometrical analysis was conducted to determine the average influence of body roll on the actual handpath (R) during the pull phase (Figure 1) using the equation:

$$R = (A_1/(A_1+A_2))*100\%$$

where A_1 is the left shaded area, and represents the influence of body roll on the handpath; and A_2 is the right shaded area, and represents of the influence of hand medial-lateral relative motion on the handpath.

RESULTS AND DISCUSSION

The results of this study indicated that the medial-lateral motions evident in the actual handpaths were due approximately equally to body roll and upper limb relative motion (Table 1).

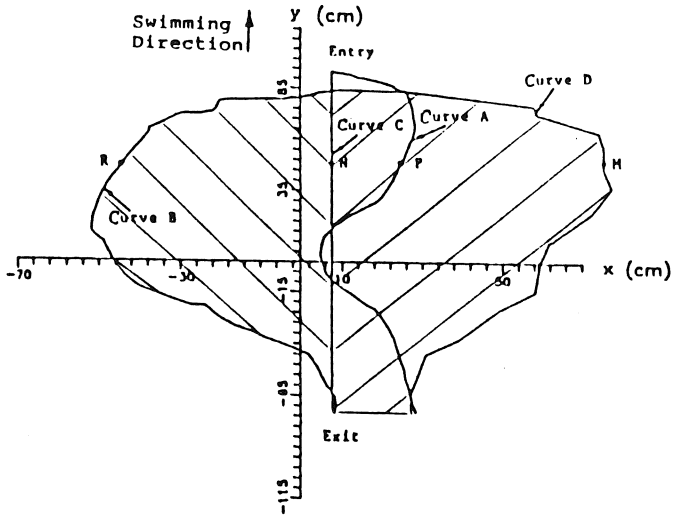


Figure 1. Geometric analysis of the influence of the body roll on handpath.

Curve A: Actual handpath.
Curve B: Model handpath for actual body roll and no relative motion of the hand.
Curve C: Model handpath for no body roll and no relative motion of the hand.
Curve D: Model handpath for no body roll but actual relative motion of the hand.
: Area A_1, contribution of body roll on the actual handpath.
: Area A_2, contribution of hand relative motion on the actual handpath.

Table 1
The Contribution of Body Roll to Actual Handpath

Subject	Total Area (graph unit)	Body Roll Area (graph unit)	R (%)
1	15.52	6.98	45.0
2	13.59	8.07	59.4
3	12.59	5.54	44.0
4	14.34	6.22	43.4
5	6.68	2.95	44.2
6	13.19	5.88	44.6
7	7.92	5.32	67.2
8	16.13	9.34	57.9
9	11.83	8.71	73.6
10	12.34	5.07	41.1
Mean			52.1
S.D.			10.9

The subjects accelerated the fingertip medially during the first 30% of the pull phase, and laterally between 60% and 80% of the pull phase. The mean value of the maximum body roll angle for the ten subjects was 61°. The greatest angular speed of body roll was recorded during the beginning and the end of the pull phase, and the least near the middle of the pull phase.

REFERENCES

1. Beekman,K.M. et al, J. of Swim Res., 4(3):11-14, 1988.
2. Hay, J.G. et al, Presentation on Proceedings, I.O.C. 1st World. Congr. on Sport Sci., 285-6, 1989.

A SPRINGBOARD RESPONSE SYSTEM FOR FEEDBACK ON DIVING PERFORMANCE

Doris I. Miller, Marc A. Pizzimenti and Ian C. Jones
Faculty of Kinesiology, University of Western Ontario
London, Ontario, CANADA N6A 3K7

INTRODUCTION

A system for providing immediate feedback on competitive diving take-offs was developed. The major component was a piezobeam accelerometer mounted under the end of the springboard with output being lowpass filtered and processed by a microcomputer at poolside. Acceleration patterns derived from digitally filtered board tip position-time information obtained from video substantiated the accelerometer output in time, configuration and magnitude. Video-based kinematic analyses of the take-offs also served as the basis for functional interpretation of the corresponding accelerometer curves. Data were collected at the 1991 World Diving Cup to establish reference acceleration-time standards for 3-m takeoffs. This springboard response system should prove of value in furnishing immediate and relevant information on a diver's boardwork as well as in addressing specific research questions related to this key aspect of performance.

REVIEW AND THEORY

Although we currently provide Canadian coaches with the results of kinematic analyses of springboard take-offs performed by the top 10 male and female divers at major national competitions within three weeks, there continues to be a need to furnish relevant biomechanical information which can be collected and used in practice. The purpose of the present project was to demonstate that such a system is feasible, that meaningful performance information can be collected and that the resulting data can be interpreted functionally from a coaching standpoint.

PROCEDURES

After several pilot studies with different types of accelerometers and methods of attachment, it was decided to employ a Kistler 8638B50 PIEZOTRON accelerometer (12 gm), threaded stud and mounting pad (2 gm) secured under the board tip with 3M 1838 epoxy adhesive. A 20-m lightweight coaxial hermetically sealed cable taped the length of the board on the torsion box conveyed the signal to a lowpass filter (corner frequency 10 Hz) linked to an Apple IIe microcomputer at poolside. The latter was equipped with an Applied Engineering 12-bit A/D converter and Transwarp accelerator card. Data for each take-off were sampled for 3 s at 500 Hz and stored on floppy disks for subsequent processing. Software was developed to analyze and display each acceleration file and to generate output in a form suitable for use by diving coaches and practitioners. The system was field tested during the 3-m competition of the 1991 Canadian Winter National Diving Championships. Data were subsequently collected on over 300 3-m springboard take-offs performed by top international divers at World Diving Cup VII. These take-offs were also videotaped and the divers' motion analyzed with a Peak 2D computerized video digitizing system to provide a basis for the functional analysis of the acceleration curves.

RESULTS AND DISCUSSION

An exemplary comparison of the board tip acceleration obtained from the accelerometer and derived by double differentiation of vertical position-time coordinates digitally filtered at 7 Hz is shown in Fig. 1. It was taken from the reverse 3 1/2 tuck (score 8.8) performed in the semifinals by U.S. diver and gold medallist Mark Lenzi. Initial and final contact in the hurdle and take-off could be identified directly from the accelerometer records thereby allowing associated support times and intervening flight time to be calculated. In addition, downward velocity of the diver at the beginning of the take-off (3.95 m/s), nature of the diver's contact with respect to the board (at maximum downward velocity) and location of maximum board depression could be inferred.

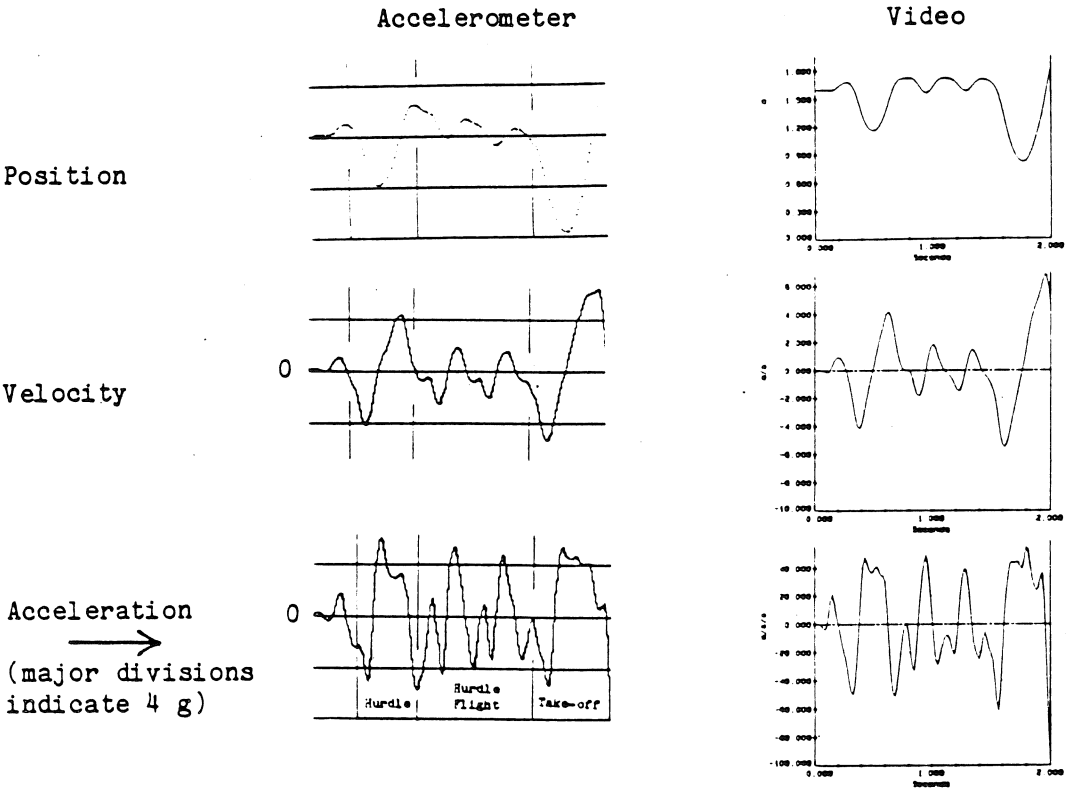


Fig. 1. Kinematic data of the board tip obtained from accelerometer (normal) and video (vertical) for a 2 s period up to and including last contact with the board before the flight. Positive signifies upward motion.

It was concluded that the direct measurement of acceleration normal to the take-off surface of the springboard when supported with appropriate analysis software and interpreted in the light of international standards of reference could provide immediate and meaningful information on a diver's take-off technique.

Acknowledgement: This project was supported by the USOC and US Diving with the cooperation of FINA and the CADA.

THREE DIMENSIONAL KINEMATIC ANALYSIS OF THE THROWING MOTION IN FOUR ELITE COLLEGE FOOTBALL QUARTERBACKS

Gregory Rash* and Robert Shapiro**

*BIO/MED Research & Consulting, Daphne, AL 36526.
**Biodynamics Laboratory, The University of Kentucky, Lexington, KY 40506.

INTRODUCTION

Several authors have investigated the kinematics of the baseball pitch, but very little work has been conducted on the throwing motion of the quarterback in American football (Atwater, 1970, 1979; Elliot, et al., 1986; Feltner, 1984; Feltner & Dapena, 1986; Gainor, et al., 1980; Pappas, et al., 1985; Sakaris, 1978; and Wisleder, et al., 1989). Therefore, the objective of this study was to determine the three dimensional kinematics of the quarterbacks' throwing motion in American football. The data reported in this study are part of an on going analysis of elite American college football quarterbacks.

METHODOLOGY

Four of the United States top senior college football quarterbacks were video taped while performing a drop-back pass into a calibrated area during a practice session for the Senior Bowl in Mobile Alabama. Synchronized 60 Hz video images from two cameras were manually digitized using a Peak Performance system and three dimensional kinematic data were calculated via a BASIC computer program. Data were digitally smoothed using a second order Butterworth filter with a cut-off frequency of 6 Hz.

RESULTS & DISCUSSION

At the point of release the mean elbow angle was 127.92 ± 6.50°. The upper arm was abducted at 98.58 ± 7.00°, horizontally abducted 14.31 ± 12.96°, and internally rotated 54.90 ± 10.09° form the vertical. Baseball pitchers typically have elbow angles of 160°, shoulder abduction angles of 90°, horizontal abduction angles of 0°, and internal rotation angles of -20° form the vertical at ball release.

The mean ball velocity for the quarterbacks analyzed in this study was 37.96 ± 7.52 mph and the maximum angular velocities of the upper extremity were: 1113.91 ± 192.92 deg/s elbow extension, 1565.46 ± 555.80 deg/s shoulder adduction, 708.5 ± 103.57 deg/s horizontal adduction, and 2461.45 ± 728.35 deg/s internal rotation. As a comparison, analyzed baseball pitchers throw the ball at an average velocity of

74 mph and typically have elbow extension velocities around 2300 deg/s, shoulder adduction velocities close to 1200 deg/s, horizontal adduction velocities at about 650 deg/s, and internal rotation velocities at approximately 7300 deg/s.

The obvious difference in ball velocity was reflected by the sizable difference in elbow extension and internal rotation velocities while the shoulder adduction and horizontal adduction velocities were somewhat similar for both quarterbacks and pitchers. Elbow and shoulder joint angles at the point of release showed differences between the two sports as well. The elbow during the football throw had not extended as far as the elbow during pitching and the shoulder had internally rotated approximately 70° further than the pitchers shoulder at release. Shoulder abduction and horizontal abduction angles at release were very similar to those angles found at release for pitching.

From these finding one can see that there are both similarities and difference between the upper body kinematics of baseball pitchers and American football quarterbacks. An understanding of kinematics and kinetics is of considerable importance to the quarterback coach, training staff, and medical community. A continued updating of the database on American football quarterbacks is presently being conducted and the addition of kinetic analysis is nearing publication status.

REFERENCES

Atwater, A. (1970). Movement characteristics of the overarm throw: A kinematic analysis of men and women performers. Doc Diss., Univ. of Wisconsin, Madison.

Atwater, A. (1979). Biomechanics of overarm throwing movements and of throwing injuries. Exer. & Sports Sci. Reviews, 7, 43-85.

Elliot, B., et al. (1986). A three dimensional cinematographic analysis of fastball and curveball pitches in baseball. ISBS, 2, 20-28.

Feltner, M., (1984). Kinetic and kinematic parameters of the shoulder joint during baseball pitching. Unpub. Master's thesis, Indiana University.

Feltner, M., & Dapena, J., (1986). Dynamics of the shoulder and elbow joints of the throwing arm during the baseball pitch. IJSB, 2, 235-259.

Gainor, et al. (1980). The throw: Biomechanics & acute injury. Am. J. Sports Med. 8(2), 114-118.

Pappas, A., et al. (1985). Biomechanics of baseball pitching: A preliminary report. Am. J. Sports Med., 13(4), 216-222.

Sakaris, J., (1979). Biomechanical analysis of overhand and sidearm fastball pitching techniques in baseball. Unpub. Master's thesis, University of Florida.

Wisleder, et al. (1989). Development of a biomechanical analysis of throwing with clinical applications for pitchers. Sports Med. Update, 4(2), 28-31.

FACTORS ACCOUNTING FOR VARIABILITY IN DISTAL END SPEED IN KICKING

Carol Putnam, School of Physical Education,
Dalhousie University, Halifax, N.S. B3H 3J5

INTRODUCTION

In an effort to understand kinematic and kinetic factors related to the coordination of the lower extremity segments in kicking, a model was developed to identify factors which determine maximum kicking speed. It was found that the variability in kicking speed demonstrated by 17 skilled performers could be accounted for by variability in the contributions made by the linear motions of the hip and of the ankle relative to the knee (the latter primarily determined by the angular speed of the leg) to the maximum ankle speed. Many kinetic factors contribute to the angular speed of the leg, but the only one found to account for the variability in maximum kicking speed was the interactive moment related to the effect of the thigh's angular velocity on the leg.

REVIEW AND THEORY

Body actions with similar objectives have similar motion patterns. For example, throwing and striking movements are performed with a proximal-to-distal sequence of segment actions(1,4). Beyond this general description, there is little understanding of the kinematic or kinetic factors constituting good performance. The timing of specific kinematic events is not related to skilled subjects' abilities to achieve maximum foot speed in high speed kicking (5). Techniques leading to good performance likely depend on the physical characteristics of the involved segments, and many mechanical and neuromuscular factors and as such, may not be readily identified on the basis of movement kinematics alone. The physical characteristics and mechanical factors can be address by considering the way segments interact dynamically during the movement. It has been shown that this interaction helps explain the proximal-to-distal pattern but it is unknown whether levels of performance can be distinguished on the basis of how segments interact. The purpose of this study was to identify factors which are most likely related to subjects' abilities to achieve fast kicking speeds and to see if levels of performance are determined by the way segments interact.

PROCEDURES

High speed film were collected from 17 skilled subjects, each performing two maximal speed kicks. Before smoothing with a digital filter, the coordinate data were linearly extrapolated beyond impact to minimize distortion prior to impact. One trial was digitized twice to check the data reduction procedure.

The kicking leg was analyzed as a two segment system, with the foot considered rigidly attached to the leg. The speed of the distal end of this linkage was taken to be the speed of the ankle. A deterministic model (2) was developed to identify factors which determine the maximum ankle speed (MAS) achieved during the performance. This speed (or the length of the vector VA in Figure 1) is the sum of the dot products of three vectors, the linear velocity of the hip (VH), the linear velocity of the knee relative to the hip (VK/H), and the linear velocity of the ankle relative to the knee (VA/K), with a unit vector in the direction of VA. The latter two dot products are determined by the angular velocity, length and orientation of thigh or leg at the instant MAS is achieved (Figure 2). Finally, using a segment interaction analysis (4), the angular velocity of the leg at the time MAS is achieved is dependent on the leg's angular velocity at some previous time (W init), the moment of inertia of the leg about its proximal end (I prox), the time interval, and the average values of the resultant joint moment at the knee (RJM) and interactive moments applied to the leg which are functions of the angular acceleration of the thigh (IM-AT), the angular velocity of the thigh (IM-VT), the linear acceleration of the hip (IM-AH) and gravity (IM-G). The first time interval considered was that between the knee passing through an angle of 90 degrees during the knee extension phase and the time of MAS. The model was then extended to include two additional time intervals, one between the beginning of knee extension and the beginning of the interval discussed above, and another between the time the knee flexed through an angle of 90 degrees and the beginning of the knee extension phase.

Correlations were calculated for all factors depicted in Figure 2 and MAS. The coefficients were considered significant if they exceeded 0.54, which is the critical value for a two-tailed test at a p value of 0.001.

RESULTS

The maximum ankle speeds ranged from 15.8 to 22.3 m/s (mean 18.8, s.d. 1.6). The MAS for the trial digitized twice differed by 0.3 m/s (5% of the range). Correlation coefficients are shown in Figure 2. Significant correlations are indicated with an asterisk.

DISCUSSION

The linear motion of the hip in the direction of the kick (i.e. in direction of the vector VA) was significantly related to MAS and therefore appears to be an important factor in accounting for the variability in MAS. Slowing down this motion could potentially increase MAS via the interactive moment IM-AH. However, IM-AH was not significantly related to MAS. Therefore, maintaining hip motion in the direction of the kick appears to important to kicking speed.

The slower the linear motion of the knee relative to the hip (and specifically the slower the forward rotation of the thigh), the more likely the subject achieved a high ankle speed, although the relationships between these factors and MAS were not significant. Although a forward rotation of the thigh could potentially have a positive contribution to MAS, performers appear to forgo this, perhaps in favour of the beneficial interactive effect of decreasing the thigh's angular velocity. While this effect has long been recognized as important (e.g. 3), it has been shown that the interactive moment related to the thigh's angular acceleration (IM-AT) will only tend to accelerate the leg in the forward direction after the knee has extended beyond 90 degrees (4). A moderate positive correlation was found between the interactive moment IM-AT and MAS during the time the knee angle is greater than 90 degrees, although the relationship was not significant.

The effect of the thigh's angular velocity on the leg (IM-VT) plays an important role in accelerating the leg forward (4) although the importance of this factor is often overlooked. The interactive moment IM-VT was significantly related to MAS while the knee was still flexing and during the initial phase of knee extension, when the knee angle was less than 90 degrees. Therefore, not only does this moment play an important role in accelerating the leg, but variations in its magnitude accounts for some of the variability in MAS.

The faster the linear motion of the ankle relative to the knee (and specifically the faster the forward rotation of the leg), the more likely the subject achieved a high ankle speed. The leg is angularly accelerated by the motion dependent interactive moments (previously discussed), the gravity-dependent interactive moment, which is not significantly related to MAS, and the resultant joint moment at the knee, which is also not significantly related to MAS.

In conclusion, subjects' abilities to achieve maximum ankle speed in high speed kicking can be distinguished by the way segments interact. Further research is required to consider what accounts for variations in this interaction, as well as to consider the interactions between factors which determine maximum ankle speed.

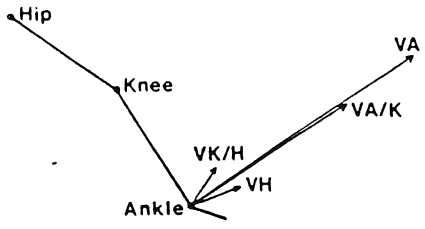


Figure 1. Vector contributions to ankle speed.

REFERENCES

1. Chapman, A.E., et al. in Multiple Muscle Systems. (Ed. J.M. Winters, et al.) Springer Verlag, pp. 607-620, 1990.
2. Hay, J.G., et al. J. Biomech., 19, 855-866, 1986.
3. Kreighbaum, E. et al. Biomechanics, Macmillan, 1990.
4. Putnam, C.A. Med. Sci. Sports. Exercise. 23,130-144, 1991.
5. Putnam, C.A. Human Locomotion VI, CSB Proceedings, 157-158, 1990.

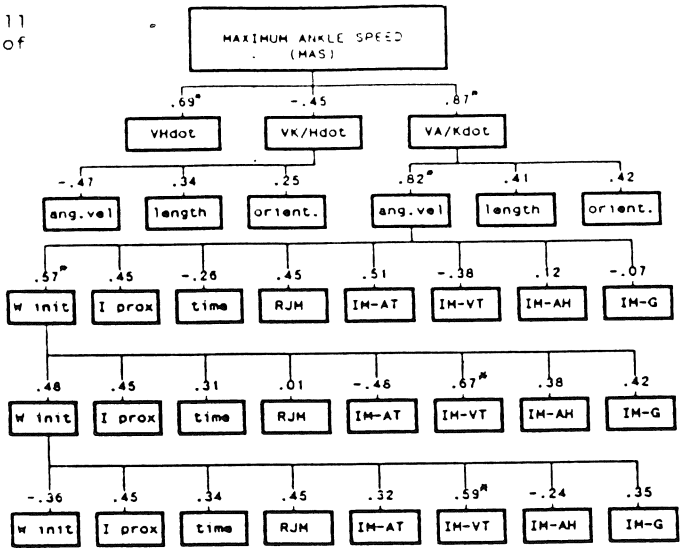


Figure 2. Deterministic model of kicking.

A 3-D Simulation of a Soccer Kick: The Effect of Varying Hip and Knee Torques

[1]DeWitt, J.K., [1]Hinrichs, R.N., and [2]Yamaguchi, G.T.
[1]Department of Exercise Science and Physical Education;
[2]Department of Chemical, Bio & Materials Engineering,
Arizona State University, Tempe, AZ 85287, USA.

INTRODUCTION

A 3-D forward dynamic simulation was used to determine the effects of the absence of hip or knee moments on a kick. The rapid reduction of hip flexor torques induces large accelerations upon the shank prior to impact. Knee flexor torques become present during follow through. The absence of knee torques does not markedly change segment actions during a kick, while eliminating hip torques significantly affected the kicking motion. This suggests large angular momentum transfers from the hip to the shank with little momentum transfer from the shank to the hip.

REVIEW AND THEORY

A soccer kick consists of a combination of hip flexion and knee extension to generate large velocities at the contact point on the foot. At impact momentum possessed by the foot may be transferred to the ball. As a soccer kick is performed, decreasing the flexor torque of the hip should act to increase the extensor torque at the knee. Therefore slowing the rate of hip flexion should increase the rate of knee extension, and thus increase the velocity of the foot. The purpose of this study was to use a computer simulation to investigate the effects of 1) altering hip torques on resultant shank motion, and 2) altering knee torques on thigh motion.

PROCEDURES

A 3-D dynamic model was formulated to represent the swing leg. Degrees of freedom were present for hip, knee, and ankle motion. Passive constraints which represent the internal structures of the joints were formulated to restrict segment movement to normal physiological ranges of motion. Joint angles during a kick for a skilled soccer player were measured experimentally. Torque histories were then adjusted by trial-and-error until a forward dynamic simulation of the model delivered segment angels that closely approximated experimental values. To determine segment motion influences upon one another, simulations were executed with hip torque inputs normal and input knee torques reduced to zero, and with knee torque inputs normal and hip torque inputs at zero.

RESULTS

Figure 1 shows a time-displacement graph of actual and simulated joint angles. Figure 2 depicts net torques at the knee and hip joints. Positive torques represent knee extensor and hip flexor torques. Figure 3 shows angle results with input knee torques at zero.

During this simulation original hip torques were input to induce thigh motion. Figure 4 shows the results of input hip torque at zero while knee torque inputs were that of a normal kick. Note that during the latter two simulations, passive torques were still present, keeping the knee from entering extreme ranges of hyperextension.

DISCUSSION

Without knee torque input, the joint angles output still approximated an actual kick. Shank acceleration occurred at about .1 seconds into the simulation, at the same time that hip torque was extremely decreased. Angular momentum inherent in the thigh was thus transferred to the shank at this time. The hip angles in Figure 3 exhibited slight peaks as the knee angle quickly moved from points of extreme extension back into normal range of motion. This suggested that the shank is acting upon the hip, but slightly.

In the simulation absent of hip torque input, joint angles did not come close to those of an actual kick. The knee entered extreme flexion after impact; This was due to the knee flexor torques present in the actual kick. As the knee extended slightly prior to impact, little action was seen in the hip, indicating that the knee motion did not appreciably affect the thigh. As the knee went into extreme flexion, hip flexion was induced, as expected. Without active hip flexion, however, the knee never extended past -50°.

It can be concluded that hip torques are for more important than knee torques during a kick because of the transfer of momentum prior to impact.

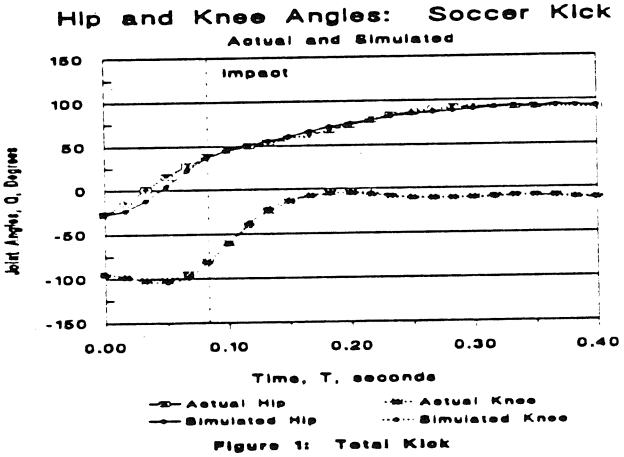


Figure 1: Total Kick

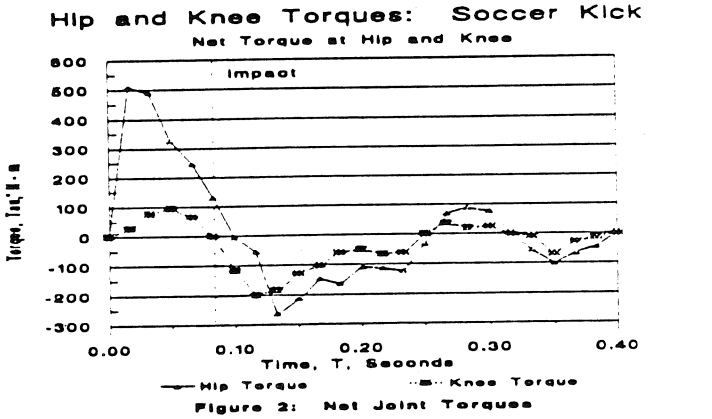


Figure 2: Net Joint Torques

Note: Positive Tau induce HIP FLEXION and KNEE EXTENSION

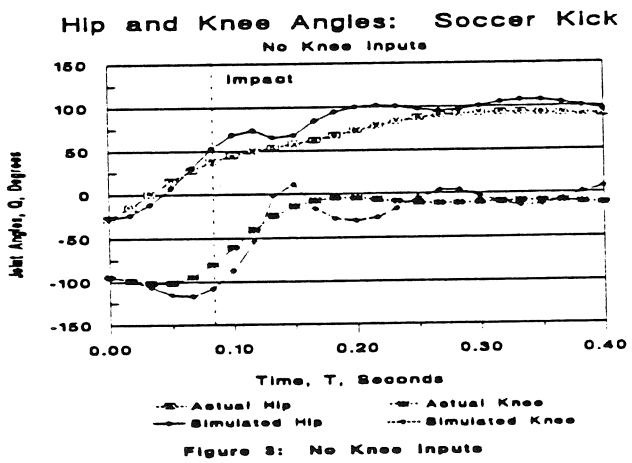


Figure 3: No Knee Inputs

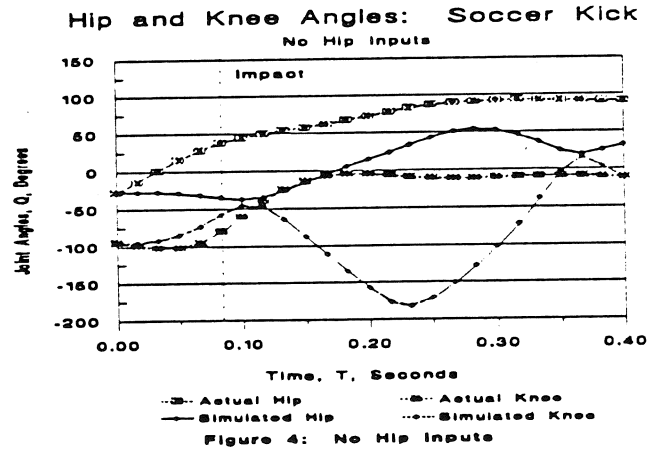


Figure 4: No Hip Inputs

SESSION 9

MATERIAL PROPERTIES OF BONE

Correlation between mechanical environment and collagen cross-linking in bone: An example from the deer calcaneus

S.Gunasekaran, PhD, Brent Constantz, PhD, John Skedros*, MD, R.D. Bloebaum*, PhD
Norian Corporation, Mountain View, CA 94043 and
*Division of Orthopedic Surgery, University of Utah Medical Center, Salt Lake City, UT 84148

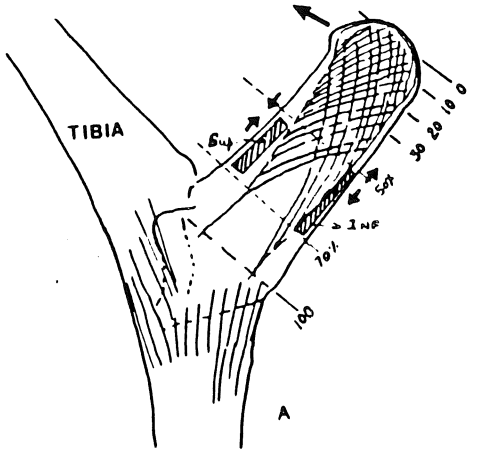
Introduction: Wolff's law teaches that bone is remodelled in response to mechanical stresses to which it is subjected. Chemical changes occurring to organic (mainly collagen) and inorganic (hydroxyapatite) components of normal bone subjected to different stresses are not well understood. Mule deer calcaneus bone can be an excellent model to study the chemical differences between the compressive and tensile portions of a given bone. The superior part is always under compression while the inferior section is in tension (Figure 1). The goal of the current investigation is to determine the possible chemical and mineralogical differences that happen due to mechanical stress on bone[1].

Methods: A total of twenty Mule deer calcaneus bones were used. We did not control the age or sex of the animal because each bone has served as its own control in our comparative study. Each specimen was carefully cleaned of muscle and connective tissues. The bone was sectioned into superior (compressive stress) and inferior (tensile stress) portions and ground to approximately 500 micron size particles. Each ground sample was first analyzed by X-ray diffraction (XRD) and Fourier Transform Infrared (FTIR). The samples were then demineralized and the proteins (mainly collagen) were characterized for amino acid composition. Subsequently, using a protocol developed at Norian, the relative amounts of protein cross-linking were estimated from the level of reactive amino groups available in the proteins. It is well understood that most of the cross-links of collagen are due to the availability of free amino-groups on the surface of the molecules. However, there is no simple reliable biochemical method presently available to assess the extent of the interaction of different cross-linking agents with the e-amino groups of the protein.[2,3] A modified Formol titration technique[4] seems to be an effective method, but this test is time consuming and has problems. Modified Formol treatment and the Schiff reagent test were used for this study. The details of the technique will be presented. The principle of the method is that when the collagen is allowed to react with formaldehyde (under optimal conditions for cross-linking), all of the possible reactive amino sites would be used up for the reaction. By assessing the remaining unreacted formaldehyde in the supernatant, one could estimate the amount of formaldehyde reacted with the amino groups of collagen.

Results and Discussion: Neither the XRD patterns nor the amino acid analyses showed any significant differences between the two test portions of the bone. However, the FTIR data showed certain differences in the amide peaks of the spectra. Highly significant changes were noticed in the relative amounts of collagen cross-linking between the two bone sections. Five out of seven samples in the first group had an average of 24% higher cross-linking of collagen in the superior (compressive stress) portion compared to that in the inferior (tensile stress) segment of the bone. We also noticed that one of the samples, as an exception, showed an increase (6%) in cross-linking at the inferior side compared to the superior. In the second group of thirteen samples, the superior portions of the bone were again significantly more cross-linked than the corresponding inferior

portions (Figure 2). These results may be interpreted that when bone is compressed, the collagen matrix may have to be more rigid mechanically. The mechanical rigidity can be attained by cross-linking. It is also interesting to correlate the fact that aldehyde cross-linked collagenous implants induce *in vivo* calcification. Further studies are being done with additional samples to verify our current data.

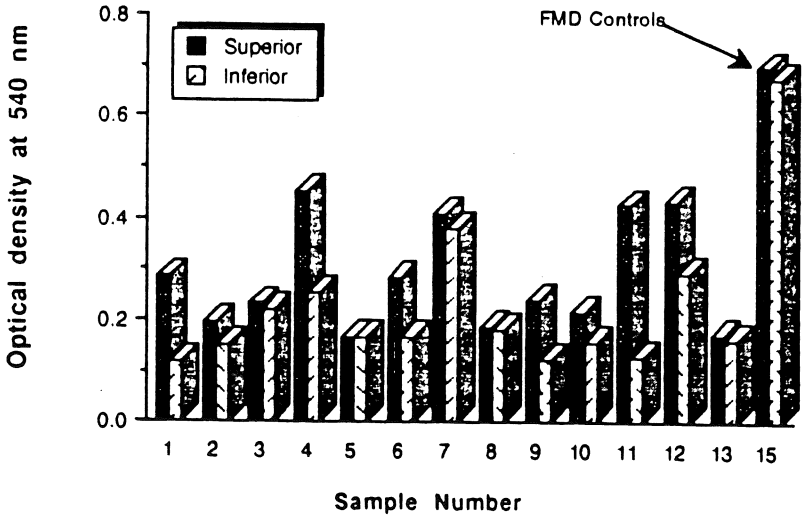
Figure 1: Test portions of the calcaneus bone.



Sup. = Cranial (Superior) portion under compression.
Inf. = Caudal (Inferior) portion under tension.

Figure 2

Collagen cross-link differences between Superior and Inferior regions of Mule Deer Calcaneus Bone



References:
1. Kuboki, Y. and Mechanic L., Calcified Tissue Interantional, 34: 306-308 (1982).
2 Weadock, K; Olson, R.M.; and Silver, F.H., Biomat. Med. Dev., Art. Org. 11(4):293-318 (1983-1984).
3. Yamauchi, M.; Katz, E.P.; and Mechanic, G.L., American Chemical Society, 4907-4913 (1986).
4. Bowers, J.H. and Cater, C.W., Biochim. Biophys. Acta., 168: 353-355 (1968).

THE EFFECTS OF DEMINERALIZATION PROTOCOLS ON THE MECHANICAL PROPERTIES OF BOVINE BONE COLLAGEN

W.R Walsh * and N. Guzelsu #
* Department of Orthopaedics , Rhode Island Hospital, Brown University, Providence, RI
# University of Medicine and Dentistry of New Jersey - SOM Biomechanics, and Rutgers University Biomedical Engineering, Piscataway, NJ

Introduction: The composite mechanical behavior of cortical bone depends upon the volume fraction, orientation, individual constituent properties and interfacial bonding between them. Bone can be considered as a fiber reinforced composite material of a stiff mineral fiber (bone mineral, hydroxyapatite) and an organic matrix (type I collagen). The mechanical properties of bone are diminished by inhibition of collagen crosslinks (1). However, either a weakening of the collagen matrix from a reduction in cross-links, a reduction in mineralization (2) or a reduction in interfacial bonding between the constituents may account for the reduced mechanical properties.

Bone constituent mechanical properties can be examined through complete removal of one phase (demineralization or deproteinzation). The organic phase has been examined by complete removal of the mineral using hydrochloric acid (3) or ethylenediamine tetraacetic acid (EDTA) (2). However, the effects of different demineralization techniques of the mechanical properties of bone collagen have not been addressed. This study examined the effect on different concentrations of hydrochloric acid and EDTA on the mechanical properties of bovine bone type I collagen.

Materials and Methods: Twenty eight bovine bone samples (5mm x 2 x 30) were prepared from the medial portion of the diaphysis of five adult femurs. A gauge length of 10 mm was marked and the ends of the samples were coated with paraffin wax. Samples were decalcified in 0.5, 1.0 or 2.0 M HCl for 48 hours at 4 ^{o}C under constant stirring or a 0.12 M EDTA solution (pH 7.4) for 42 days with daily changes. The demineralization procedure was monitored using dental x-rays and ashing. Following decalcification samples where placed in 0.145 M NaCl, pH 7.3 for 24 hours under constant stirring at room temperature. Samples were tested in uniaxial tension (strain rate of 2.65×10^{-3}) on an MTS 810 Materials Test System. The gauge length was separated into two section for histology and ash analysis. The elastic modulus, ultimate stress and strain to failure were calculated using the original cross section prior to demineralization. A Student's t-test was used to analyze mean values.

Results: The load-deformation curves of all demineralized samples demonstrated a significant initial non-linear toe region followed by a linear region. All samples did not exhibit a yield prior to failure. The ashing analysis and dental x-rays indicated all samples were completely demineralized at time of testing. The ultimate stress of the EDTA samples was statistically different than all HCl samples. The ultimate stresses of the HCl samples were not statistically different. The elastic modulus of the linear region of the 0.5 N HCl are statistically greater than the EDTA treated samples. The HCl samples have a statistically significant increase

Discussion: The ultimate stress and elastic modulus of tendon (composed almost exclusively of type I collagen) have been reported to be 60 MPa and 700 MPa respectively (4). A comparison of the values obtain for tendon with demineralized bone indicates they are indeed different. The bone mineral constitutes approximately 50% of the volume. Even if this is considered in correcting the original cross section the properties do not approach intact samples. The main difference between the organic phase in intact tendon and demineralized bone is the continuity and load transfer among the collagen fibers. In tendon, the fibers are in contact with each other and load is transferred from one fiber to another through side chains and intermolecular bonding. However, the organic phase in demineralized bone does not act as a cohesive unit. Load is transferred is interrupted where the mineral crystals used to be present. Therefore, the discontinuity among the fibers results in a reduction in the mechanical properties.

The demineralization method (EDTA versus HCl) significantly alters the mechanical and histological properties of bone's organic phase. EDTA will remove the mineral through a chelating mechanism along with those non-collagenous proteins strongly bound the mineral surface. Acid demineralization solubilizes the bone mineral, removes a different non-collagenous protein pool compared to EDTA as well as damaging the ultrastructural appearance of the remaining organic constituents. Removal of one of the phases of bone must be done to examine the contribution of the other phase to the overall mechanical properties of bone. The mechanical properties of bone however, are not predicted considering the properties of the individual constituents alone. Therefore, load transfer between the mineral and organic and interfacial bonding plays an important role in the mechanical behavior of bone tissue. Alterations in interfacial bonding may be a significant factor in various diseased states (5) and requires further investigation. Literature Cited: (1) Opsahl et al., 1982, J Nutr 112,708-716. (2) Danielsen et al., (1986) Calcif Tiss Int 39,69-73. (3) Burstein et al., (1975) JBJS 57A, 956-961. Viidik (1987) Handbook Bioengineering 6.1-6.19, McGraw Hill. (5) Bundy (1985) Ann Biomed Eng 13,119-135.

Table 1	Ultimate (MPa)	Modulus (MPa)	Strain to failure (%)
EDTA	14.7 (1.4)	54.2 (21.3)	17.0 (1.3)
0.5 M HCl	10.7 (1.8)	88.7 (28.9)	26.9 (2.6)
1.0 M HCl	9.0 (4.8)	79.4 (26.7)	23.5 (3.9)
2.0 M HCl	8.9 (2.7)	61.1 (16.3)	25.0 (2.6)

ASSOCIATION BETWEEN MECHANICAL STABILITY, CORTICAL STRAINS AND HISTOLOGY OF FEMURS RETRIEVED WITH UNCEMENTED FEMORAL PROSTHESES

James L. Comadoll, Peter T. Bianco,
Joan E. Bechtold, Ramon B. Gustilo

Orthopaedic Biomechanics Laboratory and Department of Orthopaedic Surgery, Hennepin County and Metropolitan-Mount Sinai Medical Centers

INTRODUCTION

Few reports are available on the mechanical integrity of implanted prostheses in femurs retrieved from patients who die (1,2). In the laboratory, mechanical stability and surface strains have been studied for the immediate post-operative situation, but few reports exist for strains and stability in femurs recovered from patients with functioning prostheses. In this study, two retrieved femora containing long curved stem revision femoral components with anterior and posterior ingrowth pads, and the contralateral femur of one of the subjects containing a cemented Charnley prosthesis were mechanically tested. In addition, the femora were analyzed using standard radiographs, CT and MRI scans, and were sectioned for histology to identify regions of bone ingrowth.

PROCEDURES

Three embalmed femora with prosthetic implants were obtained from two patients who died from causes unrelated to their hip replacements. One femur had a revision long curved stem uncemented titanium implant with anterior and posterior ingrowth pads which had been implanted 2-1/2 months prior to retrieval. One side of the pair of retrieved femurs was an asymptomatic fourth revision with the same uncemented stem as above, which had extensive bone grafting, and was in place for 2-1/2 years. Its contralateral femur had an asymptomatic cemented Charnley prosthesis, in place for longer than five years.

AP and ML radiographs and CT scans were obtained for all specimens; MRI scans for the uncemented implants. Thirteen rosette strain gages were attached to the femoral cortex, with one directly below the medial calcar, and three tiers of 4 rosettes (A,P,M,L). Strains were recorded for two loading configurations. First, the femora were loaded in simulated stance loading (60% compression on the prosthesis head and 40% tension in the abductor musculature, at 20 degrees to the vertical) with an electrohydraulic materials test machine (MTS). The femora were also studied in torsion, with a low torque (1 Nm -- so as not to disturb the bone/implant interface for subsequent histology). Strains were recorded, as was the relative motion between the proximal femur and prosthesis. For both load configurations, principle strains and their orientation were calculated with Micromeasurements System 4000 Strain analyzer. Loading was repeated at least 3 times to verify reproducibility.
After mechanical testing, the specimens were cut transversely at 1.0 cm intervals, embedded in methylmethacrylate without decalcification, ground to approximately 250 micrometer thickness, and stained to evaluate the type of tissue.

RESULTS AND DISCUSSION

Radiographic: Although some increased density was noted on the CT and MRI scans at the ingrowth pads, no determination could be made if this represented connective tissue or bone. The CT and MRI did give excellent delineation of the prosthesis fill of the canal. On contact radiographs of the histologic sections, the 2-1/2 year implant also showed regions of increased density corresponding to regions of contact with the prosthesis (Figure 1).
Histology:The femur with prosthesis implanted 2-1/2 years showed bone grown into the two proximal fibermetal pads (anterior and posterior), while the femur with the short 2-1/2 month history of implantation

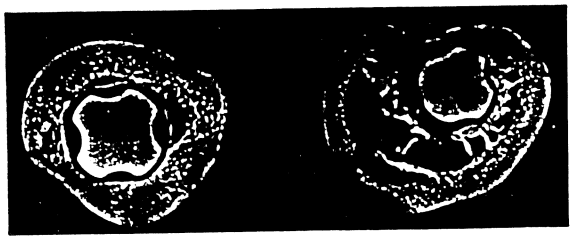
showed only connective tissue.
Mechanical stability:The relative motion in torsion of the cemented prosthesis was 10% the motion of the contralateral uncemented 2-1/2 month prosthesis (Range 0.01 - 1.0 deg @ 1.0 Nm applied torque, motion was not measured for the 2-1/2 month prosthesis). Larger motion for the uncemented femur is not unexpected in this case, because this revision femur had a large bony defect leading to an open section for the femoral shaft.
Strains - torsion: Principle strains in torsion were small in magnitude and did not vary substantially for each of the three femurs. Orientation of the principle strains was within 20 degrees of oblique for all femurs, with tension and compression of differing magnitudes, depending on the individual orientations. Comparison of cemented and uncemented prostheses in torsion shows only minimal difference. This may be related to the low torques the specimens were subjected to.
Strains - stance: Principle strains were greatest medially and laterally for all femurs, and ranged in compression from -10 to -400 microstrain, and in tension from +10 to + 200 microstrain. Anterior strains were generally small, proximally compression was greater than tension, distally tension was greater. The fourth revision femur with posterior/medial defect had generally larger magnitude strains than the contralateral cemented femur. Anterior and posterior tensile strains were larger (approximately twice) in the uncemented femur with histological evidence of bone ingrowth as compared to the uncemented femur with connective tissue. The orientation of the principle strains varied +/- 30 degrees from longitudinal, which highlights the importance of rosette gages in obtaining complete information.

REFERENCES

1. Murphy S.B. et al., JBJS, 66A:437-443 (1984).
2. Belec L et al., Trans ORS, 14:578 (1988).

ACKNOWLEDGEMENT

J. Galante, R. Turner, R. Urban at Rush-Presbyterian-St.Lukes Medical Center, Chicago IL, for generously performing histologic analyses.



REPRODUCIBILITY OF FINITE ELEMENT STRESS DISTRIBUTIONS IN MRI-DELINEATED FEMORAL HEAD OSTEONECROSIS

Kelly J. Baker, Thomas D. Brown, and Richard A. Brand
Biomechanics Laboratory, Department of Orthopaedic Surgery
The University of Iowa, Iowa City, Iowa, 52242.

Introduction: Magnetic resonance imaging (MRI) has become an important means for early detection of femoral head osteonecrosis. While late-presenting collapsed heads usually require total hip arthroplasty, pre-collapse stages are often treated successfully with head-preserving procedures such as osteotomy, core-drilling, cortical bone grafts, or electrical stimulation. The outcome of these surgical procedures appears to depend highly upon the pattern of necrotic lesion involvement. This suggests that reliable estimates of stress patterns associated with individual lesions could better delineate surgical indications.

Finite element analysis enables realistic estimation of individual lesion stresses and the associated tendency for structural collapse of the femoral head. Previous models have used only hypothetical lesions deemed representative of common infarcts. A method has now been developed for transfer of actual lesion geometry data from individual patient MRI scans to an existing 3D anatomic FEM model of the proximal femur (Fig.1), for subsequent stress analysis.

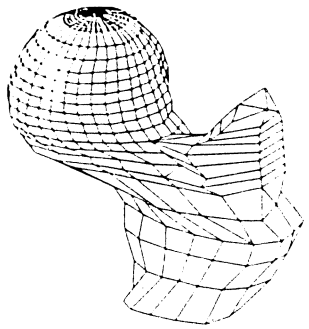


Figure 1. FEM model.



Figure 2. Lesion boundary.

Procedure: T1-weighted MR images of transverse femoral head sections are rendered as 512 x 512 8-bit grey level pixel arrays on a DEC VAXstation 3500 screen, and processed using PVWAVE software. In T1-weighted images, necrotic cancellous bone marrow is identified by a locally dark signal, contrasting with the bright signal of viable marrow of the adult femoral head. A Sobel transform is used to accentuate signal boundaries and enhance visualization of the necrotic/viable interface. The idiosyncrasies of lesion appearance on MRI render automated edge-detection routines inappropriate; manual determination of the lesion margin is necessary. At each transverse section, the lesion boundary is recorded by cursor-tracking around the infarct (Fig.2). Once all involved transverse sections in the patient MRI series have been thus digitized, each closed lesion boundary is divided into planar triangular sectors and assembled according to MRI section, creating a network of 3D wedges. This necrotic zone network is transformed from MRI-based coordinates to FEM-based coordinates, by means of appropriate rigid body translation (via head center), re-orientation (via transverse and coronal plane rotations), and scaling (via head diameter). A search algorithm then detects whether each of the 4399 femoral head mesh nodes lies in the necrotic zone. Three

distinctly different criteria are used to determine which elements are modeled as necrotic (based on the number of necrotic nodes): an element having at least one node within the necrotic zone, more than half its nodes, or all its nodes. Elements thus designated as necrotic are assigned an attenuated elastic modulus and yield strength, based on reported necrotic deficits. The result is a 3D FEM description of the MRI femoral head lesion, for which complete 3D stress fields are then computed using the ABAQUS finite element package. Since the tendency for collapse depends on the local yield strength as well as the local stress, a stress-to-strength ratio (SSR) is used as the outcome variable. The overall reproducibility of the MRI/FEM procedure, and the importance of criterion choice for necrotic element assignment, were analyzed in terms of SSR.

Results and Discussion: Coronal mid-section SSR contours were calculated for one lesion digitized six different times by the same analyst, and digitized once by six different analysts. Both the within- and between-analyst series showed qualitatively similar lesion patterns and resulting SSR contours. The percent coefficient of variation of SSR was computed for both series (solid lines, Figs.3,4), and contoured along with percentages of the peak series-averaged SSR (dashed lines; peak mean SSR = 0.639, 0.617, respectively) and shaded regions demarcating one digitized lesion. Due to the subjective nature of lesion delineation, areas of greatest variability (12-16%) were at the edges of the infarct. These variations are of consequence only at the lateral edge where high SSR values exist (although still only 50% of the maximum spatial average). In the nodal criterion series, the lesion was enlarged when only one necrotic node was required per necrotic element, and reduced when all nodes were required. For all three criteria, maximum SSR levels occurred within dense underlying cancellous bone, but decreased as the lesion size was reduced (12% decrease in maximum SSR for the all-nodes-test and 3% increase for the one-node-test, relative to the half-nodes-test).

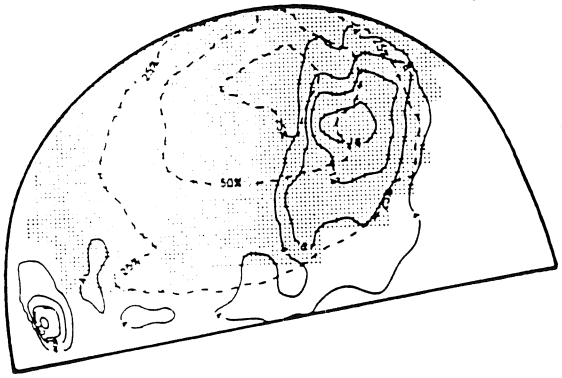


Figure 3. Within-analyst series.

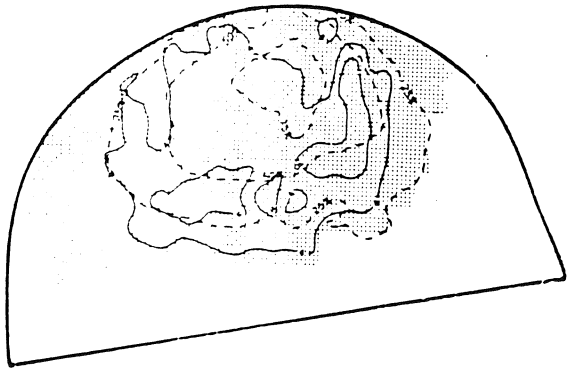


Figure 4. Between-analyst series.

The method developed for mapping MRI lesions onto the FEM mesh contains inherent variability at the infarct fringes. However, the dominant SSR levels within the infarct, and the presumably associated tendency for collapse, are only minimally affected. Similarly, criterion extremes for designating necrotic elements in the FEM model have only a minor effect on SSR levels in the MRI-defined lesion. Ongoing work involves correlation of specific patient outcomes with SSR-related values, to develop a better understanding of the clinical importance of necrotic lesion geometry.

Acknowledgment: Financial support by NIH Grant AR-35788.

ATLAS OF MECHANICAL PROPERTIES OF HUMAN CORTICAL AND CANCELLOUS BONE

Marie Christine Hobatho*, Jae Y. Rho**, Richard B. Ashman**

* Inserm U305, Centre Hospitalier Hôtel Dieu, 31052 Toulouse, FRANCE.
** Texas Scottish Rite Hospital, Research Laboratory, Dallas, Texas 75219, USA.

INTRODUCTION : Mechanical properties of bone have been presented in many reports over the last several years. Unfortunately, those reports tended to examine only a few bones from only a few poorly documented cadavers. This report of bone's mechanical properties examines tissue from eight human subjects with approximately 70 cortical and 40 cancellous specimens from the tibia, patella, femur, humerus, mandible, and L-1 to L-5 vertebrae from each subject. Of particular interest were differences between sites on particular bones, differences between properties of different bone (e.g. differences between the cortex of the tibia and femur), and differences between individuals. The results demonstrated differences exist between human subjects and between different bones. These differences may have teleological implications and should be of importance in parameterizing finite element models.

REVIEW AND THEORY : A paucity of data exists on differences between bones and individuals. Furthermore, investigations on the relationships of modulus and strength of cancellous bone to density have been of interest to those attempting to predict mechanical properties from density and those attempting to model trabecular material [3,5,6]. Though often referenced, Carter and Hayes [3] lumped human and bovine cancellous bone together as well as considered cortical bone as a dense extension of cancellous bone. Rice et al. [6] collected data obtained by several different techniques from several studies to show differences between species, differences between cancellous and cortical material and to predict the form of the relationships between modulus, strength and density. The present work attempts to address these same issues, but uses data obtained with a single technique from a larger group of individuals.

PROCEDURES : From eight unembalmed human subjects, mean age 60 years (45-68), a total of 328 samples of cortical bone were obtained (96 from the tibiae, 96-femurs, 64-humeri, 72-mandibles). Similarly, 600 specimens of cancellous bone were obtained (144 from the proximal tibiae, 128-proximal and 144-distal femora, 32-proximal humeri, 32-patellas and 120-lumbar spine). Size of the cortical specimens was 5mm cubes and 2x3x5mm parallelpipeds for bones where the cortex was thin. Cancellous specimens were 10mm cubes. Ultrasonic pulse transmission was used to measure 1) velocities in cortical specimens at 2.25MHz [1], 2) velocities in cancellous specimens at 50KHz [2]. Elastic moduli were determined from the wave propagation velocities as described previously [1,2]. Validation of this technique has been performed by comparing elastic moduli measured by the ultrasonic techniques to those measured using mechanical testing methods for both cancellous and cortical specimens [1,2,4]. Ultimate strength of the cancellous specimens was determined mechanically in compression after the ultrasonic testing was completed.

RESULTS : In comparing results between subjects, cortical moduli were found to be different for the tibia, femur and humerus ($p < 0.05$). However, density was not found to be significantly different for the tibia, femur, and humerus between subjects. Similarly, all cancellous properties were found significantly different between subjects (except for the proximal humerus where no statistical differences were found).

Differences between bone type are summarized in Table 1. Basically, for the cortical bone, properties of the humerus were found to be less than the other bones ($p < 0.05$). For the cancellous bone, properties of the proximal humerus, proximal tibia and lumbar spine were found to be less than the other bones and properties of the patella were found greater than the other cancellous bones ($p < 0.05$).

Considering the relationships between moduli and density, a general non linear model of the form $E_3 = B0 + B1\rho^{B2}$ was used to determine the best fit. Note that this model includes both a power fit (if $B0 = 0$) and a linear fit (if $B2 = 1$). T-tests of $B0 = 0$ and $B2 = 1$ were used to determine whether the general (or simpler) model would be sufficient. Linear relationships were found to be the best predictor of axial modulus from density for cortical bone (r^2 vary from 0.40 to 0.77). For cancellous bone, only the linear and power relationships are reported in Table 3.

DISCUSSION : Results show that statistical differences between subjects and bones. However, in finite element modeling elastic properties are often parameterized within a broad range. Table 2 presents

lumped cortical and cancellous properties averaged from 1) all individuals, 2) the cadaver with the minimum values of properties, and 3) the cadaver with the maximum values.

Though some statistical difference was found between power and linear density relationships. The predictive power of both types of relationship are approximately equal. However, the power fit gives a better fit of data for both low and very high density bone. Models of cellular structures predict squared relationships for open celled foams and cubic relationships for closed cell materials [6].The results presented here show best fits with powers between linear and squared, suggesting the bone tested was predominately open celled.

	CORTICAL BONE				CANCELLOUS BONE					
	Tibia	Femur	Humerus	Mandible	Prox. Femur	Distal Femur	Prox. Tibia	Prox. Humerus	Patella	Lumbar Spine
E_1	11.7±1.3	11.7±1.9	10.7±2.1 *	11.3±1.3	713±69	760±46	202±13 *	397±38 *	1484±140 *#	286±17 *
E_2	12.2±1.4	12.3±2.0	11.6±2.1 *	12.5±2.1	769±65	707±46	232±15 *	438±43 *	1197±148 *#	313±19 *
E_3	20.7±1.9	19.9±2.7	20.0±2.7	20.5±2.9	1267±79	1697±83	769±45 *	813±71 *	2801±241 *#	1087±60 *
ρ	1849±109	1811±148	1779±15 *	1858±74	350±190	395±15	198±8 *	255±16 *	731±39 *#	238±8 *
σ	-	-	-	-	4.8±0.4	5.9±0.4	2.6±0.2 *	2.7±0.4 *	8.5±1.1 *#	3.1±0.2 *

Table 1. Average and standard deviation of elastic moduli are expressed in GPa for cortical bone and in MPa for cancellous bone. Density ρ and strength σ are expressed in kg/m^3 and MPa. For the cortical data, E_1 is for the radial direction, E_2 is for the tangential direction and E_3 is for the axial direction. For the cancellous bone, E_1 is for the A-P direction, E_2 is for M-L direction and E_3 is for the S-I direction. Symbol '*' shows that the values are significantly the lowest, and '#' the highest ($p < 0.05$).

	CORTICAL BONE			CANCELLOUS BONE		
	Average	Minimum	Maximum	Average	Minimum	Maximum
E_1	11.5 ± 1.7*	9.9 ± 1.9*	13.2 ± 1.4*	614 ± 808*	347 ± 531*	721 ± 834*
E_2	12.1 ± 1.9*	10.8 ± 2.0*	13.6 ± 1.4*	544 ± 566*	293 ± 359*	659 ± 591*
E_3	20.3 ± 2.6*	19.2 ± 3.1*	21.7 ± 2.5*	1202 ± 848*	625 ± 455*	1500 ± 804*
ρ	1826 ± 140	1766 ± 178	1884 ± 201	319 ± 196*	215 ± 148*	376 ± 188*
σ	-	-	-	4.2 ± 3.5*	1.9 ± 1.4*	6.1 ± 4.0*

Table 2. Average, minimum and maximum values of mechanical properties with respective standard deviation obtained for eight subjects. Elastic moduli are expressed in GPa for cortical bone and in MPa for cancellous bone. Symbol '*' show significant difference of values between subjects ($p < 0.05$).

Cancellous Bone	Linear Relationship	Power Relationship	N samples
Proximal Tibia	$E_3 = -326 + 5.54\ \rho$ ($r^2 = 0.95$)	$E_3 = 0.51\rho^{1.37}$ ($r^2 = 0.96$)*	144
Proximal Femur	$E_3 = -331 + 4.56\ \rho$ ($r^2 = 0.95$)*	$E_3 = 0.58\ \rho^{1.30}$ ($r^2 = 0.94$)*	128
Distal Femur	$E_3 = -384 + 5.27\ \rho$ ($r^2 = 0.91$)	$E_3 = 0.82\ \rho^{1.27}$ ($r^2 = 0.95$)*	144
Proximal Humerus	$E_3 = -270 + 4.25\ \rho$ ($r^2 = 0.92$)*	$E_3 = 0.32\ \rho^{1.41}$ ($r^2 = 0.92$)*	32
Patella	$E_3 = -1327 + 5.65\ \rho$ ($r^2 = 0.85$)*	$E_3 = 0.04\ \rho^{1.68}$ ($r^2 = 0.87$)*	32
Lumbar Spine	$E_3 = -349 + 5.82\ \rho$ ($r^2 = 0.96$)*	$E_3 = 0.63\ \rho^{1.35}$ ($r^2 = 0.94$)	120

Table 3. Linear and power relationships between axial modulus expressed in MPa and density expressed in kg/m^3. Symbol '*' represents the best fit.

REFERENCES:

[1] Ashman et al., J Biomech **17** ,349-361,1984.
[2] Ashman et al., J Biomech **22** ,895-900,1989.
[3] Carter and Hayes, J Bone Jt Surg **59** ,954-962,1977.
[4] Darmana et al., ITBM **12** ,75-86,1991.
[5] Gibson , J Biomech **18** ,317-328,1985.
[6] Rice et al., J Biomech **21** ,155-168,1988.

SITE-SPECIFIC ADAPTATION OF THE GROWING SKELETON TO ALTERED MECHANICAL STIMULI

Ted S. Gross and Clinton T. Rubin
Musculo-Skeletal Research Laboratory, Department of Orthopaedics
State University of New York @ Stony Brook, Stony Brook, NY 11794

INTRODUCTION

Despite the potent influence of systemic and genetic factors, the growing skeleton remains sufficiently attuned to its daily physical milieu to respond to changes within this environment. In this study, we isolate the radius in a growing animal from its normal functional environment, substitute an experimentally applied stimulus physiologic in magnitude, and examine how the growing skeleton responds to an alternative mechanical stimulus. Interestingly, the region of greatest bone mass increase corresponded to the site of **least**, rather than greatest engendered strains.

REVIEW AND THEORY

Previous investigators have found that a daily exercise regimen, or experimental loading of bone via transcortical pins, stimulates increased bone mass versus controls in growing animals (1,2,3). Each of these regimens altered bone mass at specific cortical sites, however, the animals ambulated during non-loading periods confounding the ability to directly relate the measured adaptive response to a component of the applied stimulus. Here, we functionally isolate the turkey radius, a cylindrical bone with minimal curvature, and load the bone primarily in bending. With this model, we are able to relate specific stimuli to a measured adaptive response, and will be able to validate our observations by rotating the surgical alignment of the loading pins within the transverse plane (e.g. rotating the neutral axis of bending from the caudal/cranial to dorsal/ventral cortices).

METHODS

Using general halothane anesthesia, the right radii of three immature male turkeys (4 months) were isolated from their normal functional stimuli with parallel metaphyseal osteotomies. Stainless steel caps were filled with methylmethacrylate bone cement and placed over the exposed diaphyseal bone ends. Steinman pins (3mm diameter) were passed through matching holes in the caps and radius, extending approximately 2cm past the ventral and dorsal wing surfaces. The muscles, vascular supply, and innervation of the diaphyseal shaft was left intact. Prior to recovery from anesthesia, pins were secured with external fixators which prevented accidental loading during the experimental period. The left radius remained undisturbed and served as an intact contralateral control.

The turkeys underwent a four week experimental protocol in which, once a day, the fixators were removed, and the radius was dynamically loaded. The external loads were applied to the pins by a pneumatic cylinder with custom mating sleeves, and consisted of 100 cycles per day of a trapezoidal waveform (total period of 2.5s). The loading placed the bone primarily in bending, and was calibrated to induce a peak normal strain of $1500\mu\epsilon$, and a peak strain rate of $11{,}000\mu\epsilon$/s. The orientation of the transcutaneous pins were such that peak tension strains were induced in the dorsal/caudal cortex, peak compressive strains in the ventral/cranial cortex, and the neutral axis of bending spanned portions of the caudal and cranial cortices. Upon sacrifice, sections from the mid-diaphysis of the experimental and intact contralateral control radii were extracted. The sections were ground to 100 microns, microradiographed, magnified (15x), and digitized to determine areal properties. The area bounded by the endosteal envelope and intracortical porosities were subtracted from the periosteal envelope area to determine total bone area for a given cross-section.

Site specific adaptation was identified by anatomically aligning the experimental cross-section upon the control section using the center of the endosteal area as the point of rotation. The sections were divided into eight equal angle pie segments with sectors 1 and 5 encompassing the regions of peak tensile and compressive strain respectively, and sectors 3 and 7 encompassing the neutral axis (figure 1). Differences between experimental and control were examined using paired t-tests with p=0.05.

RESULTS

After four weeks of experimental loading, the mean (S.D.) total area of the experimental radii was nearly identical to that of the intact contralateral control bones (23.7(5.4) vs 23.2(3.1)mm^2). This net balance of bone area was attained by significantly increasing both periosteal area (10.4%) and endosteal area (16.8%) in the experimental bone compared to the contralateral control radius. Although the area of intracortical porosity increased from .06(.03)mm^2 in the control section to 0.8(0.7)mm^2 in the experimental radius, these intracortical changes were relatively small and had minimal effect upon total areal determinations. Areal changes within the eight sectors, however, were highly non-uniform. The sector corresponding to peak compressive strains (five) demonstrated an average bone loss of -14.5(8.9)%, while sector seven, corresponding to the location of the neutral axis in the caudal cortex, generated a 57.3(17.1)% increase in bone area (figure 2).

DISCUSSION

The experimental loading regimen did not stimulate an increase in total bone area, yet was sufficient to site-specifically alter the morphology of the radius. The loss of bone in five of the eight sectors was balanced by areal increases within sector six, and, most dramatically, sector seven. Surprisingly, the sectors corresponding to the greatest induced compressive and tensile strains both decreased in area, while the largest areal gain corresponded to a sector spanning the neutral axis. Increased bone near this site of minimal strain may reflect the potential regulatory effect of physical stimuli upon the growing skeleton as hypothesized by Bain et al. (5), who found that functional disuse in growing animals actually stimulated a small increase in bone mass compared to control bones. The site-specific nature of this response will be further explored by altering the location of minimal engendered strains in subsequent experimental loading studies.

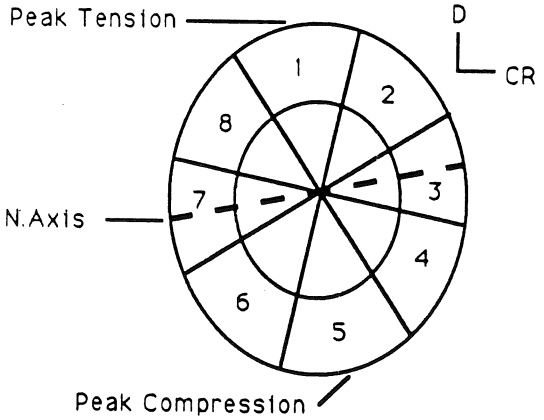


Fig. 1. Schematic of radius mid-diaphysis cross-section with sectors.

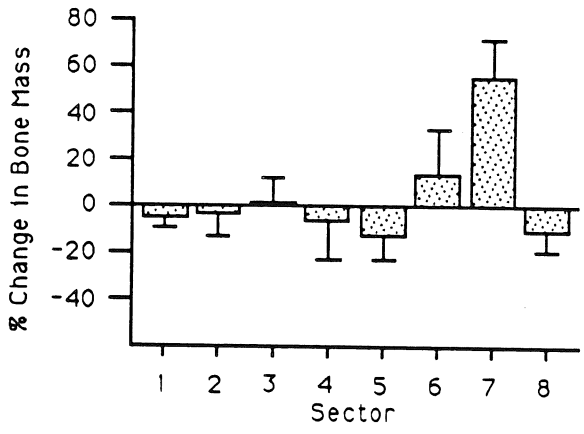


Fig. 2. Mean (S.D.) areal changes within each section versus control.

REFERENCES

1. Woo et al. (1981), J.B.J.S., 63-A:780-7. 2. Liskova & Hert (1971), Folia Morph., 19:301-17. 3. Churches et al. (1981), Trans. ASME,, 69-80. 4. Rubin & Lanyon (1984), J.B.J.S., 66-A:397-402. 5. Bain et al. (1990), Trans. 36th Orthop. Res. Soc., 418.

SESSION 10

RUNNING

3-DIMENSIONAL KINEMATICS OF THE PATELLOFEMORAL JOINT DURING RUNNING

§McClay, IS, #Cavanagh, PR, @Kalenak, A, #Sommer, HJ III

§University of Delaware, Newark, DE, 19716, #The Pennsylvania State University, University Park, PA, 16802, @Hershey Medical Center, Hershey, PA

INTRODUCTION

Patellofemoral problems are among the most common and most puzzling of knee disorders in runners. Conventional wisdom suggests that the etiology of these problems is, in part, due to maltracking of the patella with respect to the femur, and that it is often related to improper foot mechanics (ie. excessive pronation). However, patellofemoral motion is inherently difficult to measure with standard skin marker techniques. Therefore, four subjects underwent intracortical pin implantation into the patella and femur. Three-dimensional kinematics of the patellofemoral joint (PFJ) were then studied during running. Although PFJ motion was found to be somewhat variable between subjects, some trends were identified. In addition, subtle differences were noted between the normal and the patellofemoral pain subjects.

REVIEW AND THEORY

Direct measurement of patellofemoral kinematics have been obtained on cadavers through the use of roentgen stereophotogrammetric analysis[1]. Veress et al.[2] implanted tantalum balls into the patella and femur of four live subjects and used serial radiographs to study in-vivo PFJ motion while isometrically loading the quadriceps. Most of the PFJ studies in the literature incorporate protocols which do not represent normal activities of daily living. Lafortune et al.[3] were the first to study PFJ kinematics of healthy subjects during normal locomotion through the use of intracortical pins and three-dimensional cinematography. Although the PFJ is the most commonly injured joint in runners, there have been no studies, to date, that have investigated PFJ kinematics during running in either healthy or injured subjects. The purpose of the present work was to investigate the six degree of freedom (DOF) relative motion between the patella and femur during running in normal subjects compared to runners with patellofemoral pain and excessive pronation.

PROCEDURES

Four male recreational runners (ages 21-39 years) volunteered for the study. Two subjects (NL) presented with normal knees and normal rearfoot mechanics. The other two subjects (PFP) experienced anterior knee pain associated with running and exhibited excessive subtalar joint (STJ) pronation (27 deg. vs. 10 deg. for the NL). Intracortical pins (3.2 mm) were surgically inserted into the femur and patella following local anesthesia. Clusters of 4 light emitting diodes (LEDs), weighing approximately 10 grams, were attached to the pins in a triad formation with three of the LEDs attached to the end of 6 cm. long wooden struts. The fourth LED was located in the approximate center of the base of the triad. The image coordinates of the LEDs were recorded via three optoelectronic cameras (100 Hz) while the subjects ran on a treadmill operating at 3.35 m/s. The global coordinates were reconstructed using a modification of the SMAC procedure of Woltring[4]. The coordinates in the anatomical reference frame were obtained via biplanar radiographs. Six-DOF relative joint motion was calculated and motion was described about a joint coordinate system[5]. Skin markers were placed along the longitudinal axis of the posterior lower leg and heel and their coordinates were recorded via a Locam camera (100 Hz) and used to calculate the 2-D rearfoot angle. The mean values of 15 contact periods (250 ms each) were used for analysis.

RESULTS AND DISCUSSION

Figure 1a-c shows the average angular kinematics of the PFJ over 15 contacts for each of the subjects. The open symbols represent the PFP subjects. There was notable consistency in the flexion/extension patterns between the subjects. Motion in this plane comprised the largest component of the total motion. It followed closely that of the tibiofemoral joint (TFJ) with flexion occurring until 40% of

support followed by extension peaking near toe-off. The PFJ began and remained in greater extension than the TFJ and had less total excursion. No systematic differences were noted between the two groups. In the frontal plane, three of the four subjects demonstrated a general trend of abduction followed by adduction with abduction again occurring just prior to toe-off. The remaining PFP subject demonstrated a pattern opposite to the one described. Motion in the transverse plane was fairly constant across the contact period for all subjects, although offsets were noted.

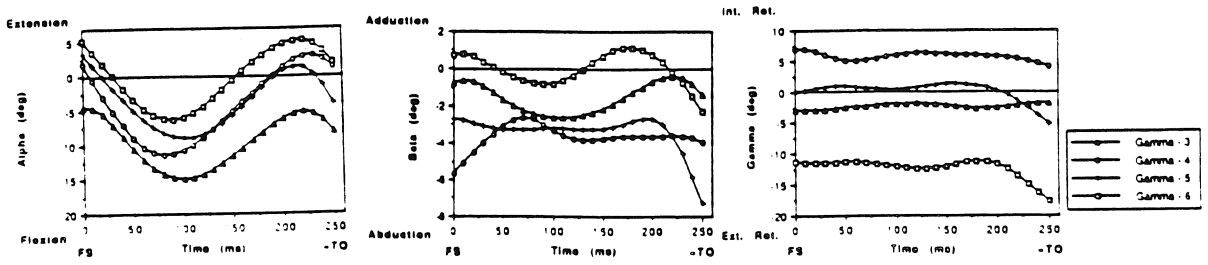


Figure 1. PFJ angular motion in the a) sagittal, b) frontal and c) transverse planes

The linear motion of the PFJ can be seen in Figure 2a-c. Along the ML axis, the PFP subjects demonstrated over 2.5 times the excursion as compared with the NL subjects (6.9 mm. vs. 2.52 mm.) This may be representative of dynamic instability often referred to in patients with PFJ disorders. Motion along the FL axis was fairly consistent in three of the four subjects with a pattern of posterior translation with knee flexion followed by anterior translation. One PFP subject exhibited a large offset placing the patella more anterior with respect to the femur. This may be an indication that it is not as well seated in the femoral groove, which could contribute to instability. Linear motion was most consistent along the DC axis. As expected, the patella moved distally (distraction) with patellar flexion and proximally (compression) with extension. The patellae of the PFP subjects remained more proximal throughout contact, especially when the knee was more extended. This has also been associated with instability as the patella is less seated in the femoral trochlea. Some care must be taken in the interpretation of the linear kinematic results as the data were not normalized for size. However, the subjects were fairly well-matched in build.

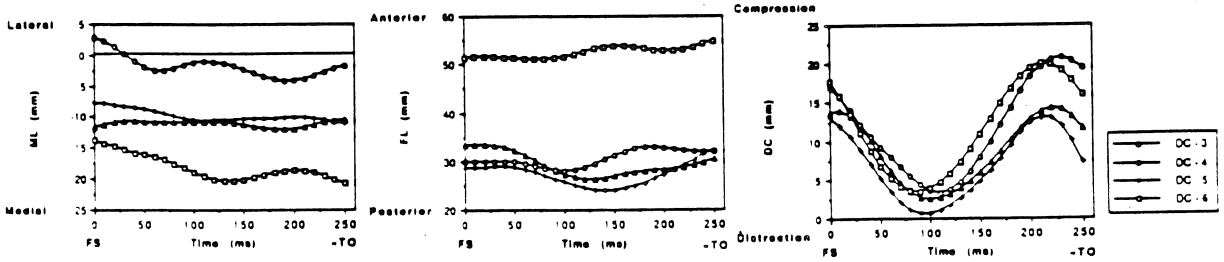


Figure 2. PFJ linear motion along the a) med-lat (ML), b) ant-post (FL) and c) prox-dist (DC) axes

In summary, a general pattern of patellar flexion, abduction, posterior and medial translation was seen with knee flexion. The differences noted between the PFP and NL subjects were relatively subtle in view of the greater than two-fold increase in maximum STJ pronation. These subtle differences, however, may be critical in enhancing the understanding the etiology of PFJ disorders.

REFERENCES

1. van Kampen, A et al.: *J. Orthop. Res.* 8:372-382, 1990
2. Veress, SA et al.: *J. Biom.* 12:639-650, 1979
3. Lafortune, MA et al.: BiomechanicsX (ed. B. Johnson), Champaign, Ill, 1986, pp 337-342
4. Woltring, HJ: *J. Biom.* 13:39-48, 1980
5. Grood, ES et al. *J. Biom. Eng.* 105:136-144, 1983

THE EFFECT OF ORTHOTICS ON ANKLE PRONATION AND KNEE ROTATION

Ksenia Kozak, Zvi Ladin, John M. Giurini*

Biomedical Engineering Dept & NeuroMuscular Research Center,Boston University
44 Cummington St.,Boston, MA 02215
*New England Deaconess Hospital

INTRODUCTION

Excessive pronation has often been linked to various injuries of the knee joint. Orthotics are often prescribed to control pronation and its associated injuries. For orthotics to achieve optimal results, they need to not only limit pronation, but to also eliminate abnormal motion at proximal joints such as the knee and hip. This study employed the use of an optoelectronic motion analysis system to assess the effects of orthotics on the kinematics of the ankle and knee joints.

REVIEW AND THEORY

As the foot pronates, the eversion of the subtalar joint causes obligatory internal rotation of the tibia (Fig.1). During gait, excessive pronation produces excessive internal rotation of the tibia which continues beyond midstance. As the knee extends during midstance the femur begins to externally rotate, while the tibia continues to internally rotate due to the excessive pronation. These opposing transverse motions, i.e. internal rotation of the tibia and external rotation of the femur, may stress the knee joint and cause stretching of the structures which stabilize and support it [1].

PROCEDURES

An experiment was conducted to investigate the kinematics of running gait for a group of eight excessive pronators. The subjects were diagnosed as excessive pronators following a clinical examination, and orthotic shoe inserts were individually prescribed and constructed for them. The WATSMART optoelectronic 3-D motion analysis system was used to monitor motion. The 3-D coordinates of infrared light emitting diodes, attached to the subject's foot, shank and thigh, were determined using two infrared-detecting cameras and a reconstruction algorithm. This 3-D data was processed using TRACK© software to calculate the six degrees of freedom of each segment. The spatial orientations of the segments were decomposed into the three anatomical joint rotations for the knee and the ankle using the ANAGAIT program. In this paper we examine two specific joint rotations:

- ankle eversion, as a measure of pronation
- transverse rotation at the knee, i.e. rotation of the tibia with respect to the femur

RESULTS AND DISCUSSION

An examination of the time trajectories of ankle inversion-eversion and knee rotation showed that in general, internal rotation of the tibia closely coincided with pronation (Fig.2). When we quantified these results by calculating the maximum values of joint angular rotation, we saw that orthotics decreased the maximum angle of pronation, and yet they increased the maximum internal rotation of the tibia. Analysis of the kinematic data showed that orthotics produced a 30% decrease in pronation and a 20% decrease in the overall range of motion of the ankle in

the frontal plane. However, orthotics increased the internal rotation of the tibia by 23% and increased the total range of tibial rotation by 8%. Statistical analysis indicated that the results were significant to the 90% confidence level.

The results seem to contradict the findings of previous investigators about the relationship between pronation and internal rotation of the tibia [1,2,3]. However, Inman and Mann [4] demonstrated that the amount of tibial rotation generated by foot pronation is determined not only by the amount of subtalar joint pronation but also by the spatial orientation of the subtalar joint axis. If the subtalar joint axis is parallel to the long axis of the tibia, each 1° of pronation will produce 1° of internal rotation. If the subtalar joint axis is perpendicular to the long axis of the tibia, each degree of pronation will produce no internal leg rotation. Our results suggest that the orthotics modified the spatial orientation of the subtalar joint, leading to an increase in the tibial internal rotation in spite of the decrease in the pronation angle.

The orthotics were designed to reduce pronation of the midtarsal joint. They did not have rearfoot posting and therefore were not designed to offer optimal rearfoot control, i.e. control of the subtalar joint motion. Thus, most of the observed decrease in pronation was probably limited to the midtarsal joint. In addition, it is the lack of rearfoot posting which might have modified the spatial orientation of the subtalar axis, orienting it more closely in parallel to the long axis of the tibia, therefore increasing the influence of pronation on internal rotation of the tibia.

These findings lead us to conclude that current prescriptive procedures for orthotics need to be supplemented with an objective biomechanical analysis, to ensure that orthotics not only limit pronation, but lead to normal function at proximal joints.

ACKNOWLEDGEMENT

This study was funded by a grant from Reebok International Ltd.

REFERENCES

1. Coplan MA, *J Orthop Sports Phys Ther*, 3:366-369, 1989
2. Vogelbach WD, *Athletic Training*, 22:6-16, 1987
3. Pagliano J, *Med Sport Sci*, 23:155-160, 1987
4. Inman VT, *DuVries' Surgery of the Foot*, Ed.3, CV Mosby, St.Louis, 1973

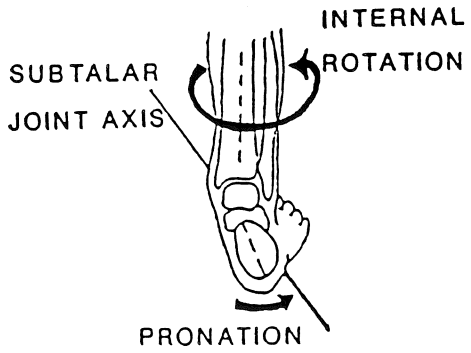


Figure 1: Eversion of the foot and rotation of the tibia

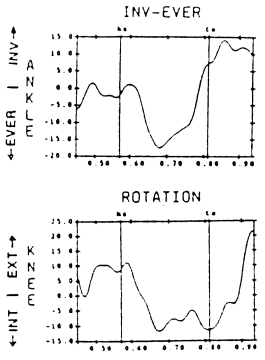


Figure 2: Kinematic data

TEMPORAL RELATIONSHIPS BETWEEN KNEE FLEXION AND PRONATION IN RUNNING: ASSESSMENT OF PRONATION EVENT SELECTION

Brian L. Caster, Timothy R. Derrick and Barry T. Bates
Biomechancis/Sports Medicine Lab, University of Oregon, Eugene, OR 97403

INTRODUCTION

Pronation characteristics were assessed under two running shoe conditions, employing three different methods of discrete event selection. Though all three methods led to similar results in the analysis of magnitude, the bi-modal nature of most pronation curves resulted in inconsistencies among the methods of evaluation for the temporal aspects of pronation. In addition, differences in the rates of change between the knee joint and pronation curves are presented as a means of identifying phase relationships between these motions.

REVIEW AND THEORY

The identification of medial knee joint disorders in association with excessive and/or prolonged pronation during mid-stance and takeoff phases of running (4,5) suggests an important temporal relationship between knee and ankle joint motions. There is a lack of documentation, however, on the temporal relationships between knee flexion/extension and pronation/supination. Furthermore, studies which assess pronation typically address only one pronation event during stance: absolute maximum pronation. The presence of bi-modal pronation curves (1,3) could result in ambiguity with regard to the pronation event being analyzed. The purpose of the study was to describe and assess the relationships among three temporally distinct pronation events and knee joint function. Events were selected with the intent of identifying a more appropriate measurement for use in addressing questions of timing between knee flexion/extension and pronation/supination.

PROCEDURES

Each of six male runners performed 20 trials for each of two shoe conditions. The shoes employed were new, top-of-line running shoes from reputable manufacturers, both containing motion control features. Subjects (S) ran at their preferred training pace (mean: 7 min/mile) while being monitored using a timing light system (+/- 3% target pace). Sagittal plane and rear view lower extremity kinematic data were acquired using a two camera automated tracking system (Motion Analysis Corp., 200 Hz). Reflective markers were attached at the hip, knee and ankle joint centers to monitor sagittal plane knee joint motion and on the heel portion of the shoe and achilles tendon to monitor rear foot motion. The pronation/supination angles were defined as the difference between the calcaneal/shoe and tibial segment angles. Stance phase variables included in the analysis were magnitudes and times of occurrence of maximum knee flexion (KNEE) and three pronation angles: absolute minimum pronation (PR1), minimum pronation occurring after KNEE (PR2), and a point (PR3) defined by a slope criterion (.18 deg / 1% stance), which identified a rapid change from the relatively stable state of pronation observed in mid-stance. Condition differences were evaluated using a single subject analysis of variance (ANOVAs) technique. In addition, slope differences between single subject ensemble knee flexion and pronation curves were generated to qualitatively assess temporal relationships between these two joint motions.

RESULTS AND DISCUSSION

Five of the six subjects exhibited non-significant differences for maximum degree of knee flexion, indicating the relative stability of this measure. All pronation magnitudes were greater for Shoe 1 ($p < 0.01$) except PR2 and PR3 for S1, and PR3 for S6. The temporal analyses, however, only identified major shoe differences for PR1 (Table 1). Temporal measurement variability as evidenced by the mean standard deviations across subjects was relatively consistent between PR2 and PR3, but considerably greater for PR1. The temporal instability of PR1 could be attributed to the bi-modal nature of most pronation curves and the tendency for the Shoe 1 condition to produce an early minimum of greater absolute magnitude than PR2, as illustrated by the representative data (Fig. 1,2). Though this apparent difference during the initial stage of pronation should not

be discounted, the greater temporal consistency of performance across shoes observed after the point of maximum knee flexion, as evidenced by the PR2 and PR3 values, suggests that these parameters might produce more appropriate measures to assess potential problems arising from a prolonged state of pronation relative to the onset of knee extension. In addition to the quantitative evaluation of discrete events, the relative rates of change between knee joint flexion/extension and pronation/supination were assessed (Fig. 1,2). Immediately following contact, a phase of greater relative pronation velocity was observed, followed by a phase of greater knee flexion velocity, as a relatively stable state of pronation was achieved. As the knee began to extend, the velocity difference tended to increase until the foot began to actively supinate. These curves, presented primarily for qualitative analysis, provide additional insight into the temporal phasing between knee flexion and pronation, suggesting a need for further investigation. In terms of potential problems associated with a prolonged state of pronation following the onset of knee extension, the critical interval defined by zero slope difference observed at maximum knee flexion and the relative maximum slope difference observed at P3 should be investigated.

Table 1. Times of Occurrence of Knee Flexion & Pronation Variables

	PR1		PR2		PR3		KNEE	
	Sh1	Sh2	Sh1	Sh2	Sh1	Sh2	Sh1	Sh2
S1	**20.9**	**36.6**	43.8	46.6	51.4	53.0	34.1	29.4
S2	**40.2**	**54.8**	**46.7**	**54.8**	**53.0**	**59.4**	38.7	43.2
S3	**45.1**	**48.4**	**45.1**	**48.4**	**49.6**	**54.3**	**38.6**	**36.8**
S4	**16.0**	**33.3**	44.2	43.6	49.8	52.2	47.0	45.9
S5	**47.2**	**56.0**	53.3	56.0	60.0	61.3	**42.3**	**39.5**
S6	45.9	51.9	52.6	53.1	57.6	58.5	**40.6**	**38.6**
Group	36.2	47.2	47.6	51.0	53.6	56.6	40.2	39.1
	(9.89)	(9.59)	(4.53)	(4.76)	(4.33)	(4.28)	(3.94)	(5.88)

Bold & Underline: $p<0.01$; Shoe condition (Sh) means are in % stance.

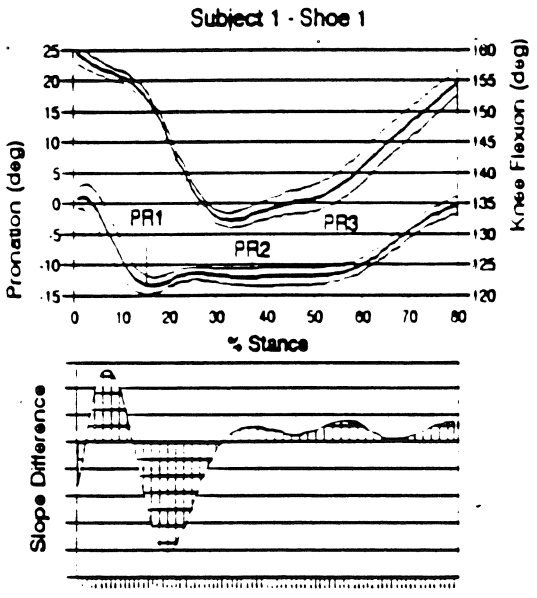


Figure 1. Ensemble Curves & Slope Differences

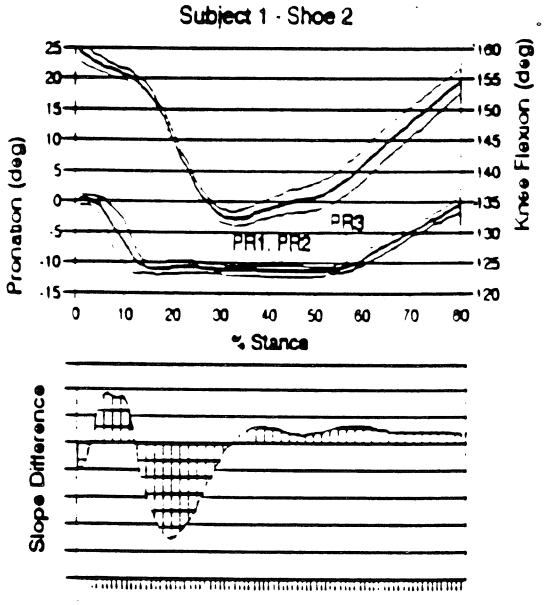


Figure 2. Ensemble Curves & Slope Differences

1. Areblad, et al. (1990). 3-D measurement of rearfoot motion during running. J. Biomechanics 23(9), 933-940.
2. Bates et al. (1978). Foot function during the support phase of running. Running 3(4), 24-31.
3. Clark et al. (1984). In Frederick (Ed.) Sport Shoes and Playing Surfaces, pp. 166-189.
4. James and Jones (1990). In Cavanagh Biomechanics of Distance Running, pp. 249-269.
5. Roy and Irvin. (1983). Sports Medicine. Englewood Cliffs, N.J.: Prentice-Hall.

TIMING OF THE KNEE AND SUB-TALAR JOINT ACTIONS DURING TREADMILL RUNNING

Joseph Hamill†, Barry T. Bates††, Kenneth G. Holt†††
Department of Exercise Science, University of Massachusetts, Amherst, MA 01003†
Department of Physical Education, University of Oregon, Eugene, OR 97403††
Department of Physical Therapy, Boston University, Boston, MA 02215†††

INTRODUCTION - In clinical studies by James et al. (1978) and Clement et al.(1981), "knee pain" accounted for over 25% of all running injuries. A disruption in timing between the knee and sub-talar joints during support has been speculated as the mechanism for this injury and has been alluded to in the biomechanics literature. To date there has been little evidence linking the mechanics of the lower extremity to knee injury. The purpose of this study was to describe the relationship between the sub-talar and knee joint actions during treadmill running in the presence of a perturbation caused by shoes of differing midsole durometer.

REVIEW AND THEORY - Bates et al. (1978) first suggested the disruptive timing mechanism. During the initial phase of support, the sub-talar joint pronates, the knee joint flexes, and the tibia internally rotates. Conversely, during the latter phase of support, the sub-talar joint supinates, the knee joint extends and the tibia externally rotates. If resupination of the sub-talar joint occurs at a different time in support than the initiation of knee extension, an antagonistic relationship may be present. This scenario could result in excessive stress at the knee joint and, with repetitive cycles as occur in running, could result in knee injury. While this mechanism of lower extremity dysfunction has been described clinically (Gray, 1985) and in theoretical papers (Tiberio, 1987), there is a dearth of data to support it.

METHODS - Twelve healthy college age males served as subjects in this investigation. All subjects ran with a heel-toe footfall pattern. Subjects ran on a heavy-duty motorized treadmill. Kinematic data were collected using two audio synchronized 200Hz NAC high speed video cameras and recorders situated to obtain a right side sagittal view and a rear view of the right lower extremity during support. Each subject was required to run in each of the three types of shoes for a period of 5 minutes with the last minute of the run being recorded. Five complete support phases for each subject/condition were digitized using a Motion Analysis VP110 micro-processor interfaced to a SUN minicomputer. The space coordinates obtained were then scaled and smoothed using a low-pass digital filter. The shoes were made specifically for this study. They were a fully slip-lasted construction and were identical except for the durometer of the midsole. The midsole durometers (shore A) were 70 (C1), 55 (C2), and 45 (C3).

RESULTS - The mean values and statistical analyses for all parameters are presented in Table 1. The response of the midsole material to a given load appeared to be linear in nature. In the four variables describing the rearfoot angle that produced significant F-ratios, there were no significant differences between C1 and C2 ($p < 0.05$). The locus of the differences in each case was revealed to be between these conditions and C3. The mean maximum rearfoot angle was greater for the 45 durometer shoe than for the two firmer midsole shoes. The significant differences in the calcaneal angle at the time of maximum rearfoot angle reflected the trend of the maximum rearfoot angle. There were no significant differences among conditions for any of these parameters describing knee kinematics. There was no significant difference between the percent time to maximum knee flexion and the percent time to maximum rearfoot angle for either C1 or C2 ($p < 0.05$). However, for C3, the time to maximum rearfoot angle was significantly less than the time to maximum knee flexion with a mean absolute difference of 7.2%.

Table 1 - Statistical analysis of rearfoot and knee angle variables (n=12).

Variable	C1	C2	C3	F-ratio
REARFOOT				
Maximum RF angle (°)	-8.5 (2.9)a	-9.4 (2.7)a	-14.7 (3.9)	12.68*
% time to max. RF angle (°)	43.8 (3.4)a	42.8 (3.1)a	38.7 (4.3)	6.52*
Shank angle at Max RF (°)	83.1 (2.2)	82.6 (2.1)	83.6 (2.3)	<1
Calc. angle at Max. RF (°)	91.6 (1.8)a	92.0 (2.5)a	98.3 (3.7)	20.91*
Max. RF velocity (°/s)	-314 (80)	-300 (72)	-339 (62)	<1
% time to Max. RF velocity	8.4 (2.6)	9.2 (2.7)	16.7 (3.1)	32.15*
KNEE				
Max. flexion angle (°)	44.1 (3.5)	43.3 (3.7)	42.7 (3.7)	<1
% time to max. flexion	44.2 (4.8)	44.1 (3.9)	45.9 (4.2)	<1
Max. knee velocity (°/s)	415 (52)	418 (45)	395 (50)	<1
% time to Max. Knee vel.	21.8 (4.8)	20.3 (4.3)	22.3 (5.3)	<1
IMPACT TEST				
Peak g	18.95	13.31	10.25	
Time to peak g (ms)	12.12	13.66	17.26	

* $p < 0.05$ (means with the same subscript are not significantly different)

DISCUSSION - The results of this experiment clearly demonstrated that a softer shoe produces a greater amount of rearfoot motion - an indicator of increased sub-talar joint pronation. In addition, the changes in lower extremity were restricted to the ankle joint complex, the knee joint showing no change in the amount of flexion and extension. It was also demonstrated that a soft midsole may disrupt the timing relationship between the motions of the sub-talar and knee joints. The rearfoot reached maximum pronation sooner in the softest shoe condition (C3), and tended to move into a neutral position later in the stance phase than the two harder shoes (C1 and C2). In the early stance phase of C3, the rearfoot reached maximum pronation and began to resupinate while the knee was still moving into flexion. In later stance, following maximum rearfoot angle, the increased time for the foot to resupinate indicated that the knee was externally rotating the tibia at a relatively faster rate than was the resupinating foot. While this may not be as crucial a disruption as the first it may nevertheless be a cause of dysfunction. Bates and associates (1978) suggested that, in a soft durometer midsole shoe, the time to maximum pronation would be reached after maximum knee flexion. This is contrary to the findings of this study. An interesting side effect of these results is the comparison of the response of the midsole material to a machine invoked load and to an in vivo load. The effect of the materials testing indicated that the influence of the durometer produced a linear response in terms of the peak impact forces. The linear response of the shoes, however, was not reflected in the in vivo measurement of the angles of the rearfoot. Lack of differences between the two harder shoes (C1 and C2) and a rather larger effect of the softer shoe (C3) indicate that the biological system can accommodate to the change in durometer up to a point, after which the foot may not have the muscular strength or control to compensate.

REFERENCES

1. Bates, B.T. et al. Running, 24-31, Fall, 1978.
2. Clement, D.B. et al. Phys. Sports Med. 9:47-58, 1981.
3. Gray, G.C. Rehabilitation Network, 1985.
4. James. S.L. et al. Am J Sports Med. 6:40-50, 1978.
5. Tiberio, D. J Orthop. Sports Phys. Ther. 9:160-165, 1987.

VELOCITY AND GROUND REACTION FORCE RELATIONSHIPS DURING WALKING AND RUNNING

J.L. Ray, A.M. Weisberger, T.S. Keller, S.S. Hasan, R. Shiavi, and D.M. Spengler
Department of Orthopaedics and Rehabilitation
Vanderbilt University, Nashville, Tennessee 37232

INTRODUCTION

The vertical ground reaction forces (GRF) produced during normal walking and running are dependent on the velocities at which the activity is performed. Few studies have examined GRF over a wide range of velocities, but instead have investigated only a subset of velocities [1,2]. In order to more completely understand this relationship tests were conducted using 23 volunteers, both male and female, over a range of velocities from 1.5 ms^{-1} to the subject's maximum speed. The vertical GRF was found to increase linearly up to approximately 60% of a subject's maximum velocity, after which the vertical GRF remained constant at 2.5 times body weight (W). Slow jogging was associated with significantly increased forces in comparison to walking at the same speed.

REVIEW AND THEORY

The popularity of recreational running has dramatically increased over the past several years. Repeated impact loading, such as that occurring during walking and running, has been thought to be responsible for several types of chronic injuries (including fatigue fractures, cartilage damage, and shin splints) [3]. The variation of vertical GRF with velocity has been one which many investigations have focused upon [2,4]. A survey of the literature [5] shows the relationship of velocity to GRF to be linear according to equation 1.

$$F_z/W = 0.47V + 0.62 \qquad (1)$$

Assuming this relationship to be true faster runners, such as sprinters, would be subject to forces in excess of five times body weight and, thus be prone to a greater degree of injury than slower runners.

PROCEDURES

Subject Population: Twenty-three subjects (13 males and 10 females) were used. All subjects were recreational athletes who participated on a regular basis in a variety of activities. Mean values for weight of the subject population were 75.6 kg (± 12.0) and 57.6 kg (± 5.8) for males and females, respectively. Mean height values were 178 cm (± 7.0) and 168 cm (± 7.0) for males and females, respectively. Mean age was 25.2 years (± 4.3) for males and 28.4 years (± 5.4) for females.

Data Collection: Subjects were asked to walk, jog, and run over a 6-channel AMTI force plate. The force plate was installed flush in the center of a 12 meter long running stage so that 6 meters were allotted for acceleration and deceleration, respectively. Eight walking and running velocities were measured in the range 1.5 ms^{-1} (± 0.2) to 6.0+ and 1.5 ms^{-1} (± 0.2) to 5.0+ for males and females, respectively. Subjects were encouraged to run as fast as possible in the 5.0+ and 6.0+ ranges. Velocity was measured by two photocells spaced 2 meters apart (1 meter each from the center of the force plate). Each subject wore a pair of Nike™ Aircraft running shoes having identical soles and cushioning. Data were collected using a Digital Equipment PDP 11/23 computer with a 12 bit A/D converter. The vertical GRF was normalized to body weight and velocity was normalized according to the subject's

was normalized to body weight and velocity was normalized according to the subject's maximum velocity. In addition, data from a subset of 12 subjects (6 males and 6 females) comprising a slow jogging group were analyzed to compare the vertical GRF between slow jogging and walking at the same velocity.

RESULTS AND DISCUSSION

Figure 1 illustrates the relationship between normalized velocity (V/V_{max}) and the peak vertical GRF (F_z/W) for males and females, respectively. The maximum values for F_z/W were 245.2% (± 12.9) W at 6 ms^{-1} for females, and 224.8% (± 25.5) W at 7 ms^{-1} for males which is dramatically less than the 5 times W predicted by equation 1 for 10 ms^{-1}. Although there was a corresponding increase in impact force and velocity, this increase only occurred up to approximately 60% of maximum velocity. No statistical differences ($P > 0.05$) between males and females were found at most speeds according to an analysis of variance. At velocities > 80-90% of maximum there was a significant decrease in force. Most of the variations in F_z/W, over the range 1.5-8 ms^{-1}, were explained by loading rate, computed by dividing the normalized peak vertical GRF at impact by the time interval between initial foot contact and the peak impact force. In the male subjects there was a significant decrease in force at the higher velocities, females exhibited this trend as well, except that the maximum velocity for two females resulted in a slight increase in force. Results from the slow jogging trials indicate that slow running involves vertical GRF of approximately 50% greater than walking at the same speed. In summary, vertical GRF does not increase linearly through the complete range of speeds, but instead remains constant or decreases at higher speeds.

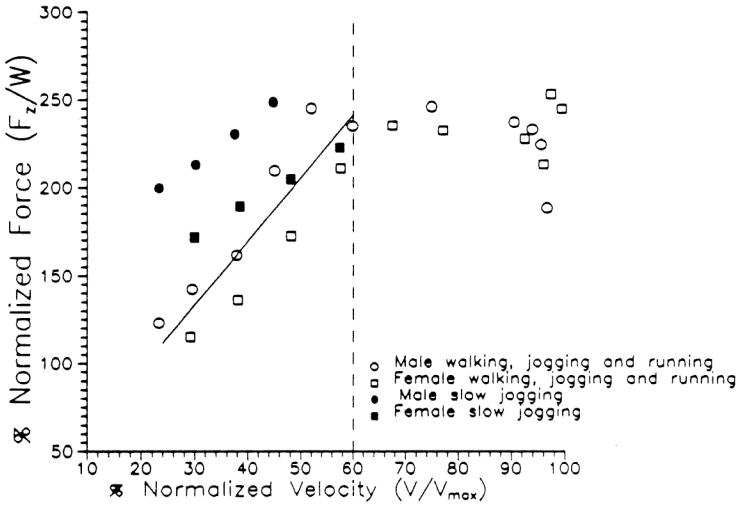


Figure 1. Data points are mean values for each velocity group (i.e. V ± 0.2 ms^{-1}). Regression equation of straight line is: $F_z/W = 3.51\ V/V_{max} + 0.31$, $R^2 = 0.59$.

REFERENCES

1)Alexander et al., J. Biomechanics 13:383-390, 1980. 2)Nigg, B.M., Biomech. Aspects of Sports Shoes and Playing Surfaces. Univ. Printing, Calgary, pp. 11-23, 1983. 3)Nigg et al., J. Biomechanics 20:951-959, 1987. 4)Munro et al., J. Biomechanics, 20:147-155, 1987. 5) TS Keller, Ph.D. dissertation, 1988.

CENTER OF PRESSURE ESTIMATION DURING RUNNING WITHOUT A FORCE PLATFORM

David Andrews, B.P.E. and James J. Dowling, PhD.
Department of Physical Education, McMaster University
Hamilton, Ontario, Canada.

INTRODUCTION

Kinetic analysis of locomotion using a linked segment model requires ground reaction forces (GRF) and centers of pressure (CP), typically obtained as output from a force platform. This study presents a new method of calculating the CP by equating the foot segment power (P) with the rate of change of mechanical energy (E), during the stance phase of running, without a force platform. Estimated CP values correlated well with the actual CP values (r=.91). RMS errors were found to be 5.3 cm in magnitude, on average.

REVIEW OF THEORY

Vertical and horizontal GRFs and CPs are required when calculations of ankle joint forces and net joint moment are made in the sagittal plane. Previous work on human gait by Robertson et al.(1980), and Quanbury et al.(1975), has shown that good estimates of the magnitude and direction of GRFs can be made without a force platform from whole body center of gravity accelerations, kinematics and anthropometrics. The point of application of the GRFs (ie) CPs, is not as easily determined. Robertson et al.(1980), estimated the CP path by linearly interpolating between foot marker positions at various times during the single support phase of gait. The purpose of this study was to examine the accuracy of a new method that solves for CP, during the stance phase of running, by equating $\dot{E}$ with P.

PROCEDURES

Five healthy subjects (3 male, 2 female) were videotaped at 60 f/s while running across a force platform (AMTI). Body landmarks were digitized (Peak Performance Technologies Inc.), creating a 13 segment sagittal plane model. The digitized data were interpolated using a cubic spline to increase the sampling rate to 200 Hz, synchronizing them with the force platform data. The raw displacement data were digitally filtered (Butterworth) and differentiated using central finite differences. $\dot{E}$ was calculated as in Robertson et al.(1980a), and joint reaction forces were calculated as in Robertson et al.(1980b). By setting $\dot{E}$=P, the CP, with respect to the center of gravity of the foot, was calculated using Equation 1. Linear interpolation of the CP path was done (Robertson et al., 1980b) when the foot angular velocity (ω_F) was between 2 and -2 rad/s. RMS errors, and correlation coefficients ("r" values) between estimated and actual CP paths, were noted.

$$Eq.1: \quad CP = \frac{I_F \cdot \alpha_F + R_x M_{R_x} + R_y M_{R_y} - F_x M_{F_x} - \frac{\dot{E} - R_x v_x - R_y v_y}{\omega_F}}{F_y}$$

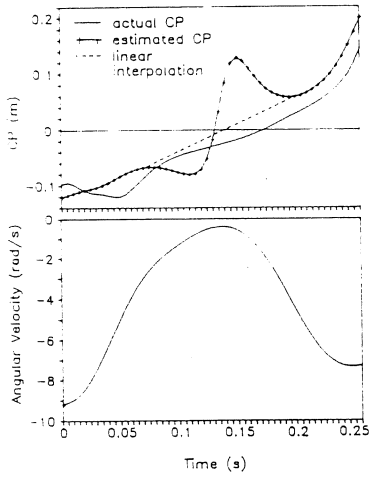
where: **CP** - center of pressure w.r.t. the foot center of gravity
$\mathbf{I_F}$ - foot moment of inertia about the center of gravity
$\boldsymbol{\omega_F, \alpha_F}$ - angular velocity & acceleration of foot, respectively
R - ankle joint reaction force
M - moment arm w.r.t. the foot center of gravity
$\dot{\mathbf{E}}$ - rate of change of foot mechanical energy
v - linear velocity of the ankle joint
F - ground reaction force
x,y - horizontal & vertical directions, respectively

RESULTS AND DISCUSSION

The estimated CP paths of each subject showed oscillations from the actual CP path at those times when the magnitude of ω_F approached zero (Figure 1). The low ω_F values typically occurred just prior to toe off or during the middle section of stance when the foot was momentarily flat on the platform. The results are shown as RMS errors and "r" values in Table 1. The average RMS error of 5.3 cm is appreciably higher than the 2.5 cm errors quoted by Robertson et al. (1980b). The larger error may be simply due to the greater GRF magnitudes involved in running as compared to walking. Future refinement of this method will include nonlinear interpolation when ω_F is near zero to better match the path of the actual CP (see Figure 1).

Table 1: RMS errors and "r" values for each subject.

SUBJECT	DA	JD	JL	CP	BP	$\bar{x}$
RMS ERROR (CM)	7.2	9.5	3.4	3.6	2.9	5.3
r	.84	.89	.97	.97	.88	.91



REFERENCES

1. Quanbury, A.O. et al., *J. Human Move. Studies*, 1:59-67, 1975.
2. Robertson, D. et al., *J. Biomechanics*, 13:845-854, 1980a.
3. Robertson, D. et al., *Human Locomotion I (CSB)* pp. 134-135, 1980b.

SESSION 11

ARTIFICIAL IMPLANTS

TORSIONAL STABILITY OF REVISION HIP STEMS

J.A. Longo*, T. McTighe+, J.B. Koeneman*
*Harrington Arthritis Research Center, Phoenix, AZ
+Joint Medical Products, Stamford, CT

INTRODUCTION

Excessive interfacial motion can be detrimental to the functioning of press fit artificial joint replacements. The proximal femur experiences torsional loading and in revision surgery there often is significant bone loss which limits the ability to achieve metaphyseal fit. The purpose of this study was to measure the torsional stability of five different revision prostheses in a composite femur with a proximal bony defect. The bones were tested in 20 degrees of flexion and a head load applied. The resulting rotation of the implant within the bone was recorded with two LVDTs. The results showed that designs which provided for proximal A/P wedging had the best stability for a revision with a proximal bone defect.

BACKGROUND

Excessive relative movement between the stem and prosthesis in non-cemented total joints can be very detrimental to the stability and clinical success of the prosthesis. Significant torsional moments are applied to the proximal femur at the extremes of flexion and extension during gait, in getting up from a chair, and in stair climbing [1]. Replacement of femoral hip stems often leaves a femur with much loss of proximal bone which normally provides torsional stability. Previous studies have examined the effect of stem length and curvature on torsional stability [2]. The purpose of this study was to investigate the torsional stability of different revision stem designs in a proximally deficient femur with a combined compression and torsional load.

METHODS

Six prostheses were tested in adult size left synthetic composite bone (Pacific Research Labs). The bones have approximately the same bending stiffness as human bones [3]. A test fixture was fabricated which provided the physiological compression force and torsion force which occurs at heel strike. The prostheses tested were the long stem PCA (size 6, 250 mm long), a long stem Osteonics (size #10, 250 mm long), a Solution (15 mm, 10 inches long), a BIAS (16 mm, 232 mm long), a straight stem SROM (20 X 15, 225 mm long), and a curved stem SROM (20 X 15, 225 mm long). A defect was prepared in the proximal femur to the lesser trochanter and the implants were implanted by an orthopaedic surgeon using the standard surgical techniques and instrumentation. The centers of all femoral heads were close to the center of the natural head. The knees of the bones were fixed in a pot with "Cerrobend," a low melting point metal. The femur was placed in 20 degrees of flexion as shown in Figure 1. A circular collar was fixed to the proximal femur. This collar was supported by a circular bushing support which allowed rotation of the femur but prevented bending. Loading was applied as shown in Figure 1 at a rate of 50 Newtons per second up to a maximum load of 2500 Newtons. Relative motion was measured by two LVDTs (050HR, Schaevitz). Holes were drilled into the lateral and medial sides of each prosthesis and pins bonded into the holes. The LVDTs

were mounted on a frame which was attached to the bone as shown in Figure 1. The pins moved the cores of the LVDTs. By comparing the output of the two LVDTs the relative lean of the prosthesis in the bone and the relative torsion of the implant with respect to the bone could be determined. The displacement at the medial interface was determined by multiplying by the ratio of the lever arms from the center of rotation. At least three runs were made for each prosthesis and then the LVDT frame was dismantled and reassembled and the tests repeated. A total of three setups with three runs per setup were conducted for each prosthesis. A/P and lateral radiographs were taken of each implant and the respective fit and fill recorded using the method of Gruen [4].

RESULTS AND DISCUSSION

All implants had excellent fit and fill (> 94%). Figure 2 shows the transverse displacement at the medial surface of the implant. Stems with both a lateral-medial and anterior-posterior wedging had the least motion except for the PCA which subsided significantly but eventually stabilized. A curved stem reduced the rotation. Collars had no effect on rotation. In similar proximally deficient prepared bones, stem design and the ability to achieve metaphyseal fit in AP and lateral planes are paramount in achieving torsional stability with revision femoral prostheses.

REFERENCES

(1) T P Andriacchi, et al, JBJS, 62-A, 749-757, (1980). (2) J E Bechtold, et al, ORS 380, (1989). (3) J A Szivek, submitted for pub (1991). (4) T Gruen, AAOS, 4003, (1991).

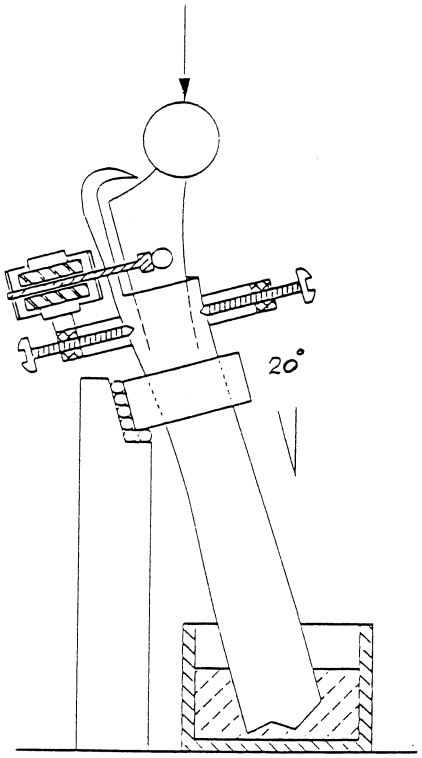
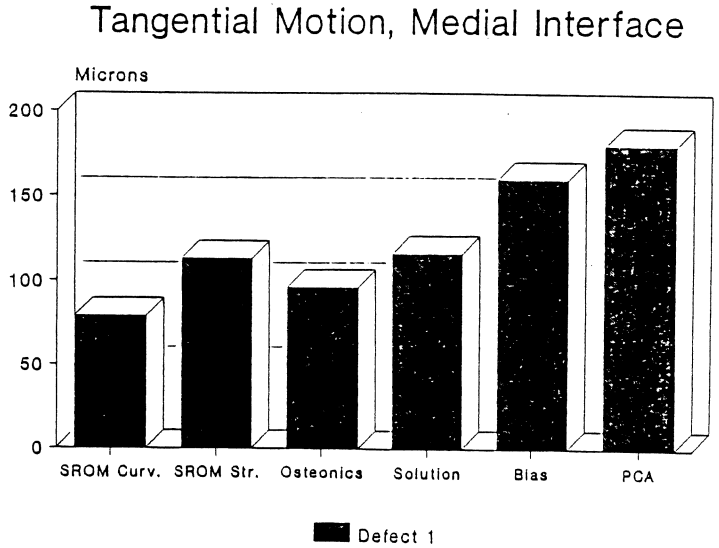


Figure 1
Test Setup



Implant Type
Figure 2

A FINITE ELEMENT ANALYSIS OF THE EFFECT OF POISSON'S RATIO OF THE COATING ON INTERFACE CONDITIONS IN POROUS COATED HIP ENDOPROSTHESES

E.A. Friis*, F.W. Cooke*, S.J. Hooper**

*Orthopaedic Research Institute, Inc.
929 N. St. Francis
Wichita, KS

**The Wichita State University
Dept. of Aerospace Engineering
Wichita, KS

INTRODUCTION

Porous coatings on orthopaedic implants provide a network into which tissue may grow. The effect of the coating properties on interfacial stresses in the bone and the coating has been a topic of study. Most studies on this subject have concentrated on the effect of the coating thickness and elastic modulus on interfacial conditions.(1,2) A new porous structural material exists which exhibits an apparent negative Poisson's ratio. This study examines the effect of varying the apparent Poisson's ratio of the coating using positive, negative, and zero ratio values in a fully-ingrown idealized finite element model of a porous coated hip endoprosthesis.

REVIEW AND THEORY

Current orthopaedic implant porous coatings include sintered metallic beads, fiber mesh and plasma sprayed surfaces. These coatings all exhibit a positive apparent Poisson's ratio. A structural material has been developed which exhibits a controllable apparent negative Poisson's ratio.(3) This structure, referred to as the re-entrant structure, is made by three-dimensional compression of an open-celled foam and can be formed from polymeric and metallic materials.(4) It is hypothesized that the re-entrant structure is a desirable material for use as the porous coating on orthopaedic implants because of its hypothetically less severe stress concentration when attached to the implant substrate as compared to the current porous coatings. However, the apparent Poisson's ratio of the re-entrant structure when used as a porous coating may have an effect on the interfacial stresses between the coating and adjacent bone. The objectives of this study were to determine the effect of the coating Poisson's ratio by estimating the stress distributions surrounding the femoral component of a fully ingrown porous coated hip endoprosthesis.

METHODOLOGY

A three-dimensional finite element model of a fully-ingrown idealized porous coated hip endoprosthesis was developed. The finite element program COSMOS/M was utilized. The model consisted of 5520 eight noded isoparametric elements and 6096 nodal points as shown in Figure 1. A linear elastic, isotropic tube of 30 mm outer diameter and 20 mm inner diameter with a total length of 150 mm and modulus of 17 GPa was used to model the femoral diaphyseal bone. The prosthestic stem was modeled as a straight cylinder with a solid core diameter of 17 mm and modulus of 110 GPa. The porous coating filled the gap between the prosthesis and bone with a thickness of 1.5 mm and constant elastic modulus of 5 GPa. The coating was assumed to be intimately attached to the bone, thus modelling an idealized fully ingrown prosthesis. The distal end of the model was fully constrained and a unit pure bending moment of 1 Nm was applied at the proximal prosthesis end to simulate the primary bending experienced by the femur in the stance phase of walking. This model was purposely made similar to that used by previous investigators (1) so that comparisons could be made. The apparent Poisson's ratio of the coating was varied between +0.30 and -0.30. Stresses in the bone and coating at the bone-coating interface were determined at the distal, midsection, and proximal locations on the tensile side of the bone.

A two-dimensional plane strain cantilever beam model with dimensions equivalent to the axial midsection of the three-dimensional model was developed to test convergence. A plane strain model with mesh density increased by a factor of four was compared with the original mesh model. Stress patterns and magnitudes at equivalent points were analyzed and found to comparable. On this basis, the overall mesh density of the three-dimensional model was assumed to be adequate for convergence.

RESULTS AND DISCUSSION

The Von Mises stress magnitudes in the bone and coating at the bone-coating interface are plotted in Figure 2 for the tensile side of the model at the distal, midsection and proximal regions. The

magnitude of Von Mises stress in the bone did not change greatly in the bone with varied coating Poisson's ratios, however the Von Mises stress in the coating increased in all regions with decreasing Poisson's ratios. The principal stress at all regions was the axial component. Individual components of stress and the overall component stress distribution were changed in both the bone and the coating with different Poisson's ratios. Figure 3 illustrates the radial stress component in the bone and coating at the three locations. As intuitively expected, the radial stress is tensile at the proximal region and compressive at the distal region. Decreasing the coating Poisson's ratio decreased the tensile stress in the proximal bone nonlinearly. At the midsection where no end effects are occurring, the magnitude of radial stress was low. However, this stress component may be critical for initial bone ingrowth and/or maintenance. Figure 4 illustrates the radial stress at the midsection of the model. The radial stress changed from a tensile to compressive stress with decreasing coating Poisson's ratio.

CONCLUSIONS

The potential benefits of using an open-celled foam with a negative Poisson's ratio were investigated. As a first approximation, this study has shown that the coating Poisson's ratio can effect the stress distribution and stress component magnitude and direction in both the bone and coating. Coating Poisson's ratios and elastic moduli may be tailored to provide the desired interfacial stress conditions.

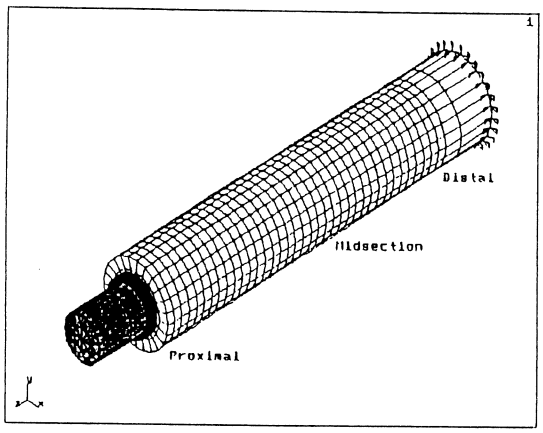


Figure 1. 3-D FEM Model

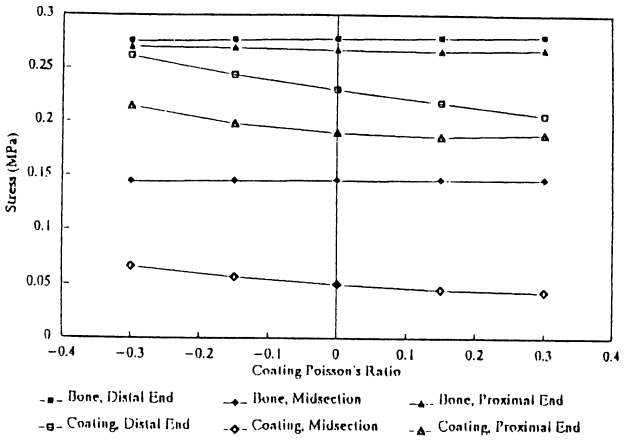


Figure 2. Von Mises Stress at the Bone-Coating Interface

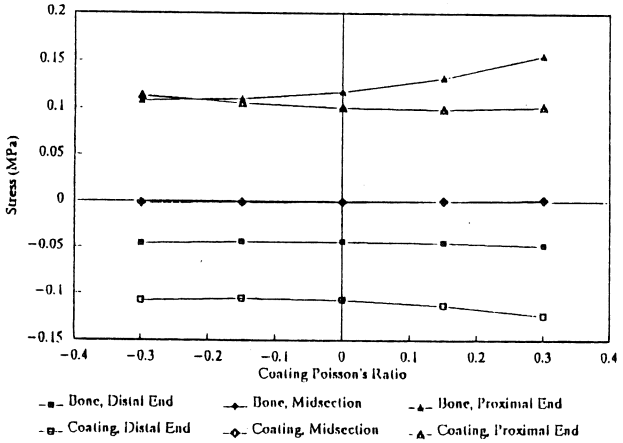


Figure 3. Radial Stresses at the Bone-Coating Interface

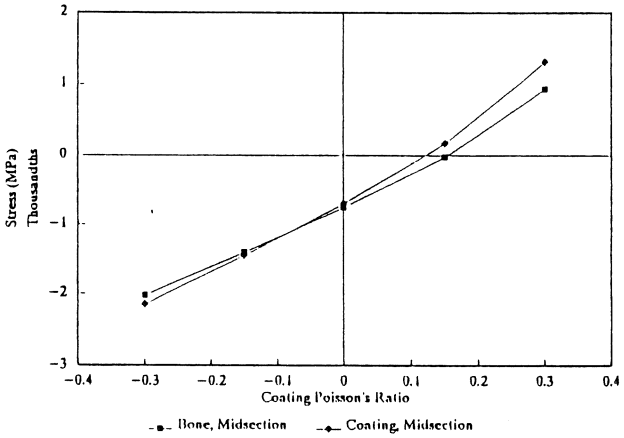


Figure 4. Midsection Radial Stress at the Bone-Coating Interface

REFERENCES

1. Rohlmann, A., et al. J Biomechanics, 21(7):695-611 (1988). 2. Ducheyne, P., et al. J Biomechanics, 11:297-307 (1978). 3. Lakes, R.S. Science, 235:1038-1040 (1987). 4. Friis, E.A., Lakes, R.S., Park, J.B. J Materials Science, 23:4406-4414 (1988).

A FINITE ELEMENT ANALYSIS OF THE SIMMONS AND STEFFEE BONE BOLTS

Mark E. Harbaugh
Smith & Nephew Richards Inc., Memphis, TN 38116

INTRODUCTION

Finite element analysis was used to study the peak stress in the Simmons and Steffee bone bolts. Three different bolts were analyzed: Simmons, new Steffee, and old Steffee. Each bolt was loaded with a 445 Newton transverse force to simulate the load carried by the bolt and a 8.47 Newton-meter nut torque. The results indicate that the stress in the new Steffee bolt is 1.6 times higher than the Simmons bolt and the stress in the old Steffee bolt is 2.6 times higher than the Simmons bolt.

REVIEW AND THEORY

Spinal fixation devices are used primarily to stabilize the vertebrae for fusion of the spine. Plating systems consist of a plate along with two or more bolts or screws with bone threads on one end and machine threads on the other. One of the complications of spinal plating systems is fatigue failure of the bolt[1-4]. In a recent study by Liu et al [2] most of the failures occurred at the first bone thread; indicating the existence of a stress riser. This study uses the finite element method to compare the stress distributions in the Steffee (Acromed Inc.) and Simmons (Smith & Nephew Richards Inc.) bolts. Finite element models were created for both bolts. Each model was loaded with a 8.47 Newton-meter pretorque and a 445 Newton transverse force [5]. Stress values were determined in both the bone and machine threads.

PROCEDURES

Three different bolts were analyzed: Simmons, new Steffee, and old Steffee. An axisymmetric finite element model was created for each bolt (Figure 1). The bolts were loaded with a 445 Newton transverse force and fixed at the bolt plate interface. The nut pretorque was simulated by applying a displacement constraint to the machine threads. The finite element geometry was meshed with quadratic axisymmetric harmonic structural solid elements (Figure 2). Because large stress gradients were found to exist at the bone threads, submodeling was used. The submodeling technique involves creating a refined finite element model of a small part of a model and then using the results from the larger model to 'load' the submodel. Figure 3 shows the submodel for the critical bone thread region. Both parts are made from stainless steel; Simmons from 316L and Steffee from 22-13-5. The materials were assumed linear, isotropic, and elastic (E=200 GPa, v=0.30, yield=862 MPa).

RESULTS & DISCUSSION

Figures 4-6 are plots of the effective stress for the Simmons, new Steffee, and old Steffee bolts. The contours plot the stress as a fraction of the peak stress in the Simmons bolt (862 MPa). The peak stress in the new Steffee bolt is 1.6 times higher than the Simmons bolt and the peak stress in the old Steffee bolt is 2.5 times higher. This relationship holds until the material begins to yield. At the yield point the material behavior becomes nonlinear. All computational runs assumed that the bolts are connected to an infinitely stiff plate. In reality the plates have a finite stiffness. This finite stiffness will reduce the stress in the actual part.

The section modulus of the Steffee bolt is 1.8 times less than the Simmons bolt if the effect of the bone threads is ignored. Because stress is inversely related to section modulus in bending, the peak

stress difference can partly be explained by the section modulus difference. Other contributing factors to the peak stress include the thread design and the amount of taper between the root diameter and the mid-shank outside diameter.

Transpedicular fixation of spinal instrumentation is currently indicated for use only by clinical investigators participating in an FDA approved study.

[1] Steffee, et al, Clin Orthop, 203:45-53, 1986; [2] Liu, et al, SPINE, Vol 15, No 4, pp. 311-317, 1990; [3] Ashman, R.B., et al, SPINE, V 14, N 12, pp. 1398-1405, 1989; [4] Zand, M.S., et al, J. Bio, Vol 16, No 5, pp. 305-311, 1983; [5] Ashman, R.B., et al, Clin Orthop, No 227, pp. 113-125, Feb 1988

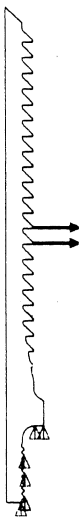


Figure 1 - Model



Figure 2 - Mesh

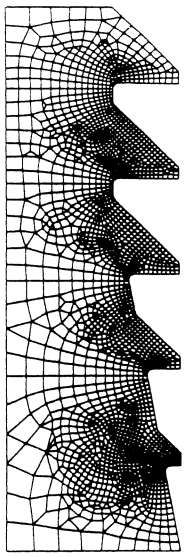


Figure 3 - Submodel

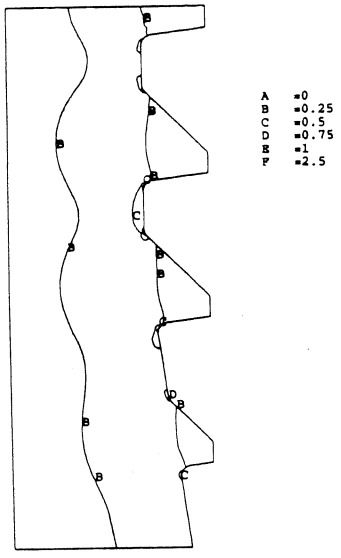


Figure 4 - Simmons

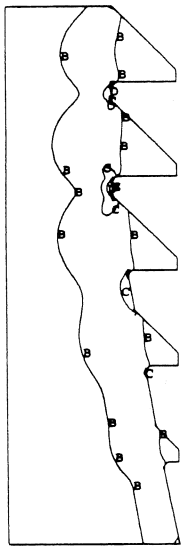


Figure 5 - New Steffee

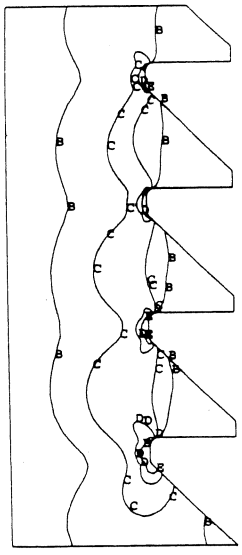


Figure 6 - Old Steffee

GLENOID IMPLANT TECHNOLOGY - PART I: DEVELOPMENT OF A THREE-DIMENSIONAL FINITE ELEMENT MODEL

C.M. Smith[1], U.P. Wyss[1], D.R. Pichora[2], H.L. Ploeg[1]
Departments of (1) Mechanical Engineering and (2) Orthopaedic Surgery
Clinical Mechanics Group, Queen's University
Kingston, Ontario, Canada K7L 2V7

INTRODUCTION

To address the problem of glenoid component loosening in current shoulder replacements, a three-dimensional (3-D) finite element (FE) model has been developed. Three models have been created representing the natural joint and the resurfaced joint with two different glenoid components. Using bone material properties and joint loading from the literature, three functional load cases per model have been established.

REVIEW AND THEORY

Painful loss of motion and function in the shoulder arises from post traumatic arthritis, rotator cuff deficiency, osteoarthritis, and most commonly, rheumatoid arthritis. Progress in the development of successful shoulder arthroplasties has been modest and generally, prostheses currently in use do not accurately replicate the anatomy or biomechanics of the shoulder. Although pain relief is usually satisfactory and some function is restored, the high incidence of loosening of the glenoid component is a primary concern. This problem arises because of the small amount of bone stock available for fixation and the relatively high and excursatory nature of the loading. Joint forces have been reported to be as high as 10.2 times the weight of the extremity [1] and 0.89 times body weight [2]. The modeling of glenoid fixation using the FE method was first done on a two-dimensional scale [3] but to fully address biomechanical and kinematic deficiences, a 3-D study is needed due to the asymmetry of the joint. To date, one known 3-D model exists [4] but is too coarse for analyzing implant design parameters. The purpose of this study is (1) To develop a 3-D FE model of the glenohumeral joint and (2) To assess basic stress and deformation characteristics of the natural and resurfaced glenoid with the intent of determining the fundamental design parameters of a new glenoid component with a reduced tendency of loosening.

PROCEDURES

A normal, male cadaver shoulder was used to obtain the basic geometry and material property distribution of the joint. The scapula was mounted on a specially designed computer tomography (CT) frame and alignment of the scapula was achieved using the inferior pole, intersection of the scapular spine and the vertebral border, and the centre of the glenoid face. The frame and aligned scapula were fed through the CT machine in the inferior-superior direction and CT scans were performed in the horizontal plane. Scans were taken with a bone filter at 2 mm increments using a 1 mm beam width. Each scan produced a horizontal cross section of the scapula from which the outer contours and the different bone property boundaries could be seen. These lines were traced and digitized to form a series of 2-D layered contours. This information was transferred to AutoCAD where each

contour layer was meshed to its adjacent layer to form a 3-D surface model of the scapula. These surface and bone property interface data were then converted to finite element data (keypoints, lines and areas) and transferred to the FE package ANSYS.

RESULTS AND DISCUSSION

Solid modeling techniques were used to construct three FE models representing the natural joint and two uniquely resurfaced joints. Each model employs over 4000 8-noded brick and surface contact elements and includes four different materials (assumed linear elastic and isotropic): the metallic prothesis (E=117 GPa, v=.30), cortical bone (E=8 GPa, v=.35), cancellous bone (E=.25 GPa, v=.21) and transition bone (E=1.5 GPa, v=.25). Joint loading consists of a 1000 N compression force on the face of the glenoid and a 500 N tensile deltoid load. The orientation of the compressive force is based on three positions of the arm: (1) 90 degrees abduction (central load), (2) 60 degrees abduction (superior excursion of 4 mm) [5] and (3) cocked phase of throwing (posterior excursion of 4 mm) [6].

To minimize computing requirements, only the primary areas of interest were modeled - the glenoid fossa and adjacent bone, coracoid process, lateral portion of the spine and the superior lateral border. To further minimize the number of elements without sacrificing accuracy, an effort was made to use brick-shaped elements as opposed to tertrahedral elements. The FE mesh is designed to include the prostheses within the bone of the natural joint which allows the resurfaced models to be generated by simply changing the material properties of the appropriate elements. The mesh exhibits a flexibility in defining bone density regions permitting the cortical shell and adjacent cancellous bone (transition layer) to be altered in thickness depending on the integrity of the joint.

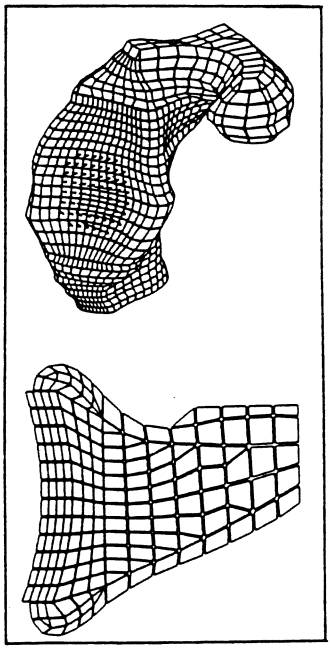


Fig. 1: FE Mesh

Meshing irregular 3-D shapes with brick-shaped elements while maintaining minimum element distortion is a cumbersome task due to the inherent preference for tetrahedral elements. The brick element produces a simple, more physically conceptual mesh (especially in 3-D) than its tetrahedral counterpart and greatly reduces the number of elements needed to obtain a specified accuracy. In Part II of this study, various glenoid component design parameters will be evaluated.

REFERENCES

[1] Inman VT et al. (1944) J Bone Jt Surg, **26A**, p1-30.
[2] Poppen NK et al. (1978) Clin Orthop, **135**, p165-170.
[3] Orr TE et al. (1988) Clin Orthop, **232**, p217-224.
[4] Rohlmann A et al. (1984) 4th Meeting European Soc Biom, Switzerland.
[5] Poppen NK et al. (1976) J Bone Jt Surg, **58A**, p195-201.
[6] Howell SM et al. (1988) J Bone Jt Surg, **70A**, p227-232.

A 3D FINITE ELEMENT ANALYSIS IN THE DEVELOPMENT OF A TOTAL JOINT REPLACEMENT FOR THE GREAT TOE

H.L. Ploeg[1], T.D.V. Cooke[2], A.R. Dujovne[1], C.M. Smith[1] and U.P. Wyss[1]
Clinical Mechanics Group, Kingston General Hospital
Departments of (1) Mechanical Engineering and (2) Orthopaedic Surgery
Queen's University at Kingston, Ontario, Canada, K7L 2V7

INTRODUCTION

Finite element analysis (FEA) has been used to aid the development of a resurfacing prosthesis for the great toe joint. A three-dimensional (3D) finite element (FE) model was constructed to study various designs of the metatarsal component. The stability of the implant designs was evaluated, as well as their effects on the stress distribution in the head of the metatarsal bone. Successful designs produced stress fields most similar to the normal bone model and little or no motion between the implant and the bone.

REVIEW AND THEORY

The Clinical Mechanics Group of Queen's University is developing an anatomic joint replacement for the treatment of arthritic first metatarsal phalangeal (MTP) joints. The goal of this design is to provide a long lasting MTP joint replacement by considering anatomic geometry, fixation, and surgical accessibility. This non-constrained joint replacement provides resurfacing prostheses for the metatarsal head and phalangeal base. The pathologic metatarsal head is resurfaced with an anatomic metal "cap" with plantar grooves for the sesamoid bones. A frustum (cut-off cone shape) is used for the bone prosthesis interface, allowing for a frontal surgical approach and a gentle transfer of load from the prosthesis to the bone. The bone-prosthesis interface includes three keyways, for torsional stability: two plantar, and one sagittal. A centre peg may be included to aid translational stability.

The purpose of this FE study is to examine the stability of the metatatarsal component of the great toe total joint replacement and its effect on the stress situation in the metatarsal head.

PROCEDURES

Combining results of previous studies on the MTP joint geometry [1], material properties, alignment [2], and loading [3] 3D FE models were constructed using ANSYS (version 4.4a). Several models are involved in this study; however, care was taken to create one general model which could be modified with little effort to create the required models.

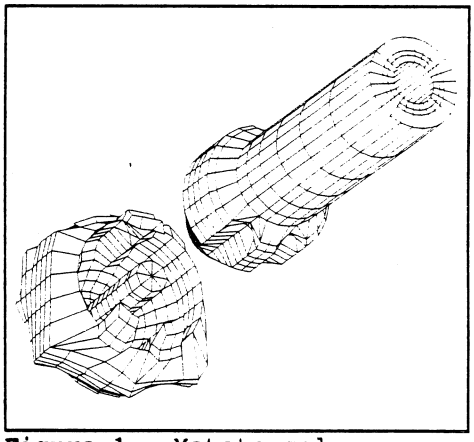


Figure 1. Metatarsal Resurfacing Prosthesis - FE Model

Geometry: The surface geometry of the metatarsal head was prepared into a wire frame mesh using Autocad (release 10). The inner part of the model was constructed as a solid model using ANSYS 4.4a. Subsequently, the surface and inner models were merged and converted into a FE model. The general FE model is composed of bricks, wedges, pyramids, and tetrahedrons with emphasis on the eight noded brick element. Each node has three translational degrees

of freedom. A 3D interface element models the bone-prosthesis interface. The interface is assumed frictionless, therefore avoiding a non-linear analysis in preference to a bi-linear analysis. The resulting general model has 2602 elements, 2628 nodes, and 7596 unconstrained degrees of freedom.

Material Properties: The model assumes linear elasticity and isotropy, though it attempts to model the non-homogeneity of bone. A total of nine material properties are used in the general model, including interface elements and elements which are required to take on different material properties to accommodate design variations. The material of the prosthesis is a titanium based alloy. The bone is simplified into three types: cortical (E = 15 000 MPa), transition (E = 1 500 MPa), and cancellous bone (E = 150 MPa). A Poisson's ratio of 0.3 is assumed for all the bone types.

Boundary Conditions: The metatarsal head is loaded at three contact areas, from the phalanx and the two sesamoid bones. A representative load from the push off phase during gait was assigned to the models. The resultant force on the metatarsal head is distributed approximately 2:1 between the phalanx and the sesamoids. The force from the sesamoids is asymmetric, roughly proportional to the size of each sesamoid. A 10 MPa surface pressure is assigned over a 56 mm^2 area to represent the phalangeal load. The sesamoid loads are modelled with 7 MPa pressures over a 32 mm^2 area (tibial side) and a 21 mm^2 area (fibular side). The proximal end of the metatarsal bone model is fixed at all nodes, in all degrees of freedom.

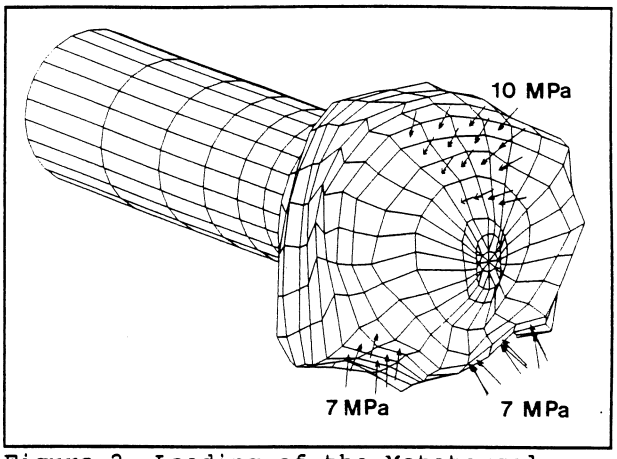


Figure 2. Loading of the Metatarsal

RESULTS AND DISCUSSION

A 3D FE model was constructed to study the stability of the metatarsal component and its effects on the stress situation on the bone. There was no lift off of the implant from the bone, and the rotation of the implant about the bone's long axis was less than one degree. In general, the stress levels were greater in the normal bone model than in the models with implants. It is uncertain whether this is an indication of stress shielding of the bone by the implant, since the difference in the stress levels was within the calculated error. The presence of a centre peg was not found to add to the stability of the implant or to affect the stress situation in the bone any differently than the model of the implant without a centre peg. Therefore, in the interest of minimal bone removal, it is suggested that the centre peg is not necessary and should not be included in the final design. It is expected that, within the next year, the MTP total joint replacement will be ready for implantation. The FE study has provided a glimpse at the effects that the implant may have on the metatarsal bone. The knowledge gained in a comparison of the FE results with the implanted MTP joint replacements can be used to refine the FE model and examine further modifications of the MTP total joint replacement.

REFERENCES

[1] Yoshioka, Y., et al., J Orthop Res 6:878-885, 1988.
[2] Wyss, U.P., et al., J Biomed Eng 11:19-24, 1989.
[3] Wyss, U.P., et al., J Biomech 23:977-984, 1990.

SESSION 12

EMG AND MUSCLE MECHANICS

LIGAMENT FORCE FEEDBACK AND THE REGULATION OF JOINT STABILITY

Thomas S. Buchanan, Scott Beckman and W. Zev Rymer

Departments of Rehabilitation Medicine and Biomedical Engineering, Northwestern University, and Sensory Motor Performance Program, Rehabilitation Institute of Chicago, 345 East Superior Street, Chicago, IL 60611

INTRODUCTION

In order to investigate the role that knee joint mechanoreceptors play in regulating force in muscles acting at the knee, we applied a mechanical perturbation to the joint and examined the electromyographic activity that resulted. Our hypothesis was that by applying a sudden varus or valgus torque to the knee joint, the ligaments would be loaded, thus stimulating the mechanoreceptors on the medial or lateral side of the joint. If mechanoreceptors are used as active feedback elements to control muscle activation levels in order to maintain joint integrity and stability, this perturbation should cause an increased activation of the muscles that have moment arms orientated such that they could relieve the ligaments of these loads. Our results suggest that EMGs are modulated by sudden knee torques that would prejudice joint stability and that this modulation is most likely mediated by mechanoreceptors in ligaments or joint capsule.

REVIEW AND THEORY

It has long been known that ligaments generally contain mechanoreceptors—sensory organs that respond to mechanical perturbations. However, the exact role that these play in modulating muscle force activation levels in humans is not understood. For example, it has been shown in cat knees that direct mechanical stimulation of the anterior cruciate ligament can result in increased activation of hamstrings and inhibition of quadriceps [1]. However, it is not clear from this report whether or not the investigators simply induced a flexion withdrawal via stimulation of nociceptors and these results have been contested on the basis of contrary data [2]. Clearly, the neurosensory role of ligaments is still a matter of great debate.

PROCEDURES

In this study, the mechanical perturbation was actually applied at the foot. The subject stood with one foot on a hinged platform which could rotate the lower limb in the medial or lateral direction. Sudden medial displacements at the foot will be transmitted to the knee in the form of varus torques which put stress on the lateral collateral ligaments as well as the lateral side of the capsule. Similarly, lateral displacements of the foot should transmit valgus torques to the knee. During this study, the other foot was placed on a stationary platform of equal height, with the feet separated by a natural distance comfortable to the subject. The test foot was initially kept from moving by wooden support blocks that laid under each side of the platform. At the time of the actual experiment, one of these support blocks was suddenly and unexpectedly removed, which, under the subject's weight, caused rotation of the foot resulting in a medial or lateral translation of 2.5cm. During the perturbations, EMGs were recorded with surface electrodes from four muscle groups: the medial and lateral parts of the quadriceps and hamstrings. Three seconds of data were digitally recorded at 500 Hz. The perturbation was applied approximately one second after the initiation of data acquisition.

RESULTS

To quantify the EMG activity, we examined the first 200ms of activity following the initiation of movement. From this average, rectified EMG was subtracted the baseline (resting)

TABLE 1: Ratio of rectified, averaged, EMG values for medial to lateral quadriceps and hamstrings associated with the two different perturbation directions. Each ratio represents the average of five to ten trials.

EMG ratio	Subject RB1		Subject SJ1		Subject PT1	
	Varus	Valgus	Varus	Valgus	Varus	Valgus
Q_{qm}/Q_{ql}	0.69	5.00	1.03	1.26	0.67	1.87
Q_{hm}/Q_{hl}	0.85	0.58	1.85	2.06	0.96	2.39

EMG, which was determined by the average, rectified EMG of the 200ms *preceding* movement initiation. This final, processed EMG value we will call Q_{qm}, Q_{ql}, Q_{hm}, and Q_{hl} for the EMG activity in the medial quadriceps (vastus medialis), lateral quadriceps (vastus lateralis), medial hamstrings (semitendinosus), and lateral hamstrings (biceps femoris longus), respectively.

If our hypothesis is valid, it suggests that EMGs of the medial knee muscles would be increased more than EMGs from lateral muscles when valgus torque perturbations were applied. For the quadriceps, this can be stated mathematically as follows:

$$\left(\frac{Q_{qm}}{Q_{ql}}\right)^{valgus} > \left(\frac{Q_{qm}}{Q_{ql}}\right)^{varus}$$

The same should hold true for the hamstrings. EMG ratios for three subjects are presented in Table 1. Note that a comparison of these ratios for the quadriceps shows, for all three subjects, that the vastus medialis is more significantly activated by valgus perturbations than the vastus lateralis. The drop in the activation ratio during varus loads and the increase with valgus loads was exactly what we predicted. Similarly, although not as powerful, is the same observation made for the hamstrings. Only for one subject (RB1) was this ratio not greater in valgus in the hamstrings muscles. This could be due to the very low EMG values we obtained in the medial head (possibly due to bad electrode placement) or they could be due to the subject shifting most of the weight backward, relying more heavily on the quadriceps and thereby resulting in inhibition of hamstrings in these tests.

DISCUSSION

Because the perturbation and, hence, the EMG response, was slow to evolve, we cannot be sure that vestibular reflexes were not influencing the EMGs. Also, no precautions were taken to ensure that stretch reflex from ankle or knee muscles did not play a significant role. However, we have no reason to believe that vestibular reflex or stretch reflex from ankle muscles would cause any difference in the ratio of the EMGs—it should influence both medial and lateral portions of these muscles equally. Also, we believe that although a medial/lateral torque was transmitted to the knee, motion, and hence muscle stretch, was negligible.

These problems notwithstanding, we believe that these data do indicate that EMGs are modulated by knee varus/valgus torques that would prejudice joint stability and that the most likely sensory element responsible for this modulation is the ligament and/or joint capsule mechanoreceptor. We believe that they also demonstrate that this type of study of ligament mechanoreceptors warrants further investigation, because, to our knowledge, no other work has shown such an imbalance of EMG activity.

REFERENCES

[1] Solomonow, M., et al. *Am. J. Sports Med.* 15: 207-213, 1987.
[2] Grabiner, M.D., et al. *J. Orthop. Res.* 7:152-155, 1989.

TORQUE AND MUSCLE ACTIVITY IN VARIOUS ISOMETRIC ELBOW TASKS

J.C. Jamison and G.E. Caldwell
Department of Kinesiology, University of Maryland
College Park, MD, USA 20742

INTRODUCTION

The effect of a simultaneous task in a second degree of freedom (*df*) on torque and muscle activity (EMG) was studied in isometric torque production at the elbow. Previous work has shown differences in torque and EMG measures with an additional task when both are maximal effort (Caldwell *et al.*, *in press*). The present study was designed to examine the relationship between the *magnitude* of this additional task and associated changes in torque and EMG, and to determine if surface EMG techniques are able to detect differences in the location of task-specific motor unit activity. Results indicate that both torque and EMG can be affected by various levels of torque in the second *df*, and that surface electrodes are able to detect localized differences in muscle activity within m. biceps.

REVIEW AND THEORY

Research on m. biceps brachii (BB) has demonstrated the existence of task-specific motor units (ter Haar Romeny *et al.*, 1984). The critical firing level (CFL) at which BB motor units are recruited depends on the torque production task required of this multifunctional muscle. Further, the motor units recruited specifically for supination are located in the medial portion of BB while units recruited for flexion are located more laterally. Although the CFL indwelling electrode technique is ineffective at higher magnitudes of elbow torque, surface EMG studies have supported the notion of task-specificity at both lower (Buchanan *et al.*, 1989) and at higher torque levels (Caldwell *et al.*, *in press*). However, the relationship between the magnitude of a second *df* torque task and the associated changes in torque production and EMG has not been shown. Further, it is unclear if surface EMG studies can detect differences in the localization of activity within the BB. The present study was undertaken to address these latter two points.

PROCEDURES

Four healthy male subjects produced isometric torque in both single and dual *df* elbow tasks while securely seated (shoulder angle = 20°; elbow angle = 90°; forearm in mid-prone position) and grasping a handle instrumented to measure flexor (F) and supination/pronation (S/P) torque. Pairs of miniature (2 mm) surface electrodes were placed on the belly of brachioradialis (BRAD) and the short head of biceps (BBSH). Two pairs of electrodes were placed on the long head of biceps, one on the medial aspect (BBLM) and one in a more lateral position (BBLL). Subjects produced maximal effort contractions (MVC) in each single *df* task - flexion (F), supination (S) and pronation (P). Each subject then attempted a series of similar MVC contractions while simultaneously maintaining a targeted torque level (33%, 67% or 100% of MVC) in a second *df* (e.g. MVC pronation and 67% flexion [P(F67)]). All data were collected with a 12 bit A/D convertor sampling at 1000 Hz per channel. The digitized data were processed to obtain averaged steady state levels of torque and RMS EMG. All torques were normalized with respect to the corresponding single *df* MVC. EMG data were normalized with respect to the single *df* flexion MVC.

RESULTS

MVC flexion torque magnitude was altered by the presence of *any* of the torque target levels in the second (S/P) *df* (fig. 1A). In contrast, MVC supination and pronation torque magnitudes were affected by only the higher levels of torque in the second (F) *df* (fig. 1B). During flexion MVCs, a linear relationship exists between the magnitude of the second *df* (S/P) torque and EMG level at all BB sites (fig. 1C). BRAD EMG activity is reduced by about 20% from that in single *df* F MVC at all levels of S/P torque (fig. 1C). Another EMG effect is divergent behavior between the long and short heads of BB, with BBLL and BBLM showing

a stronger response to the addition of a second *df* S task (F[S]) than the BBSH (fig. 1C). The BB EMG responses above 100% in F(S) and S(F) tasks indicate possible recruitment of both task-specific motor unit sub-populations (fig. 1C & 1D). Further, BBLM displays less EMG activity than BBLL in the conditions F(P) and P(F) (fig. 1C & 1D) possibly due to an inhibition of the medially-located supination units.

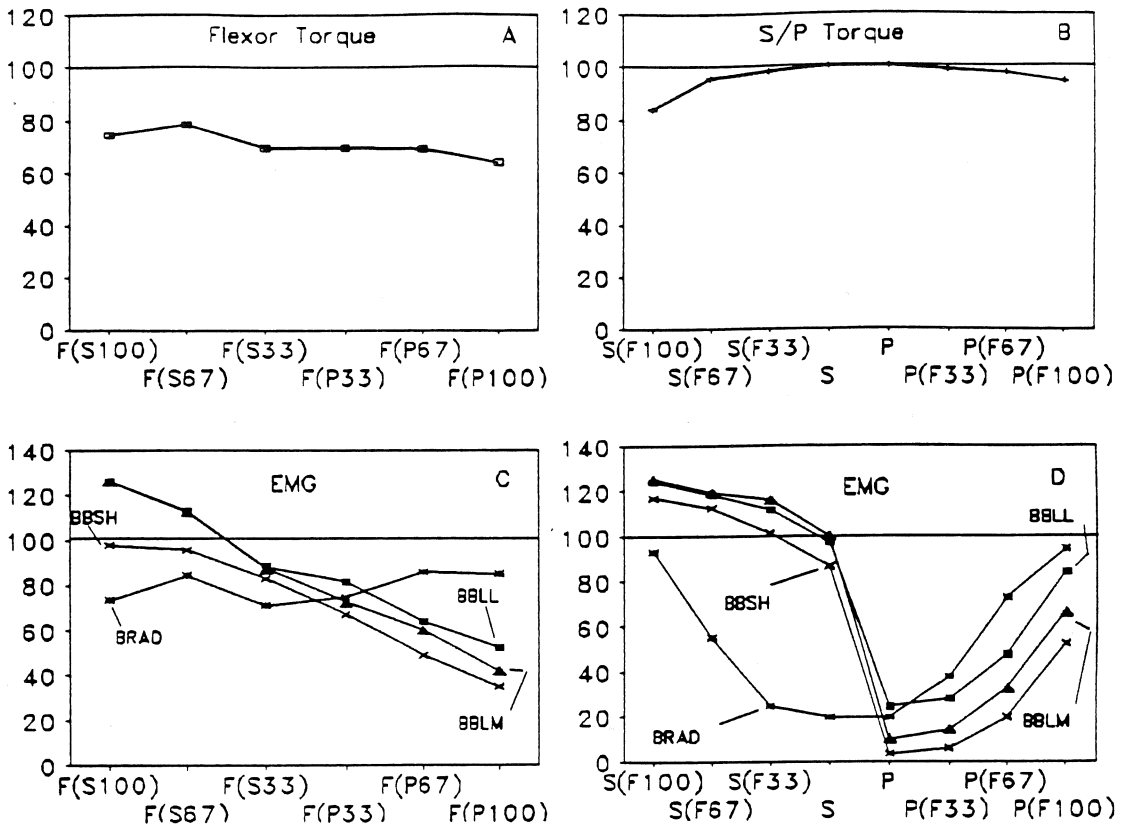


Figure 1: Mean torque (A & B) and EMG (C & D) responses in different task conditions.

DISCUSSION

The ability to produce flexion torque in an MVC is decreased by even low levels of torque in a second (S/P) *df*. The strong dependence of BB EMG on S/P torque indicates that one should control this variable in investigations of BB muscle activity during elbow flexion. The divergent behavior noted among all electrode sites refutes the 'flexor equivalent' concept (Bouisset, 1973) under these conditions of dual *df* tasks. These findings should be considered by those attempting to model bi-functional muscles such as the BB. Additionally surface EMG techniques may be able to detect differences in activity related to the location of task-specific motor units.

References

Bouisset, S., *New Devel. Electromyogr. Clin. Neurophys.* 1:607-622, 1973.
Buchanan, T.S. *et al.*, *J. Neurophys.* 62(6):1201-1212, 1989.
Caldwell *et al.*, *EMG & Clin. Neurophys. in press.*
ter Haar Romeny *et al.*, *Exp. Neurol.* 85:631-650, 1984.

ASSESSMENT OF THE DOUBLE DIFFERENTIAL TECHNIQUE AT IDENTIFYING AND ELIMINATING EMG CROSSTALK

Christine V. Portfors, BSc. and James J. Dowling, PhD.
Department of Physical Education, McMaster University
Hamilton, Ontario, Canada

INTRODUCTION

The ability of the double differential technique to identify and eliminate EMG crosstalk was assessed during voluntary contractions of the upper arm muscles of 10 subjects. Significant amounts of crosstalk were removed in each condition. The double differential technique may be beneficial for more valid assessments of muscle activity, although not all of the crosstalk was removed.

REVIEW AND THEORY

The double differential technique developed by Broman et al. (1985) is the only method to date which detects and eliminates EMG crosstalk. It has been used effectively to eliminate crosstalk in lower extremity muscles under both stimulation and voluntary conditions (Deluca,1988; Dowling and Kennedy,1990). A better test of the effectiveness of the technique would be in a situation where the activity of the neighbouring muscles is known. The upper arm muscles exhibit a classic triphasic pattern of activity which gives reasonable confidence that when the triceps are active the biceps and brachialis are inactive. The purpose of this study was to further examine the validity of the double differential technique under voluntary conditions in muscles of the upper arm.

PROCEDURES

Surface electrodes were placed over the biceps, triceps, and brachialis muscles of seven male and three female subjects. A three electrode configuration over the brachialis allowed two single differential myoelectric signals (SDMES) to be collected. One trial each of isometric flexion, extension, and dynamic flexion/extension was performed. The second digital differential amplifier created the double differential myoelectric signals (DDMES). The integrated SDMES was compared to the integrated DDMES to determine the percent crosstalk removed from the signal. Mean crosstalk percentages were calculated for each contraction condition.

RESULTS AND DISCUSSION

Mean crosstalk percentages were 33.5%, 26.5%, and 20.5% for extension, dynamic, and flexion trials respectively. Isometric extension resulted in the most crosstalk on the brachialis electrodes which was expected as the triceps were active and both the flexors were quiet. According to the classic triphasic

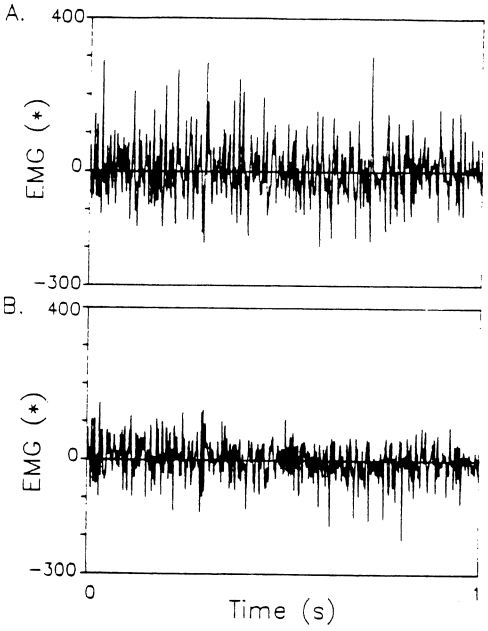
activity pattern (Angel,1974), during triceps activity the flexors should both be quiet. Visual inspection of the raw EMG did not reveal a triphasic pattern. Substantial activity on the brachialis channel indicated crosstalk was being recorded from the triceps. For this reason, values closer to 100% crosstalk during the dynamic movements would seem more appropriate. Since the triceps are inactive during flexion, the crosstalk detected during flexion may have been due to volume conduction from the biceps.

Table 1 shows the percent crosstalk values for the three contraction conditions. The high variability between subjects may be an important consideration when obtaining EMG data in that standard electrode placement sites may result in very different amounts of crosstalk with different subjects.

Table 1. Percent crosstalk values of 10 subjects under three contraction conditions.

	Subjects									
Condition	1	2	3	4	5	6	7	8	9	10
Extension	38.3	26.5	56.1	13.7	18.2	36.8	61.8	67.0	2.0	14.3
Dynamic	17.4	34.5	34.3	27.7	23.7	30.1	23.5	59.0	7.5	9.5
Flexion	14.0	21.6	16.3	28.5	26.4	26.6	26.8	35.1	8.5	0.6

In each condition the double differential technique removed a significant amount of crosstalk as supported by a two-way repeated measures ANOVA. Figure 1A-B shows the SDMES and DDMES of an isometric extension trial in which 36.8% crosstalk was removed. There is still activity on the brachialis channel after the crosstalk was removed indicating the double differential technique did not eliminate all the crosstalk effectively. This may be due to the placement of the brachialis electrodes. The technique requires the same amount of nondelayed activity on both channels to accurately determine the amount of crosstalk or all of the crosstalk is not eliminated resulting in an underestimation of crosstalk and an overestimation of muscle activity.



REFERENCES

Angel,R.W.(1974), EEG. Clin. Neurophysiol., 36: 493-498
Broman et al.(1985), IEEE Trans. Biomed. Eng., BME-32: 341-344
Deluca et al.(1988), EEG. Clin. Neurophysiol., 69: 568-575
Dowling et al.(1990), J.Biomech., 23: 728

OLDER HUMAN SUBJECTS EXPERIENCE LESS OF A CHANGE IN EMG FREQUENCY CONTENT DURING A FATIGUING CONTRACTION

R.M. Enoka, A. J. Fuglevand, and P. M. Barreto
Department of Exercise & Sport Sciences, University of Arizona, Tucson, AZ 85721.

As humans age, common experience develops the perception that performance capabilities diminish. This perception is underscored by the decline in muscle mass and strength with age (Aniansson et al., 1986) and the associated reduction in the number and size of motor units innervating a muscle, including an apparent reduction in the proportion of fast-twitch muscle fibers (Campbell et al., 1973; Kanda & Hashizume, 1989). In contrast, there are several reports of the counter-intuitive finding that muscle does not become more fatigable with age (Klein et al., 1988; Laforest et al., 1990). These observations have shown that older subjects are equally capable of sustaining a submaximal force as younger subjects. However, given the motor-unit reorganization that occurs with age, it appears uncertain, despite a similar endurance limit, whether the neuromuscular adaptations that occur with fatigue are similar for older and younger subjects. We focused on the adaptations that influence the frequency content of the EMG; these include the effect of metabolite accumulation on the conduction velocity of action potentials (DeLuca, 1984). The purpose of this study was to compare the age-related changes in the frequency content of the EMG during a fatiguing contraction.

Experiments were performed on older human subjects (64-79 years) and their results were compared to younger adults (18-40 years) who had been tested in the laboratory. The older subjects were carefully screened to eliminate those candidates with a history of neuromuscular deficits, including the use of medication that might impair neuromuscular function. The test muscle was first dorsal interosseus (FDI) of the left hand; FDI is located between the thumb and the index finger and it is the only muscle that abducts the index finger. The hand was placed so that the proximal interphalangeal joint of the index finger was aligned with two force transducers, one that sensed an abduction force and another that sensed a flexion force. EMG signals were obtained from bipolar surface electrodes (4-mm diameter, silver-silver chloride, 1.2 cm interelectrode distance) placed on the skin overlying FDI and abductor digiti minimi (the abductor of the little finger, which, like FDI, is innervated by the ulnar nerve). Electrical stimulation was applied percutaneously to the ulnar nerve, first at the wrist and then at the elbow. The supramaximal stimulus, which had a duration of 1.0 ms and was delivered once every 3 seconds, was used to elicit direct motor responses (M waves) in FDI. Concurrent measurement of M waves in abductor digiti minimi assured stability of the stimulating electrode.

The central element of the experimental protocol was the fatiguing contraction that involved sustaining an isometric abduction force with the index finger to exhaustion. Prior to this fatiguing contraction, subjects performed 2-4 trials in which the abduction force was gradually (2-5 s) increased up to maximum (MVC). The greatest force that was achieved consistently was taken as MVC and the target force for the fatiguing contraction was set at 35% MVC. Five M waves were elicited before and immediately after the fatiguing contraction. The force and EMG data were stored on FM tape and were replayed and analyzed with Spike2 (CED 1401), an event and waveform data-capture and data-analysis system. For the fatiguing contraction, time was normalized as a percentage of the endurance time. The EMG was rectified and averaged over epochs that represented 10% of the endurance time. In addition, a Fourier transformation of the EMG was performed on each epoch to obtain the power spectrum from which the mean power frequency was calculated. The M waves, which were generally biphasic, were quantified by the measurement of peak-to-peak amplitude and duration.

Table 1. Despite a similar performance during the fatiguing contraction, the EMG frequency content changed less in the older subjects.

	Gender	Young		Old	
Age (years)	F+M	27.3 ± 5.2	(44)	67.2 ± 5.6	(19)
	F	27.6 ± 5.2	(17)	73.3 ± 7.4	(3)
	M	27.0 ± 5.3	(27)	66.0 ± 4.6	(16)
MVC (N)	F+M	33.3 ± 8.3	(44)	29.8 ± 8.5	(19)
	F	25.5 ± 4.8	(17)	17.2 ± 0.8*	(3)
	M	38.2 ± 5.9	(27)	32.1 ± 7.0*	(16)
Endurance time (s)	F+M	204.0 ± 85.0	(22)	194.0 ± 84.0	(15)
	F	196.0 ± 54.0	(7)	209.0 ± 134.0	(3)
	M	208.0 ± 98.0	(15)	191.0 ± 75.0	(12)
Average EMG (%MVC)†	F+M	55.1 ± 16.2	(11)	57.4 ± 14.2	(15)
Mean power frequency:					
Initial (Hz)	F+M	128.1 ± 26.4	(11)	131.9 ± 20.6	(15)
Final (% initial)†	F+M	43.6 ± 6.1	(11)	55.9 ± 12.1*	(15)
M wave (% initial):					
Peak-to-peak amplitude†	F+M	77.1 ± 19.7	(20)	72.3 ± 19.0	(16)
Peak-to-peak duration†	F+M	138.5 ± 23.5	(20)	117.6 ± 33.7*	(16)

Values are mean ± SD (n). * $p < 0.05$. † value at the end of the fatiguing contraction.

Table 1 indicates two significant features of the performance by the young and old subjects during the fatiguing contraction: (1) there was no difference between the two groups in endurance time for FDI; (2) although the average EMG increased to the same extent (initial = 35%) for the two groups during the fatiguing contraction, the mean power frequency declined less for the older subjects. Similarly, there was less of a change in peak-to-peak duration of the M waves for the older subjects. These data indicate that although the two groups of subjects had a similar endurance limit, the older subjects experienced less of a change in the mechanisms underlying the reduction in propagation velocity of muscle action potentials.

Aniansson A, Hedberg M, Henning G-B, Grimby G: Muscle morphology, enzymatic activity, and muscle strength in elderly men: a follow-up study. *Muscle Nerve* 9: 585-591, 1986.

Campbell MJ, McComas AJ, Petito F: Physiological changes in ageing muscle. *J Neurol Neurosurg Psychiat* 36: 174-182, 1973.

DeLuca CJ: Myoelectric manifestations of localized muscular fatigue in humans. *CRC Crti Rev Biomed Eng* 11: 251-279, 1984.

Kanda K, Hashizume K: Changes in properties of the medial gastrocnemius motor units with aging. *J Neurophysiol* 61: 737-746, 1989.

Klein C, Cunningham DA, Paterson DH, Taylor AWF: Fatigue and recovery contractile properties of young and elderly men. *Eur J Appl Physiol* 57: 684-690, 1988.

Laforest S, St-Pierre DMM, Cyr J, Gayton D: Effects of age and regular exercise on muscle strength and endurance. *Eur J Appl Physiol* 60: 104-111, 1990.

Supported by USPHS grants AG 09000, NS 20544, NS 07039 and NS 08634.

SINGLE MUSCLE CONTRACTIONS CAN PRODUCE MUSCLE-TENDON INJURY

Jon W. Feuerbach[1], James G. Hay[2], Warren G. Darling[2]
[1]Department of Biomedical Engineering and Applied Therapeutics,
The Cleveland Clinic Foundation, Cleveland, OH 44195, USA
[2]Department of Exercise Science, The University of Iowa, Iowa City, IA 52240, USA

INTRODUCTION: Garrett *et al.* modeled muscle injury by lengthening both active and passive muscle-tendon units until they suffered a complete functional and structural failure at the distal muscle-tendon junction (1). However, the muscle-tendon lengths obtained with this model probably exceeded the maximum physiological length of the unit. McCulley *et al.* modeled muscle injury by subjecting the muscle-tendon unit to 450 slow eccentric contractions that were maintained within the maximum physiological length of the unit (2). This eccentric protocol caused functional and structural losses on a much smaller scale than those produced by Garrett *et al.*'s model and probably simulated the muscle damage associated with the phenomena of delayed onset of muscle soreness (DOMS). Concentric or isometric protocols did not cause either functional or structural losses. McCulley *et al.* clearly established that muscle injury can be produced by repeated slow eccentric contractions even if the contractions are restricted to physiological length limits. However, it has not been established that muscle injury can result from a single eccentric contraction that is maintained within the physiological length limit.

The purpose of this study was to examine the effect of a single eccentric contraction on the incidence and severity of muscle-tendon injury in a rat model. The eccentric contraction was maintained within physiological limits of length and velocity. Injury was defined functionally as a statistically significant reduction in the isometric force production of the muscle-tendon unit. It was hypothesized that: (1) injury could occur as a result of a single eccentric contraction that is maintained within physiological length and velocity limits; (2) as the velocity of the eccentric contraction increases, the severity of the injury increases; and (3) units that contract concentrically immediately after contracting eccentrically will be more severely injured than units that contract eccentrically only.

METHODS: Thirty male Sprague Dawley rats were separated into three groups of ten rats. The tibialis anterior (TA) of one limb was subjected to an experimental protocol and the contralateral TA served as a control. Each animal was anesthetized and the skin over the TA of one limb was removed. The neurovascular supply to the TA was left intact. The maximum length of the TA muscle fibers ($L_{f\text{-}max}$) was measured with the ankle placed in extreme plantarflexion. The femur and tibia were then stabilized on a testing jig that was mounted on the piston of a Materials Test System and the distal tendon of the TA was released from its insertion and clamped to a load cell. The initial length of the TA muscle fibers was set at 90% $L_{f\text{-}max}$ and the sciatic nerve was stimulated to produce a pre-test maximal isometric contraction of the TA. Two minutes later the experimental TAs were subjected to one of three test eccentric contractions:

Group 1/Experimental TA: slow eccentric (1 $L_{f\text{-}max}$/s);
Group 2/Experimental TA: fast eccentric (10 $L_{f\text{-}max}$/s); or
Group 3/Experimental TA: fast eccentric followed by fast concentric (10 $L_{f\text{-}max}$/s).

Eccentric contractions were performed by stimulating the sciatic nerve while lengthening the TA fibers from 90% $L_{f\text{-}max}$ to $L_{f\text{-}max}$. This change in muscle fiber length was, on average, 3 mm. Care was taken not to exceed $L_{f\text{-}max}$ during the protocol. A post-test isometric contraction was then performed two minutes after the test contraction. This protocol, without the test eccentric contraction, was performed on the contralateral control TA. A 2 by 3 (test type by Group) ANOVA and a Tukey's post-hoc analysis were used to test for significant differences in the reduction of isometric force production among the groups (experimental and control).

RESULTS AND DISCUSSION: The mean percentage change in TA isometric force production from the pre-test to the post-test is shown in Table I.

Table I. Mean (SD) percentage change in TA isometric force production.

Test Type	Group 1	Group 2	Group 3
Experimental TA	-1.5 (0.8)	-7.9*(3.8)	-9.4*(4.6)
Control TA	+0.3 (0.5)	+1.6 (2.2)	+0.6 (0.9)

*Significantly different from control values and Group 1 experimental value ($p<0.05$).

The definition of injury used in this study was a statistically significant reduction in isometric force production. These results suggest that a fast eccentric contraction (Group 2/Exp. TA), and a fast eccentric contraction followed immediately by a fast concentric contraction (Group 3/Exp. TA) will produce more injury than a slow eccentric contraction (Group 1/Exp. TA). Thus, these results support the first and second hypotheses which state that injury can be produced by a single eccentric contraction that is maintained within physiological limits of length and velocity, and that as the velocity of the eccentric contraction increases, the severity of the injury increases. However, the results do not support the third hypothesis since no significant difference existed between the amount of injury produced by a fast eccentric contraction (Group 2/Exp. TA) and a fast eccentric contraction followed immediately by a fast concentric contraction (Group 3/Exp. TA). Fast eccentric contractions and rapid changes in contraction state were performed to simulate the conditions experienced in activities such as sprint running. While the severity of injury appears to be influenced by the velocity of contraction, these data do not support the proposition that injuries are more likely to occur during a rapid change in contraction state (from eccentric to concentric) than during a single contraction state.

No isometric force could be produced by the muscle-tendon units that Garrett *et al.* lengthened to rupture. This is obviously a more severe injury than the deficits observed in the present study. Although the macrotrauma of Garrett *et al.*'s model has been seen in human muscle-tendon units, it has not been shown that these units, undergoing normal activity such as sprint running, are subjected to the extreme length changes of their model. McCulley *et al.* subjected the units to 450 slow (1 L_f/s) eccentric contractions and found that the isometric force production of the unit was reduced by 28% (taking into account fatigue). This is also greater than the functional deficit observed in the present study. This suggests that repeated slow eccentric contractions will produce a more severe injury than one fast eccentric contraction. McCulley, *et al.* found no evidence of macrotrauma, but instead found histological alterations near the center of the muscle belly. No macrotrauma was evident in the present study and a histological analysis was not performed.

In conclusion, a muscle-tendon injury was produced by a single eccentric contraction which was maintained within physiological limits of length and velocity. Because the severity of human muscle-tendon injury is difficult to quantify, it is not yet known how it corresponds to the severity of experimentally induced injury. It is also not known if similar mechanisms are responsible for both single event injuries and multiple event injuries.

REFERENCES:

(1) Garrett, WE, *et al.*, Am J. Sports Med. 15(5):448-454, 1987.
(2) McCulley, KK, *et al.*, J. App. Physiol. 59(1):119-126, 1985.

POSTER PRESENTATIONS

ANATOMICAL JOINTS

FACTORS AFFECTING ELASTIC ENERGY RECOVERY IN STRETCH-SHORTENING MOVEMENTS

Michael Mungiole[1] and Jack M. Winters[2]
[1] Exercise & Sport Research Inst. [2]Chemical, Bio, and Materials Engrg., Arizona State University, Tempe, AZ 85287, USA

INTRODUCTION

Previous experiments which have considered factors affecting series elastic component (SEC) energy contributions to the stretch-shortening cycle (SSC) have resulted in equivocal conclusions in extrapolating external measures to internal phenomena. A muscle model was used to investigate the influence of fiber type proportion, amplitude of movement, and SEC compliance on elastic energy recovered and the performance of an ankle plantarflexion movement task. When compared to the nominal case, each of these factors influenced the relative proportions of the contractile component (CC) and SEC to overall muscle power, although performance (joint excursion in a particular time period) was affected to a lesser extent. The interaction of the CC and SEC influenced the power developed and the amount of elastic energy recovered during the concentric phase. Also, an increase in the SEC energy recovered does not necessarily imply improved movement performance.

REVIEW AND THEORY

Enhanced performance of SSC movements vs.those without prior muscle stretch has usually been attributed to the increased utilization (recovery) of SEC energy. Several factors have been considered or manipulated to determine their influence on the energy recovered. Equivocal conclusions have been made regarding such factors as fiber type proportion (1), eccentric phase movement amplitude (2), and SEC compliance (3,4). Also, the implications of muscle mechanics principles (e.g., force-velocity relationship) have often been neglected. This study was conducted to determine the influence of these factors on SSC performance and the SEC power (rate of recovery) during the concentric phase.

PROCEDURES

A validated muscle model (5) was used to simulate an ankle joint movement task. Neural and external loading inputs were based on an experimental study in which subjects performed ankle dorsi/plantarflexion movements (6). A nominal (baseline) simulation run was compared to cases in which model parameters were individually varied to simulate changes in fiber type proportion, muscle optimal length, and SEC compliance. A trial and error procedure was necessary so that each simulation run had the same joint torque and position at the initiation of the concentric phase (turnaround), resulting in equivalent amounts of SEC stored energy at this instant. The first 100 ms of the concentric phase was emphasized for analysis.

RESULTS

Nearly 75% of the energy recovered occurred in the first 100 ms (Figure 1 (a)). SEC power peaked earlier than that for the CC, providing most of the joint power early in the concentric phase. Model parameter manipulations resulted in joint excursion differences less than 4% from the nominal run, while average (0-100 ms) SEC power differences were 7-11% (Table 1). Also, the manipulations caused changes in CC and SEC power which were in opposite directions. Although an increase in SEC compliance resulted in a larger amount of SEC power output, it had little effect on the CC power.

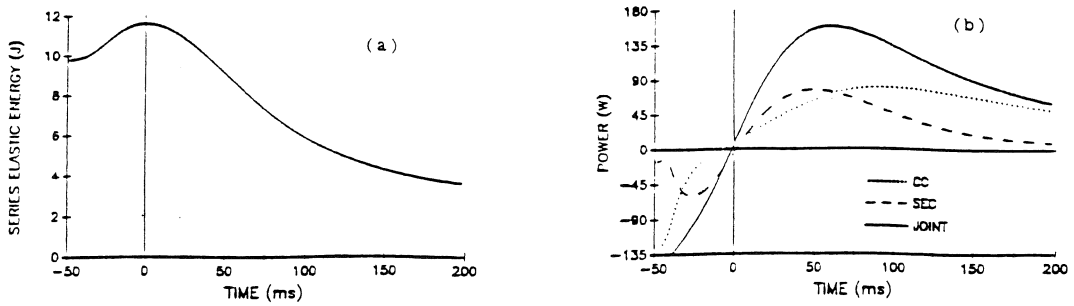


Figure 1. SEC energy (a) and joint and component power (b) for a typical simulation of an ankle joint movement task. Time = 0 represents the initiation of the concentric phase.

Table 1. Joint excursion and average (0-100 ms) power results for nominal and manipulated model parameter runs. Numbers in parentheses denote difference from the nominal run.

	joint excur (°)	joint power (W)	CC power (W)	SEC power (W)	SEC power (% nom)
nominal run	8.85	118.7	56.5	50.9	-----
increase in maximum CC velocity (14 cm/s)	9.20	127.8	69.6	46.6	91.6
increased dev from optimal angle (5°)	8.65	111.4	45.9	54.5	106.9
increased SEC max ang extension (3°)	9.15	123.8	55.9	56.3	110.6

DISCUSSION

The relative CC and SEC contributions can be explained by the interaction of these components and muscle mechanics principles. With an increase in the maximum unloaded CC velocity (as compared to the nominal run), the CC force did not drop off as much during a particular concentric phase time period. This corresponded to a reduced amount of SEC recoil and less energy recovered. In contrast, the CC force was reduced to a greater extent as turnaround was further from the optimal angle and the concentric phase was on the ascending part of the length-tension relationship. This resulted in more energy recovered by the SEC and an increased SEC shortening velocity and power developed. The more compliant SEC produced an increased amount of SEC shortening for a given drop in force. These simulation results indicate that moderate changes in elastic energy recovered may likely result in little change in performance. In addition, the changes in performance and energy recovered are not necessarily in the same direction.

REFERENCES

1. Bosco, C. et al. Acta Physiol Scand 106: 467-472, 1979.
2. Bosco, C. et al. Acta Physiol Scand 116: 343-349, 1982.
3. Aura, O. et al. Int J Sports Med 7: 137-143, 1986.
4. Shorten, M.R. Current research in sports biomech. Karger, Basel, 1987.
5. Winters, J.M. et al. IEEE Trans Biomed Eng BME32: 826-839, 1985.
6. Mungiole, M. Ph.D. dissertation, Arizona State University, 1991.

HIGH PRECISION PLANAR AND SPATIAL MEASUREMENTS BETWEEN A TALAR BONE VECTOR AND THE MALLEOLUS-METATARSAL VECTOR DURING THE MOVEMENTS OF DORSIFLEXION AND PLANTAR FLEXION FOR THE FOOT

Norman Murphy [1, 2], Paul Allard [1, 2] and Rachid Aissaoui [1]
1) Pediatric Research Center, Sainte-Justine Hospital, Montreal, Que., Can., H3T 1C5.
2) Faculty of Physical Education, University of Montreal, Montreal, Que., Can., H3C 3J7.

INTRODUCTION

This paper reports findings between the planar (sagittal) angle and spatial angle defined between a talar bone vector and the malleolus-metatarsal vector during the movements of dorsiflexion and plantar flexion for the foot. The purpose of this study was to illustrate the presence of spatial motion at the ankle. The results, which support the existance of spatial motion, confirm that in biomechanical foot and ankle investigations a three-dimensional (3-D) approach and analysis must be used.

REVIEW AND THEORY

Cinephotography and roentgenograms are primary methods used to investigate and analyse normal and pathological biomechanical functions of the ankle. These methods are mostly used in planar (2-D) investigations. The absence of 3-D investigations forestalls the true understanding of the biomechanical function of the ankle (1). Presently, most link segment representations and modelling of the human lower limb consider the foot and ankle complex to be rigid, rotating in the sagittal plane. More specifically, a vector extending between the lateral malleolus and base of the fifth metatarsal is used to represent the 2-D rotation of the foot and ankle complex. The degree to which this vector corresponds to true rotation of the foot, the talar bone at the ankle, remains unknown. In this investigation, a stereophotogrammetric set-up, (2) combined with the Direct Linear Transformation (DLT) technique (3), was used to obtain high precision 3-D osseous marker displacement data. The degree to which the malleolus-metatarsal vector corresponds to true rotation of the foot, via the talar bone, was then calculated.

METHODOLOGY

The experimental set-up consisted of four motorized still cameras, one mounted at each corner of a rectangular baseboard. At the center of the baseboard, a calibration object having 36 fiducial marks was used for the calibration. The device removed, a fresh amputated human lower limb was fixed into position. Windows were dissected and osseous markers were then embedded directly into the talar bone, malleolus and fifth metatarsal. Stereophotographs of the markers were taken for five consecutive positions during dorsiflexion and plantar flexion. The movements were induced by a pulley and weight system attached to the primary muscle tendons. The 2-D coordinates of the osseous marker displacements were obtained by manual hand digitization. The 3-D coordinates were reconstructed and then smoothed (4) using the GCVSPL procedure (5). With the availability of three more specimens, the procedure was repeated. A talar bone vector (T) and a malleolus-metatarsal vector (M) were defined from the osseous markers. The planar (sagittal) angle (α_p) and spatial angle (α_s) between the two vectors for each of the five positions for each specimen were analytically calulated. Their respective angular errors ($\Delta\alpha_p$, $\Delta\alpha_s$) were also calulated. Finally, the spatial angles between each successive positions 1 to 5, for each vector, were calculated.

RESULTS

The 3-D reconstruction error was calculated to be 0.36mm. The spatial angles, calculated between the malleolus-metatarsal and talar bone vectors at each one of the five positions, were significantly greater than the planar angles. More precisely, for the combined four

specimens, the spatial angles were greater by a mean of 4.79 ± 0.80° (angular error of 0.21 ± 0.04°) for dorsiflexion and 5.25 ± 1.55° (angular error of 0.40 ± 0.04°) for plantar flexion. Table 1. reports the results for dorsiflexion in one specimen.

Table 1. Angles between vectors T and M for dorsiflexion.

	Planar angle (deg)		Spatial angle (deg)		Angular difference (deg)	
Position	α_p	$\Delta\alpha_p$	α_s	$\Delta\alpha_s$	α_{s-p}	$\Delta\alpha_{s+p}$
1	60.23	0.03	64.22	0.04	3.99	0.07
2	60.48	0.04	65.47	0.04	4.99	0.08
3	59.82	0.04	65.98	0.04	6.16	0.08
4	58.33	0.04	66.04	0.05	7.71	0.09
5	56.77	0.04	66.40	0.05	9.63	0.09
				Mean	5.64	0.16

The spatial angles calculated for the malleolus-metatarsal vector, within each successive postions 1 to 5, were significantly greater than those for the talar bone vector angles. More precisely, for the combined four specimens, they were greater by a mean of 3.20 ± 1.48° (angular error of 0.30 ± 0.03°) for dorsiflexion and 3.47 ± 1.27° (angular error of 0.33 ± 0.09°) for plantar flexion. Table 2. reports the results for dorsiflexion in one specimen.

Table 2. Angles for each successive postion of vectors T and M for dorsiflexion.

	Vector T (deg)		Vector M (deg)		Angular difference (deg)	
Position	α_{sT}	$\Delta\alpha_{sT}$	α_{sM}	$\Delta\alpha_{sM}$	α_{sM-T}	$\Delta\alpha_{sM+T}$
1 - 2	6.51	0.13	6.86	0.02	0.35	0.15
2 - 3	6.44	0.12	7.58	0.02	1.14	0.14
3 - 4	6.55	0.11	8.53	0.02	1.98	0.13
4 - 5	6.16	0.10	8.22	0.02	2.06	0.12
				Mean	1.71	0.27

DISCUSSION

For all conditions, the spatial angles were significantly greater than the planar angles. This finding can be partially explained by the projection of the vectors out of the sagittal plane. The calculated angles estimate a projection of approximately 4 to 5°. The spatial angles for the malleolus-metatarsal vector were significantly greater than the talar bone vector spatial angles. The calculated angles estimate a projection of approximately 3°. This finding can be partially explained by the increase in range of motion observed due to interosseous movement of the bones within the foot. Caution must therefore be exhibited when interpreting ankle motion via the malleolus-metatarsal vector. These results do illustrate and confirm that for close-range biomechanical foot and ankle investigations, such as in foot modelling, a three-dimensional (3-D) approach and analysis must be used.

REFERENCES

1. AREBLAD M et al.: J Biomech 23: 933-940, 1990
2. ALLARD P et al.: Eng Med & Bio Sept: 31-36, I987.
3. MARZAN GT et al.: Symp on Close-Range Photogram Syst: 420-473, 1975.
4. de LANGE A et al.: J. Biomech Eng 112: 107-112, 1990
5. WOLTRING HJ: Adv.Eng Software 8: 104-113, 1986.

KINEMATICS OF THE ANKLE: A HINGE AXIS MODEL

by
ANOOP K. SINGH, F.R.C.S., KEITH D.STARKWEATHER, M.S.,
SANJAY JATANA, M.D., ANNE M. HOLLISTER, M.D.and ANDREI G.LUPICHUK, B.S.E.E
Orthopaedic Laboratory, Harbor-UCLA Medical Centre, Torrance, California.

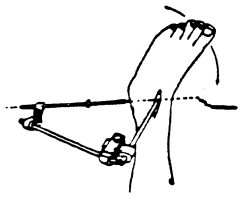
ABSTRACT

We used a mechanical method to locate the axis of rotation of the talocrural joint . A single constant axis of rotation was found just distal to the tips of the malleoli . Light emitting diodes mounted on a talar pin were photographed during flexion-extension, so as to record their arced trajectories in time-lapse frames. These trajectories were analysed both in the sagittal plane and in a plane perpendicular to the determined axis of rotation. Results obtained from sagittal plane studies were distorted by perspective error. The plane used to analyze joint motion or shape must be the plane of motion. Models of the talocrural joint for gait analysis, reconstructive surgery and prosthetic design should have a single offset axis of rotation.

INTRODUCTION

Ankle motion has been studied by many researchers over the years. Three talocrural models have emerged . **Goodsir** [3](1868) implied that the talocrural joint had a single axis passing through the centre of the talar body . **Fick** [2] proposed a variable hinge axis, the axis changing as the talocrural joint moved. **Barnett and Napier** [1] suggested two axes, a claim reaffirmed by **Hicks** [4] who attached a mechanical device to the calcaneus to locate the flexion-extension axis of the ankle. a**Sammarco, Burstein and Frankel** [11] used reuleaux analysis of sagittal plane x-rays of the ankle to suggest instant centres of rotation for the talocrural joint.

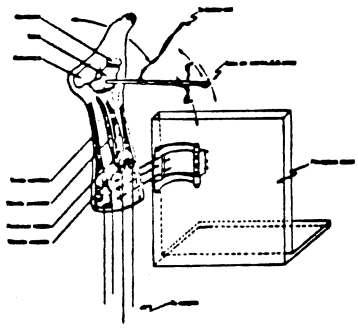
Inman [5,6,7] used a mechanical method to locate a single axis of rotation of the human talocrural joint which lies just distal to the tips of the malleoli. . Interestingly enough, all the researchers suggesting multiple axes, analysed data obtained from sagittal plane studies. Inman - on the other hand - studied the talocrural joint in a plane perpendicular to the axis suggested by his model.With these contending models of talocrural kinematics, we decided to use a mechanical method to determine the axis of rotation. We also wanted to see whether perspective contributed to the wide disparity in the various models of the ankle.



MATERIALS AND METHODS: EXPERIMENTAL

Six fresh-frozen cadaver legs amputated below the knee were used. The Tibia was attached to a frame by an Ace external fixator. The joint was stabilized by loading tvarious tendons. A Steinmann pin was drilled into the neck of the Talus, and the mechanical device used to locate the axis was then attached to the pin.

We then used the mechanical device - the axis finder - to locate the axis of the ankle joint. Once the axis had been located, the camera was aligned with the axis finder's Steinmann pin at a distance of six feet. A flashing 3-Light Emmiting Diodes (LED) tree was attached to the talar pin. Time-lapse photography was performed to record the three arcs described by the LEDs, as the ankle joint was moved from dorsi to plantarflexion. The camera was then aligned in the sagittal plane (non-axial lateral view) and the arcs recorded once again. The experimental setup determined that about 70 degrees of talocrural movement was represented by the three arcs. The ankles were then drilled using a special jig and the specimens were then scanned by Magnetic Resonance so as to illustrate the anatomic relationships, prior to dissection. T1 images were obtained for all the specimens in the antero-posterior plane and also in a plane perpendicular to the axis.



The photographs of the LED paths so obtained were scanned into a computer. The LED paths were digitized, resulting in "X" and "Y" coordinates of the data points.Since the arcs appeared circular, the data from each arc was entered into a non-linear optimization programme wnich determined the radius of the circle, the circle's centre and the amount of Least Squares Error between the calculated radius and the optimized radius.Data from concentric circular arcs would generate a common center and minimal residual error (F value at convergence), and data from non-circular or nonconcenric arcs would be optimized with the circle model yeilding different centers and / or higher residual error. If the camera were aligned with the axis of rotation and the axis were constant, the three arcs formed by the three LEDs would form three concentric circles. LED arcs shot at a true lateral position (sagittal plane motion) would have an elliptical shape, and would have different x/y values for their centers of rotation. We compared the range of (x_c,y_c) center values to the mean radius r of the three arcs (A=delta X/mean R; B=delta Y/mean R). Arcs with low A and B values are sections of concentric circles (having a common center). Arcs with large A and B values are sections of ellipses.

RESULTS

The arcs obtained in the axial projection demonstrated center coordinates clustered significantly more closely than those

from the lateral projections.($p < 0.0192$ for Xc and $p < 0.0274$ for the Yc coordinates using the Student t-test, with a 95% confidence interval). The Circular Error of Probability (CEP) is a percentage ratio. It compares the area within which the centres of rotation of the three arcs lie to the total area of a circle of radius equal ot the mean radius of that data set (Xc x Yc / mean R) x 100. A low CEP would mean a tighter spread of the centres. No meaningful comparison can be drawn between the axial projection data of one ankle and the analysis from a lateral view of another. This - we feel - is due to the wide variation of the talocrural joint axis ($^{+/-}$ 20 degrees). This in turn may result in the axis of a given ankle being very close to the plane of the lateral projection. The A and B values of such an ankle would show close clustering even in the lateral projection. However, the axial clustering of this ankle would still be significantly tighter.Analysis of the shape of the talar joint surface shape from the MRI's showed the arcs to be very circular (mean 0.59% error +/- 0.15 s.d.) if the images were made in a plane perpendicular to the axis of rotation The flexion-extension axis of the talocrural joint as suggested by Inman lies just distal to the tips of the malleoli. Magnetic resonance imaging of the ankles revealed that the drill path (i.e. the axis of rotation) followed this trend.

DISCUSSION

Our investigation of the axis of rotation of the talocrural joint revealed that experiments that approached the joint from the true lateral position could not identify the axis of rotation, as the curves generated were elliptical - a geometric shape composed of curves of varying radii and axes of rotation. An analogy can be drawn to that of a log cut in cross-section. A two dimensional recording device is subject to perspective error (unless corrected for) and will be unable to faithfully find an axis of rotation that lies in three dimensional space.Our photographic data confirms that a single flexion-extension axis for the talocrural joint exists, as the curves generated by the moving LEDs (when photographed down the axis) formed concentric arcs throughout the physiologic range of motion. The location of this axis is similar to that described by Inman [5,6,7]. We propose that this common centre is the location of the flexion-extension axis of the talocrural joint. However, arcs with large A and B values are sections of ellipses (non-axial viewing of a circle). Reuleaux analysis of these curves will give variable axes of rotation [10,11].

In addition, we found that erroneous kinematic conclusions can be made by studying the talocrural joint from the true lateral perspective. The axis of rotation is offset in two planes. It is offset by approximately 23 degrees posterior and lateral to the long axis of the foot, and downward laterally to the long axis of the tibia in the coronal plane. This would introduce complementary movement in both the valgus-varus and pronation-supination planes. These conjoint movements would have to be compensated for if one tries to reduce three dimensional ankle motion to two dimensions. One way of correcting for this factor is by recording motion of a joint along its axis of rotation.

This would introduce complementary movement in both the valgus-varus and pronation-supination planes. These conjoint movements would have to be compensated for if one tries to reduce three dimensional ankle motion to two dimensions. One way of correcting for this factor is by recording motion of a joint along its axis of rotation. Current prosthetic designs of ankles [13,14] still heavily rely on a cylindrical configuration for the talus, with an axis of rotation parallel to the floor and perpendicular to the long axis of the foot. This concept is emulated by the model in **figure I.** We feel the axes of such prostheses are misaligned by 20 degrees in both these planes. This would not only profoundly alter joint moments and joint reaction forces but would make these implants incapable of mimicing normal motion. The accurate location of a joint's axis is an essential perquisite for torque and joint force analysis. Tendon transfers and other dynamic musculo-skeletal reconstructive procedures can profoundly alter joint moments and stresses. A precise three-dimensional analysis of musculo-tendinous moments about a joint is essential prior to embarking on reconstructive surgery.

REFERENCES

1. **Barnett, C.H.; and Napier, J.R.**: The axis of rotation of the ankle joint in man: Its influence upon the form of the talus and the mobility of the fibula.: J. Anat.,86:1, 1952.
2. **Fick, R**: Handbuch der Anatomie und Mechanik der Gelenke unter Berucksichtigung der bewegenden Muskeln. Part 1. Gustav Fischer Verlag, Jena, 1904.
3. **Goodsir, J.**: On the curvatures and movements of the acting facets of articular surfaces. In Turner, W. (Editor): Anatomical Memoirs. Edinburgh, Adam and Charles Black, Vol.2, 246-264, 1868.
4. **Hicks, J.H.**: The mechanics of the foot.1. the Joints. J. Anat.,87: 345-357, 1953.
5. **Inman, V.T.**: The joints of the ankle. Baltimore, The Williams and Wilkins Company, 1976.
6. **Inman, V.T.; Mann, R.A.**: Biomechanics of the foot and ankle. In DuVries' Surgery of the foot . Saint Louis, The C.V.Mosby Co. 1978.
7. **Isman, R.E.; and Inman, V.T.**: Anthropometric studies of the human foot and ankle. Bull. Pros. Res., 10-11: 97-129, 1969.
8. **Kahaner, D.; Moler, C.; and Nash, S.**: Numerical Methods and Software. Prentice Hall, New Jersey, 9:1989.
9. **Lundberg, A.; Svensson, O.A.; et al.**: Kinematics of the ankle/foot complex Pt. 1-3. Foot and Ankle, 9: 4, 1989.
10. **Reuleaux, F.**: Theoretische Kinematik. Grundzug einer Theorie des Maschinenwesens. Braunschweig, Germany, F. Vieweg & Sohn, 1875.(Translated by A.B.W. Kennedy: The Kinematics of Machinery: Outline of a Theory of Machines. London, MacMillan, 1876.)
11 **Sammarco, G.J.; Burstein, A.H.; and Frankel, V.H.**: Biomechanics of the ankle: A kinematic study. Orthop. Clin. North. Am., 4: 75, 1973.
12. **Soudan, K.; Audekercke, R.V.**: Methods, difficulties and inaccuracies in the study of human joint kinematics and pathokinematics by the instant axis concept. Example: the knee joint.. J. Biomech., 12: 27-33, 1979.
13. **Stauffer, R.N.**: Total ankle replacement. Arch. Surg., 112: 1105-1109, 1977.
14 **Stauffer, R.N.; and Segal, N.M.**: Total ankle arthroplasty: four years experience. Clin. Orthop., 160: 217-221, 1981.

INTRA- AND INTERDAY ASSESSMENT OF BILATERAL SYMMETRY IN ISOKINETIC KNEE EXTENSION MOMENTS

Steven T. McCaw, Biomechanics Laboratory, Dept of HPERD, Illinois State University, Normal, Illinois 61761

Introduction and Review: Knee injuries occur frequently as the result of athletic, industrial and automobile accidents. The subsequent decrement in performance following injury, surgery and rehabilitation, and the ability of the knee to avoid reoccurrence of severe injury is dependent on the restoration of pre-injury joint range of motion and strength. The effectiveness of a knee rehab program is frequently evaluated by measuring joint strength using an isokinetic dynamometer. A criterion commonly used to assess a patients rehabilitation is the ratio between the strength of the injured and uninjured limb. A patient will be cleared to resume normal training when the injured limb has regained 90% of the strength of the uninjured limb (Charteris, 1979). Although the 90% criterion is widely used, there is a paucity of data on the bilateral symmetry of knee strength in the uninjured population at a variety of different isokinetic speeds. The purpose of this study was to evaluate bilateral symmetry in knee extensor strength of healthy males, and to evaluate the symmetry measure on consecutive days.

Methods: Four males from the university community volunteered for the study. All subjects were free of recent knee trauma. Informed consent was obtained in accordance with university policy. Subjects were asked to restrict heavy loading of the legs for 48 hours prior to the first data collection.

Knee joint moment of force and angular displacement data were sampled (1000 Hz) during maximum knee extension using a Biodex isokinetic dynamometer. The dynamometer was calibrated using a known weight and angles on each of the 2 days of testing. A gravity correction factor (Nelson et al, 1983) was calculated for each leg on each day. Surface EMG was used to monitor quadriceps and hamstring activity during collection of the gravity correction factor data to ensure that knee flexion occurred passively. Wide straps immobilized the trunk, pelvis and thigh of the subject, the trunk angle was fixed, and the dynamometer arm was securely attached to the distal shank during testing.

On each day of testing, data were recorded from the right and left leg for 4 trials at 8 angular velocities between 30 and 300°/s. Right and left leg starting order and the sequence of velocity performance were randomized across days. Ample time was provided between trials to avoid fatigue effects. Moment and angle data were smoothed (10 Hz) using a recursive low-pass Butterworth digital filter (Winter et al, 1981), the gravity correction factor was added to the moment data, and the period of constant angular velocity was identified from the differentiated angle data. The peak extensor moment (PEM) and the angle at which the peak moment (PEMang) was produced were identified for each trial and saved in a data file. Data were analyzed on a within-subject basis using ANOVA procedures from SPSS. The design of the study allowed for 16 comparisons of right/left symmetry (8 speeds * 2 days) and within-leg between-day comparisons (8 speeds * 2 legs) for both PEM and PEMang data. Alpha was set at 0.05.

Results: There was no consistent trend across the subjects for one leg to exhibit greater PEMs. Two subjects exhibited greater PEMs for a single leg at all speeds on both days. However, for Subject 1 (S1) the left leg PEM was consistently greater while for S4 the right leg PEM was consistently greater. The other two subjects also exhibited a similar trend in PEMs. For both of these subjects, the PEM for one leg was consistently greater at the low speeds (<135 °/s) while the opposite leg was consistently greater at higher speeds. For S2 the left leg PEMs were greater at low speeds and right leg PEMs were greater at high speeds. The opposite trend was evident

for S3, with his right and left leg PEMs greater at low and high speeds, respectively. To graphically demonstrate these trends, the right and left leg mean PEM data for S1, day 2 and S2, day 1 are plotted in Figures 1 and 2, respectively. Table 1 presents the number of significant Right/Left PEM comparisons, and the number of comparisons where the mean difference was greater than 10% for each subject. S1 had the greatest number of significant R/L differences (11 of 16) and S2 had the least (5 of 16). However, it can be seen that the R/L difference was less than 10% for the majority of the differences. Table 1 also presents the number of significant within-leg between-day comparisons. These values indicate that the interday variability within a leg was as great as the intraday bilateral differences. This suggests that the observed bilateral asymmetry is more reflective of normal biological variation in knee extensor moments than a true functional difference.

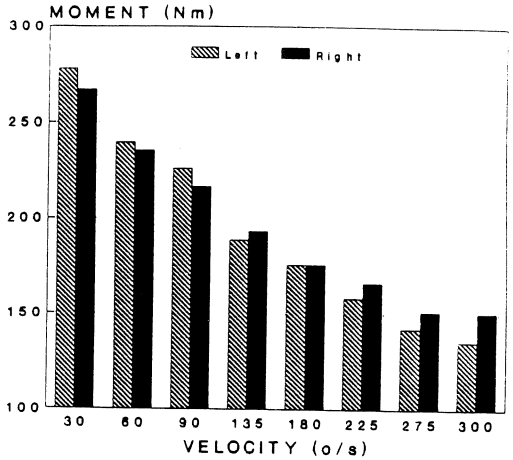


Fig 2. Peak Knee Extensor Moment, S2D1

Table 1. Number of significant bilateral and interday PEM comparisons ($p<.05$) and number of comparisons with mean PEM difference > 10%.

	Right/Left Comparisons		Day1/Day2 Comparisons	
	# Significant	#Diffs >10%	# Significant	#Diffs >10%
S1	11	2	8	3
S2	5	2	7	2
S3	7	0	8	4
S4	8	3	6	3

Similar inconsistencies were evident in the PEMang data. S1 exhibited no significant bilateral or interday differences in PEMang. S2, S3 and S4 all exhibited significant bilateral differences in PEMang, but only S2 did not exhibit significant interday differences. As with the PEM data, these results suggest that the observed bilateral differences in PEMang reflect normal biological variability.

Conclusion: The data support the assumption that bilateral differences of 10% in PEM values are acceptable. However, the inter-individual differences in asymmetry direction and the interday variability present in the data of healthy subjects emphasizes the need to collect bilateral PEM data before injury occurs to best evaluate knee joint rehabilitation.

References:
Charteris, J. (1979) Scan. J. Rehab. Med., 11:105-109.
Nelson, S.G et al (1983) Phys. Ther.,63:5:674-676.
Winter, D.A. et al (1981) Eur. J. Appl. Physiol., 46:397-408.

This study was supported by an Illinois State University Research Grant.

THE EFFECTS OF COLD APPLICATION AND MODIFIED PNF STRETCHING TECHNIQUES ON ACUTE HIP JOINT FLEXIBILITY IN COLLEGE MALES

William L. Cornelius, Khosrow Ebrahim, and Jack Watson
Department of Kinesiology, Health Promotion, and Recreation
University of North Texas, Denton, TX 76203-3857

INTRODUCTION

Modified Proprioceptive Neuromuscular Facilitation (PNF) and conventional stretching techniques were examined under conditions of cold and no-cold application. Joint range of motion (ROM) data were collected to determine the status of hip flexion. PNF stretching techniques are believed to be more effective than conventional stretching maneuvers. Furthermore, local cold application has been used as an important modality in athletics and as a medical treatment. Few studies, however, have been conducted with the use of cold application and subsequent flexibility maneuvers. Results suggested that PNF stretching techniques can provide greater acute ROM than a passive stretch, with or without cold.

REVIEW AND THEORY

PNF stretching techniques have been shown to significantly improve ROM over more conventional stretching techniques (Cornelius et al., 1987; Etnyre and Abraham, 1986; Wallin et al., 1985). Few investigations have utilized therapeutic modalities, such as cold application, in conjunction with PNF stretching techniques. Several studies reported significant increases in ROM when a 10 minute cold application was used prior to modified PNF (Rosenberg et al., 1990; Cornelius and Jackson, 1984). Furthermore, significant main effects were found in these studies, with the PI_3CP technique reported superior to the PCP technique in producing increased ROM at the hip joint. A three-second maximum voluntary isometric contraction (MVIC) of the stretched antagonist was incorporated. Earlier, no significant difference between three- and six-second MVIC, without the use of cold, was found utilizing modified PNF stretching procedures (Cornelius and Hinson, 1980). Consequently, the purpose of this study was to determine the efficacy of the use of particular modified PNF flexibility techniques under two conditions, cold and no-cold application.

PROCEDURES

The sample for the study consisted of males (N=120) from physical education classes. Criteria for the selection of subjects included those who were free from injury and had body fat of 18 percent or less. The investigation met guidelines set by the University of North Texas Human Subjects Review Board. Subjects were randomly assigned to a cold or no-cold condition in one of eight groups. Groups assigned the cold condition received a ten minute application. A Leighton Flexometer was used to determine degrees of passive hip flexion at the terminal point in the PNF (PCP, 3-PI_eCP, 3-

PI_fCP) and P techniques. The average of the three trials was used to determine ROM attained during each treatment. A passive stretch of the agonist served as a baseline measure (control) and preceded the treatments for all subjects in order to determine whether or not there were any significant differences among the groups.
The research design was a two (cold/no-cold condition) by four (techniques) ANOVA. Data were analyzed with analysis of variance techniques (Winer, 1971). A Tukey multiple comparison test was used as a post-hoc test in comparing mean differences between the groups.

RESULTS AND DISCUSSION

Descriptive statistics were summarized in Table 1 for the entire sample (N=120) on fat (10.9±3.8 %), age (21.5±2.7 yrs), weight (158.7±15.9 lbs), height (69.6±2.6 in), and baseline ROM (95.2±13.2 deg) measures. An ANOVA on the pretest data indicated there was no significant difference between the groups on the baseline (no-cold) passive stretch ($F_{3,119}$=1.200, p=0.313). Descriptive statistics were calculated on ROM for all possible treatment conditions.

	Treatments			
Condition	3-PI_fCP	PCP	3PI_eCP	P
Cold	112.1±08.8	110.6±10.8	113.4±09.9	98.4±12.8
No-cold	106.0±12.0	108.0±10.7	115.7±15.6	100.7±11.1

The reliability of the ROM data between trials ranged from 0.944 and 0.9684. No significant (main) effect of the cold verses no-cold condition ($F_{1,112}$=0.239, p>.05) was found. There was a strong effect of treatment ($F_{3,112}$=8.677, p<.001). Tukey post-hoc tests indicated that only the P treatment differed from the other stretching techniques, with 3-PI_fCP, PCP, and 3-PI_eCP all superior to the P treatment (<.05).
These findings were in agreement with other studies which found modified PNF maneuvers to be superior to conventional stretching techniques. The three PNF techniques were equally effective at increasing ROM. It was concluded that PCP, 3-PI_eCP, and 3-PI_fCP modified PNF stretching techniques can be utilized more effectively than the common pasive stretch technique to enhance hip joint flexibility in college males, with or without cold application.

References

Cornelius, W., et al., J of Sp Med & Phys Fit, 20:75-80, 1980.
Cornelius, W., et al., Ath Train, 19:183-184, 199, 1984.
Cornelius, W., et al., J of Appl Sp Sci Res, 1:39-41, 1987.
Etnyre, B., et al., Am J of Phy Med, 65:189-196, 1986.
Lippold, O., et al., J of physio (Lond), 153:218-231, 1960.
Rosenberg, B., et al., J of Phys Educ & Sp Sci, 2:31-36, 1990.
Wallin, D., et al., The Am J of Sp Med, 13:263-268, 1985.

QUANTIFYING TWO-DIMENSIONAL JOINT INCONGRUITY IN THE OSTEOARTHROTIC HIP

John A. Miller, Jr. and James G. Andrews, Department of Exercise Science, and Richard A. Brand, Department of Orthopaedic Surgery, The University of Iowa, Iowa City, IA, and Paul G.J. Maquet, Aywaille, Belgium.

INTRODUCTION

Osteoarthrosis (OA) distorts the articulating surfaces of the hip through articular cartilage deterioration and osteophyte formation. In general, this distortion decreases the congruity of the joint. With this decreased congruity may come an increase in the looseness of the hip over the range of motion (ROM) encountered during normal activities of daily living. The increased looseness of the hip might then provide the setting for abnormal stressing of the articulating surfaces of the hip which would encourage the continuation of OA.

There are basically two ways to change the looseness exhibited in a given joint: (1) by altering the geometry of one or both of the articulating surfaces, and (2) by realigning unmatched surfaces so that they match or fit together better over the specified ROM. In either case, it is necessary to quantify some biomechanical measure or measures of joint behavior so that a comparison can be made before and after the change takes place to determine its effect on joint incongruity or looseness.

The purposes of this investigation were to define the looseness of the hip in a clinically relevant way, and to calculate the looseness of the hip over the range of hip configurations encountered during normal activities of daily living.

PROCEDURES

Three possible and potentially useful measures for quantifying the looseness of a joint were identified. The first measure used the locus of a characteristic point (CP) embedded in the femoral head (FH) as the femur was moved relative to the acetabulum (A) to quantify the looseness present in the joint. The second and third measures used the joint space (JS) and the contact region (CR), respectively, that existed at small (0.1 mm) discrete steps during this translatory motion, to quantify the looseness of the joint. Three standard, anterior-posterior X-rays showing the OA affected hip in the neutral, maximum abduction and maximum adduction positions for each of 38 subjects were used to obtain the input data required in the 2D algorithm developed

for this investigation. To determine each looseness measure, the FH first was rotated to reflect the hip orientation being considered, and then translated along A in that orientation through a sequence of surface contacts. A subgroup of these surface contacts was then used to determine the three overall looseness measures for each hip orientation.

RESULTS

The algorithm generated CP locus, JS and CR looseness measure values at 5^{o} increments ranging from 30^{o} varus rotation to 30^{o} valgus rotation. Average values and ranges for the looseness measures are presented in the following table.

Average minimum and maximum, and ranges for looseness measures of the osteoarthrotic hip (n=38)

Looseness Measure	Average Minimum	Range	Average Maximum	Range
CP locus (cm)	0.77	0.26-1.76	1.03	0.43-2.13
Joint space (cm^2)	1.60	0.96-3.61	3.64	1.32-9.33
Contact region (cm)	0.90	0.05-2.09	2.16	0.32-4.23

DISCUSSION

Each of the three looseness measures (i.e., the characteristic point locus, the joint space, and the contact region) defined and calculated in this investigation varied from subject to subject, and each varied with hip orientation for each subject. This was expected as the extent to which osteoarthrosis had affected each hip was unique in each subject.

One potential use for one or more of the looseness measures might be in the treatment of OA. One surgical method of treating OA, the intertrochanteric osteotomy, is based on realigning the unmatched surfaces of the femoral head and the acetabulum to achieve a better fit or congruity. Currently, the osteotomy is determined by the surgeon in a subjective manner. By identifying a looseness measure which is either minimized or maximized at a certain osteotomy angle, the surgeon would have additional quantitative information to support the subjective evaluation.

INVIVO EULER BUCKLING AT THE ELBOW

Joseph J. Crisco III, Ph.D., .Manohar M. Panjabi, Ph.D, Kristina Rath. Biomechanics Laboratory and Section of Sports Medicine, Department of Orthopaedics and Rehabilitation, Yale University School of Medicine, 333 Cedar Street, New Haven, Connecticut, 06510, USA

INTRODUCTION

Clinical instability is a widely used term, but its is difficult to define. The definition of mechanical stability can also be complex. One simple definition is based on the Euler column: an axially loaded column remains stable if it remains upright after being perturbed. *In vitro* studies of the ligamentous spinal column have shown that it behaves as an Euler column, and buckles at loads less than 20N (Lucas, Crisco). Thus, muscular activity is necessary for the stability of the spinal column. Since we assumed that the neuromuscular system is "energy efficient", we hypothesized that muscular activity would increase to stabilize the spinal column as loads were increased. This hypothesis predicts coactivation is necessary for stability. Coactivation of muscles has been recorded during many tasks (Sherrington), but a well accepted generalized model predicting coactivation is lacking (Hughes). The goal of this study was to test our hypothesis with the simplest *in vivo* model of a column available: the rigid forearm and the 1DOF elbow joint. We recorded the EMG activity of the biceps and triceps, and the motion of the vertical forearm as it was axially loaded. Contrary to our hypothesis we recorded minimal coactivation levels of the biceps and triceps as the load increased. Moreover, in the majority of tests buckling was avoided as the subjects placed their forearm eccentrically to the load. Buckling was observed in 25% of the tests, and we recorded significant levels of coactivation only after the onset of buckling. In these tests, simple buckling theory was demonstrated to be in excellent agreement with the experimental data.

MATERIALS AND METHODS

The right arms of four healthy male volunteers were tested. With the elbow flexed and supported from below, a hand jig was held and strapped to the forearm (Fig. 1). The jig was attached by a linkage of linear bearings that permitted unconstrained elbow flexion and extension. We applied a compressive vertical load to the top of the jig and recorded the flexion/extension displacement, from which elbow rotation and acceleration were calculated. Random perturbations could be introduced with a free flowing air-line fastened to the the top of the hand jig with a section of spring steel. We digitally recorded (250 Hz) the surface EMG activity over the midbelly of the biceps brachii and over the bellies of the medial and long triceps. The RMS was determined with a sliding window of 0.8 sec. A test consisted of increasing the load to 350 N as the subject attempted to keep the forearm vertical, while the load, displacement, and EMGs were recorded. Two protocols were followed. In the first (4 subjects, 28 tests), random perturbations were introduced at the hand jig. In the second (2 subjects, 12 tests), no perturbations were introduced. Only the second protocol will be presented here.

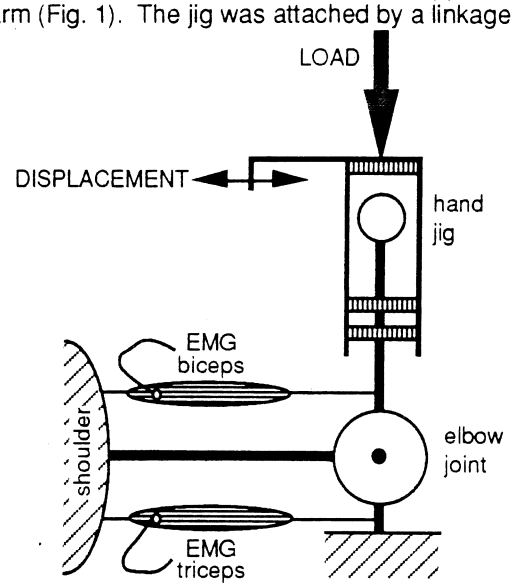


Figure 1. Lateral schematic view of the elbow supported from below and the forearm vertical.

RESULTS AND DISCUSSION

The 12 tests were qualitatively categorized into three groups, based upon the observed buckling behavior. In the first group (n=8), no buckling behavior was observed because elbow rotation steadily increased (4 in flexion, 4 in extension) as the loading increased. In this group EMG activity clearly

showed that the increasing load was solely supported by the agonist muscle. In the second group (n=1), the forearm remained vertical as the load reached its maximum and decreased with *no* increase in EMG activity. In the third group (n=3), buckling behavior was observed. Buckling was defined as a change in elbow position with an acceleration greater than 60 degrees/second^2. The buckling loads for these three tests were 288, 279, and 298 N. We plotted the applied load, displacement of the hand jig, and the RMS of the biceps and triceps activity for one such test in Fig. 2. As the load was increased, we see a slight fluctuation in hand position at about 10 seconds that is dampened with minimal activity. However, at 17 seconds buckling occurs with a sudden increase in *both* EMG levels and significant displacements with high accelerations of elbow rotation.

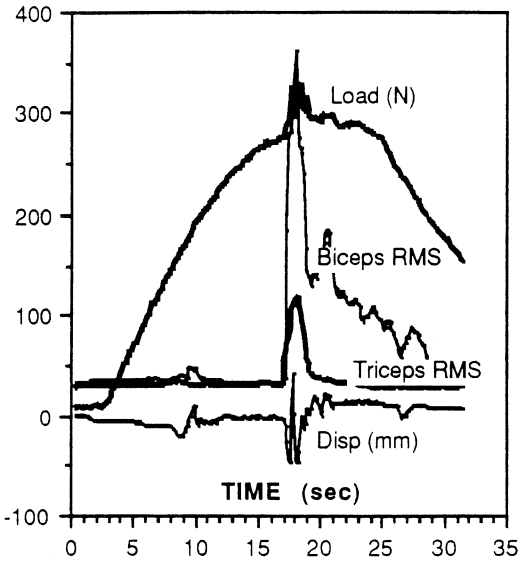


Figure 2. Experimental data.

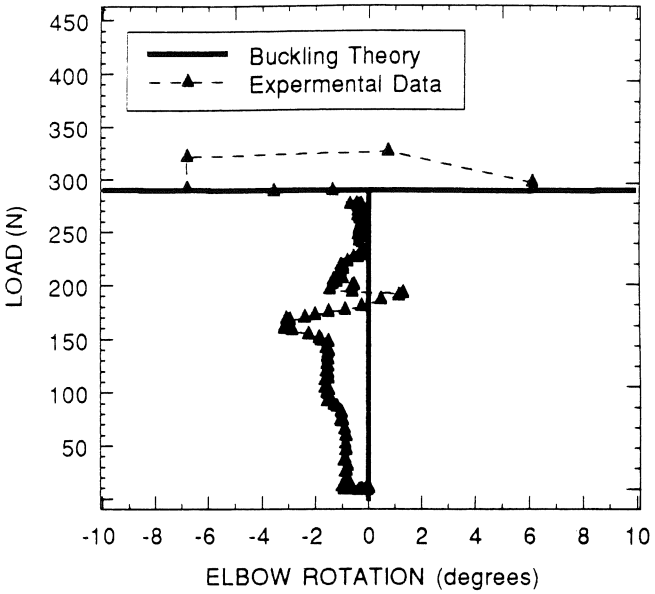


Figure 3. Comparison of load-displacement buckling theory and experimental data.

The forearm and elbow joint was then modeled as a rigid Euler column simply fixed at it base. Assuming that biceps and triceps activity provide a variable torsional stiffness at the elbow joint, we compared Euler buckling theory to the experimental data by plotting load versus the elbow rotation of Fig. 2. In Fig. 3, the theoretical displacements remain at zero as the the load is increased until the buckling load is reached. At the theoretical buckling load there is a bifurcation of the load-displacement curve, indicative of instability, since there is equal probability that the displacements will occur in either direction.

The control of posture and movement is complex. Numerous studies have determined the task specific roles of muscles. This study is believed to be the first on the Euler buckling phenomena *in vivo* . We found that buckling did not occur in the majority of tests. To allow a compressive load to remain axial, with the possibility of large displacements and loads arising with instability, may not be a natural response. The more natural, and safer, response was to place the load eccentrically and resist the increasing load with agonist activity.

In tests were buckling did occur, the load-displacement behavior of the buckling theory was in excellent agreement with the experimental data. Coactivation of the biceps and triceps can increase the stiffness of the elbow joint and hence the buckling load. However, such coactivation was not observed as a normal response until the onset of buckling. One interpretation of these findings is that the elbow joint cannot sense increases in pure compressive loading, but responds only to displacements that result from the buckling.

REFERENCES

Crisco et al. Multiple Muscles, Springer Verlag, 1990
Lucas et al. Tech. Report. Univ. Cal. San Francisco
Sherrington Selected Writings, Hoeber, N.Y., 1940
Hughes et al. Proc. Am. Soc. Biom. 1988

POSTURE

OPTIMIZATION AS APPLIED TO LARGE-SCALE 3-D HUMAN POSTURAL SYSTEMS: A SYNTHESIS OF CONCEPTS AND APPROACHES

Jack M. Winters
Bioengineering Program, Arizona State University, Tempe, AZ 85287-6006, and
Mechanical Engineering, The Catholic University of America, Washington, D.C. 20064

INTRODUCTION

Many human movement tasks appear to reflect underlying goal-directed behavior, including a variety of activities of daily living (ADL). This suggests that the tools of optimization represent a useful approach for studying movement coordination strategies. As computational power continues to improve, optimization techniques can be applied to more realistic larger-scale systems such as three-dimensional (3-D) posture. In the past the terms "dynamic optimization" (DO) and "static optimization" (SO) have been utilized to distinguish between two classes of optimization approaches [1,2]. However, when applied to ADL tasks involving postural adjustments, this terminology is confusing, and not as descriptive as is possible. A different classification is proposed here - forward optimization (FO) versus inverse optimization (IO) - that helps distinguish more explicitly between cases where optimization is utilized to solve a problem involving neuro-motor strategy versus cases where it is used to load-share between "redundant" muscles. The key is whether geometry is pre-specified. From this foundation, several of intriguing and computationally efficient approaches - based on utilizing performance criteria that are intricately tied to mechanical stability considerations - evolve for solving large-scale 3-D FO (yet quasi-static) problems. These techniques are relevant both toward synthesizing concepts in postural control and toward better understanding of ADL tasks of interest in rehabilitation and ergonomics.

REVIEW AND THEORY

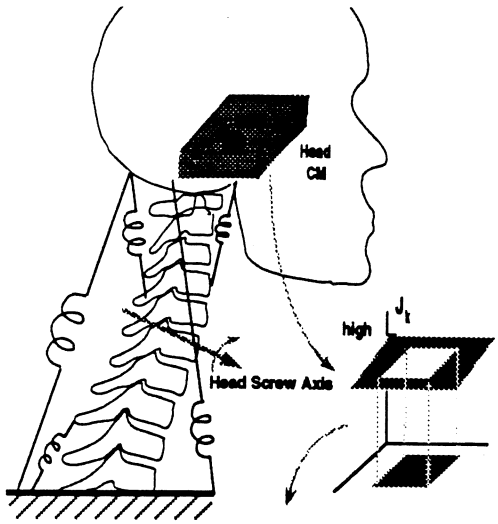
There are two general categories of useful musculoskeletal models: dynamic and steady-state (quasi-static). Within the first are models where either inertial or viscous terms are significant and behavior unfolds over time. Within the second are elasto-static models of posture and most applications of finite element methods. For each of these there are two types of mechanical formulations: forward and inverse. Thus, there are at minimum four distinct representations. It might be argued that the static (steady-state) case is simply a special case of dynamics. However, consider the following important classes of tasks: choosing a stable body posture when performing simple tasks while sitting or standing. Because of the large number of degrees of freedom of the spine and limbs and the wealth of potentially relevant muscles, this is a challenging problem since there exists a large number of kinematically admissible solutions. Thus, given both kinematic and muscle redundancy, the human brain must discern between various options such that the overall system - and any subsystem - is not only in equilibrium but also mechanically stable. This problem is considerably more complex than prespecifying a posture, making a free body diagram cut, and solving a SO problem; thus the concept of SO, as traditionally defined [1], has lost descriptive value. Interestingly, it has been suggested that the vast majority of ADL tasks are essentially quasi-static [3], and that concepts such as equilibrium "virtual" trajectories, in conjunction with impedance modulation, could drive such postural movements [4].

PROCEDURES

It is suggested that there are two fundamental approaches for finding solutions to the optimization problem: ***i) forward optimization*** (FO), where the specified (or optimized) inputs are muscle activations and the determined outputs are the geometric configuration and perhaps movement kinematics; and ***ii) inverse optimization*** (IO), where the geometric configuration and necessary kinematics are known (or pre-specified based on reducing measured data) and typically the muscle forces are determined outputs. This distinction can be seen from the form of the scaler performance (cost) criterion (PC) that is to be minimized (or maximized). For IO, this criterion is typically a function of muscle forces (e.g. muscle stress) or joint loading - a "cost" or "penalty" function that is independent of "performance"

measures based on system geometry or kinematics (since these are assumed *a-priori*) and is minimized at independent instants in time (hence the definition SO). In contrast, the FO PC includes a specification of the neuromotor task goal, which typically includes some measure of kinematic performance [2]. We define four possibilities: *i)* inverse optimization with a static model (IO_s); *ii)* inverse optimization with a dynamic model (IO_d); *iii)* forward optimization with a static (steady-state) model (FO_s); and *iv)* forward optimization with a dynamic model (FO_d). For groups interested in rehabilitation or workplace ergonomics, FO_s may indeed be the most appropriate current investigative approach.

The control parameters being modulated here are muscle excitation inputs. One FO_s approach has utilized a PC that includes "reference" head screw axis parameters during head tracking transitions (see Figure) in tandem with traditional measures such as muscle stress. Despite use of the Harris and Cray (as well as PC-386) computers, each solution takes time (hours or usually days). Recently, several intriguing, computationally efficient approaches have been developed for solving such large-scale FO_s problems. In these the PC includes a *discontinuous* subcriterion based on kinematic task performance (e.g. for the head in Figure) plus system potential energy (PE). There is thus a nonlinear mapping between the PC-control space and the PE-geometry space. Thus, the mechanics and optimization problems are solved simultaneously - essentially optimization via a single iteration. Additionally, there are similarities between the process of converging from a prior solution to a new equilibrium and the concept of "virtual trajectories" as developed in [4].



Two Examples: High Penalty Only if Outside of "Allowable" Task Region (e.g. Head Postion/Orientation Range)

$J_c = J_k + J_{pe}$ ← Potential Energy of System

$J_c = J_k + J_{ms}$ ← Summed Muscle Stresses

RMS difference from "reference" head screw axis parameters

RESULTS AND DISCUSSION

Three applications of FO_s have been or are currently under investigation: *i)* head "tracking" movements using the screw axis approach to contrast previous results with a medium-scale head-neck model with the current large-scale versions; *ii)* a simple 3 degree-of-freedom inverted pendulum model designed to contrast these various optimization approaches and establish theoretical implications; and *iii)* a large-scale head-neck-torso-pelvis model (150 nonlinear muscles; 100 ligaments plus relevant bones/facets/disks) designed to explore neck loading and muscle strategies, given various types of simulated neck "injuries" and a head-torso that is constrained within simulated halo orthotic devices. Both nonlinear and bilinear models of muscle are in use. Perhaps the most intriguing result to date is related to the tradeoffs between the primary postural task and maintenance of postural stability - without some "antagonist" and or certain types of "synergistic" cocontraction, stable postures often cannot be obtained within certain regions of the workspace.

Acknowledgement. This work was supported in part by a grant from the U.S. Dept. of Education (Nat. Inst. Disab. & Rehab. Res. grant number H133C90140-89).

References:

[1] Zajac, F.E. and Gordon, M.E., CRC Crit. Rev. Biomed. Engng., 17:359-411, 1989.
[2] Zajac, F.E. and Winters, J.M., in Multiple Muscle Systems (Winters and Woo, eds), pp. 121-148, Springer-Verlag, New York, 1990.
[3] Hogan, N. and Winters, J.M., in Multiple Muscle Systems (Winters, J.M. and Woo, S.L-Y., eds), pp. 182-194, Springer-Verlag, New York, 1990.
[4] Hogan et al., Exerc. & Sport Sci. Rev., 15: 153-189, 1987.

ANALYSIS OF HUMAN STANDING POSTURE: CONSTRAINTS & OBJECTIVES

A.D. Kuo and F.E. Zajac
Stanford University and Veterans Affairs Rehabilitation R & D Center
Palo Alto, California, USA

INTRODUCTION

We analyzed the biomechanics of standing posture as an optimization problem. The musculoskeletal system imposes constraints on achievable accelerations of the joints. We computed the set of all feasible accelerations, and examined the limits to acceleration of the body center of mass. In addition, we analyzed the effect of constraining the knee to be fixed (an experimentally observed strategy), and found that it limits vertical acceleration of the center of mass without hindering horizontal acceleration.

REVIEW & THEORY

Due to redundancy in the number of actuators and joints, the control of the human musculoskeletal system is a problem of optimization; that is, the choice of objectives to find one solution among potentially many possibilities. Viewing motor control as an optimization problem necessitates that one specifies objectives and constraints. This transforms the problem into one of finding the objectives and constraints. Unfortunately, motor control research has not, in general, provided applicable optimization parameters. We have found, however, that analysis of biomechanical and behavioral constraints can provide greater understanding of the motor control problem. Specifically, we can visualize geometrically the biomechanical constraints on joint torques, and the corresponding "Feasible Acceleration Set" (FAS) for a three-joint (ankle, knee, hip) model of motion in the sagittal plane (1,2).

We hypothesized that a critical objective in human standing is achieving acceleration of the body center of mass. The three-joint FAS, a polyhedron, can be projected into a 2D space representing horizontal and vertical acceleration if the center of mass in the sagittal plane.

We also examined behavioral constraints in the form of a knee constraint. Horak et al. (4) found that subjects tend to respond to postural perturbations with combinations of an "ankle strategy," meaning that the motion takes place about the ankle joint with the knee and hip rotation nearly constrained, and a "hip strategy," in which the motion is primarily about the hip, with the knee constrained. Keeping the knee constrained is equivalent to intersecting the plane representing constrained knee motion with the FAS polyhedron. This intersection can also be projected onto the two-dimensional center of mass acceleration space.

PROCEDURES

We modeled human standing posture as a quasi-static motion of four body segments (foot,shank, thigh, head-arms-trunk) in the sagittal plane. We combined 33 muscles of the lower limb into 14 muscle groups according to anatomical position, modeling the force-length and moment arm characteristics of muscle (3). The equations of motion were written as

$$\ddot{\theta} = I^{-1}(R \cdot F_0^M \cdot F_\ell \cdot a + G) \qquad (1)$$

where I is the inertia tensor, R is the matrix of joint moment arms, G is the gravity vector, and $\ddot{\theta}$ is the joint angular acceleration vector (for ankle, knee, and hip). F_ℓ scales peak isometric force F_0^M according to normalized force-length relationships Normalized neural activation a is constrained between 0 and 1. Equation 1 maps the activation constraints into acceleration constraints, which define the FAS polyhedron. Note that this FAS does not account for neural connectivity constraints, which would further constrain the achievable accelerations.

We then projected the FAS onto the two-dimensional space representing acceleration of the body center of mass horizontally and vertically. We also projected onto this space the subset of the FAS corresponding constrained knee motion.

RESULTS & DISCUSSION

As noted in (2), the FAS polyhedron (Figure 1) associated with near-vertical posture is significantly oriented along a single direction (approximately 15 times longer than it is wide), indicating a "preferred" movement mobility in that direction. Figure 2 (shaded region) shows the projection of the FAS onto the center of mass acceleration plane, with x and y directions corresponding to horizontal and vertical movement, respectively (-x is forward). The narrow black region corresponds to the intersection of the knee constraint with the FAS. Though the major effect is to limit the range of vertical accelerations to approximately 2.4% of the unconstrained case, constraining knee motion does not greatly limit mobility for balancing objectives, since the horizontal acceleration for this range of vertical motion is undiminished.

Therefore, we conclude that limiting motion of the knee is nearly equivalent to constraining the vertical acceleration of the center of mass, and represents a reasonable strategy for maintaining balance. This view of posture as an optimization problems helps us understand the mechancal effects of such strategies.

ACKNOWLEDGEMENTS

This work was supported in part by a NSF Pre-Doctoral Fellowship to A.K., NIH grant NS17662 to F.Z., and the Rehabilitation R & D Service, Dept. of Veternas Affairs.

REFERENCES

1. Gordon, M.E. PhD Thesis, Stanford University, 1990.
2. Kuo, A.D. et al. Proc. XIIIth Int. Congr. on Biomech., 1991, submitted.
3. Hoy, M.G. et al. J Biomechanics 23:157-169, 1990.
4. Horak, F.B. et al. J. Neurophys. 55:1369-1381, 1986.

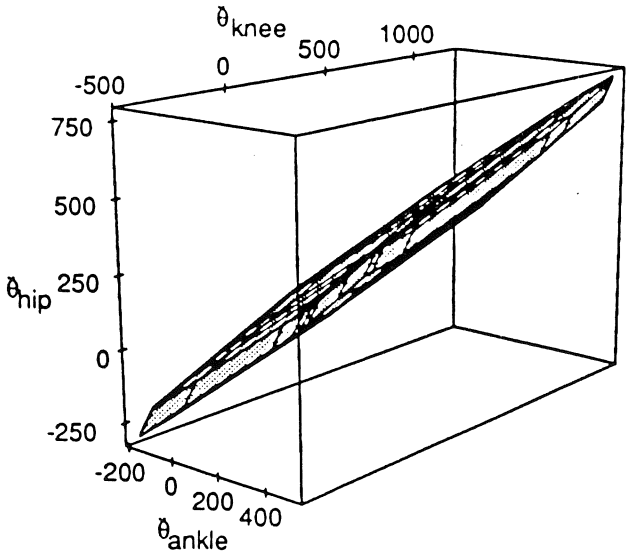


Fig 1. Feasible Acceleration Set for standing posture in sagittal plane. Units are rad/s^2

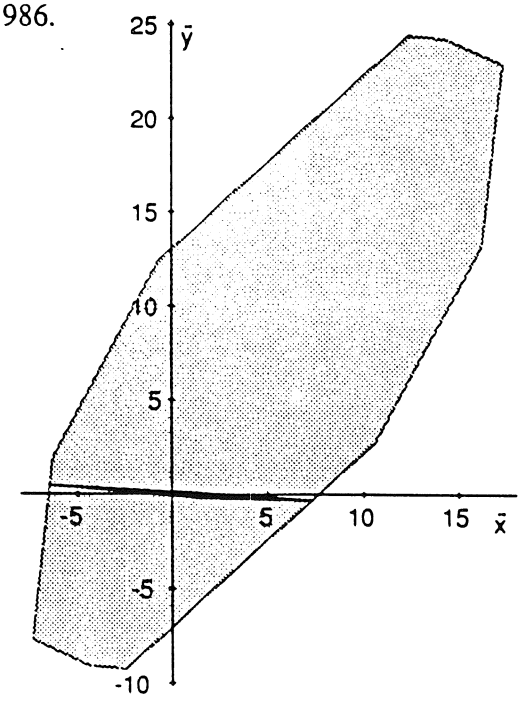


Fig. 2. FAS of body center of mass. Knee constraint shown in black region. Units are m/s.^{2}

PREDICTING TORSO MUSCLE ACTIVITY DURING ASYMMETRIC LOADING: A COMPARISON OF THREE OPTIMIZATION MODELS

Maury A. Nussbaum*, Steven A. Lavender+, Richard E. Hughes*,
Don B. Chaffin*, and Gunnar B.J. Andersson+
*Center for Ergonomics, University of Michigan, Ann Arbor, MI 48109-2117
+Rush Presbyterian-St. Lukes Medical Center, Chicago, IL 60612-3864

INTRODUCTION

The risks associated with asymmetric loading of the torso are becoming increasingly apparent. An understanding of the etiology of injury formation resulting from asymmetric loading is hampered by the complexity of the physiological responses. Optimization techniques are commonly used to overcome the indeterminacy problem and predict muscle forces over a wide range of loading conditions. Few empirical attempts have been made, however, in comparing and contrasting different model formulations. An experiment was performed which systematically applied symmetric and asymmetric loads to the spine. The data facilitated detailed comparisons of three optimization procedures.

REVIEW AND THEORY

The optimization model developed by Schultz *et al.* (1983) generated predictions of torso muscle forces from intervertebral moments. A reformulation (**BCS**) was presented by Bean *et al.* (1988). The model has been widely studied and shown to successfully represent the activity of major individual agonist muscles. The model solves two linear programs to resolve the indeterminacy caused by having more variables than constraints. The first step involves determining a minimum upper bound on muscle intensity (force/area) subject to the conditions of moment equilibrium. The second step chooses a set of muscle forces which minimize the spinal compression force. A variant of the Bean *et al.* model (**1.4BCS**) was achieved by increasing the upper bounds on muscle intensities obtained from the first step. Optimal performance was reached when the upper bounds were multiplied by 1.4. This modification allowed for increased recruitment of muscles which, because of their orientations or moment arms, were well suited to develop a particular moment about the spine.

The approach taken by Crowninshield and Brand (1981) employed a different objective function (**C-B**). They demonstrated that maximal endurance of an activity occurs when the sum of the $\mathbf{n}^{th}$ power of muscle stresses is minimized: **n** is a constant in the force endurance relationship and considered equal to 3.0. The method tends to keep individual muscle stresses low by preferential activation of muscles with large cross-sectional areas and long moment arms.

PROCEDURES

Ten male volunteers (age 20-40) were studied during external loading in the upright static posture. Loads were applied at shoulder level using weights attached to a webbed harness. Moments about the L3/L4 level were determined by measuring the distance from the force application to the midpoint of the L3 and L4 spinous processes. By varying the weights, five levels of moments (10, 20, 30, 40, and 50 Nm) were applied from seven directions. The moment directions included sagitally symmetric loading to the front and rear, and all asymmetric angles to the right side in 30 degree increments. One trial of each of the 35 loading combinations was used in a randomized order of presentation.

EMG activity of 4 pairs of muscles (ES, LD, EO, RA) were monitored using surface electrodes. Electrode placements were: ES at L3/L4 level 3 cm. lateral to midline; LD over muscle belly at T7 level; EO at umbilicus level 2 cm. medially from the ilium at an angle of 45 degrees; RA at umbilicus level 2 cm. lateral to midline. The signals were amplified and rectified

with a bandpass range of 20-600 Hz, from which RMS data were sampled at 10 Hz. The RMS data were averaged over a ten second collection period and normalized relative to maximal values observed during MVC trials and baseline values. Normalized EMG (NEMG) values were averaged over the ten subjects for comparison with model predictions.

RESULTS

The three optimization models (BCS, 1.4BCS, and C-B) were used to generate predictions of muscle forces for the 35 loading conditions. The predicted forces were compared to the averaged NEMG using linear regression. The coefficients of simple determination (R^2) are shown in Figure 1. With the exception of the latissimus dorsi, all three models account for more than 55% of the variance in the major torso muscles. The variant of the BCS model demonstrated improved performance for the rectus abdomini and erector spinae, but was inferior to the standard model for the external obliques and latissimus. The Crowninshield and Brand model achieved the best correlations for all muscles excepting the right ES and left LD, with 5 of 8 correlations on the order of 0.9.

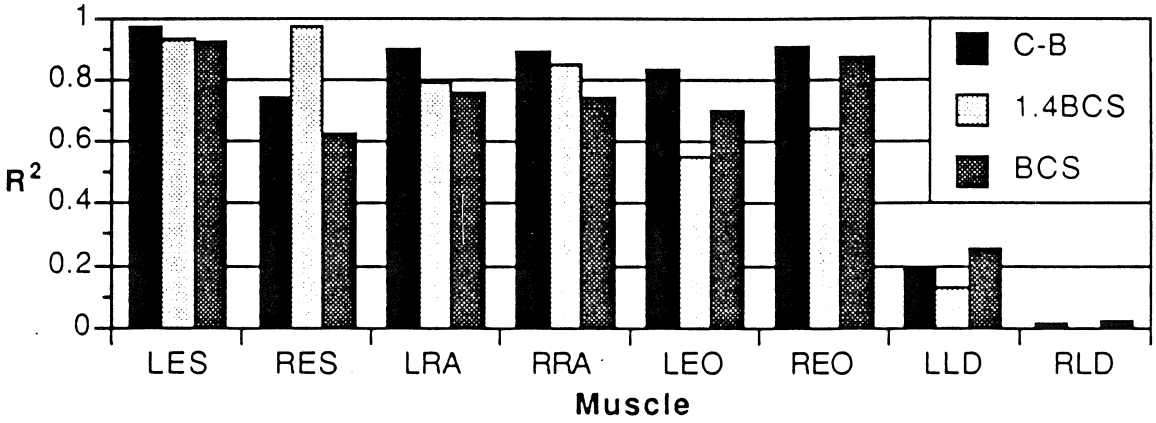


Figure 1. R^2 Values for Predicted Muscle Force vs. NEMG

DISCUSSION

The results suggest that the non-linear Crowninshield and Brand optimization criterion is superior for lumbar muscle force prediction. This conclusion, however, can only be made for loading in the horizontal plane. Comparisons have yet to be made for torsional loads and for loads that are fully three-dimensional. All three models failed to predict latissimus dorsi activity. It is suggested that this failure is due in part to the low activity of the latissimus observed in the data (ie., <10%MVC). In addition, the activity of the latissimus showed no obvious relationship to either the magnitude or the orientation of the load.

None of the models specifically accounted for individual subject anthropometry. Instead, the EMG data were averaged over all subjects, thereby eliminating a significant degree of existing variability. In this study a single set of muscle moment arms and orientations, from an idealized 50-%tile male, were utilized. Future models, in order to be applicable to individual subjects, will to incorporate inter-subject geometric differences to improve predictions of muscle recruitment.

REFERENCES

Bean, et al. (1988) *J. Biomechanics* **21**:59-66.
Crowninshield, et al. (1981) *J. Biomechanics* **14**:793-801.
Schultz, et al. (1983) *J. Orthop. Res.* **1**:77-91.

Acknowledgements: This work was supported by NIH Grant-1R01-AR39599

CYCLING

MEASUREMENT OF THE DYNAMIC FORCES DURING MANUAL WHEELCHAIR PROPULSION

Mark G. Strauss Ph.D., Jerry Maloney, Frank Ngo, Matthew Phillips
Division of Rehabilitation, University of Illinois at Urbana-Champaign
1207 S. Oak Street, Champaign, Illinois 61820, USA

INTRODUCTION

Nichols et al. sent a survey to 708 people who use manual wheelchairs. The responses showed that approximately half of all the respondents (n=563) indicated that they currently have or had pain in their shoulder(s). One third indicated that the pain was prominent enough to cause loss of sleep. It is reasonable to assume that this pain reduced their mobility and independence. The ramifications of this are lost wages, job insecurity, missed classes, increased dependence and overall increased discomfort. The cause of this pain is unknown.

In the not too distant past, wheelchairs were made basically as one size fits all (no adjustments) even though the anatomy of the wheelchair user varied. What we understand better now is that the proper wheelchair-to-user fit provides important advantages such as comfort, reduced high pressure areas and increased attention to tasks. With this realization, and increased competition, wheelchair vendors have allowed for the alteration of certain chair characteristics by the user or therapist, ie., rear axle position with respect to the seat and wheel camber.

REVIEW

In retrospect the variables in the wheelchair-user-interface were within the user, as the chair characteristics were fixed. Now, there exists variables within the user and the chair. The question is how can the chair characteristics be optimized to each user in order to provide increased performance and elimination of pain? This is an increasingly important issue as the wheelchair using population is increasing. What is needed is a tool and a method to examine the interaction between this man and machine system. In the past, others have explored the power output, or the effect of variables on torque production but a three dimensional kinetic examination of the manual propulsion system and how the configuration of the system effects the stresses in the joints has not been performed. The long term goals of this research are examining how various propulsion techniques and alterations in wheelchair geometry effect the efficiency of manual propulsion and the reaction forces in the joints of the upper limb. This paper discusses the immediate objective of developing the system necessary to obtain this information. The history and the problems of the development will be discussed.

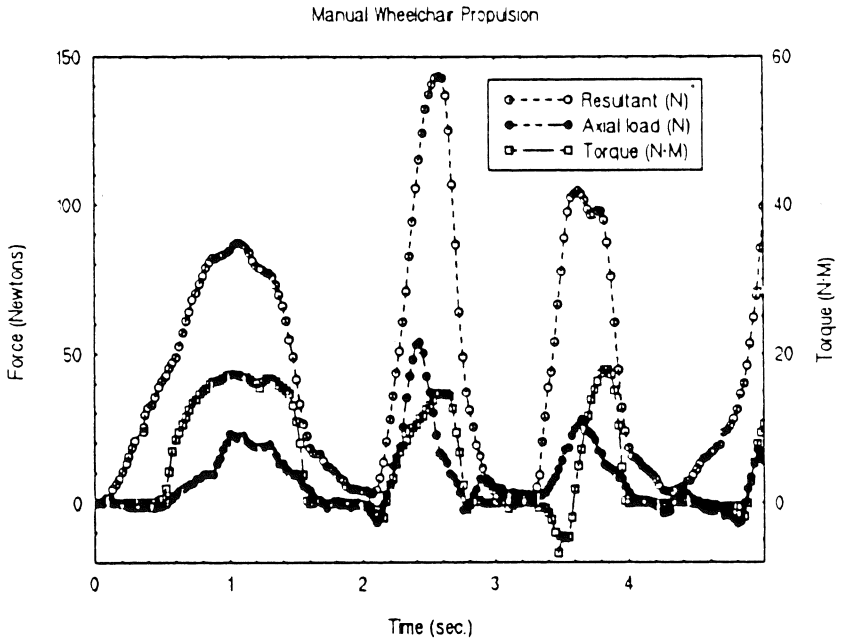
DISCUSSION

Although it is still difficult to determine the joint loads due to intrinsic muscle forces, the joint loads due to extrinsic dynamic reactions can be examined if the external loads can be measured. These external loads are the forces of the handrim of the wheelchair wheel on the palm of the user. In 1988, the development of an instrumented handrim for examining these forces was initiated. The mode of force determination was via a strain gaged based, 'in-house' developed transducer. Since the most desirable goal would be to create a measuring system which would not alter the propulsion patterns of the subjects, frequency modulated, radio linked data telemetry was planned to eliminate the need for a tether cable. The calibration of this first prototype demonstrated that the transducer was not sufficiently linear and could not be corrected. Although the bridge circuits were AC excited and the transmission was rectified at the receiver output, the capacitive coupling and drift inherent in the system crippled this data transmission scheme. The only channel with adequate sensitivity and linearity measured torque and some initial results were reported (Strauss and Moeinzadeh, 1989).

The second prototype was designed around an AMTI six degree of freedom strain gage based force transducer, which was more costly than the original transducer but possessed the required linearity and sensitivity. Analog Devices 1B31AN strain gage signal conditioning modules are used to excite the bridges, and act as a first stage instrumentation amplifier and low pass filter. At the output of the second stage amplifier (AD8471JN), the original microvolt strain gage signal appears as +/- 10 volts, more than adequate to pass through a slip ring untainted by noise. Experience with the first prototype demonstrated the difficulties of transmitting analog signals, especially from an antenna mounted on the rotating wheel. The current system has two means of communicating the data to the PC based data acquisition system. For calibrating at high data acquisition rates, a wired link is used. For clinical testing, a microprocessor based digital transmission system has been built. An Intel 80C196KB receives the six channels of amplified force and encoder data and the integrated multiplexer and analog to digital converter digitizes the information. The now digitized signal is sent serially to a single miniature FM transmitter and a wheelchair frame-mounted antenna. The received signal is preprocessed by a another Intel 80C196KB before it is sent directly to the PC serial port, eliminating the need for any other A/D conversion. The microprocessor algorithm to ensure received data integrity is being updated currently to include parity checks and intentional data transmission redundancy.

RESULTS

Preliminary propulsion profiles of an individual who propelled a manual wheelchair bent over at 45 degrees is shown below. The figure shows the torque, the resultant forces in the plane of the wheel and the axial loads on the wheel during three propulsion cycles. An optical encoder keeps track of the position of the wheel as the chair is propelled around the room but is not shown in the figure. With the data from the encoder, the position of hand contact on the rim can be shown dynamically.



REFERENCES

Nichols, P.J.R., Norman, P.A. and Ennis, J.R. (1979) Wheelchair user's shoulder, Scan. J. of Rehab. Med.; 11:29-32.

Strauss, M.G., Moeinzadeh, M.M., Schneller, M., Trimble, J. (1989) The development of an instrumented wheel to determine the handrim forces during wheelchair propulsion. 1989 ASME Winter Annual Meeting, San Francisco, CA., Dec. 10 - 15, 53-54.

A COMPARISON OF TORQUE PRODUCTION OF CLIP-IN PEDALS AND CONVENTIONAL TOE CLIPS AND CLEATS

Marcia E. Cooper, Rory A. Cooper*, Irvin E. Faria, Annette Vosse*, and James F. Ster III*
Human Performance Laboratory and Human Engineering Laboratory*
Departments of Health and Physical Education and Biomedical Engineering*
California State University, Sacramento, CA 95819-6019, USA

INTRODUCTION

Advances in pedal connection technology, such as clip-in pedal systems, have yet to be examined for their effect on biomechanical efficiency. The purpose of this investigation was to compare torque, as function of crank angle, produced at 9 m/s for two workloads (37 Watts, and 14 Watts) during submaximal cycling tests using clip-in pedals and conventional toe clips and cleats. Seven competitive cyclists participated in submaximal cycling tests conducted using the Look Pedal System and a Conventional Toe-Clip Pedal System. During the tests crank arm torque, angle and speed were measured. The potentiameter, tachometer and strain gage (torque) signals were interfaced to 12 bit A/D Board (National Instruments) installed in an AT&T 6386 computer. All signals were sampled at 100 Hz, and data were collected during the fifth minute of each six minute constant speed and workload exercise test. There were no differences in the graphical representations of the torque curves for the two types of pedals. There were differences in the torques produced with workload with higher workloads eliciting higher torques for both pedals. Our results suggest there are no differences in torque production as a function of crank angle for the two pedal types.

REVIEW AND THEORY

Instrumentation designed for kinetic investigations include strain gages, pedal dynamometers, force transducers, and computer simulation. Most of these methods record the deformation which occurs during the pedal cycle. McCartney et al. (1983) determined force applied by bonding strain gages to several surfaces of the crank arms. Strain gages have also been applied directly to the pedals to determine the amount of pedal force. Lollgen et al. (1980) studied the tangential forces produced throughout the pedal cycle. A strain gage based pedal dynamometer described by Hull and Davis (1981) has been used to measure all six degrees of freedom. Sanderson and Cavanagh (1987) described a force transducer designed as a shoe insole which measured pressure exerted on the sole by the bottom of the foot. Benecke et al. (1983) measured torque applied to the pedals along with spasticity in the lower limbs during cycling for patients with spastic motor disorders. Bolourchi and Hull (1985) further investigated measurements of rider induced loads on the seat, handlebars, and pedals. Force production studies indicated that for the three pedal connections, riding without toe clips, riding with toe clips without cleats and riding with toe clips and cleats, riding with toe clips and cleats allowed cyclists to produce force throughout the entire pedal cycle and produced higher efficiencies.

PROCEDURES

Subjects. Seven male competitive cyclists, age 17 to 30 years, participated in this study. All subjects were training a minimum of 100 miles per week at the time of testing and were free of any current musculoskeletal injuries. Fitness was ensured by making peak oxygen consumption and anthropometric measurements prior to testing.

Testing. Each subject rode a 57 cm Schwinn Peleton bicycle, with Look racing pedals for two tests and with KKT pedals with metal toe clips for two tests, on a modified Blackburn Mag Trainer. Each cyclist fit the height of the saddle to their own preference. A wire wound potentiameter was

attached to the crank via a gear train to measure crank angle. Both crank arm torques were measured by dc strain gage bridges with temperature compensation and signal conditioning. Measurements Group (P-3500) strain indicators received the torque signals which were sampled, along with the crank angle signal, at 100 Hz by an analog to digital converter inserted into an AT&T 6386 computer. The data acquisition and storage program was written with LabWindows Software (National Instruments Company). Torque, angle, and speed were measured during the fifth minute of each six minute test.

Each subject completed four submaximal test sessions. Two tests at different workloads (14 Watts, and 37 Watts) for a pedal type were conducted on the same day, with the other pedal type being tested a week later. Pedal rate was held constant at 90 rpm with a metronome and speed was held a constant 8 m/s using a Maxon dc tachometer. Each subject wore his own cleated shoes.

Statistics. Peak torque, angle at peak torque and mean revolution torque were compared for each pedal and workload, respectively. A 2 factor design was used with one between tests factor (Look vs. conventional pedals) and one within tests factor (workload). Consequently, a 2x2 ANOVA statistical design was used for analysis with Tukey's post hoc tests used for follow up testing when appropriate.

RESULTS

The mean positive peak torques were 93.08 N-m at 91^{o} for Look at 37W, 45.05 N-m at 91^{o} for Look at 14W, 89.70 N-m at 97^{o} for conventional at 37W, and 42.57 N-m at 91^{o} for conventional at 14W. The mean negative peak torques were -18.64 N-m at 268^{o} for Look at 37W, -26.77 N-m at 263^{o} for Look at 14W, -19.22 N-m at 274^{o} for conventional at 37W, and -26.62 N-m at 257^{o} for conventional at 14W. The analysis revealed no significant differences ($p>.05$) between the peak torque, angle at peak torque or mean revolution torque for the two types of pedals. The angle at peak torque was not significantly different ($p>.05$) between pedals or workload. However, the peak torque and mean revolution torque were significantly different ($p<.05$) between workloads for both pedals.

DISCUSSION

Results indicate that there may be no difference between the mechanical efficiency of the two pedal systems tested. The torque curves appear virtually identical for the two types of pedals, and statistical analysis did not identify any differences. The torque curves did change with workload as was to be expected. The selection of pedal type appears to be an issue of personal preference and convenience. Differences may become apparent if lateral forces were measured, and/or if clip-in pedals which allow rotation of the foot during the pedal cycles were tested.

McCartney et al. (1983), A constant-velocity cycle ergometer for the study of dynamic muscle function, J. App. Phys., 55, pp.212-217.

Lollgen et al. (1980), Muscle metabolites, force, and perceived exertion bicycling at varying pedal rates, Med. Sci. Sports Ex, 12, pp.345-351.

Hull and Davis. (1981), Measurement of pedal loading in bicycling: I Instrumentation. J Biomech., 12, pp.843-856.

Sanderson and Cavanagh. (1987), An investigation of in shoe pressure distribution during cycling in conventional cycling shoes or running shoes. In B. Johsson (Ed.), Biomechanics X-B, pp. 907-930, Human Kinetics.

Benecke et al. (1983), Electromyographic analysis of bicycling on an ergometer for evaluation of spasticity of lower limbs in man, Adv. in Neurology, 39, pp.1035-1046.

Bolourchi and Hull. (1985), Measurement of rider induced loads during simulated bicycling, Int. J. Sport Biomech., 1, pp.308-329.

A 3-D MODEL OF THE LOWER LIMB IN A CYCLING MOVEMENT

Tony Marsh and G.T. Yamaguchi
Departments of Exercise Science and Physical Education and Chemical, Bio and Materials Engineering, Arizona State University, Tempe, AZ, 85287.

INTRODUCTION

Biomechanists have usually examined cycling performance based on a human factors perspective. However, many of these investigations have been based on the constraints imposed by the structure of a conventional bicycle and/or have modelled the motion as 2-D (e.g., 1,2,3,5,6,7,8). However, we have found that the pelvis rocks on the seat through an angle of 16-20° consistent with the results of Nordeen et al. (5). The model presented in this report represents a basic step in the development of a 3-D model, that was not constrained in the conventional manner, to examine the effects of removing kinematic constraints.

METHODS

The pelvis and lower limb were modelled as an unconstrained, four segment, 5 DOF system (Figure 1). External forces were obtained from the data collected and published by Krauz et al. (4). Since these values were normal and tangential to the pedal surface, another reference frame oriented at 40° from the foot was included so that these forces did not have to be changed to a global reference frame. The joint moment inputs used were based initially on the results of Hull et al. (3). The success of the model was evaluated by comparison with the joint angular position data of Nordeen et al. (5). Although the simulation occurred relative to time results are presented in terms of theoretical crank position for ease of interpretation.

RESULTS AND DISCUSSION

The use of the experimentally derived joint moments for the hip, knee and ankle (3) produced unsatisfactory results. In general the pelvis was forced into a CW spin by the effect of the pedal forces acting with a moment arm of half the pelvic width. Following this initial trial the moments at each joint were manipulated in turn starting with the pelvis. The results of initial simulations showed that the joint moments had to be changed at least 30° prior to the time when an angular position change was desired.

Initially a positive moment forced the pelvis to rotate CCW. The pelvis was approximately level at 90° and continued to rotate CCW to approximately 10°. The joint moments were decreased as BDC approached so that the pelvis rotated CW back to the starting position at TDC. The hip abduction/adduction moment was set to zero and the angle (q2) with respect to the vertical did not deviate more than 2-3° for the entire simulation. The lower limb therefore remained in the sagittal plane despite the movement of the pelvis.

The model was able to reproduce the hip flexion/extension movement of cycling with

reasonable results. The movement was accomplished by input of positive moments to move the thigh down. Negative moments were used to brake the movement as the angle approached 60°. These negative moments also started the segment moving up to the start position where the application of positive moments arrested the upward movement of the thigh at a joint angle of approximately 10°. Since the motion was unconstrained (due to the lack of a crank) the knee was forced into full extension during the power phase as the thigh accelerated. However, the changes in the joint moments necessary to extend the knee to 40° at BDC and then return to 110° at TDC produced large changes in the angle at the hip. Those moments needed to arrest the extension motion of the knee dominated the movement at the hip and the pelvis, although there was little change in the hip frontal plane angle (q2). Attempts to then correct the angle at the hip produced undesirable effects at the knee. Similarly, manipulation of the ankle angle produced undesirable motion at the hip and knee. Clearly the absence of kinematic constraints and the dynamic linking of the segments, even though a joint apart, were the overriding influences in these results.

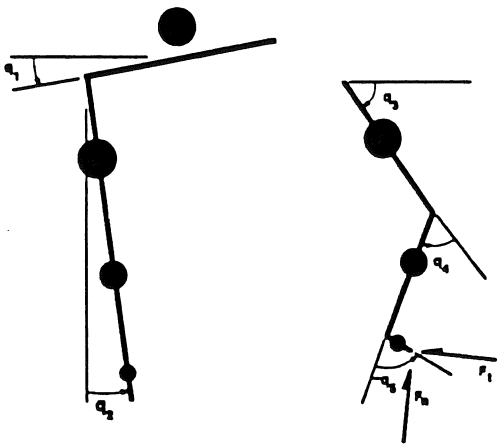
Although difficult to interpret, the trend was for the total system energy to increase slightly, decrease to BDC and then increase. One possible explanation for this was that initially the relatively heavy thigh segment contributed to the kinetic energy of the system as its velocity increased, after which the segments slowed and dropped in height as BDC approached therefore decreasing the total energy of the system. After BDC the segments gained potential energy and kinetic energy as they moved up to TDC. The thigh appeared to have a significant influence on the total energy of the system as it accelerated to TDC.

CONCLUSIONS

The model results showed that the more distal segments were far more difficult to control than the proximal segments. Certainly the moments at the distal joints had a profound effect on the more proximal segment. Dynamic linking of the segments would appear to be the major contributor to these interactions. It was clear that the joint moments of the model bore little resemblance to experimentally derived joint moments. This suggested the importance of formulating dynamic models that are neither overconstrained (as in planar models) nor underconstrained (as in this model). Future attempts will continue to pursue a 3-D model using a constrained end-point.

REFERENCES

1. Hull, M.L. et al. J. Biom., 21, 10: 839-849, 1988.
2. Hull, M.L. et al. Int. J. Sports Biom., 4: 1-20, 1988.
3. Hull, M.L. et al. J. Biom., 18, 9: 631-644, 1985.
4. Krauz, S.A. et al. Int. J. Sports Biom., 7: 29-53, 1990.
5. Nordeen, K.S et al. Biomechanics V-B, 26-33, 1976.
6. Redfield, R. et al. J. Biom., 19, 4: 317-329, 1986a.
7. Redfield, R. et al. J Biom., 19, 7: 523-539, 1986b.
8. Yoshihuku, Y. et al. J. Biom., 23, 10: 1069-1079, 1990.



A NOVEL PROPULSION DEVICE FOR A HUMAN-POWERED WATER VEHICLE

Andrew D. Aswad, M. S.
Baxter Healthcare Corporation
Renal Division
Rt. 120 & Wilson Road
Round Lake, IL 60073

Manssour H. Moeinzadeh, Ph.D.
University of Illinois at Urbana-Champaign
117 Transportation Building
104 S. Mathews Avenue
Urbana, IL 61801

INTRODUCTION

The concept of deriving propulsive thrust from a traveling sinusoidal wave in an aqueous medium is based on reports of high hydromechanical efficiency achieved using undulatory propulsion systems [1]. The ultimate goal of the design and development of such a propulsion system is to achieve a mechanical means of propulsion that surpasses contemporary conventional systems and rivals that provided by nature, as exemplified by the dolphin. The immediate motivation for pursuing the development of such a system lies in its integration into an efficient human-powered water vehicle, an example of which is provided by the *Flying Fish II* [2]. An in-depth feasibility study is conducted, including an extensive literature review of aquatic propulsion in nature, and prototype construction and evaluation.

THEORY

The main component of the propulsion device, figure 1, is a thin flexible band, 1, of a material of such modulus of elasticity as to provide a resistance to the surrounding fluid medium without itself yielding to local buckling. The band is laterally compressed beyond the first (global) buckling load and constrained by longitudinal walls or bars, 2. As a result of this arrangement, the band acquires an equilibrium configuration, I, consisting of segments of Euler elastica as determined by the compression level and distance between the walls. Two shafts, 3, attached to the ends of the band translate and rotate along assigned paths, 4. As the shafts undergo a cyclic motion, the band sequentially acquires configurations II-III-IV-I, generating a sinuous transverse wave that propagates along the band.

METHODOLOGY

Several iterations of design and prototype evaluation lead to the mechanism configuration depicted in figure 2. Viewed from the side, the propulsion mechanism consists of a sprocket, a series of bars, linear bearings, links, and a flexible band. Rotation of the sprocket drives the bars, creating a nearly parallel rocking motion of the pivot arms about two fixed points with an imposed phase lag between the two. This rocking motion is translated through the struts to the links and the flexible band, resulting in the generation of a simple harmonic waveform along its length. The configuration of the mechanism allows for the production of the two concurrent and dependent motions necessary for generation of the desired waveform: the vertical displacement of either endpoint of the band and the angular rotational displacement at either end of the band. The combined motions act to "scoop up" the water and force it backwards, creating a reactive thrust.

RESULTS AND DISCUSSION

The propulsion mechanism is evaluated as incorporated into the vehicle shown in figure 3. An evaluation of the mechanism consists of both qualitative and quantitative assessments of the operating parameters and efficiency of the propulsion system. Measurements of velocity and drag are recorded, and propulsive efficiency are determined from the ratio of output

power to input power. Maximum theoretical design efficiency is calculated, and its ratio to a calculated trial efficiency is used to determine an efficiency loss ratio. In general, it is concluded that the feasibility of such a novel propulsion system has been proven, however further development is required before the system can be considered optimized.

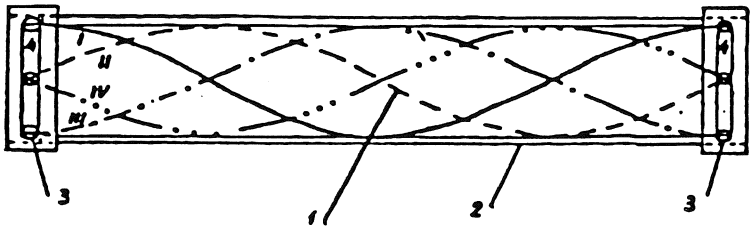


Figure 1: Concept for Propulsion Device

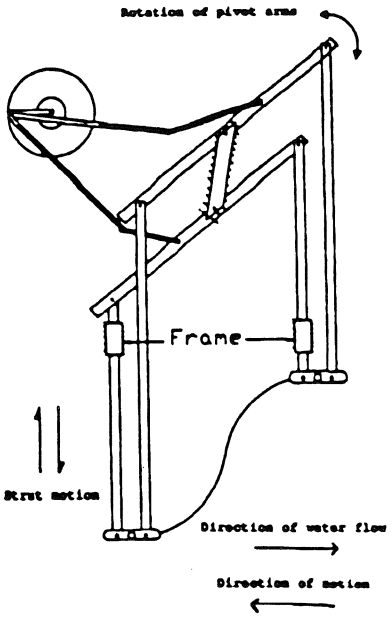


Figure 2: Model of Propulsion Device.

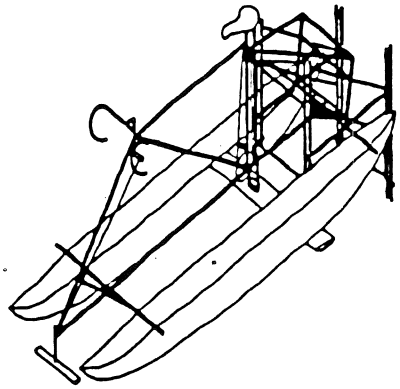


Figure 3: Human-Powered Water Vehicle.

REFERENCES

[1] Katz, J., and Weihs, D., *Journal of Fluid Mechanics*, pp. 485-497, Volume 88, Part 3, 13 October 1978.

[2] Brooks, Alec N., Abbott, Allan V., and Wilson, David Gordon, *Scientific American*, December 1986, pp. 120-130.

ACKNOWLEDGEMENTS

The design and development work for this novel propulsion system was generously funded by an interdisciplinary research grant from the Bioengineering Program at the University of Illinois, Urbana-Champaign.

INFLUENCE OF ORTHOTICS ON LOWER EXTREMITY FUNCTION IN CYCLING

Timothy G. Joganich and Philip E. Martin
Exercise and Sport Research Institute
Arizona State University, Tempe, AZ 85287-0404

INTRODUCTION

Selected lower extremity kinematic and kinetic variables relating to knee pain were compared between cyclists with knee pain (P) and with cyclists who were pain-free (PF). In addition, the effects of orthotics on these variables were quantified for the P cyclists. Dependent variables were associated with pronatory movement and included maximum values for rearfoot pronation (MRP), rearfoot pronation relative to an anatomical neutral position (MRPN), medial knee position from the pedal center (MKP), internal tibial rotation (TROT) and internal pedal torque (TOR). Results failed to demonstrate expected differences in rearfoot motion and related kinetics between P and PF cyclists. Orthotic treatment had a modest effect on rearfoot pronation and internal tibial rotation in the direction opposite than expected. Despite these limited and unexpected results, five of nine P subjects reported that knee pain was abated following two weeks of cycling with the orthotics.

REVIEW AND THEORY

Overuse knee injuries are a common occurrence in cycling with chondromalacia of the patella and patellar tendinitis being the most common diagnosed sources of knee pain (Dickson, 1985). Excessive pronation and internal tibial rotation was suggested by Francis (1988) as a mechanism leading to knee injury. While the relationship between excessive pronation and knee injuries has been considered extensively for running, the potential relationship between lower extremity kinematics and knee pain in cycling has received little attention. Orthotic inserts in running shoes have been shown to be effective in reducing excessive pronation (Bates et al., 1979) and consequently reducing knee injuries (Blake & Denton, 1985). Several researchers (Francis, 1988; Hannaford, 1985; Moran, 1988) have asserted that orthotics would also be beneficial for cyclists. There is little empirical data, however, to support this speculation. Thus, the purposes of this study were: 1) to compare selected lower extremity kinematic and kinetic variables between the PF and P cyclists, and 2) to quantify the effects of orthotics on these variables for the P cyclists. A secondary purpose was to clinically assess the effects of the orthotics.

PROCEDURES

Two groups of experienced cyclists were subjects: one comprised of cyclists who had not suffered from knee pain in the last year (n=14, $\bar{X}$age= 27.0 yr) and a second comprised of cyclists who suffered from knee pain at the time of the study (n=9, $\bar{X}$age= 27.4 yr). PF subjects completed a single test session whereas the P subjects completed two sessions, one before and one after orthotic treatment. Comparisons of the variables between the P and PF groups were based on tests using control shoes to minimize confounding due to footwear. The P subjects were prescribed orthotics after the first test session. After an orthotic adaptation period of two weeks, the P group completed a second test session with and without the orthotics. All subjects rode a lab bike installed on a wind trainer. They pedaled at 90 rpm in a 52 x 19 gear (32.2 $km \cdot hr^{-1}$) that simulated an approximate metabolic cost of 2.8 $l \cdot min^{-1}$ (Coast et al., 1988) and a 200 watt workload. An instrumented pedal was designed and built to measure torsional load about the normal axis. Crank position data were obtained with an optical encoder and kinematic data were recorded with a 3D Watsmart system. The rearfoot and tibial rotation measures were computed using a 3D joint coordinate system as outlined by Arebald et al. (1990). Kinematic data were filtered at 5 Hz while kinetic data were filtered at 10 Hz. A multivariate MANOVA was used to perform statistical comparisons ($p < .05$).

RESULTS

Results are summarized in Table 1. There were no significant differences for P vs PF comparisons. For the orthotic analysis, only TROT reflected a significant difference but in a direction opposite to that expected.

Table 1. Summary of P vs. PF cyclists and with vs. without orthotic comparisons.

Variable	Pain	Pain-free	With orthotics	Without orthotics
MRP (deg)	6.0 ± 5.5	9.6 ± 8.7	10.6 ± 4.4	8.7 ± 4.4
MRPN (deg)	1.8 ± 1.8	4.3 ± 9.0	6.4 ± 6.0	4.6 ± 5.7
MKP (cm)	1.4 ± 1.7	1.8 ± 0.9	1.5 ± 1.5	1.7 ± 1.2
TROT (deg)	7.7 ± 5.0	4.9 ± 3.8	6.8 ± 3.5	4.9 ± 3.8*
TOR (N·m)	1.6 ± 1.8	1.6 ± 1.3	1.3 ± 1.9	1.5 ± 1.7

* Statistically significant difference ($p < .05$)

DISCUSSION

It was hypothesized that the P group would exhibit significantly larger values for the dependent variables than the PF group. Results failed to support this which is in contrast with observations by several researchers. Francis (1988) stated that cyclists suffering from knee pain tended to show a greater internal tibial twist during the downstroke. Hannaford et al. (1986) and Moran (1988) have shown a more linear path of the knee in the frontal plane for cyclists who are pain-free than those experiencing knee pain. The absence of differences between P and PF cyclists in this study suggests that the descriptors may not have adequately reflected internal knee stresses responsible for knee pain. It was also hypothesized that orthotics would significantly decrease the dependent variables for the P group. Results did not support this hypothesis which was based on observations by several researchers (Francis, 1988; Hannaford et al., 1986; Moran, 1988). Orthotic treatment had a modest effect on rearfoot pronation and internal tibial rotation, but in a direction opposite to that expected. MKP results are in agreement with Sanderson (personal communication, March 20, 1991) who failed to find any differences in medial-lateral knee deviations with severe 10 degree canting of the foot in varus and valgus. Several reasons may explain the results of this study. The tight orthotic fit in the subject's own shoes may not have allowed the orthotic to do the job for which it was designed. Additionally, it was assumed that all the subjects would require a varus correction. The subjects corrections were characterized as: 5-modest varus, 2-none, and 2-modest valgus. Despite the results, five of nine subjects indicated a reduction in knee pain with use of the orthotics. In conclusion, P and PF cyclists did not exhibit any lower extremity kinematic and kinetic differences and despite the numerous speculations that the orthotics would result in a significant reduction in the variables, the results did not support this.

REFERENCES

Arebald et al. (1990). Three-dimensional measurement of rearfoot motion during running. J Biomech, 23(9), 933-940.

Bates et al. (1979). Foot orthotic devices to modify selected aspects of lower extremity mechanics. Am J of SportsMed, 7(6), 338-42.

Blake et al. (1985). Functional foot orthoses for athletic injuries. J Am Podiatry Ass,75(7), 359-62.

Coast et al. (1988). Metabolic requirements of riding windload simulators as compared to cycling on the road. Burke & Newsom (Eds.), Medical and Scientific Aspects of Cycling (pp. 109-116). Champaign Il: Human Kinetics.

Dickson, T.B. (1985). Preventing overuse cycling injuries. Phys Sportsmed, 13,(10), 116-123.

Francis, P. R. (1988). Pathomechanics of the lower extremity in cycling. In E. R. Burke & M. M. Newsom (Eds.), Medical and Scientific Aspects of Cycling (pp. 3-16). Champaign Il: Human Kinetics.

Hannaford et al. (1986). Video analysis and treatment of overuse knee injury in cycling: a limited clinical study. Clinics in Podiatric Medicine and Surgery, 3(4), 671-678.

Moran, G.T. (1988). Biomechanics of cycling-the role of the foot pedal interface. In Kreighbaum, E. & McNeill, A. (Eds.), Proceedings of the 6th ISBS Symposium, (pp. 43-49).

Funded by Nike, Inc.

JUMPING AND LANDING

A NEW MODEL FOR THE COMPUTER SIMULATION OF POLE VAULTING

Wang Qin and Wei Wen-Yi Biomechanics Laboratory,Shanghai Institute of Physical Education,Shanghai 200433,P.R.China

Introduction: In recent Years,Several mehods of computer simultion of pole vaulting have been presented.However,due to the complexity of the movement,it is very difficult to establish a model that can describe both the vaulter and the pole completely and accurately.The model developed by Walker et al.(1973) is too simple.In Hubbard's(1980) method,there is the evident difference between the model of vaulter and real vaulter. In addition to that, the control variables employed are the joint torques which can not be measured very easily so that very much estimation has to be done to determine the proper control variables before simulation. The simulation method of Dapena et al,(1985) uses too much computer time and the model can not determine the joint torques of the vaulter. In this paper,We apply the dynamics of multi-body systems with closed chains to the simulation of pole vaulting and develop a method which is more complete and accurate, less computer-time consuming.It is more suitable to investigate the casual relations of the motions and it can determine the muscular torques.

Models and Theories: The physical model of the systerm is established as following: the vaulter and the pole segment between upper and lower hand grips are treated as a multi-body system of ten rigid segments with a closed chain; the pole segment under the lower hand grip is modeled as an inextensive elasca which has variable flexual stiffness along the lenth of pole, no mass, and very small initial bending. These two submodels are coupled by a pin hinge with a nonlinear torsinal spring.The motion of the model is restricted in a plane vertical to the crossbar. The mathematical model is also composed of two parts. One describes the relation between the configuration of the elastica and the external force exerted on it.For this part, the Broyden's(1969) iteration method and fourth-order Runge- Kutta integration are used to find the solution of differential equations of the deflection curve which satisfies the given boundary condi-tion.The calculation showed convergence was rapid. The other,when the motions of contiguous segments in system relative to one another are prescribed, describes the motion of multi-body system relative to an inertial reference base fixed on the ground. The system is under the action of reaction force of the elastica. For this part, first of all,the closed chain must be cut to transform the multibody system with a closed chain into a tree-structrue system,for a tree-structure system without coupling to an external body whose motion is prescribed, Wittenburg(1977) provided the equations.Based on the equations,the kinematic constraints of the cut hinge

are re-introduced and D'Alembert's Principleis is formulated for the complete system with a closed chain. Lagrange equation of motion of the first kind can be established by applying Lagrange's method of mutiplietrs.To integrate the equation numerically, the unknown Lagrangian multipliers must be eliminated.Finally,in order to arrive at equations which can be solved by a half-inverse dynamics approach,controll variables(i.e the reltive motions of the body segments)and controlled variablees are separated. For these equations,numerical integration used is still a fourth-order Runge-Kutta Procedure.

Coputer Programs: All of the computational processes have been programmed by IBM-PC FORTRAN LANGUAGE. The program can caculate the state of motion of every joint point. segment, and the center of grvity of the vaulter.Besides,it also can caculate the the muscular torques in the joints of vaulter,and the forces exerted by the upper and lower hands at each time step size.

Results: To evaluate the feasiablity of the simultation method, the films recording a real pole vaulting process were analysed. The initial conditions at take-off(posture of the vaulter,the velocity of lower hand grip), the orientation and angular velocity of the pole between the upper and lower hard grip,the time histories of the relative motions of segments, the parameters of the vaulter(lengths,masses,inertial moments),and the flexual stiffness of the pole have been put into the program. The result of caculation shows the error between the simulation and the real process of pole vaulting are acceptable : the absolute value of the errors of horizontal and vertical coordinates of lower hand grip are not larger than 0.41 rad (All the errors of the orienta-tion have the same sign of minus). The simulation of the performance is from leaving ground of the take-off foot to releasing pole of the lower hand. The amount of the simulaton time is about 2 hours.

Conclusion: Using this method, we can keep the initial conditions and change controlling variables of flexual stiffness of the pole to investigate their influence upon the overall motion and further more to look for the more suitable or optimal technique of performance.

References

Broyden,C.G.(1969)The Computer Journal,Vol.12,No.1,94-99
Walker,H.S.et al.(1973)ASME Symposium on mechanics and sport,AMD-Vol.4,131-141
Wittenburg,J,(1977)Dynamics of Systems of Rigid Bodies. Teubner Stuttgart.
Hubbard.M et al.(1980)Journal of Biomechanics,Vol.13,965-976
Dapena,J et al.(1985)Biomechanics IX-B,Human Kinetics Publishers,458-463

INDIVIDUAL JOINT CONTRIBUTIONS TO SHOCK ABSORPTION DURING VERTICAL DROP LANDINGS

Philip K. Schot[1], Janet S. Dufek[2], and Barry T. Bates[2]

Department of Human Kinetics[1]
University of Wisconsin-Milwaukee
Milwaukee, WI 53201

Biomechanics/Sports Medicine Lab[2]
University of Oregon
Eugene, OR 97403

INTRODUCTION AND REVIEW

Ground reaction forces (GRFs) are the net reaction to the actions of individual body segment motion. The GRFs experienced by performers during various types of landings have been documented by several researchers (1,2,3,4). However, it is impossible to gain information regarding the functional demands placed upon individual joints from the GRF record. Recent research (6) has indicated that the maximum forces experienced at articulating surfaces do not coincide temporally with GRF peaks. The function of the lower extremity during landings is to control the downward momentum of the body. This is generally accomplished by performing negative work through lower extremity joint flexions via eccentric muscle activity. Joint kinetic records have recently been examined for landing activities (1) and have focused on maximum joint moment values. Shock absorption characteristics of the lower extremity joints have not been as detailed in the literature. The purpose of this study was to document the individual shock absorption contribution of the lower extremity joints during vertical drop landings.

PROCEDURES

Nine volunteer subjects (4 male, 5 female) performed 75 vertical drop landings (0.6 m) onto a dual force platform system (1000 Hz). Concurrent bilateral sagittal plane kinematic records were obtained using a dual camera video system (200 Hz). Anthropometric measures were made and lower extremity joint kinetic records were calculated using an inverse dynamics model for the 100 ms after initial surface contact. Previous examination of this data set (5) indicated no left/right leg pattern differences within subjects, therefore, a pooled set of 150 "legs" of data were analyzed for each subject (1350 total). From a visual inspection of the ensemble vertical GRF records (VGRF), three landing style preferences were apparent. These were labelled as soft (S: 2 subjects), medium (M: 5 subjects), and hard (H: 2 subjects) based on the apparent magnitude differences among VGRF peaks.

RESULTS AND DISCUSSION

Statistical VGRF peak differences were found (ANOVA, $p < 0.01$) between styles, confirming the categorizations based on visual inspection. Functional differences for select joint work measures and for the negative work performed by individual joints were also analyzed across landing styles via ANOVA ($p < 0.01$).

Prior to addressing the shock absorption role of the ankle (AJ), knee (KJ), and hip (HJ) joints individually, comparisons were made to assess select joint work characteristics for different landing styles. The joint power patterns indicated distinct work phases across joints. The AJ record indicated negative work throughout the analysis period, while the KJ and HJ records each demonstrated three work phases (see Figure 1). Overall negative and net lower extremity work output indicated no style differences (-2.23 and -1.95 J/kg, respectively), which was expected given the controlled drop distance. Identified landing style differences generally indicated that the H style resulted in greater work magnitudes than either the S or M styles. AJ work differences were not indicated, with one and two work differences for the KJ and HJ, respectively. A previously unreported phenomenon was observed for the KJ power records. A positive work phase between approximately 20 and 34 ms after contact (0.059, 0.097, and 0.176 J/kg for S, M, and H, respectively) was observed. The H style demonstrated a significantly greater magnitude for this measure than the S and M landings. The biarticular musculature serving the KJ and HJ result in opposite functions. The strong functional association of this system has been well documented and partially explains the negative work difference identified for the HJ between the H and S styles (-0.325 and -0.191 J/kg, respectively). The third HJ work phase indicated that the S style evoked slight negative work,

conversely the M and H landings demonstrated positive work output (-0.048, 0.097, and 0.128 J/kg, respectively).

Examination of the negative work performed by each joint for all styles indicated that the HJ contributed significantly less to shock absorption than either the AJ or KJ (-0.270, -0.954, and -1.003 J/kg, respectively). This pattern was also demonstrated within the S and H landings, whereas for the M style each joint contributed significantly different negative work quantities to the overall task (-0.887, -1.024, and -0.279 J/kg for the AJ, KJ, and HJ, respectively). The net joint work exhibited similar trends when data were pooled across styles. Examination of within style joint work indicated no individual differences for the M and H landings, with the S style resulting in significant differences for all three joints (-1.029, -0.805, and -0.153 J/kg for the AJ, KJ, and HJ, respectively).

The results indicate that the AJ and KJ serve as the primary functional shock absorbers during landings, with the HJ contributing only minimally. In contrast, the KJ clearly serves as the major shock absorber during locomotion. This difference is attributable to foot orientation at initial contact (ie; forefoot vs rearfoot for landing and locomotion, respectively). The positive KJ work phase was initially thought to occur due to biarticular gastrocnemius actions where, due to a controlled lowering of the foot, tension was transmitted to the femur, possibly causing a KJ flexor effect. This is the reverse of an argument advanced for the functional interaction of the KJ and AJ during jumping (7). Upon closer examination, this does not appear to be a valid explanation; the subjects with the most controlled rearfoot lowering (S style) demonstrated the smallest KJ flexor magnitudes. It is suggested that the mechanical properties of the musculoskeletal system and/or the orientation of the leg at contact are responsible for the phenomenon. The prominent features of the joint power records occur within approximately 60 ms after contact. It has been suggested that events occurring within 50 ms of contact are passive and that it is impossible for the muscles to contribute to shock absorption (4). While it is likely that the neuromuscular system cannot react to the initial landing conditions directly, it is incorrect to state that the muscles do not contribute to shock absorption prior to 50 ms. Landing strategies are certainly pre-selected, and can mediate the stresses imposed by landing impacts, as evidenced by the different GRF and joint work results observed in this study. Finally, in spite of the rigid constraints of this movement task, several preferred landing styles were evidenced within a relatively small sample. Such findings suggest that researchers consider this factor prior to pooling data for analysis.

ACKNOWLEDGEMENT

Partial research support provided by Sigma Xi, The Scientific Research Society.

REFERENCES

1. Dufek, J.S., et al. Med Sci Sport and Exer., 1990.
2. McNitt-Gray, J., et al. Int. J. Sport Biomech., 1991.
3. Panzer, V., et al. Biomech. XI, 1988
4. Ricard, M., et al. Int. J. Sport Biomech., 1990.
5. Schot. P. Unpublished dissertation, 1991
6. Scott, S., et al. Med Sci Sport and Exer., 1990.
7. Van Ingen Schenau, G. Human Movement Science, 1989.

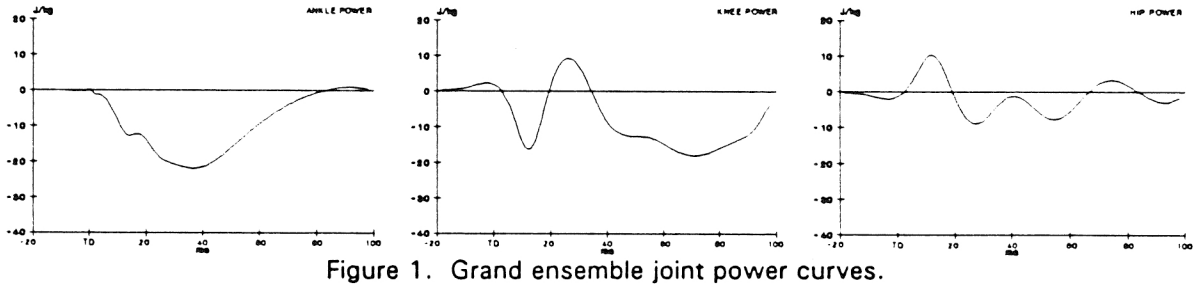


Figure 1. Grand ensemble joint power curves.

EVALUATION OF POSITION CONSTRAINTS ON LANDING PERFORMANCE

J.S. Dufek, B.L. Caster and B.T. Bates
Biomechanics / Sports Medicine Laboratory
University of Oregon
Eugene, Oregon 97403, USA.

INTRODUCTION

The initial position of the body prior to landing affects the maximum vertical forefoot (F1) and rearfoot (F2) and antero-posterior (AP) braking (FB) and propulsive (FP) ground reaction force (GRF) values as well as knee joint function during landings. Results of a systematic evaluation of these phenomena identified a flatfoot landing style for horizontal jump-landings which displayed no peak F2 and FP forces. A lesser degree of knee joint flexion during landings resulted in greater vertical and AP GRF values.

REVIEW AND THEORY

Constraints of position during landing can be defined relative to the entire system in space (initial jumping position) or with respect to body segment relationships (joint angles). Recent experimental protocols have primarily concentrated on vertical landings or drops (1,4) while it is apparent that many sport and movement activities include horizontal as well as vertical position changes of the body center of gravity. In addition, the effects of joint position during landing, primarily the knee joint angle, have been implicated to affect the magnitude of vertical GRFs experienced by the performer (3,4,5). The purpose of the study was to systematically evaluate the effects of selected take-off heights, distances and knee joint flexion angles on lower extremity function during landings.

METHODOLOGY

Five male collegiate student volunteers performed two landing techniques defined by knee joint range of motion (mean stiff [ST]=57 deg; mean soft [SO]=62 deg) during the initial 100 ms of the landing phase from three jump-position locations including horizontal (Hz: height=0 cm, distance=120 cm), vertical (Vr: height=120 cm, distance=0 cm) and combination (HV: height=120 cm, distance=120 cm). Retro-reflective markers were attached to selected right side lower extremity anatomical landmarks and sagittal plane motion of the markers was obtained using a video-based automated tracking system (Motion Analysis Corporation; 200 Hz) while subjects performed landings onto a dual force platform system (A.M.T.I.; 1000 Hz). Fifteen successful trials using each technique from each location (n=90 trials per subject) were evaluated for all subjects. The order of condition presentation was the same for all subjects: Hz, Vr, and HV with SO followed by ST at each location.

Maximum forefoot (F1) and rearfoot (F2) vertical GRF values, maximum AP braking (FB) and propulsive (FP) force values and times of occurrence of these events were obtained for each subject-trial. ExpertVision™ software was incorporated to obtain position coordinate data which was synchronized with the force platform data via an external pulse. Knee joint range of motion (K_{ROM}) and average angular velocity (K_{ω}) values were calculated for the initial 100 ms of the landing phase.

RESULTS AND DISCUSSION

Asymmetry of landing was first assessed by comparing right and left leg F1 and F2 vertical GRF values as well as times of occurrence of the respective events for all subject-conditions ($p < 0.05$) using a Model Statistic procedure (2). Results across all subjects identified 35 and 50% significant differences in magnitude and temporal force characteristics, respectively. Only one subject-condition (S1, HV-ST) exhibited a left leg force dominance (F1).

Position x Technique group ANOVAs were computed on F1, F2, FB, FP, K_{ROM} and K_{ω} for the right lower extremity. The omnibus-F as well as main effects were significant ($p < 0.01$) for all variables. *Post hoc* contrasts of the simple main effects were conducted and are summarized in Table 1.

F1 and F2 for ST were 1.6 and 2.3 times greater than the corresponding SO values while FB and FP were 1.2 times SO. K_{ROM} and K_{ω} for ST were 90% of the corresponding SO values. These results are consistent with previous research (1,3,5) and further suggest the importance of knee joint function regardless of initial jumping position. As body position moved up and away from the landing target, K_{ROM} and K_{ω} increased in magnitude. HV kinematic values averaged 1.4 times Hz across subjects. Due to the flatfoot nature of Hz landings, F2 and FP values were not observed. The single peak vertical and AP forces for Hz averaged 66 and 46% of the (F1+F2)/2 and FB values for Vr and HV, respectively, which suggest the more demanding nature of these two landing conditions.

In summary, the jump-landing positions evaluated identified 50% significant performance differences of which 79% were observed for Hz. Landing technique exhibited 75% significant differences within position. A more thorough understanding of the interactive effects between these components requires further investigation.

Table 1. Group Descriptive Data and ANOVA Summary

	Hz-SO	Hz-ST	Vr-SO	Vr-ST	HV-SO	HV-ST
K_{ROM}	50.0*ST	44.3	65.9*ST	63.6	67.0*ST	63.9
	(7.8)	(7.6)	(4.6)	(3.3)	(9.3)	(4.9)
K_{ω}	499.6*ST	442.5	661.1*Hz	636.1*Hz	672.6*ST,	639.1*Hz
	(73.9)	(65.3)	(46.5)	(32.3)	(85.3)*Hz	(40.1)
F1	17.94	32.12*SO	29.38*Hz	31.57*SO	27.79*Hz	29.43*Hz
	(3.95)	(5.13)	(6.58)	(5.56)	(6.33)	(5.20)
F2	----	----	37.90	47.23*SO	43.60*Vr	53.87*SO
			(8.14)	(9.00)	(7.32)	(10.03)
FB	4.92	8.80*SO	13.68*Hz	14.91*SO,	15.25*Vr,	16.05*Hz
	(0.97)	(2.83)	(3.07)	(2.54)*Hz	(3.17)*Hz	(3.08)
FP	----	----	6.81*HV	8.52*SO	5.62	6.12
			(3.01)	(3.09)	(2.21)	(2.30)

Note: K_{ROM} = deg; K_{ω} = deg/s; F1, F2, FB, FP = N/Kg; * $p < 0.01$.

REFERENCES

1. DeVita et al. Proc. 13th ASB. 186-186, 1989.
2. Dufek et al. Med. Sci. Spt. Exerc. in press.
3. Dufek et al. Med. Sci. Spt. Exerc. 22:370-377, 1990.
4. McNitt-Gray. Int. Jrl. Spt. Biomech. 7:201-224, 1991.
5. Tant et al. Proc. 12th ISB. # 118, 1989.

DIFFERENCES IN REACTION FORCES EXPERIENCED BY GYMNASTS DURING LANDINGS OF FRONT AND BACK SALTOS

Jill L. McNitt-Gray, Ph.D., Carolyn A. Barbieri, David D. Anderson, and Dawn M.E. Irvine
USC Biomechanics Research Laboratory, Department of Exercise Sciences
University of Southern California, Los Angeles, CA, USA 90089-0652

INTRODUCTION

Landings of gymnastics skills have produced some of the largest peak reaction forces encountered in sport (Nigg, 1985; Panzer, 1987). The peak magnitude of these forces have been shown to increase as the impact velocity (McNitt-Gray, 1991) and skill complexity increase (Panzer, 1987). For example, landings of a single back tucked saltos have produced peak vertical reaction forces of 8 times the body weight (BW), whereas, double back tucked saltos have produced peak vertical reaction forces exceeding 18 BW (Panzer, 1987). These impact forces have been shown to reach even higher magnitudes when the landing is uncontrolled and the lower extremities are asymmetrically loaded (Panzer, 1987; Bruggemann, 1987). In addition, the ability of the gymnast to safely attenuate the forces experienced during landing may be compromised by the visual conditions and segment configurations prior to contact (Nigg, 1985; McNitt-Gray & Nelson, 1988; McNitt-Gray, 1989; Sidaway, McNitt-Gray, & Davis, 1989), as well as, the technique restrictions imposed by the Federation Internationale de Gymnastique. Although no causal relationship has been shown between reaction forces and injury, the high forces encountered during landings of aerial gymnastics skills may be responsible for the high incidence of injury to the lower extremities of gymnasts (McAuley et al., 1987; NCAA, 1986, 1990). The purpose of this study is to systematically examine the influence of forward and backward rotation prior to contact on the magnitude, timing, and symmetry of the vertical and horizontal forces experienced by gymnasts during landings.

METHODS

Six healthy male gymnasts, who were members of a team ranked among the top five of all collegiate gymnastics teams within the United States, volunteered to serve as subjects. During data collection, each subject successfully landed three drop landings (McNitt-Gray, 1991), three front tucked saltos, and three back tucked saltos in a randomized order using their normal competitive landing style. All three tasks were initiated from a height of .72 meters above the top surface of two regulation gymnastics mats (200 mm by 400 mm; 100 ILD). The mats were fully supported by two Kistler force plates (200 mm by 400 mm). The reaction forces at the mat-plate interface were quantified for each foot using a sampling frequency of 800 Hz. Segment kinematics were recorded simultaneously using high speed video (200 fps; NAC Motion Analysis System). The interval of interest, identified as the landing phase, was defined as the time required to bring the vertical velocity of the total body center of mass to zero. Significant differences in horizontal and vertical reaction forces were compared between tasks and feet within subjects using analysis of variance ($p<.05$).

RESULTS AND DISCUSSION

Examination of the peak vertical forces measured at the mat/plate interface under each foot indicated the mean differences in peak vertical force (Pk2) between feet were on average .50(.3)BW for drop landings, .78 (.7)BW for front salto landings, and .95 (1.1)BW for back salto landings. Although the differences in peak vertical forces (Pk2) between feet were not found to be significantly different between tasks, the higher means and standard deviations observed during the salto landings suggest that landings of more difficult skills may produce a higher degree of asymmetrical loading. Differences in time to peak vertical force (Pk2) between feet did not produce significant differences between tasks (Drop, .004 (.003)s; Front, .003

(.002)s; Back, .002 (.002)s). Landings of front and back saltos did, however, result in significant increases (~50%) in peak resultant vertical forces (Pk2) over those experienced during drop landings (Figure 1). This observed increase in peak vertical force with increases in rotation was consistent for all subjects and is supported by the findings of Panzer (1987). The lack of significant difference in peak vertical forces between landings of forward and backward rotating skills indicates that the magnitudes of the peak vertical forces may not be influenced by the direction of rotation. In contrast, the peak anterior/posterior (A/P) forces do appear to be sensitive to the direction of rotation. Comparisons of the peak horizontal forces directed posterior with respect to the anatomical reference system resulted in significantly higher initial peaks (Pk1) during the back salto landings than during the drop and front salto landings (Figure 2). However, no significant differences in secondary peak posterior forces (Pk2) were noted between tasks. Examination of the peak horizontal forces opposing the direction of rotation (Front Salto: Anterior force; Back Salto: Posterior force; open arrows, Figure 2) produced significantly higher initial peaks and lower secondary peaks during the landings of the back saltos, as compared to the front saltos. The tendency for back saltos to produce larger initial peaks and the front saltos to produce larger secondary peaks was found to be consistent among all subjects. These significant differences in horizontal peak magnitudes and relative timing of the peaks, along with the differences in segment orientation at contact, may have important implications as to the loading and control of the lower extremity joints. Further examination of the kinematics and kinetics may also identify specific injury risk factors (e.g. cruciate tears, tendon ruptures) associated with the mechanics of forward and backward tumbling.

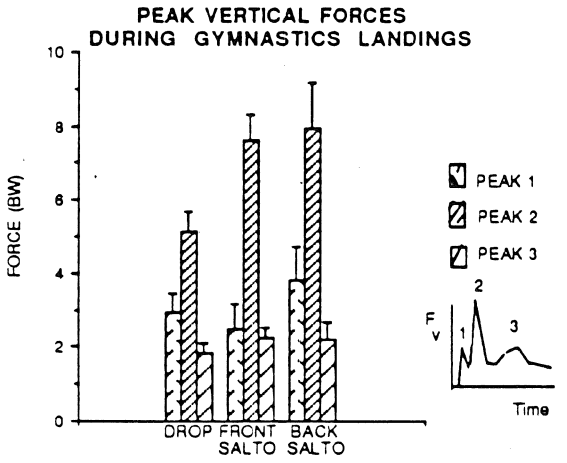


Figure1. Mean (SD) peak vertical forces.

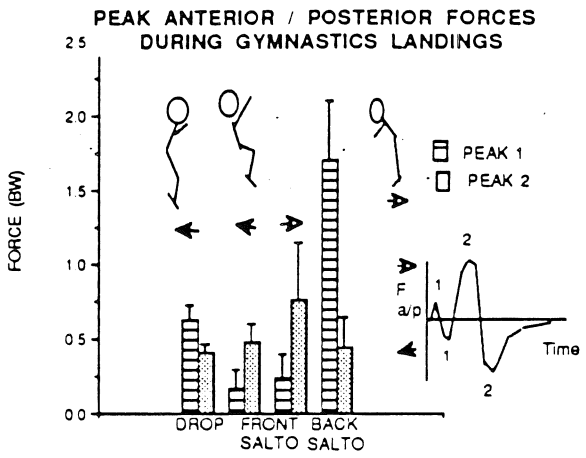


Figure 2. Mean (SD) peak ant./post. forces.

REFERENCES

Bruggemann, G. P. MSSE, 25:142-176, 1987.
McAuley, E. et al., Am J Spts Med, 15, 558-565, 1987.
McNitt-Gray, J.L. Doc.Dissert. Penn State, 1989.
McNitt-Gray, J.L. IJSB, 7,201-224, 1991.
McNitt-Gray, J.L. et al. Proc of ASB, 1989.
National Collegiate Athletic Association, 1986, 1990.
Nigg, B. M., Sprts Med 2, 367-379, 1985.
Panzer, V.P., Doc. Dissert, U of Oregon, 1987.
Sidaway, B. et al. J of Eco Psych, 3, 1989.

Acknowledgements: US Olympic Committee and members of the USC Biomechanics Lab.

THE EFFECT OF LANDING SURFACE ON MUSCLE ACTIVITY IN PREPARATION FOR LANDING

Jill L. McNitt-Gray, Ph.D., Dawn M.E. Irvine, Carolyn A. Barbieri, and David D. Anderson
USC Biomechanics Research Lab, Department of Exercise Science
University of Southern California, Los Angeles, CA 90089-0652

INTRODUCTION

Interaction between humans and support surfaces during landing involves prospective action as demonstrated by the activation of muscles prior to contact (Melvill Jones & Watt, 1971; Viitasalo & Aura, 1987; Dietz, Noth, & Schmidtbleicher, 1981; Sidaway, McNitt-Gray, & Davis, 1989). The duration of muscle preactivation for an individual has been shown to be relatively constant for the medial gastrocnemius (MG) when landing on a variety of surfaces from a given height (Fukuda, Miyashita, & Fukuoka, 1987; Gollhofer, 1987). However, examination of the amplitude of MG muscle activity prior to contact has produced mixed results. Gollhofer (1987) found that the amplitude of medial gastrocnemius (MG) activity prior to contact increased as surface compliance decreased, where as, Fukuda et al. (1987) observed a decrease in amplitude. This study continues to explore the relationship between muscle preactivation characteristics and surface compliance by examining the differences in time of muscle onset and amplitude for the soleus (SO), as well as, the medial gastrocnemius (MG) during landings on two surfaces.

METHODS

Nine male recreational athletes consented to serve as subjects. Each subject performed a series of drop landings from a stationary platform positioned .72 meters above the top of two different landing surfaces. Nine landings were performed onto two Kistler force plates and nine landings were performed onto two landing mats fully supported by the two force plates, in a randomized order. The landing mats were constructed with a top layer of stiff ethafoam (3.2 cm) and a bottom layer of polyurethane foam (6.8 cm; 100 ILD). The reaction forces at the mat-plate interface were quantified for each foot using a sampling frequency of 800 Hz. Segment kinematics were recorded simultaneously using high speed film (100 fps). The muscle activation patterns of the Medial Gastrocnemius (MG), Soleus (SO), and Tibialis Anterior (TA), prior to and during the landing were quantified using surface electromyography (1800 Hz; Beckman Silver-Silver Chloride electrodes; Differential amps, Data, Inc.). The reaction forces, kinematics, and EMG were synchronized at the time of contact. The EMG signals from each muscle were processed using a high and low pass filter, rectified, and integrated from the time of first EMG onset to ground contact (SNIP, 1988, Digital Dynamics, Inc). Time and relative amplitudes for each muscle were compared across surface conditions (ANOVA; $p<.05$).

RESULTS AND DISCUSSION

The results indicate the onset of MG activity generally occurred earlier than the onset of SO activity. The MG onset times across surface conditions were consistent with the findings of Gollhofer (1987) and Fukuda et al. (1987) in that no significant differences in time of MG activation prior to contact were noted between landings on the forceplates and landings on the mats (Figure 1). In contrast, the SO tended to turn on significantly earlier prior to landing on the force plates as compared to the mats (Figure 2). Comparison of MG EMG amplitudes also support the findings of Gollhofer (1987) and Fukuda et al. (1987) in that some subjects demonstrated increases in amplitude with increases in surface compliance, whereas, some subjects demonstrated decreases. In contrast, EMG amplitudes for the SO significantly increased as surface compliance decreased. The adjustment in onset times and amplitudes for

the soleus muscle in response to landing surface indicates the soleus may be responsible compensating for differences in surface compliance. These differences between the gastrocnemius and the soleus prospective response to surfaces may be due to the difference in fiber type make-up, muscle architecture, and/or the number of joints they cross. Examination of the preactivation patterns of other lower extremity muscles under the same surface conditions may provide additional insight as to the reasons for differences in prospective response observed for the medial gastrocnemius and soleus muscles.

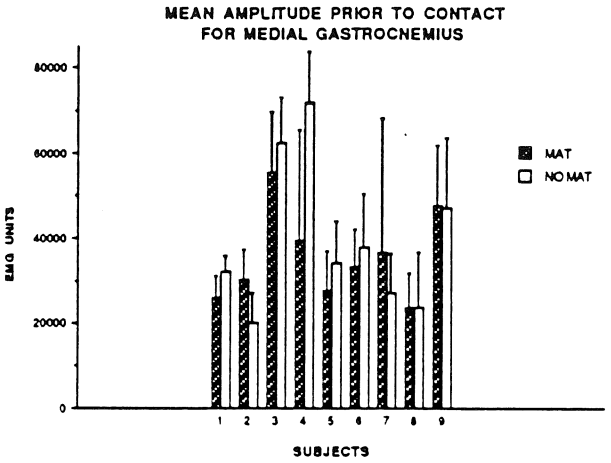


Figure 1. Medial gastrocnemius preactivation.

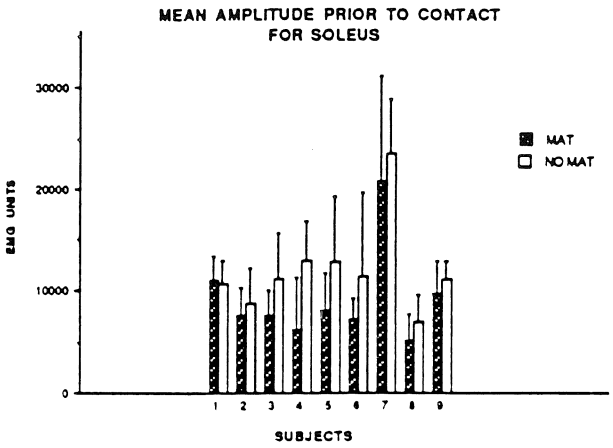


Figure 2. Soleus preactivation.

REFERENCES

Dietz, Noth, & Schmidtbleicher, J of Phys, 113-125, 1981.
Fukuda, H., Miyashita, M., Fukuoka, M., Biomech X-A, 301-305, 1985.
Gollhofer, A. Biomech X-B, 701-706, 1987
Melvill Jones & Watt, 1971, J of Phys, 709-727, 1971.
Saito, S. et at., B Hlth Spts Sc, Tsukuba, 5:201-206, 1982.
Sidaway, B., McNitt-Gray, J., Davis, G., Ecological Psychology 1(3) 253-264, 1989.
Viitasalo & Aura, 1987, Biomechanics X-B, 695-700,1981.
Acknowledgements: USC Faculty Research and Innovation Fund and members of the USC Biomechanics Research Lab.

ARM SWING AND TOE-TOUCH MOVEMENT EFFECTS ON VERTICAL JUMP PERFORMANCE

Barry A. Munkasy and Richard N. Hinrichs

Biomechanics Research Laboratory
Department of Exercise Sciences
University of Southern California
Los Angeles, CA 90089-0652

Exercise and Sport Research Institute
Arizona State University
Tempe, AZ 85287-0404

INTRODUCTION

This study investigated the effects of a sagittal ("normal") or frontal plane ("whip") arm swing approach (WA) and the presence or absence of an airborne toe-touch maneuver (TJ) on the performance of a vertical jump (VJ). Specifically, it investigated approach and movement effects on takeoff height (TH), landing height (LH), and flight height (FH) of the body center of mass (BCM); and the vertical and mediolateral velocities of the ankle at touchdown. TH, FH, and LH were defined as the height of the BCM at the instant of takeoff, touchdown, and the maximum height of rise of the BCM from the takeoff point, respectively. Twenty-two female subjects were videotaped and their performances were digitized. The positions and velocities of the (BCM) and ankle joints were computed as functions of time. FH was found to be significantly lower with the WA, but TH and LH were not significantly different between approach conditions. Although TH did not differ between movement conditions, FH and LH were significantly lower; yet, time in the air was significantly greater, with the TJ. The lower LH facilitated the increased time in the air needed to complete the TJ. Ankle velocity at touchdown was found to be significantly higher with a TJ as compared to a VJ.

REVIEW AND THEORY

Vertical jumping is an important movement in sports such as basketball and volleyball. It also plays a major role in gymnastics, skating, dance, and cheerleading. Little research has been done on how different arm movements and preparation for movement in the air affect the takeoff, flight or landing of a VJ. For example, cheerleaders often perform VJs in non-standard ways. They sometimes swing their arms in the frontal plane in preparation for takeoff (whip approach) and perform toe-touch maneuvers while in the air.

It was anticipated that the WA would decrease TH and FH when compared to the normal approach (NA) and would have no affect on LH. It was also expected that the performance of a TJ would decrease the FH as compared to a VJ but not TH or LH. Finally, vertical and mediolateral ankle velocities at touchdown were expected to be greater in a TJ when compared with a VJ.

PROCEDURES

Twenty-two female subjects (Age: 15.78 ± 1.02 years, Height: 1.61 ± 0.07 m, Mass: 50.45 ± 4.56 kg) participated in one session in which each performed a normal approach vertical jump, a whip approach vertical jump, a normal approach toe-touch jump, and a whip approach toe-touch jump. All subjects normally performed both types of arm swings and the TJ during practice, games, and performances. The NA-VJ was a standing VJ with a countermovement. Initial arm movement was lateral, and the forward and upward swing was mostly in the sagittal plane. WA trials started out in the same way, but the subjects initially swung their arms medially and the entire movement occurred mostly in the frontal plane. For the TJ, the subjects, once in the air, abducted and flexed their hips. With both legs extended and moving toward a straddled horizontal or above horizontal position, the jumpers flexed forward at the waist and moved their arms into a toe-touch position.

A Panasonic AG-450 Super VHS camcorder recorded the subject's frontal plane movements at 60 Hz. The camera setup (approx. 25-30 m away from the subjects) limited perspective error caused by out of plane motion to less than three percent. Twenty-one points defining a 14 segment model of the human body were digitized. Body segment masses and centers of mass were derived from the mean data of Clauser, et al. (1969) as adjusted by Hinrichs (1990). The data were smoothed at 5 Hz with a Butterworth digital filter, but for ankle velocity analysis at touchdown, a cutoff frequency of 7 Hz was determined to be appropriate. To be as accurate as possible, the timing of events such as takeoff and touchdown were estimated to the nearest half of a digitized frame. Linear interpolation was then used to compute position and velocity data at the specific events. Statistically, two factor repeated measures ANOVAs and a MANOVA were conducted. Tukey post hoc follow up tests were used if significant interactions were found. Because 10 statistical comparisons were made the level of significance was set at .005.

RESULTS AND DISCUSSION

THs were not found to be significantly different between conditions. FH, however, was significantly less when using the WA (NA: 0.305 ± .041 vs. WA: .289 ± .041 m, $p<.005$) and when performing a TJ (VJ: 0.306 ± 0.044 vs. TJ: 0.288 ± 0.037 m, $p<.005$). In addition LH was significantly less when performing a TJ (VJ: 1.071 ± 0.055 vs. TJ: .985 ± 0.053 m, $p<.005$). Even though FH was less for a TJ as compared to a VJ, time in the air was greater when performing a TJ. The increased time in the air was a result of a differing arm position and a lower BCM at touchdown. A longer time in the air may have allowed the subjects more time to complete the TJ.

Although the BCM vertical velocity at touchdown was not statistically different between conditions, the mean ankle vertical velocity was significantly higher for the TJ than for the VJ (3.032 ± 0.672 vs. 1.883 ± 0.197 m/s, $p<.005$). In addition, TJ mean ankle vertical velocity was significantly greater than BCM vertical velocity (3.032 ± 0.672 vs. 2.613 ± 0.164 m/s, $p<.005$). Further investigation revealed that in a VJ, the vertical velocity of the ankles relative to the BCM was reduced by hip and/or knee flexion and by reciprocal upward leg movement due to airborne downward arm movement. The antithesis occurred in a TJ. In terms of ankle mediolateral movement, velocity was significantly less in a VJ as compared to a TJ (0.180 ± 0.067 vs. 3.26 ± 0.698 m/s, $p < .005$). Therefore, a TJ landing created a greater resultant touchdown ankle velocity - implying that the body would have to dissipate a greater impact force.

Preparation for and performance of a toe-touch maneuver alters many characteristics of a vertical jump. The typical subject did not execute a toe-touch jump as a vertical jump with an in-flight toe-touch movement added in. It had unique characteristics which affected FH, LH, and ankle velocity at touchdown. In the toe-touch jump the subjects utilized the ground not only to decelerate medial leg movement, but also to decrease additional ankle vertical velocity. This indicates that a jumper may not be able to prepare for or handle impact with appropriate joint and muscle action when performing a toe-touch jump. It is suggested that if the arms are moving down at impact the jumpers would increase their time in the air, decrease their ankle vertical velocity at touchdown and may make these jumps safer to perform.

REFERENCES

Clauser, et al. (1969). *Weight, Volume, and Center of Mass of Segments of the Human Body*. Ohio: Wright-Patterson Air Force Base (AMRL-TR-69-70).

Hinrichs, R. N. (1990). *J. Biomech.* 23:949-951.

KINETIC EVALUATION OF A SPORTS TILE SYSTEM WITH HORIZONTAL DISPLACEMENT

Anita M. Bagley, Orthopedic Biomechanics Institute
359 8th Avenue, Suite 206, Salt Lake City, UT 84103

INTRODUCTION

Performance of a sports flooring system was evaluated via force platform testing. It was proposed that the "lateral forgiveness" feature of this flooring would reduce the magnitude of forces experienced by the lower extremity upon contact, and thus diminish stress on the musculoskeletal system. Fourteen normal recreational athletes performed four trials of three tasks: running, braking and jumping, on the test flooring and on linoleum. Orthogonal force data was collected and compared via two-tailed paired t-tests. For all tasks, maximum braking force was reduced with the tile flooring versus linoleum, and for the two tasks involving acceleration, the time to peak acceleration was diminished. Maximum vertical moment was reduced in the running task with the use of the tile flooring, but peak vertical force for the braking task was increased.

REVIEW AND THEORY

The magnitude of contact forces during sports activities have been investigated in studies to design equipment that enhances performance (1) and reduces injury (3). Repeated impact forces have been implicated in degenerative changes to the musculoskeletal system, including osteoarthritis in an animal model (2). The purpose of this study was to quantify performance characteristics of a flooring consisting of interconnected tiles that allow a limited amount of horizontal displacement via the tile linkages. It was proposed that the behavior of this flooring may reduce the forces experienced by the lower extremity and diminish injurious stress to the musculoskeletal system.

PROCEDURES

A 32 foot walkway with an AMTI OR6-5-1 Biomechanics Platform positioned centrally along the walkway length was covered with linoleum to form a level surface. To install the floor tile system, a thin pad was placed over the walkway and then covered with tiles fitted along the length to assure proper function of the horizontal displacement feature. The force platform was recalibrated after installation of the tiles. 14 recreational athletes (20 to 45 y.o.) with no history of injury to the lower extremities were randomly tested with either their right or left leg. Shoe type was not restricted and included running, tennis and aerobic designs. Subjects were allowed to practice to generate consistent behavior on the force platform. Four trials of each task (running, braking and jumping) were collected for both floor types. Orthogonal force and moment data were collected at 120 Hz for three trials, and at 480 Hz for one trial of each task. Forces were normalized to body weight. Two-tailed paired t-tests were used to evaluate differences between the two floor types at a significance level of alpha > 0.05. Parameters analyzed included vertical force peaks and minimums, braking and acceleration force maximums, maximum vertical moment and maximum medio-lateral force in the running task, the timing of the listed force extremes, and the timing of cross-over from braking to propulsion.

RESULTS AND DISCUSSION

Parameter averages are listed in Table 1. The floor tiling dissipated some impact force as evidenced by the reduction in maximum braking force. In addition, athletic performance may by enhanced by the tiles since in the running and jumping tasks, maximum acceleration was achieved faster. The increase in vertical force exhibitted during the braking task with the tiles may reflect differences in floor/shoe friction, with more sliding occurring on the linoleum. A trend for a more pronounced vertical minimum during the jumping task was noted with use of the tiles. This spring behavior may by exploited if the compliance of the floor is altered to match the inherent resonance of the muscle system (1).

(1) McMahon TA, Greene PR: Scientific American 239:148-163, 1978.
(2) Radin EL, et al.: Journal of Biomechanics 15:487-492, 1982.
(3) Steele JR, Milburn PD: Int'l Journal of Sports Biomechanics 4:130-145, 1988.

TABLE 1: Parameter Averages

	SPORT TILING		LINOLEUM	
RUN (% stance follows magnitude):				
VERTICAL CONTACT PEAK	2.00	(13.4)	1.93	(12.4)
VERTICAL MINIMUM	1.69	(18.9)	1.56	(18.7)
VERTICAL PUSH-OFF PEAK	2.46	(42.0)	2.45	(42.1)
BRAKING MAXIMUM	0.30*	(28.7)	0.43	(30.7)
ACCELERATION MAXIMUM	0.36	(72.5)*	0.36	(74.5)
MEDIOLATERAL MAXIMUM	0.18	(31.3)	0.19	(26.3)
VERT. MOMENT MAX (NM)	5.28*	(35.8)	10.05	(30.7)
CROSS-OVER	37.6		39.9	
DURATION (sec)	0.245		0.247	
BRAKE (duration follows magnitude):				
VERTICAL CONTACT PEAK	3.18*	(0.041)	2.89	(0.037)
BRAKING MAXIMUM	0.81*	(0.046)	0.94	(0.047)
JUMP (% stance follows magnitude):				
VERTICAL CONTACT PEAK	3.09	(9.3)	3.24	(9.4)
VERTICAL MINIMUM	1.44	(17.9)	1.73	(17.9)
VERTICAL PUSH-OFF PEAK	2.84	(46.2)	2.78	(44.5)
BRAKING MAXIMUM	0.51*	(18.0)	0.72	(23.7)
ACCELERATION MAXIMUM	0.49	(76.9)*	0.46	(79.8)
CROSS-OVER	31.3*		36.3	
DURATION (sec)	0.379		0.378	

*significance at alpha > 0.05.

ERGONOMICS

THORACIC CRUSH INJURIES IN A TRACTOR WHEEL ROLLOVER: ESTIMATION OF 3-D FORCES

Narayan Yoganandan, PhD, Y. King Liu,* PhD,
John Winterbottom,* MS, Anthony Sances, Jr, PhD

Department of Neurosurgery, Medical College of Wisconsin,
Department of Veterans Affairs Medical Center, Milwaukee, WI
and *Department of Biomedical Engineering,
University of Iowa, Iowa City, IA

ABSTRACT

While significant efforts have been undertaken to evaluate the biomechanics of injuries induced during a motor vehicle crash, little research has been done to determine the biomechanics of crush injuries that are routinely seen in a rural environment. The objective of the present study was to determine the generalized dynamic force (and moment) histories which are primarily responsible for crush injuries to the human thorax during a tractor wheel rollover. A three-dimensional force and moment measuring load cell was used to collect dynamic data. A sandbag of approximately 22.7 kg simulating the human torso was placed on the load cell. Tractor wheel rollover tests were conducted at velocities ranging from 0 to 86 cm/s. Peak compressive forces ranged from 3,500 to 13,430 N. Off-axis (shear) forces were considerably smaller. Moments along the three directions and the off-axis forces developed after the development of the peak compressive force. This indicates that crushing injuries are primarily due to the principal (vertical) component during *in vivo* situations.

INTRODUCTION

Injury in the United States has considerable impact on our society. According to a recent estimate, injuries cost our nation $158 billion annually. While significant efforts have been advanced to study the epidemiological and biomechanical aspects of trauma induced during motor vehicle crashes, little emphasis has been placed on rural injuries. It should be noted that farming is the occupation resulting in the highest fatality rates. Equipment injuries produce high rates of morbidity and mortality with tractor trauma identified as one of the leading killers. Tractor rollovers account for almost one-half of all tractor accidents. Crushing injuries often result due to tractor rollovers. The present study was designed to determine the generalized dynamic force histories during a tractor wheel rollover.

MATERIALS AND METHODS

Tractor wheel rollover studies were conducted to determine the dynamic triaxial force and moment histories at speeds of 0 to 86 cm/s, representative of rural accidents. A Bobcat with a static weight of 2400 kg and a six axes force plate, 60x120x10 cm (Bertec Inc., Worthington, Ohio) capable of recording the dynamic forces and moments were used. The weight ratio of the front to the rear wheels was around 0.55. The width of the tractor tire was 178 mm. Initial force plate calibration tests were conducted and the testing sequence included a static load on the force plate from the front and rear tires of the tractor followed by loading the force plate at velocities ranging from 0 to 86 cm/s. A guiding platform 12.8 m long was constructed to roll the tractor wheels at the above velocities. The force plate was firmly positioned in the middle region of the platform. The platform was rigidly fixed to the floor and interconnected by transverse struts to minimize lateral (sway) motion. The tractor movement was controlled such that a uniform velocity was achieved in the region where the force place was positioned. A sandbag of approximately 22.7 kg was placed on the force plate simulating the human thorax. Triaxial force and moment data were collected as a function of time using accepted procedures

for dynamic testing. All channels were sampled digitally at a rate of 2500 Hz per channel frequency. The data was collected in a personal computer and further processing included a computation of the resultant forces, a temporal identification of the peak magnitudes of the force and moment histories, and computation of the impulse. The coordinate system used in the study was such that z-axis was vertically downwards with the x and y axis perpendicular to z and conforming to the right hand rule. In biomechanical terms, forces in the z, x, and y directions represented the compressive (superior-inferior) force and lateral shears (postero-anterior and left to right) and moments along the xy, yz, and zx planes represent the axial, lateral bending and flexion-extension components.

RESULTS AND DISCUSSION

At velocities ranging from 0 to 86 cm/s, peak dynamic compressive forces ranged from 3,500 to 13,430 N. Figure 1 illustrates the compressive force-time response for the left front wheel. The off-axis shear forces which ranged from 0 to 1120 N in the x direction and 250 to 4000 N in the y direction were considerably smaller the principal compressive component. The moments also indicated similar characteristics. The off-axis forces and moment histories reached their peak values following the development of the peak compressive component. This suggests that crush injuries in the initial impact phase may be primarily due to the principal component. The development of the off-axis forces and moment histories after this peak can be considered as a secondary phenomenon. These studies were conducted with sandbags, thus, a correlation of the primary and secondary forces and moments with the trauma is not possible. However, it is to be expected that the above mechanism of the transfer of the external quasistatic force is indicative of a majority of the crush injuries routinely encountered in a rural environment.

ACKNOWLEDGEMENT

This research was supported in part by PHS CDC Grants R49CCR703640, R49CCR502508, and the Department of Veterans Affairs Medical Research Funds.

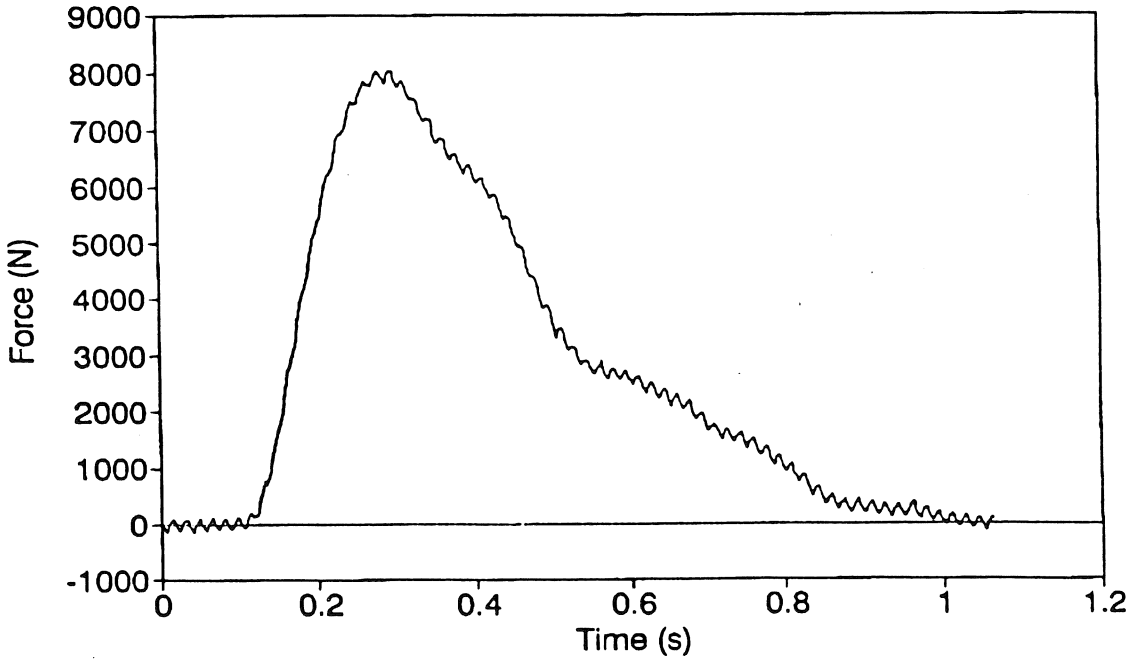


Figure 1: Compressive force-time response for the left front wheel.

AN APPLICATION OF THE BIOMECHANICAL SIMULATION OF HUMAN MOVEMENT TO THE EVALUATION OF DWELLING SPACE DESIGN

Takashi Yokoi
Industrial Products Research Inst., Tsukuba, Ibaraki 305, Japan.

INTRODUCTION

Muscle stress occurring through the interaction between dwellers and equipment during dwelling activities is a consideration for the evaluation of dwelling space design. This viewpoint is indispensable for evaluating the design of dwelling spaces and equipment appropriate for elderly people.

One useful method to identify muscle stress may be biomechanical simulation of dwelling activities based on musculo-skeletal model of the human body. Individual muscle forces as well as joint torques estimated through the simulation are used for describing muscle stress. Also, the simulation may enable the identification of energy consumption during the dwelling life of various people by using equipment sizes and human body dimensions as the input data sets. However, there was a dearth of published research on the above application of biomechanical simulation.

The purpose of the present study was to apply the biomechanical simulation to the evaluation of cooking table height from the viewpoint of muscle stress.

METHODOLOGY

The eight-segment link model of the human body(i.e. head, torso, upper arms, forearms, hands, thighs, shanks and feet) and musculo-skeletal model of the lower limb (Figure 1)[2] were used in the present biomechanical simulation. The simulation adopted inverse dynamic approach and estimated individual muscle forces of the lower limb and joint torques. An optimization model using linear programing technique was adopted for the estimation of individual muscle forces.

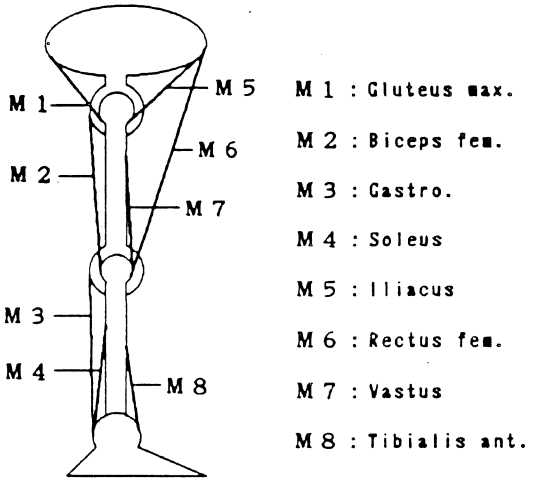


Figure 1 A musculo-skeletal model of the lower limb.

Static postures used for cooking activity on several work surface heights from 0.65 to 1.2m were constructed as an input data set for the simulation. The worker was assumed to be a standard Japanese adult female(Height=1.6m, Weight=529.2N) for constructing the postures. Body segment parameters were obtained based on the regression equations proposed by Ae, et al[1].

RESULTS AND DISCUSSION

Figure 2 shows the cooking postures at 0.65, 0.80 and 1.00m of work surface heights and the joint torques to maintain static postures. The amount of torques were indicated by the radii of sectors. Torques apply to the direction decreasing central angles of the sectors. Figure 3 shows the changes in individual muscle forces to maintain cooking postures with the increase of work surface height.

At a surface height lower than 0.8m, joint torques and muscle forces for the lower limb increased due to the forward bent of the trunk segment. At a surface height higher than 0.8m, these parameters exhibited some increase due to the change in the relative arm position. The results may indicate that the optimum range of work surface height in cooking is from 0.80 to 0.90m for the worker whose stature is 1.6m. Similar results were obtained in the previous experimental investigations using EMG and interview[3].

Within the limitation of this study, it was confirmed that the biomechanical simulation can be applied to the evaluation of dwelling spaces and equipment from the viewpoint of muscle stress. The improvement of the human body model as well as the collection of input data may be necessary for more flexible application of the simulation to the evaluation of dwelling spaces and equipment.

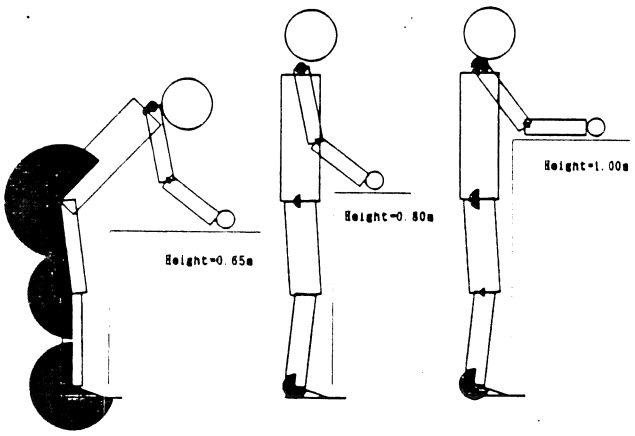


Figure 2 Examples of postures and joint torques at several work surface height.

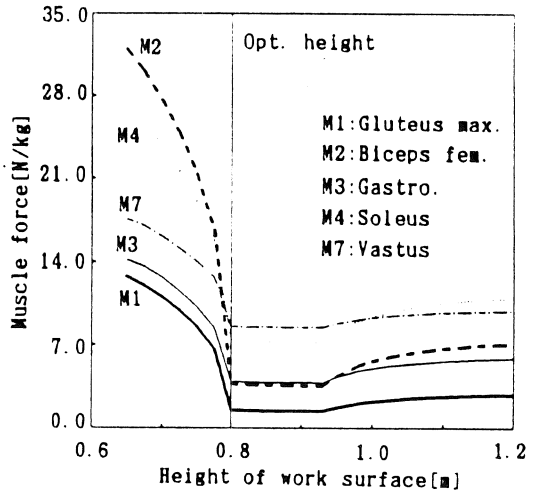


Figure 3 Change in individual muscle forces with the increase in work surface height.

1)Ae, et al., Proceedings of 41th Annual meeting of the Japanese Society of Physical Education B, pp.135, 1990.
2)Yamazaki, Japanese Journal of Ergonomics, 11-4, 1975.
3)Yoshinaga, Bulletin of Industrial Product Research Inst., 55, 33-46, 1968.

ASSESSMENT OF RISK FACTORS FOR CUMULATIVE TRAUMA DISORDERS (CTD) USING A VIDEO/COMPUTER GRAPHICS APPROACH

R. Wells and A. Moore
Department of Kinesiology, University of Waterloo
Waterloo, Ontario, Canada, N2L 3G1

INTRODUCTION

This paper describes an approach to assessing manual tasks for the potential of causing work related chronic musculoskeletal (cumulative trauma) disorders. Instrumentation combining a video image of the worker performing the task together with superimposed quantitative information on risk factors, has been found very useful in obtaining semi-quantitative assessments in many types of workplace.

REVIEW AND THEORY

While it is now relatively common knowledge that studies of upper limb musculoskeletal disorders must consider, at least, risk factors of force, repetitiveness and posture, as well as inadequate rests, the practical aspects of assessing tasks for musculoskeletal injury potential, in the absence of any agreed upon quantitative guidelines, remains problematic. In order to analyze such tasks a system was developed which allows one to assess the major risk factors simultaneously. The recent availability of affordable and portable video and computer systems as well as commercial instrumentation has allowed the marriage of these technologies to permit both quantitative and semi-quantitative monitoring and analysis of upper extremity work.

PROCEDURES

Data on musculoskeletal stresses were collected using the video and EMG system described by Moore et al., (1991). The system allowed the recording of quantitative estimates of the hand, wrist and shoulder loads during manipulative tasks simultaneously with the video. Despite the availability of the other information, the video image remains an important resource for interpretation. A non-restrictive goniometer (Penny and Giles, Gwent, U.K.) was used to transduce wrist flexion/extension and ab/adduction. The linear envelope EMG and wrist angle data were collected on a custom battery powered signal processing unit (10 channels, bandwidth 0-10Hz), worn as a waist pack. The EMG and wrist transducer data were then encoded and transmitted in pulse code modulated form onto one stereo sound channel of the video camcorder via an infra-red fibre optic link. Hence, data on muscle activity(force), posture and repetition were available directly or later, upon playback of the video tape, synchronised to the activity. Upon playback of the tape, or directly during the task, the multiplexed signals were decoded, analog to digital (A/D) converted at 30Hz on a portable computer and the information used to drive various types of graphic representations. These were then superimposed upon the video image using commercial hardware (VGA Producer, Magni Corp, Beverton). A commercial windowing system (Windows 3, Microsoft Corp) running custom software on the computer allowed flexible sizing and positioning of the graphic information as well as labelling of traces. The graphic representation chosen to depict the rapidly changing data was an "oscilloscope" display with long persistence and a 5 to 10 second sweep duration with up to eight channels displayed simultaneously. A base line and another predetermined level, often some fraction of the MVC, was also superimposed for estimating values. This representation allowed recognition of cyclic patterns and provided sufficient persistence to allow comparisons between channels and between cycles in tasks with high repetition rates.(Fig 1).

There are many parameters which have been used to provide estimates of musculoskeletal injury potential of a job. These include measured or estimated force, posture of the limbs, wrist and fingers, repetition of tasks or task elements or muscle activations in the shoulders or arms. In estimating the musculoskeletal loads incurred in performing a task, a typical display may include the following parameters superimposed on the video (4 each both left and right): 1) Shoulder muscle activation; 2) forearm muscle activation; 3) wrist angles and; 4) the coincidence of wrist flexion and forearm flexor muscle activation. Factor 1) was deemed critical as shoulder loading, especially "static" contraction, has been implicated in development of chronic shoulder troubles, (Aaras and Westgaard, 1987). Although not yet proven through epidemiological methods, we believe that forearm muscle activation can be used in similar ways to shoulder myoelectric signals, Moore et al., (1991). Poor wrist posture has long been regarded as risk factor for hand/wrist

problems, eg. Armstrong and Silverstein (1987). Factor 4) is a combination of wrist flexion and forearm muscle activation which loads the median nerve directly and is a potential contributor to the development of carpal tunnel syndrome, (Drury, 1987, Smith et al., 1979). For tasks in which low back loads give rise to concern, electrode placements to monitor the myoelectric activity of the thoracic spinal musculature have been found useful in assessing low back demands over time using known calibration loads and postures, Potvin et al., (1990).

RESULTS AND DISCUSSION

Fig. 1 shows a person doing a cashiers job. The subject shown used a typical 'scan and bag' technique whereby the worker reached for an appropriate item, grasped and turned it so the bar code passes over the scanner, and placed the item in a bag. The bags were then loaded into tote boxes and the tote box carried to a conveyor. EMG from five muscle sites is shown. Using this technique for analysis, parts of the job which required high muscle loading were quickly identified. When compared with alternative analysis methods, this was found to allow quick identification of specific stressful points within a job. It is faster for identifying the specific action, than separate processing of quantitative and video image. The video image alone, while useful for functional analysis, can be difficult to use for postural analysis, especially in the upper limb, due to the multiple degrees of freedom and the loss of the upper limb from view. In analysis of sewing tasks, for example, the upper limb can often be under the material, out of sight. By incorporating a reading of wrist angle with the video image, the hand function and a wrist angle can be assessed simultaneously. Also, this technique allows for a simultaneous qualitative assessment of variables that are not readily apparent from the video image such as muscle loading (eg. static loads in the shoulder girdle) or hand force. While the process does not identify the overall stressfulness of the job, the quantitative data is still available for further analysis. Overall, the technique presented was found to be an excellent tool for quickly identifying the most physically stressful parts of a task.



Figure 1 Typical video frame showing work postures and quantitative information. The arrow represents the time of the frame. See text for details.

REFERENCES

Aaras, A. and Westgaard, R.H. (1987). Applied Ergonomics ,18.3, 211-219.

Armstrong, T.J. and Silverstein, B.A. (1987). Clinical Concepts in Regional Musculoskeletal Illness, (pp.333-354), Grune and Stratton.

Drury, C.G. (1987). Seminars in Occupational Medicine, 2, 1, 41-49.

Moore, A.E., Wells, R., Ranney, D.A. and Cholewicki, J. (1991) Quantification of exposure in tasks with cumulative trauma disorder potential, Ergonomics, (*in Press*).

Potvin, J., Norman, R. and Wells, R. (1990), Proceedings of the Human Factors Association of Canada, Ottawa.

Smith, E.M., Sonstegard, D.A., and Anderson, W.H. 1977,, Archives of Physical Medicine and Rehabilitation, **58**, 379-385.

RESONANCE BEHAVIOR OF THE HUMAN EXPOSED TO WHOLE-BODY VIBRATION

Suzanne D. Smith and Leon E. Kazarian
Armstrong Laboratory Wright-Patterson AFB Ohio 45433-6573

INTRODUCTION

Previous whole-body vibration studies conducted to define human dynamic response have demonstrated at least one and possibly two regions of resonance between 3 and 30 Hz. Among these studies, some have shown that the location of the resonant peaks are dependent on the acceleration level. The present study evaluated the impedance response of the seated human exposed to sinusoidal vibration between 3-20 Hz at three acceleration levels. The results of this study indicated that the location of the primary resonant frequency shifted as a function of the acceleration. Up to three additional regions of resonance were also observed in both the magnitude and phase data. The results led to the formulation of a 5-mass, 4-degree-of-freedom lumped parameter model for simulating the observed human vibration response.

REVIEW AND THEORY

Using the apparent mass ratio of transmitted force to input acceleration, Hinz and Seidel (1987) and Fairley and Griffin (1988) demonstrated that the primary resonant frequency decreased with increasing acceleration level (from 4.5 to 4 Hz for acceleration increases from .15 to .31 g_{rms} and 6 to 4 Hz for acceleration increases from .026 to .2 g_{rms}). In addition to the occurrence of a primary resonant peak between 4 and 6 Hz, a second peak was usually observed between 10-12 Hz. Several models have been formulated to describe this response. Using the driving-point impedance technique, Smith and Kazarian (1990) observed that the vibration response of the Rhesus monkey was dependent on the acceleration level. A similar methodology of testing and analysis was used in the present study to investigate the acceleration dependence and resonance behavior in the human.

PROCEDURES

A triangular arrangement of load cells and two accelerometers, secured beneath the human test seat, were used to measure the transmitted force and input velocity for calculating the impedance ratio. The seat was mounted onto an Unholtz-Dickie vibration platform. A Fast Fourier algorithm was used to calculate the phase differences. To obtain the subject impedance magnitude and phase, the seat impedance was subtracted from the total impedance at each load cell site and the results summed. Four male subjects were loosely restrained in the seat and tested a total of 4 times each between 3-20 Hz at .05, .1 and .25 g's peak acceleration.

RESULTS

The mean primary resonant frequency shifted from 5 Hz at .25 g peak to 6 Hz at .10 g peak to 7 Hz at .05 g peak acceleration. The impedance magnitude curves also showed up to three additional regions of resonance between 7 and 9 Hz, 12 and 14 Hz, and 14 and 20 Hz. The magnitude curves were

relatively linear up to the first resonant peak. The phase data showed the expected response associated with resonance behavior. At .10 and .25 g's peak acceleration, the first resonant peak corresponded to the primary resonant frequency in the majority of tests. At .05 g peak there was a tendency for an increased magnitude response at the location of the second resonant peak and, in several cases, the second peak (observed between 7 and 9 Hz at .05 g peak acceleration) was observed as the highest or primary peak with an initial lower resonance region also appearing between 5 and 7 Hz. At the higher acceleration levels, the peak between 7 and 9 Hz was not always present in the magnitude data. Figure 1 illustrates the impedance magnitude results for a subject and is typical of all other subject responses. A human model was formulated from an existing model of the Rhesus (Smith and Kazarian, 1990). In addition to representations for the pelvis, spine and legs, two sprung-mass subsystems were added to represent the intra-thoracic and intra-abdominal viscera. Typical responses of the model are presented in Figure 2.

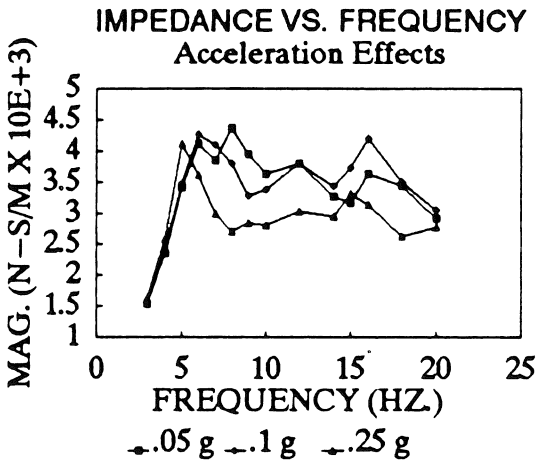


Figure 1

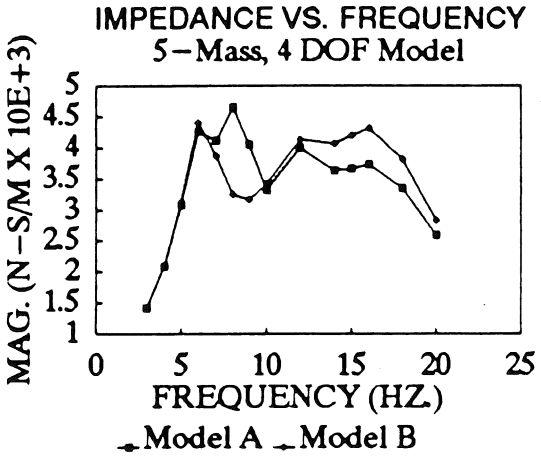


Figure 2

DISCUSSION

The observed shifts in the primary resonant frequency with changes in acceleration level are in agreement with Hinz and Seidel (1987) and Fairley and Griffin (1988), however, the additional regions of resonance have not been consistently observed. At the lowest g level, the transmission of vibration may not be as effective in exciting the intrathoracic components of the upper torso to produce the primary resonant peak. From the results of this study, it is speculated that the leg mass subsystem, in direct contact with the seat, could produce the primary resonance observed between 7 and 9 Hz. In Figure 2, it was possible to eliminate the resonance between 7 and 9 Hz by reducing the stiffness and increasing the damping associated with the leg mass subsystem in Model B. The model can be used to evaluate the significance of the resonance shifts relative to changes in the stiffness and damping characteristics.

Hinz and Seidel, Indust. Health, 25, 169-181, (1987)
Fairley and Griffin, J. Biomechanics, 22, 81-94, (1988)
Smith and Kazarian, J. Biomechanics, (Abstr), 23, 712, (1990)

FLUID MECHANICS

FLOW DYNAMICS AND TURBULENCE MEASUREMENTS PAST MITRAL VALVE PROSTHESES IN A MODEL LEFT VENTRICLE: EXPERIMENTAL AND NUMERICAL RESULTS

Richard T. Schoephoerster
Department of Mechanical Engineering
Florida International University
Miami, FL 33199

and

Krishnan B. Chandran
Department of Biomedical Engineering
University of Iowa
Iowa City, IA 52242

INTRODUCTION

The nature of the flow dynamics past heart valve prostheses of various geometries and the mechanical stresses associated with the flow have been linked to thrombotic complications with the clinical use of the prostheses. To gain an understanding of the detailed flow dynamics near the valve and within the left ventricle(LV), *in vitro* experimental and numerical analyses were performed. The experimental methods included velocity and turbulent shear stress measurements past various prosthetic mitral valves(MV) in an acrylic rigid model of the LV using laser Doppler anemometry(LDA). The 2-D Navier-Stokes equations for fluid flow were then solved numerically for the flow past several of these geometries of MV in a 2-D representation of the physical model of the LV using the finite analytic(FA) method.

REVIEW AND THEORY

The velocity profiles and turbulent shear stresses produced downstream of prosthetic MV are critical parameters in the evaluation of the flow dynamics associated with thrombosis and hemolysis. Velocity profiles have been obtained past prosthetic MV in an axisymmetric flow chamber[1]. It is intuitively obvious that overall LV flow dynamics, including vortex formation distal to the MV, will be a functon of the flow chamber geometry. A very limited amount of work has been done to numerically predict the flow dynamics in the LV past MV prostheses. Solutions of the laminar Navier-Stokes equations using a finite difference technique in 2-D models of the LV and MV have been reported in the literature[2]. Any detailed comparison of numerical simulations with experimental data is lacking. No detailed velocity and turbulence measurements in flow chambers representing the physiological geometry of the LV have been reported in the literature. This study consists of LDA measurements downstream of various prosthetic MV in a model LV flow chamber, and also a numerical simulation of flow in a 2-D representation of this model using the FA method.

PROCEDURES

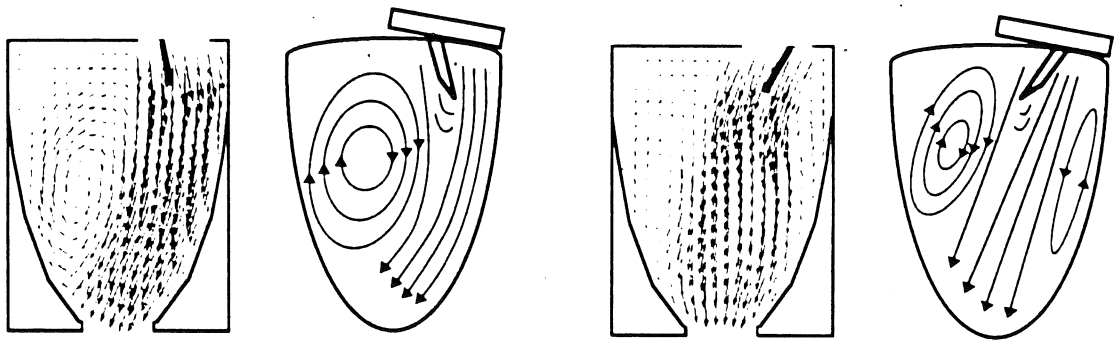
The details of the experimental and numerical procedures are contained in [3]. Flow visualizations and fluid velocity and turbulence measurements were obtained past Starr-Edwards caged ball, Bjork-Shiley tilting disc, St. Jude bileaflet, and polyurethane trileaflet valves mounted in the mitral position of an acrylic rigid model of the LV. The model LV cavity is essentially one-half of an ellipsoid. The dimensions of the cavity and the orientation and positioning of the MV annulus are based on an *in situ* casting of a human LV as well as average LV volumes. The LV flow chamber is connected to a pulse duplicator which simulates physiological flow and pressure waveforms. Flow visualizations were obtained by suspending neutrally buoyant resin beads in the blood analog fluid and illuminating with a high intensity split light. Velocity measurements were made using a three beam two-component LDA.

The LV was modelled numerically in 2-D as one half of an ellipse with a 2-D representation of the MV. The LV walls and the MV leaflets are rigid and stationary. The fluid is viscous(Newtonian) and the flow is laminar. The governing equations for the flow are the Navier-Stokes equations for incompressible, unsteady flow with constant properties. The

velocity profile at the MV inlet as well as the outlet at the apex is uniform and periodic with $U(t) = U_O \sin t$. The flow is initially assumed to be stationary. The numerical solution was obtained by discretizing the governing differential equations using the FA method described in [4]. Solutions were obtained at successive time steps from t=0 to t=π at peak Re=300.

RESULTS AND DISCUSSION

Representative results for a tilting disc valve(Bjork-Shiley) in two orientations are shown. A large stabilizing vortex is produced with this valve in the posterior position which appears to provide a smooth washout of the fluid with minimal disurbance of flow compared to the anterior position. The turbulent shear stresses are somewhat elevated in the region of the jets for both orientations, with maximum values of 172 dyn/cm^2 (posterior) and 211 dyn/cm^2(anterior). The velocity and turbulent shear profiles obtained across the entire diametrical axis of the flow chamber differ greatly from the data of [1], and this can at least in part be attributed to the stabilizing vortex produced in this model due to the geometry of the flow chamber. The measured turbulent shear stress magnitudes for all valves studied did not exceed the reported value for hemolytic damage(1500 dyn/cm^2). However, the measured turbulent shear stresses were near or exceeded the critical shear stress reported in the literature for platelet lysis(100 dyn/cm^2), a known precursor to thrombus formation. The numerical solutions agree well enough with experimental measurements and observations to warrant further modifications to the model to better simulate *in vivo* conditions, including wall motion boundary conditions obtained from cine-angiography. The maximum computed wall shear stress on the rigid valve leaflets ranged from 60 to 91 dyn/cm^2. However, the computed shear stresses would most likely increase dramatically for flows at physiological Reynolds numbers as well as with the introduction of turbulence and three-dimensional effects.



(a) (b)

Fig. 1. Computed velocity vectors(left) and streamlines drawn from flow visualization(right) for the tilting disc valve in the posterior(a) and anterior(b) position.

REFERENCES

1. Woo, Y-R, et al. (1986) J. Biomechanics. 19:39-51.
2. Peskin, C.S., et al. (1980) J. Comp. Physics. 37:113-132.
3. Schoephoerster, R.T. (1989) Ph.D. Thesis, University of Iowa.
4. Chen, C.J., et al. (1984) J. Comp. Physics. 53:209-226.

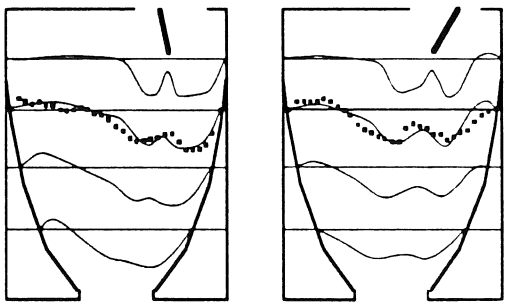


Fig. 2. Velocity profiles for the tilting disc valve. Solid line = numerical results, square markers = LDA measurements.

QUANTITATIVE TECHNIQUES

ENDPOINT PROBLEMS IN SMOOTHING RAW KINEMATIC DATA: AN EVALUATION OF FOUR POPULAR SMOOTHING TECHNIQUES

Richard N. Hinrichs, Exercise and Sport Research Institute,
Arizona State University, Tempe, AZ 85287-0404 USA

INTRODUCTION

The question of which method is best for smoothing and differentiating raw kinematic data has been debated for more than a decade. Pezzack et al. (1977) promoted the use of a Butterworth digital filter (DF) followed by finite difference differentiation and provided raw data for others to use to evaluate other smoothing methods. Subsequently, other authors used the Pezzack data to demonstrate accuracy equal to that reported for DF using cubic spline (CS), quintic spline (QS), and optimally regularized Fourier series (FS). None of the methods showed "endpoint problems" (erratic behavior at the ends of the data set) commonly associated with smoothing and differentiating raw kinematic data. In order to create a data set more "stressful" to the smoothing algorithms (and therefore expected to reveal endpoint problems), the present study truncated the Pezzack data set at three locations corresponding to large peaks in the second derivative. The three data subsets were smoothed and differentiated using FS, CS, QS, and DF to obtain acceleration values. These were compared with the "true" acceleration values reported by Pezzack et al. The results demonstrated clear superiority of the quintic spline over the other methods in producing more accurate acceleration values close to the endpoints of the data set.

REVIEW AND THEORY

The most commonly-referenced article on smoothing and differentiation of raw kinematic data in biomechanics is by Pezzack et al. (1977). These researchers used an accelerometer to provide analog acceleration values to compare to those obtained from film. They concluded that filtering the raw displacement data with a Butterworth digital filter followed by finite difference differentiation provided accurate acceleration values. They provided their raw displacement data so as to let others evaluate different smoothing methods. Subsequently, other authors used the Pezzack data to demonstrate accuracy equal to that reported for DF using cubic spline (Soudan & Dierckx, 1979), quintic spline (Wood & Jennings, 1979), and optimally regularized Fourier series (Hatze, 1981). When applied to the Pezzack data, none of the methods showed "endpoint problems" (erratic behavior at the ends of the data set) commonly associated with smoothing and differentiating raw kinematic data. The DF known to be especially prone to these endpoint problems. A common way to handle this is by digitizing additional frames at the beginning and ends of the data set. Alternately, artificial extra frames ("padding") can be added by extrapolating the data beyond the endpoints before smoothing and differentiating (Smith, 1989).

The fact that Pezzack et al. did not show any endpoint problems with their use of the DF is curious. Re-analysis of their data with a DF using a cutoff frequency of 7.2 Hz (which is equal to a double pass of the 9 Hz filter used by Pezzack et al.) reveals significant endpoint problems with their data (see Figure 1). Evidently Pezzack et al. only reported the results for the middle portion of a larger data set, thus giving the misleading impression that the DF did not suffer from endpoint problems with their data set. The purpose of the present study was to use subsets of the Pezzack et al. data to evaluate the endpoint problems associated with FS, CS, QS, and DF methods of smoothing and differentiating.

PROCEDURES

The original Pezzack data set (122 points) was truncated at three different locations corresponding to the major acceleration peaks. These were points 74, 84, and 98 (see Figure 1). The resulting data subsets were smoothed and differentiated using a software package "SMOOTH" available from Graeme Wood

at the University of Western Australia. In this software package, Wood provides the programs for FS, CS, QS, and DF. The standard DF option, however, pads the data with 10 extra frames at the beginning and end of the data set using linear extrapolation. Therefore the data were also analyzed with the DF without these extra frames added, in order to provide a true "stress test" for endpoint problems. For the DF, the cutoff frequency was set at 7.2 Hz as mentioned above. For the splines, smoothing factors were chosen to produce curves which most closely approximated the Pezzack analog acceleration data. For the FS, the program automatically selected the optimum harmonic.

RESULTS AND DISCUSSION

Figure 1 shows the results for the entire Pezzack data set using DF with and without padding. The padded curve closely approximates the analog acceleration curve reported in Pezzack et al. This padded DF curve was used to represent the "true" curve for subsequent comparisons. The endpoint problems become most noticeable 4-5 points from the ends, although small deviations were still present 10 frames from the end.

Figure 2 shows the results for the 74 point data subset. All methods suffered from endpoint problems to some extent. The QS, however, performed best with accelerations closest to the "true" values. The DF without padding performed the worst. The CS, FS, and DF with padding fell in the middle. Results for data subsets up to points 84 and 98 showed similar trends. In each case the QS suffered the least endpoint problems and DF without padding suffered the worst endpoint problems. The results clearly demonstrated the superiority of the QS over the other methods of smoothing. If DF is to be used, then the researcher should be sure to digitize at least 10 extra frames at the beginning and end of the data set. Alternately, padding the data set with extrapolated frames reduces, but does not eliminate, the endpoint problems suffered by the DF.

REFERENCES

Hatze, H. (1981). Journal of Biomechanics, 14:13-18.
Pezzack, J.C. et al. (1977). Journal of Biomechanics, 10:377-382.
Smith, G. (1989). Journal of Biomechanics, 22:967-971.
Soudan K, and Dierckx, P. (1979). Journal of Biomechanics, 12:21-26.
Wood, G.A. and Jennings, L.S. (1979). Journal of Biomechanics, 12:477-479.

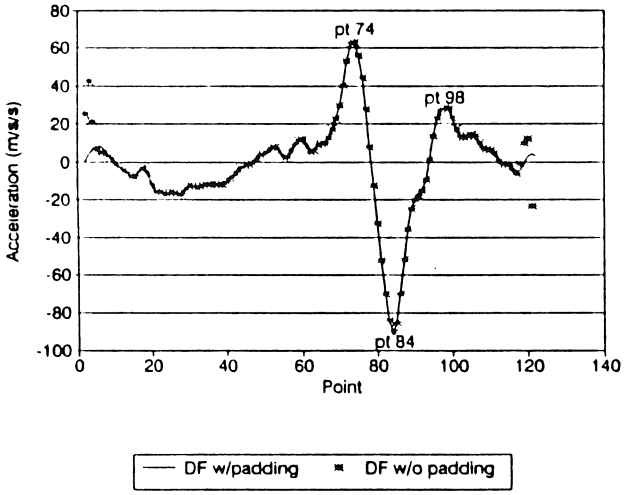


Figure 1. Full Pezzack et al. acceleration curves comparing DF with and without padding.

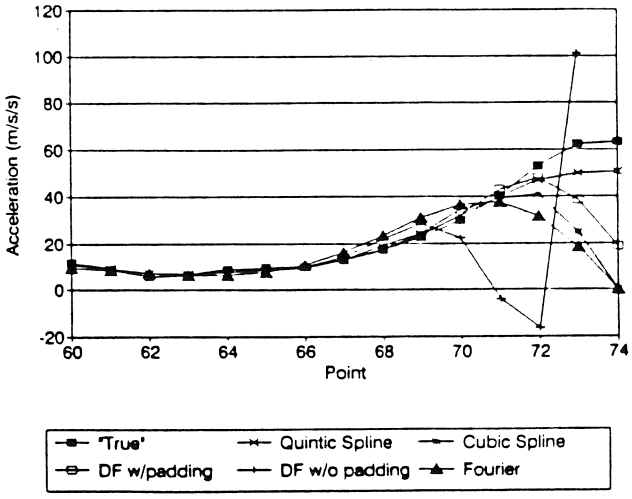


Figure 2. Truncated Pezzack et al. acceleration curves produced by FS, CS, QS, and DF with and without padding.

A COMPARISON OF DLT WITH AND WITHOUT EXTRAPOLATION AND NLT 3-D CINEMATOGRAPHY METHODS

S. McLean, R. Hinrichs, J. DeWitt, G. Heise, A. Hreljac, T. Joganich, T. Marsh, & B. Munkasy
(Exercise and Sport Research Institute - Arizona State University, Tempe, AZ 85287-0404, U.S.A.)

INTRODUCTION

Many human movements such as walking, running and jumping can effectively be analyzed in two dimensions. However, other activities such as throwing or hitting require a three-dimensional (3-D) treatment. For this purpose various methods of 3-D cinematography have been proposed. In choosing one of these methods, problems arise relating to the size of the control object and the ability to effectively use this control object outside of the laboratory. This study compared the accuracy of a standard DLT calibration (Abdel-Aziz & Karara, 1971) to an extrapolated DLT calibration (Wood & Marshall, 1986) and an NLT calibration (Dapena, Harman & Miller, 1982). The results indicated that for the best accuracy the standard DLT should be used with a control object large enough to encompass the entire activity volume. However, if the experimenter is limited by financial or size considerations both the extrapolation and NLT calibrations provided reasonable accuracies. These conclusions became clearer when the accuracy was expressed as a percentage of the activity volume's longest dimension.

REVIEW AND THEORY

Two methods of 3-D cinematography are the Direct Linear Transformation, DLT and the Non-Linear Transformation, NLT. The accuracy of the DLT when used within the limits of its control volume has been shown to be acceptable for 3-D cinematography (Wood & Marshall, 1986; Dapena, 1985; & Shapiro, 1978). Wood & Marshall (1986) caution against the use of an activity volume larger than the defined control volume with the DLT method as this extrapolation would lead to reduced accuracy. With this logic, studying activities covering a large area would require a large, expensive control object. The NLT offered an alternative which was more flexible with respect to the cost and size of the control object. Dapena (1985) showed the DLT and NLT to be comparable in terms of the errors of prediction. The criticism of the NLT centered on increased computational requirements (Dapena, 1985). The purpose of this study was to compare a standard DLT calibration to extrapolated DLT and standard NLT calibrations with respect to their accuracy of prediction to evaluate their use in situations requiring a large activity volume.

PROCEDURES

A large cuboid DLT object of approximately 180 cm x 460 cm x 260 cm (X, Y, Z respectively) with 28 points (surveyed within 1 cm) was used with a two camera video based analysis system. A control volume was defined using the 8 points located at the corners of the control object. Camera parameters based on these 8 control points were used to predict the locations of the remaining 20 non-control points inside the control volume.

A smaller cuboid control volume was defined by 8 points locating the corners of this shape. This control volume was located on one side of the original control object. New camera parameters based on these control points were used to predict the locations of 20 non-control points (4 inside and 16 outside the control volume) which defined the activity volume. This process is known as extrapolation (Wood and Marshall, 1986). The points predicted inside the control volume were referred to as being at 0% extrapolation while the 16 remaining points were divided into three levels of extrapolation (104%, 175%, and 341%) based on the distance extrapolated outside the control volume expressed as a percentage of the activity volume Y-dimension (as this was the direction of extrapolation).

An NLT calibration was conducted on a prescribed activity volume of approximately the same dimensions of the DLT control object. The NLT object consisted of a single pole made from PVC tubing with 6 points marked on it with three known lengths defined. The pole was moved to 14 different vertical and 2 horizontal positions encompassing the activity volume providing 99 control points for calibration. To evaluate the NLT the points of the DLT control object were predicted with the NLT camera parameters.

To compare all three methods the absolute error of prediction was calculated as the difference between the predicted and surveyed locations of the DLT control object points. The absolute errors of prediction for all three methods were normalized by dividing by the activity volume Y-dimension (the longest activity volume dimension) and expressing as a percent.

RESULTS

From the mean absolute errors of prediction (Table 1), the standard DLT provided the best accuracy. As extrapolation grew the absolute errors increased (0.008 m to 0.059 m). The NLT's absolute measures were similar to those for extrapolation at 175%. However, normalizing these results showed that the NLT (0.90%) was more accurate than the extrapolated DLT (1.10%).

Table 1 - Mean Errors of Prediction

3-D method	Y-dimension	Absolute Error	Normalized Error
Large DLT	4.66 m	0.020 m	0.44%
Small DLT	1.06 m	0.008 m	0.72%
104% Extrapolation	2.17 m	0.024 m	1.09%
175% Extrapolation	2.92 m	0.032 m	1.10%
341% Extrapolation	4.66 m	0.059 m	1.26%
NLT	4.10 m	0.037 m	0.90%

DISCUSSION

Comparing these methods based on their absolute terms showed clearly that the standard DLT calibration was the best choice. However, sometimes factors of cost and transportation of the required control object limit the flexibility of this method. Both an NLT calibration and an extrapolation of a smaller, less expensive DLT control object provided viable alternatives which may be more field oriented.

The normalized results showed that both extrapolation of a control volume and the NLT produced usable calibrations. However, the extrapolation errors became much larger at the 341% level. Given a reasonably sized control object it would be unlikely that one would need to extrapolate to this level.

The NLT produced prediction errors which were approximately twice those of the standard DLT. These results conflicted with Dapena (1985) who reported the opposite trend between DLT and NLT (1.5% versus 0.80% error respectively). In each case, however, the values reported here remained relatively small (less than 1%). The flexibility and minimal expenses of this method make a strong argument for using this method with activities which require a large control volume or are studied in the field.

The DLT results represent a "stressful" test for that method. Only 8 control points were used to calibrate the control volume. The accuracy of surveying was less than most commercially available control objects. If more control points were used (Wood and Marshall, 1986, recommended 12-20) and/or a better survey of the control object obtained, then the accuracy would probably increase, strengthening these conclusions.

REFERENCES

Abdel-Aziz, Y.I. & Karara, H.M.; *ASP Symposium on Close Range Photogrammetry*; 1971; 1-18.
Dapena, J.; *et al.*; *J. Biomechanics*; **15**; 11-19; 1982.
Dapena, J.; *J. Biomechanics*; **18**; 1985; 230.
Shapiro, R.; *Research Quarterly*, **49**; 197-205; 1978.
Wood, G.A. & Marshall, R.N.; *J. Biomechanics*; **19**; 781-785; 1986.

THE APPLICATION OF THE INTEGRATED KINEMATIC SEGMENT TO THE STUDY OF HUMAN LOCOMOTION, I - KINEMATICS

Ge Wu and Zvi Ladin
Biomedical Engineering Department and NeuroMuscular Research Center
Boston University, Boston, MA 02215

Introduction

The study of the kinematics of body segments is important for the purpose of objectively and accurately quantifying the motion, and estimating the dynamic variables such as joint forces and moments associated with the motion. However, the complete kinematics of human lower limb during locomotion has not been fully documented. A new approach, called the Integrated Kinematic Segment (IKS) approach is utilized for the study of the three dimensional kinematics of human lower limb during normal walking and running.

Methodology

Three healthy young male subjects were tested. The WATSMART optoelectronic system with two cameras was utilized. Three IKSs, composed of a rigid fixture that includes one triaxial linear accelerometer and one angular rate sensor, and an array of markers for determining the position and orientation in order to dynamically calibrate the accelerometer's output [2] [1], were attached to the foot, shank, and thigh of lower right limb, respectively. A timer was used to monitor the average speed over a distance of $3.66m$. All the kinematic variables were low pass filtered at $100Hz$ and digitized at $200Hz$. All the experiments were done with bare foot. The average speed for normal walking was $4.7km/h$, and for running was $13.84km/h$.

Results and Discussion

The results are presented in three orthogonal directions fixed in the lab coordinate system. The angular velocities and linear accelerations of the shank segment during normal walking and running are shown in figures 1 and 2, respectively. Since the motion was mainly along the anterior direction, the angular velocity about the M-L axis were dominant over other directions for both cases. They both reached maximum peaks at around mid-swing and relatively small values during stance. They also showed some amount of discontinuity at HS (heel strike) due to the HS impact. In both the A-P and vertical directions, the angular velocities for walking and running were small except at HS and TO (toe off).

Comparing normal walking to running, the maximum magnitudes of corresponding components increased substantially. The HS impact was more significant in running than in walking. The A-P angular velocities at TO also showed large changes.

The linear accelerations in the sagittal plane (i.e. the A-P and vertical directions) were dominant. Except at HS, the sagittal plane accelerations for walking showed larger peak values in swing than in stance, whereas the ones for running showed comparable values for both phases. Although the motion was mainly in the sagittal plane, large M-L accelerations were also observed at HS and TO.

Similar to the angular velocity, the maximum values of the linear accelerations showed substantial increase from walking to running (about 4~5 times). In addition, the high frequency HS spikes in running was larger than in walking. The results indicated that the

acceleration measurement is very sensitive to the HS impact and also increases with the increase of speed of the tasks.

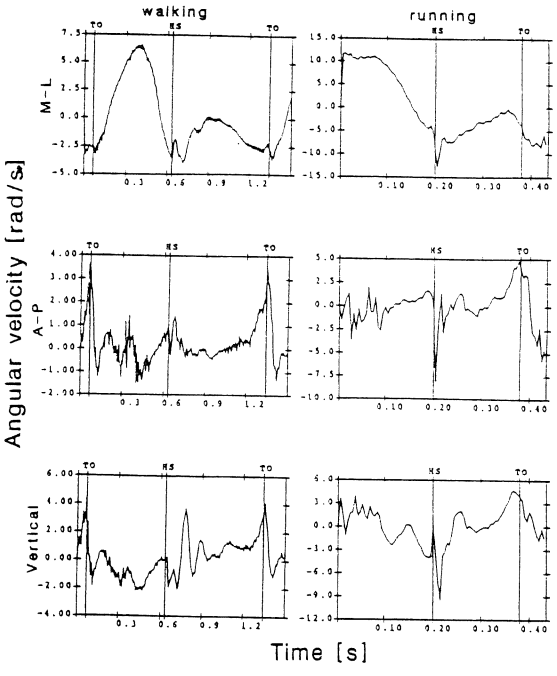


Fig. 1. Angular velocities of shank in normal walking and running

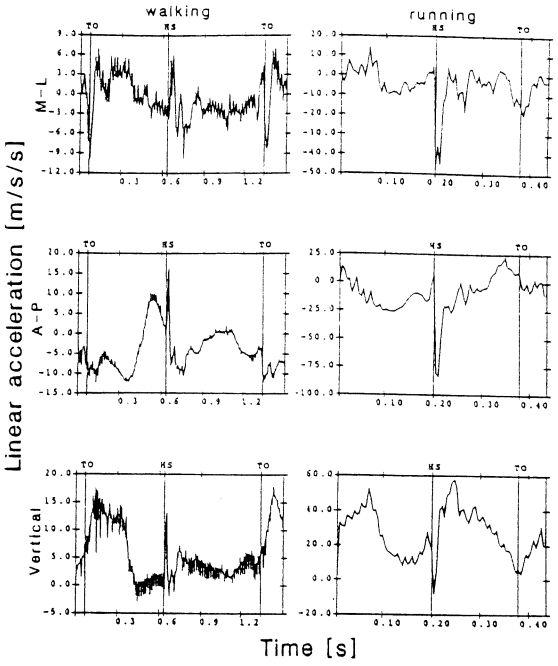


Fig. 2. Linear accelerations at c.m. of shank in normal walking and running

Conclusion

The IKS approach is able to provide high quality measurements of complete segmental kinematics at any time or location during locomotion. Since there is no low-pass filtering associated with it, the frequency range is only limited by the capacity of data collection system.

References

[1] Ladin, Z. and Wu, G. (1991): *Combining position and acceleration measurements for joint force estimation.* J. Biomech., in print

[2] Wu, G. (1991): *Dynamic estimation of human joint loading during locomotion.* Doctoral dissertation, Boston University, Boston, Mass.

Acknowledgement: This work was supported by a National Science Foundation Grant No. EET-8809060 and by a grant from the Whitaker Foundation.

OPTICAL SCANNER CALIBRATION BY OBJECT-IMAGE PLANAR MAPPING AND 3-D OBJECT-SHAPE RECONSTRUCTION ACCURACY

J. Kofman, B. Lindström, A. Karlsson and K. Öberg.
Department of Biomechanics and Orthopaedic Technology
University College of Health and Care
S-551 11, Jönköping, Sweden

INTRODUCTION

Calibration of an optical scanner for stump-shape measurement was achieved by mapping object coordinates in the plane of light to image screen coordinates (X,Y). Curve fitting of the dependent variables X and Y with the true radius (R) and height (Z) values permitted interpolation of (R,Z) values corresponding to integral (X,Y) values. Object-shape reconstruction accuracy was determined from scans of cylinders 30-175 mm in diameter. The average absolute errors were 0.4 mm ± 0.3 mm (SD), 1.4 mm ± 1.0 mm (SD), 0.7 mm ± 0.5 mm (SD), for diameter, circumference and length measurements. The accuracy was more than adequate for stump-shape measurement input to CAD/CAM systems for prosthetic sockets.

REVIEW AND THEORY

Non-contacting laser scanning offers the possibility of accurate stump-shape measurement required for prosthetic CAD/CAM systems (1, 2, 3). Rotation of the laser-light plane and camera about the object reduces the calibration for 3-D object-shape measurement to determination of object-distances within the light plane. This paper presents the calibration of a single-camera optical scanner by object-image planar mapping, and the 3-D object-shape reconstruction and accuracy.

PROCEDURES

A calibration plate was stepped through the light plane (Fig. 1) at constant height (Z) and video camera images were taken for each increment in radius (R) from the center of camera-laser rotation. Bright spots on the illuminated horizontal white strips appeared in the camera image.

Computer screen (X,Y) coordinates of the center of each spot were determined for each image resulting in a final array of 15 x 17 points covering the range R: 0-140 mm and Z: 0-320 mm. Least-squares curve fitting was done with X, Y dependent (having errors) and R, Z independent (true values). An (R,Z) pair for each (X,Y) pixel was obtained by interpolating X and Y for varying R at constant Z, interpolating Z at constant R for Y integral pixel steps, and obtaining the corresponding X. (R,Z) were stored in a lookup table for all integral (X,Y).

For object-shape measurement, the center contour along the laser image is determined first. Least squares smoothing of the curve results in non-integral values of X. Object-shape reconstruction proceeds by interpolation of R and Z between integral X values. Measurements of diameter and circumference were made by scans of a cylinder having diameters ranging 30-150 mm, in 7 vertical positions. Longitudinal measurements were made on grooved cylinders 50 mm, 100 mm, and 175 mm in diameter.

RESULTS AND DISCUSSION

The measurement accuracy is summarized in Table 1. All errors are the differences between measurements made by scanning the object based on the calibration and object-shape reconstruction, and those assumed to be the true values, made by caliper. Diameter and length measurement was limited by the CAD software. The precisions in measuring on the computer screen of 0.2 mm (diameters) and 0.5 mm (lengths), contribute to the variation in these measurements. The measurement accuracy is a slight improvement over other scanners, where accuracies of 1 mm radially and longitudinally (4), 1% circumferentially (2), and 0.76 mm radially and 1.27 mm longitudinally (3) were obtained. The measurement accuracy is more than adequate for the purposes of stump-shape measurement and prosthetic fitting. Whereas conventional and CAD/CAM fitting has succeeded in fitting sockets based on caliper and tape measurement (5), and plaster casting which deform the stump surface, more accurate measurement was found to be required (6). Clinical experience with the present system suggests that the greater accuracy offered by the present scanning method would tend to improve the socket fit and minimize the number of sockets required to achieve a good fit (7).

Calibration by mapping the light-plane coordinates to the screen image accounts for lens distortion, bending of mirrors and camera alignment errors. With raw data filtering the method achieves an accuracy greater than the camera and frame-grabber resolutions. The calibration procedure is simple to carry out for the user.

References

1) Öberg et al., J Prosthet Orthot. 1:139-148, 1989.
2) Fernie et al., Prosthet Orthot Int. 9:12-16, 1985.
3) Walsh et al., J Prosthet Orthot. 1:165-181, 1989.
4) Fernie et al., Prosthet Orthot Int. 8:87-90, 1984.
5) Saunders et al., J Prosthet Orthot. 1:122-130, 1989.
6) Topper et al., Prosthet Orthot Int. 14:136-142, 1990.
7) Kofman et al., Adv. in ECHE X. 475-481, 1990.

Supported by Sahva BS, Denmark; Prosthetic Foundation, Finland; Ortopedfyran, Sweden.

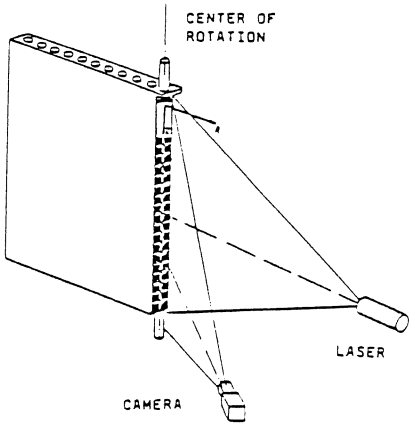


Fig. 1 Calibration setup

Table 1. Measurement errors in object-shape reconstruction

MEASUREMENT	AVERAGE ABSOLUTE ERROR (mm)		S.D. (mm)	RMS ERROR (mm)	MAXIMUM ABSOLUTE ERROR (mm)
DIAMETER (n = 146)	0.4	±	0.3	0.4	1.2
CIRCUMFERENCE (n = 73)	1.4	±	1.0	1.7	4.8
LENGTH (n = 80)	0.7	±	0.5	0.9	1.9

GAIT

VARIANT AND INVARIANT CHARACTERISTICS OF THE HUMAN STEP CYCLE DURING SPEED AND GRADE PERTURBATIONS

Patrick Hannon, David Fukumoto, Scott Fleming, *Rebecca Long, and Angelo Pappas
Departments of Physical Education and Physical Therapy, Northern Arizona University, Flagstaff, Az 86011, USA
*Jefferson Medical College, Department of Neurology, Philadelphia, PA 19107, USA

INTRODUCTION:

The discovery of invariant features common to a class of movements provides evidence for the existence of generalized motor programs. These characteristics of the motor program remain fixed while the variant features change as the demands for movement change (eg. movement speed), (Schmidt, 1985). The finding that certain features for a class of movements such as a walking or running gait remain unchanged while other variables are experimentally manipulated (e.g. movement speed) suggests that specific control mechanisms are operating while other control mechanisms may be ruled out, (Schmidt, 1985). This hypothesis was recently tested in the present study of human gait kinematics on 3 treadmill grades (0%, 10%, 20%) across 4 locomotor speeds (3km/hr, 4km/hr, 6km/hr, and 9km/hr). Kinematic data was collected with a 3 camera Watsmart system for 8 male and female subjects. Stance and swing phases were calculated from the kinematic data combined with Fz data from the AMTI force platform. The results indicated that the relative swing and stance phases during walking were not affected by changes in gait speed. However, grade perturbations from 0% to +10% to +20% resulted in a progressive lengthening of the stance phase and a progressive shortening of the swing phase.

REVIEW AND THEORY:

A locomotor response demands both a spatial organization (muscle selection) and a temporal organization (timing of appropriate muscles). It has been proposed that the control of these features is by a motor program stored within the central nervous system and further that a motor program exists for each class of movements (i.e. motor schema, Schmidt, 1985). Schmidt emphasized that when independent variables such as movement speed are manipulated, perhaps it is the invariances within a class of movements that are most salient (eg., temporal organization of the movement). This search for invariances in order to examine the control of human locomotion in relation to the generalized motor program model was the objective of the present research. Specifically, this study addressed the effect of gait speed changes and treadmill grade changes upon walking and running human locomotion kinematics.

PROCEDURES:

Eight male and female volunteers, age 20-29 participated in this study. Infrared light emitting diodes were applied to the left side #5 metatarsophalangeal juncture, lateral malleolus, lateral epicondyle of the distal femur, and the greater trochanter of the femur (Shapiro, D.D., Zernicke, R.F., Gregor, R.J. and Diestal, J.D., 1981). Recording was at 200 hz. Additionally, foot strikes were determined by placing the base of the treadmill on the AMTI force platform (recording at 800 Hz). The force plate input to the Northern Digital A-D converter simply permitted an on-off stance time recording coincident with the recording of the Watsmart kinematic data. Data reduction permitted the examination of gait

parameters in relation to stance and swing phases through 2 walking speeds (3km/hr and 4km/hr), 2 running speeds (6km/hr and 9km/hr) and 3 treadmill grades (0%, +10%, +20%).

RESULTS AND DISCUSSION:

A factorial anova was used to test the effects of speed and running grade on walking and running gait performance. Walking performance showed a significant grade effect $F = 6.294$, $p < .011$ for both stance and swing, and a non-significant speed effect at 3 km/hr and 4km/hr. Running performance did not show significant differences for speed (6km/hr and 9km/hr) or grade perturbations at 0%, +10%, or +20%. The invariant motor control pattern during changes in speed is in line with Shapiro's (1981) work where subjects increased walking and running speed (1.5-2.0 fold respectively) and the relative time durations within walking or running remained approximately the same. Further, in agreement with the present study, Hannon, Rasmussen and DeRosa (1985) found that kinematic changes in relative swing and stance phases occurred in level, -10% grade, and +10% grade running at (4.47 m/s) in elite male middle distance runners. On the one hand, invariances in kinematics during speed changes provide evidence for a single generalized motor pattern within each gait. The changes in stance and swing during grade changes may be explained by the impulse equation, FT = delta M. A strong first order polynomial test of order (linear) was evident in walking locomotion for both stance, $F = 12.211$, $p < .01$ and swing, $F = 12.211$, $p < .01$. The 0%, +10% and the +20% grades resulted in progressively longer stance phases and progressively shorter swing phases in the walking gait cycle. Although by no means surprising, this experimental result confirms the advantage of a longer time epoch during which a force may be applied to the ground surface resulting in a greater Force x Time impulse. This is particularly important in very steep uphill running where an enormous amount of work must be performed. Unfortunately, only 4 of the 8 subjects were able to complete the protocol at +20% grade at 9 km/hr. The statistical analysis for running locomotion proceeded with 4 cases for the 3 grades, but with much less statistical power perhaps accounting for the nonsignificant grade effects in running.

REFERENCES

Hannon, Patrick R., Rasmussen, Stanley A., and DeRosa, Carl P. (1985) Electromyographic patterns during level inclined treadmill running and their relationship to step cycle measures. Research Quarterly for Exercise and Sport, 56, (4), pp. 334-338.

Schmidt, R.A. (1985) The search for invariance in skilled movement behavior. Research Quarterly for Exercise and Sport, 56(2), pp. 188-200.

Shapiro, D.D., Zernicke, R.F., Gregor, R.J. and Diestal, J.D. (1981) Evidence for generalized motor programs using gait pattern analysis. Journal of Motor Behavior, 13:33-47.

This research study was funded by Integrative Neural Sciences, NSF, Grant # BSN-86-09779.

EFFECTS OF MUSIC AND RHYTHM ON GAIT CHARACTERISTICS OF NORMAL INDIVIDUALS.

Spiros Prassas+ and Michael Thaut*
+Department of Exercise and Sport Science; *Department of Music, Theater and Dance,
Colorado State University, Fort Collins, CO 80523, U.S.A.

The unique emotional benefits of musical experiences for human behavior are well documented by research in music therapy and psychology of music (Unkefer, 1990). It is also documented that music and rhythm have been utilized universally to accompany motor activity (Merriam, 1964). The biomechanics of gait have also been studied extensively, in electromyographic, kinematic, and to a lesser degree, kinetic studies. Although gait movement patterns remain relatively steady until late in life, deterioration occurs due to age, injury and disease. When deterioration occurs, mechanisms to restore normal patterns are desirable. Musical-rhythmic stimuli as a superimposed pacing signal might be one of those mechanisms. We believe that before a study involving individuals with deteriorated or abnormal walking patterns is undertaken to investigate the effects of music and rhythm on their walking patterns, the effects, if any, of this medium on gait characteristics of normal subjects is warranted. Therefore, the purpose of this study was to investigate the impact of music and rhythm on gait kinematic parameters of normal individuals.

Methods

Three female subjects (age 36, 35, and 28 yrs; weight 61.2, 52.2, and 54 kg) participated in the study. The subjects were videotaped with a Panasonic PV-330 60 Hz videocamera while walking at a normal self-selected speed without music and when music adjusted to their walking pattern and rhythm was superimposed. For each subject, a "without-music" and a "with-music" full walking cycle from heel strike (HS) to HS of the same foot was digitized. The raw data was digitally filtered with a cutoff frequency of 6Hz before being submitted to further analysis.

Results and Conclusion

Table one presents the results of the study. Swing time (ST) was defined as the time of the (swinging) limb from toe-off to HS, stance time (ST) was the time of the supporting limb from HS to toe-off (including single and double-support time), stride length (SL) was the

distance from HS to HS of the same foot expressed as a percentage of height, hip and knee joint range of motion (ROM) was the difference in minimum and maximum hip and knee joint angles of the swinging extremity, center of mass (CM) velocity was the average velocity of the CM in the horizontal direction, CM vertical displacement was the difference between its maximum and minimum vertical position, and trunk angle was the

TABLE 1

SELECTIVE KINEMATIC PARAMETERS OF GAIT

	Sub.1		Sub.2		Sub.3	
VARIABLE	NM	M	NM	M	NM	M
Swing Time (SW) (sec)	0.33	0.363	0.33	0.33	0.363	0.363
Stance Time (ST) (sec)	0.594	0.594	0.594	0.627	0.627	0.693
Ratio of SW/ST	0.555	0.611	0.555	0.526	0.578	0.523
Stride Length (SL)	95	95	78	84	88	93
% change in SL	0		+6		+5	
Hip Joint ROM (degrees)	33	30	37	35	39	38
Knee Joint ROM (degrees)	65	66	63	64	64	62
CM velocity (m/sec)	1.73	1.72	1.36	1.47	1.50	1.44
CM vertical displacement (m)	0.028	0.037	0.033	0.042	0.046	0.058
Trunk Angle (degrees)	87.6	86.8	87.8	85.6	91.8	89.5

NM: *without music*; M: *with music*

posterior angle of the segment with the right horizontal. The results indicate that the effects of music and rhythm on kinematic parameters of normal individuals are mostly minimal and non-directional. However, before conclusive remarks regarding the effects of musical-rhythmic stimuli on gait characteristics of normal individuals can be made, a larger sample size should be tested.

References

Merriam, A. (1964). The anthropology of music. Evanston, IL: Northwestern University Press.

Unkefer, R. (1990). Music therapy in the treatment of adults with mental disorders. New York: Schirmer Books.

NEW STRIDE PHASES AND THE DEVELOPMENT OF SPORT SHOE PROTOTYPE TO ASSIST THE CALF MUSCLES DURING HEEL-OFF

Mark R. Pitkin, Ph.D.
Newman Laboratory for Biomechanics and Human Rehabilitation,
Department of Mechanical Engineering,
Massachusetts Institute of Technology, Cambridge, MA 02139

INTRODUCTION: Investigation of a stride stucture was conducted which allowed to select the new stride phases according to the mobility of metatarsal, ankle, and hip joints. It was found that during support phase of walking stride, after sufficient and free mobility of the ankle joint, calf muscles provide almost total fixation of the ankle joint, and therefore the heel takes off and the foot begins a rotation around the metatarsal heads. That rotation happens due to inertia of the whole body, and calf muscles lift the heel indirectly by fixation of the ankle mobility. Recuperating energy stored at that phase, calf muscles also provide a further plantar flexion of the foot, which can be considered a component of the propulsion of the body. The fatigue of calf muscles decreases the level and quality of performances. To assist said muscles and therefore to increase the level and quality of performances, a new sport shoe prototype was developed. An elastic force generator and a means for its positioning were included in an otherwise conventionally constructed sport shoe. Said generator consists of a number of elastic elements which can be mounted to or taken off depending on the wearer's needs.

REVIEW AND THEORY: There are many ways to select the stride phases depending on research purposes [1]. An approach presented in this study is based on results of [2], where a criterion for tuning out of the resonance during walking was found. Due to that investigation it is now possible to use the following phases: 1) Ankle-Phase (AP); 2) Metatarsal-Phase (MP); 3) Metatarsal-Ankle-Hip-Ankle$_2$-Phase ($MAHA_2P$), where a symbol A_2 relates to the ankle of second leg. **Fig.1** is schematic illustration depicting the sequence of said phases.

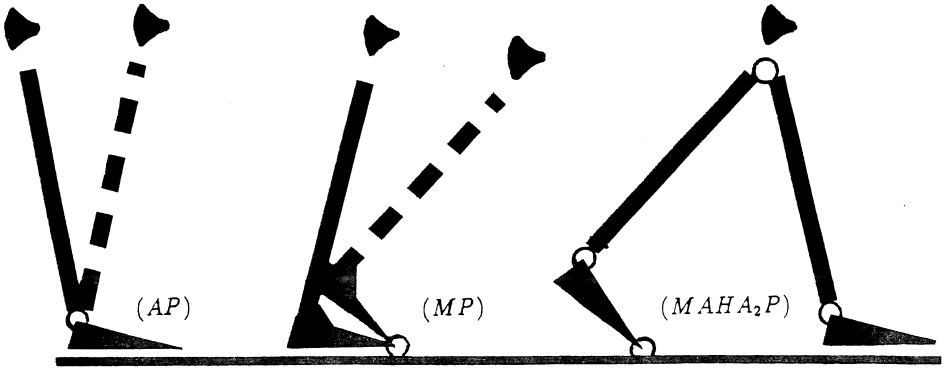


Fig.1 New stride phases: AP; MP; $MAHA_2P$.

The beginning of AP is defined a moment of toes-off of the rear leg, which is not shown on AP and MP, and appears on $MAHA_2P$ as a fore leg with its ankle marked A_2P.

The MP starts at the moment of heel-off, and $MAHA_2P$ starts from the heel-on of the second leg, swinging during AP and MP. In each of these phases a human body is representable by a system of one freedom degree under the mobility restriction in all "extra" joints. The purpose of this study was to create a device for storing energy in MP and releasing it in $MAHA_2P$. Also the device should not affect during AP. A zone of a shoe flexibility taken place at MP and $MAHA_2P$, metatarsal head's area of a sole, was excluded from the consideration since according to [3] its rigidity G had to be limited: $G < pS/h$, where h - width of that area of a sole, S - the square of the sensitive zone of the toes on which the maximal pressure allowed is p.

PROCEDURE: Said device, mounted to the conventional sport shoe was designed to assist calf muscles during MP to fixate ankle and to propel the wearer's body during $MAHA_2P$ by dorsiflection of the foot.

It can be seen from **Fig.2** that a sport shoe 1, having a standard upper 2, is provided with an elastic force generator 3, and frame 4 for its positioning. The lower part of the generator is attached to the counter 5 by the joints 6, forward (parameter δ) to the lower part of generator 3. Activation of the generator by means of elongation of its elastic elements starts from the beginning of MP (see **Fig.1**) simultaneously with the calf muscles, when the frame 4 and elastic elements provide a rectangule with sides δ and l_0.

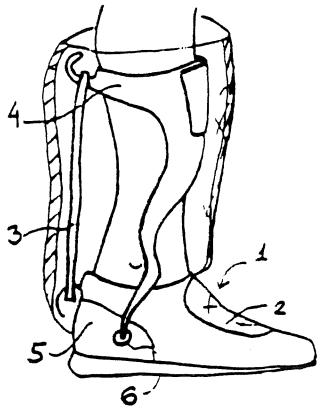


Fig.2

RESULTS AND DISCUSSION: Using linear elastic elements of initial length l_0 an assisting force produced by generator can be estimated by its absolute elongation Δ :

$$\Delta = \sqrt{(\delta - \delta\cos\varphi)^2 + (l_0\cos\varphi + \delta\sin\varphi)^2} - l_0,$$

where φ is a current angle of rotation of the frame 4. During MP angle φ takes its values from an interval $(0^0 - 45^0)$, where 0^0 corresponds to the vertical position of the elastic elements. Matching said elements of different elasticity enables to provide desirable assistant force (torque). The substantial difference from the existing devices is a "zone of silence" during AP, when the assistant force equals to zero, and there is no resistance to the free mobility of the ankle joint. The prototype of a shoe presented allows also to provide an easy triggering of mobility from ankle to metatarsal joint which increases the effectiveness of locomotion.

REFERENCES:

1. Pitkin M.R. *Proc. XII Int. Congress of Biomechanics, UCLA, 336-337,* 1989.
2. Hof A.L., et al. *J.of Biomechanics, 20, 167-178,* 1987.
3. Pitkin M.R. *Proc. The First World Congress of Biomechanics, UCSD, Vol.1, 130,* 1990.

GAIT ANALYSIS IN PATIENTS AFTER VAN NES ROTATIONPLASTY

Catani F.*, Capanna R.**, Benedetti M.G.*, Battistini A.*, Leardini A.*, Cinque G*, Giannini S.*.

* Dept. of Orthopaedic Surgery, Biomechanics Laboratory, Istituto Ortopedico Rizzoli, Bologna, Italy
** Bone Tumor Center, Istituto Ortopedico Rizzoli, Bologna, Italy

INTRODUCTION

The Van Nes rotationplasty is a new procedure used in children with primary bone tumors of the distal part of femur. This procedure permit to convert the ankle joint into a knee joint after en bloc resection of the distal femur with a portion of the tibia and 180 external rotation and fixation of the distal tibial fragment to the femur such that the posteriorly directed foot serves as "pseudo-knee". This pseudo-knee is fit into a below-knee prosthesis with a socket modified with a plantar shelf to permit full weight-bearing at the foot. Gait analysis through kinetic, kinematic and temporo-spatial parameters assesment is the aim of this paper to evaluate functional performance of this patients.

REVIEW AND THEORY

The Van Nes procedure is a worth-wile limb salvage alternative to above knee amputation and to the segmental replacement with a custom knee endoprosthesis in patients with primary bone tumors of distal femur (1,2). The functional advantages of this procedure are the weight-bearing capacity of extremity, the functionally better result of prosthetic management with the ankle joint serving as a knee joint allowing the patient to have an active control of this one and to be able to perform all functional activity of daily life such as run, jump climb stairs and play sports. Moreover, foot proprioceptive afferences are maintaned and complications such as plantar pain are avoided. Psycological problems are related to the aesthetical aspect of lower limb (3,4).

Other investigators described functional performance in this patients compared with above-knee amputes or endoprosthesis, measuring muscle strenght, joint motion, gait parameters and electromyographic activity of the ankle and knee during walking, running and stairs climbing (5)
and oxygen consumption, stride analysis and isometric torque production (6). Their results indicate this procedure as very acceptable from a functional and biomechanical point of view.

PROCEDURES

Ten children underwent to the Van Nes procedure for osteosarcoma (8 pz) or Ewing's sarcoma (2 pz) of the distal femur: these patients -six male and four female (mean age 10.7, range 7.5-14)- were tested in our biomechanical laboratory. The mean follow-up was 23.9 months (range10-50).

Quantitative assessment of gait was obtained:

- with a force -plate (KISTLER) for ground reaction forces;
- with a motion analyser (ELITE) for kinematic (joint angular displacement) and spatial-temporal measurement (stance, swing, stride lenght, cadence, velocity).

Kinetic data (force ground reaction) were discussed as Chao suggests (7).

Data obtained were compared with measurement of a normal population of ten health subject (mean age 29.9) since other investigators have found that a mature gait pattern is developed in children after seven year old (8).

Statistical analysis (T-Test of comparison) was introduced to better evaluate differencies with normal subjects.

RESULTS

Spatial-temporal measurement: significant differences ($P<0.05$) in stride duration, stride lenght, cadence and velocity respect to the normal subject. Alterated stance-swing ratio with increased duration of stance on the sound side ($P<0.05$), more evident in the younger patients and in patients with a shorter follow-up from operation.

Ground reaction forces: significant differences ($P<0.05$) in parameters defining the propulsive phase in the prosthesis side (F3-F6 decreased) and the acceptance phase in the sound side (F1-F5 increased) and in corresponding time in % of stance.

Kinematic assessment: tendence to increase the hip flexion at heel strike and later extension in toe-off phase in the operated side. Quite normal displacement of controlateral limb joints except a certain variability on articolar behaviour of the ankle. The parameters corresponding to joint motion were not submitted to statistical analysis for the lack of normative data. Data discussed are presented in Fig.1-2.

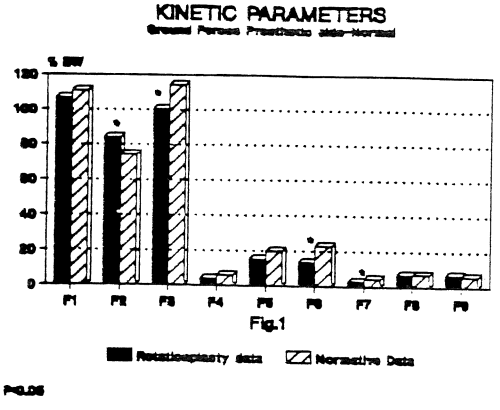


Fig.1

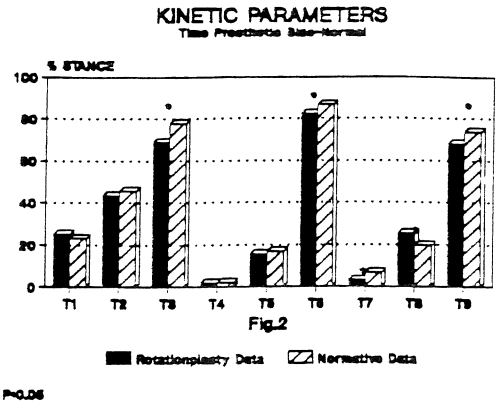


Fig.2

DISCUSSION

According with the other AutorsVan Nes rotationplasty seems to be a valid procedure from a biomechanical-functional perspective, particularly respect to the active control of the "pseudo-knee" that allows a smooth and coordinate gait pattern, slower than normal. Kinematic and kinetic differences are probably due to the rigidity of the ankle and foot joints of the below-knee prosthesis used as a "pivot" during all stance phase , while flexor-exstensor control of the new knee is appropriated for gait function (may be that knee control results difficult in some activities requiring more of 90 degree of flexion) . Hip joint changes in displacement and the lack of a ripetible pattern of movement at the controlateral ankle joint associated to the anticipation of the weight-bearing phase of the sound side are functional to provide a brief and secure support on the "pseudo-knee" during single limb support phase and to permit the forward progression of the artificial foot in the swing phase .

REFERENCES

1 . Van Nes C.P., "Rotationplasty for Congenital Defects of the femur" , J.Bone and Joint Surg. 32-B(1): 12-16, 1950.

2 . Jacobs P.A., "Limb Salvage and rotationplasty for Osteosarcoma in children", Clin.Orthop.,188:217-222, 1985.

3. Kotz R., Salzer M., "Rotationplasty for childhood Osteosarcoma of the distal part of the femur" J.Bone and Joint Surg. 64-A:959-969, Sept.1982.

4. Fixsen J.A. "Rotation-Plasty" J.Bone and Joint Surg. 65-B(5): 529-530,1983.

5. Cammisa F.P., Otis J.C., Lane J.M., Kroll M.A., and Glasser D. "Gait performance after Van Nes tibial rotationplasty in children" , 32nd Annual ORS, New Orleans, Lousiana, Feb.17-20,1986.

6. Murray P. et al. "Functional performance after Tibial Rotationplasty", J of Bone and Joint Surg. Vol.67-A,No.3, March1985.

7. Laughman et al., "Functional Evaluation of the lower extremity using instrumented gait analysis", IEEE, 1983

8. Sutherland et al., "The Development of Mature Walking", Mac Keith Press, 1988.

BONE

STRUCTURAL TRANSFORMATIONS INDISTINGUISHABLE BY POINT-COUNT STEREOLOGY

D.P. Fyhrie, S.J. Hollister*, M.M. Schaffler, J. Kimura

Bone and Joint Center, Henry Ford Hospital
2799 W. Grand Blvd. Detroit, MI 48202 USA
*Orthopaedic Research Laboratories, University of Michigan**

INTRODUCTION It will be shown that the mean intercept length, a stereological measure used for trabecular bone, cannot distinquish certain types of structures which have different material properties.

BACKGROUND Many investigators have used stereology to study the morphology of trabecular bone, including: Whitehouse (1974), Carter and Hayes (1977), Hayes and Snyder (1981), Harrigan and Mann (1984), Cowin (1985), Goldstein et al (1990), Snyder and Hayes (1990). Many investigations had the goal of determining trabecular bone mechanical properties from measurements of the apparent density and mean intercept length. The first of these is closely related to the bone volume fraction, BV/TV, (the total area of hard tissue per unit volume of bone tissue). The second is related to the number of intersections which a grid of parallel lines makes with the bone-marrow interface as a function of grid orientation which is denoted $P_l(\theta)$.

As noted by Philofsky and Hilliard (1969) and more recently by Odgaard et al (1990) the mean intercept measure cannot distinguish between structures which have the same orientation distribution. In 2D this means that if the lines defining the structure on the plane are broken into small segments and moved arbitrarily *without rotation* of any piece, the mean intercept measure is unchanged (See Hilliard; 1962).

METHODS Mechanical models of three idealized trabecular bone models were made which had exactly the same area fraction (BA/TA) and mean intercept measurements, P_l (Fig 1). The models are known to have identical measurements as they were each simple rearrangements of identical circular holes over identical areas. The mechanical properties of these models were estimated using the method of homogenization (Hollister, Fyhrie et al, in press).

RESULTS AND DISCUSSION The Young's modulus varied by 12% and the shear modulus by 21% in these three structures with identical P_l and area fraction. Additional stereological measures are needed to characterize trabecular bone. Consideration of the standard deviation of the intercept lengths in addition to the mean should prove helpful.

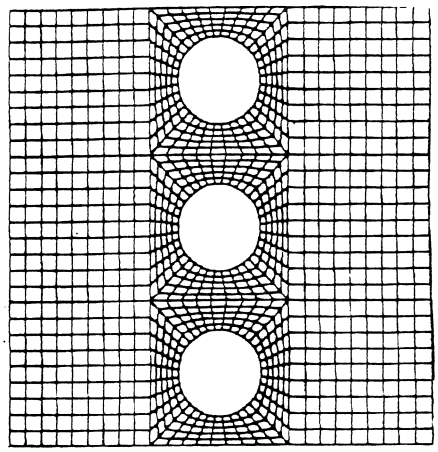
REFERENCES

Carter and Hayes (1977) J Bone and Joint Surg, 59A(7):954-962; Cowin (1985) Mech and Mat, 4:137-147; Goldstein et al (1990) Biomech Diarthrodial Jts (II), Springer-Verlag; Harrigan and Mann (1984) J Mat Sci, 19:761-767; Hayes and Snyder (1981) Amer Soc Mech Eng, 45: 43-68; Hilliard (1962) Trans Metallurg Soc AIME, Vol 224. Hollister, Fyhrie et al (in press), J Biomech; Odgaard et al (1990) 36th Mtg ORS, 53; Philofsky and Hilliard (1969) Q appl Maths, 28, 79-86. Snyder and Hayes (1990) Biomech Diarthrodial Jts (II), Springer-Verlag; Whitehouse (1974) J Micros., 101:153-168;

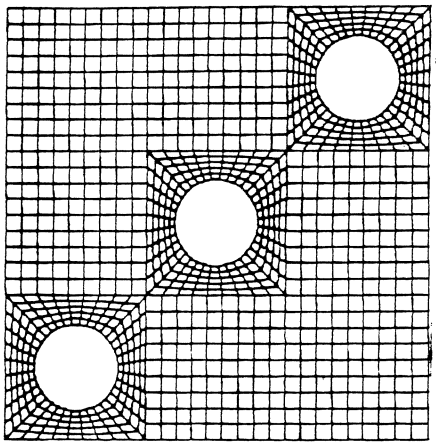
This research was supported in part by The Whitaker Foundation and NIH Grant AR34399.

Figure One: The three panels (A-C) represent the finite element meshes of three homogenization models of idealized trabecular bone structures. The mean intercept measures and area fraction of each are the same, yet the stiffnesses (Young's moduli and Poisson's ratios) are different. In each case the tissue modulus was 5 GPa with a Poisson's ratio of 0.3. Note that the ratios of the largest to smallest Young's Modulus, Shear Modulus and Poisson's ratios are: 1.13, 1.22 and 1.27, respectively.

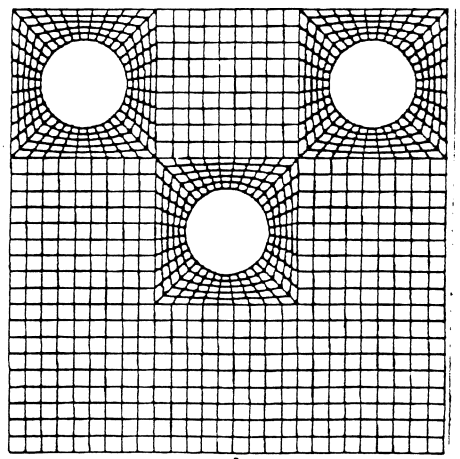
A) $E_x = 3.77GPa$, $E_y = 4.18GPa$, $G_{xy} = 1.25GPa$, $\nu_{xy} = 0.26$, $\nu_{yx} = 0.29$. This model has orthotropic symmetry and has the the largest Young's modulus, smallest shear modulus and smallest Poisson's ratio.



B) $E_x = 3.71GPa$, $E_y = 3.71GPa$, $G_{xy} = 1.52GPa$, $\nu_{xy} = 0.33$, $\nu_{yx} = 0.33$ This model has the largest shear modulus and Poisson's ratios.



C) $E_x = 3.90GPa$, $E_y = 3.74GPa$, $G_{xy} = 1.45GPa$, $\nu_{xy} = 0.31$, $\nu_{yx} = 0.30$ This model is intermediate in all of its properties.



Contact Stress Distributions in Malreduced Intra-articular Distal Radius Fractures

Donald D. Anderson†, Alexander L. Bell*, Michael B. Gaffney*, and Joseph E. Imbriglia‡

†Biomechanics Research Laboratory, Allegheny-Singer Research Institute,
‡Department of Orthopaedic Surgery, Allegheny General Hospital,
320 E. North Ave., Pittsburgh, PA 15212
*Dept. of Orthopaedics, University Health Centers of Pittsburgh,
121 Meyran Ave., Pittsburgh, PA 15213

INTRODUCTION

Radiographically-evident residual articular surface incongruity of the distal radius following intra-articular fracture has been highly correlated with the onset of early osteoarthritis (OA) and, in many cases, a poor clinical outcome.[1,2] A simple in vitro fracture model of the distal radius has been developed to investigate the relationship between the initial degree of surface incongruity and the associated distribution of radiocarpal contact stress.

PROCEDURES

Twelve cadaver forearms were dissected free of all skin, subcutaneous tissues, and muscles, while retaining elbow and wrist ligaments, the radio-ulnar interosseous membrane, and the wrist flexor and extensor tendons. Following dissection, each forearm was mounted in a frame to allow quasi-physiologic static loading of the wrist (elbow flexed 90°, forearm fully pronated) through the hanging of weights from the flexor and extensor tendons (total load 100 N). Following dorsal capsulotomy, a packet of pressure-sensitive film enclosed in a thin layer of plastic was inserted into the radiocarpal joint space to assess the "normal" stress distribution for that wrist.

A simple intra-articular fracture in the distal radius was created with a combination of longitudinal and transverse osteotomy. A proximal segment of the freed fragment was resected and replaced by a family of precision brass shims,[3] allowing controlled fragment reapproximation. The articular surface of the distal radius was examined to assure congruity, and then the fragment was secured with several Kirchner wires. Loading trials for this "anatomically reduced" radius were performed to assure maintained "normal" contact stresses. Progressive intra-articular step-offs of 0.4, 1, 2, and 3 mm were introduced through sequential shim removal. Loading trials were run at each step-off with a packet of pressure-sensitive film placed in the joint space.

The experimental stains were scanned into a computer, and subjected to digital image analysis. The analysis yielded measurements of mean and maximum contact stress as well as engaged contact area. The technique was verified through discrete integration of contact stress distributions to recover the applied load.

RESULTS AND DISCUSSION

The force recovered at anatomical reduction was in close agreement with the applied load. Stains obtained for progressively larger intra-articular step-offs changed from

smoothly rounded toward more oblong patterns, oriented lengthwise along the fracture line, especially in the scaphoid fossa. This spreading began consistently in the 0.4 or 1 mm step-off case, and once a 2 mm step-off was reached, only slight additional changes were observed in the gross appearance of experimental stains. Increased articular step-off was accompanied by only slight increases in the mean stress (Figure 1) and by virtually no change in the maximum stress. There were statistically significant increases in overall contact area associated with increased step-off. During testing, it was observed that with increasing step-off, an increasingly unstable loading configuration existed.

The data obtained suggest that substantially elevated contact stresses are not necessarily associated with simple incongruities of less than 3 mm on the articular surface of the distal radius. Elevated contact stresses associated with the presence of residual surface incongruities is but one mechanism by which the details of stress transfer across the joint could be changed following distal radius fracture. Qualitative observations during laboratory investigation indicate that changes in the proximal carpal row kinematics may accompany irregularities in articular surface geometry.

REFERENCES: (1) Knirk and Jupiter: J Bone Joint Surg (Am) 68:647-59, 1986. (2) Bradway et al.: J Bone Joint Surg (Am) 71:839-47, 1989. (3) Brown et al.: J Orthop Res, 6(6):851-62, 1988.

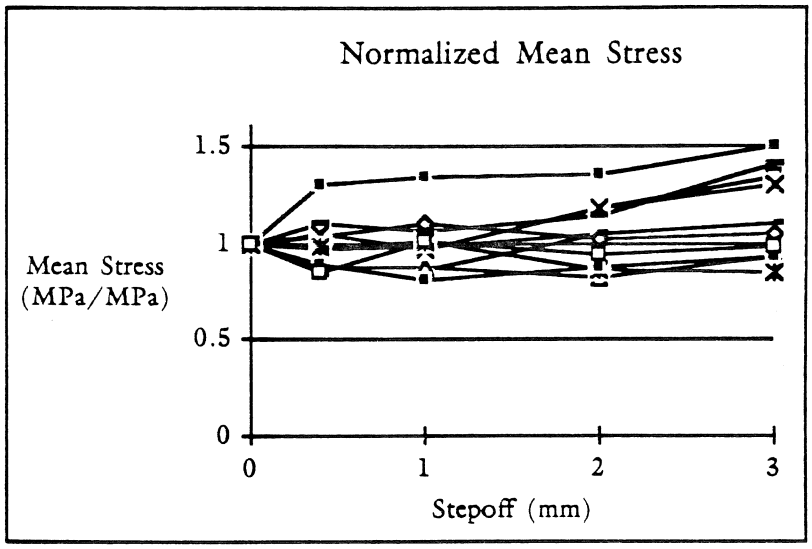


Figure 1. Variation of mean stress with respect to imposed step-off.

NORMAL AND SHEAR STRAIN DISTRIBUTIONS OF THE EQUINE THIRD METACARPAL DURING LOCOMOTION: CHARACTERIZING BONE'S FUNCTIONAL MILIEU

Ted S. Gross, Kenneth J. McLeod, and Clinton T. Rubin
Musculo-Skeletal Research Laboratory, Department of Orthopaedics
State University of New York @ Stony Brook, NY 11794

INTRODUCTION

Deformations induced in the skeleton during functional activity are considered powerful determinants of skeletal morphology. Previous efforts to characterize functionally induced strains have presumed the manner by which the skeleton was loaded, resulting in a potentially inaccurate description of the bone's mechanical environment. In this study, we characterize bone's functional strain milieu without simplifying assumptions of inertial loading. Once defined, these strains, and the loading conditions required to generate them, will serve to further elucidate the relationship between function and form in the skeleton.

REVIEW AND THEORY

Many parameters of the strain milieu have been proposed as the dominant influence of skeletal morphology, including strain rate (1), strain magnitude (2), strain energy density (3), and the strain tensor (4). Unfortunately, until a full characterization of bone's functional strain milieu is completed, the physiologic relevance of these parameters can only be estimated. Recent studies have used multiple site strain gauge attachments to provide critical descriptions of the skeleton's functional strain environment (5,6,7), yet each has relied upon simplifying assumptions regarding the inertial loading of the skeleton to define strains acting upon a given cross-section. In this study, we characterize normal and shear strain and strain energy density (SED) distributions acting upon the equine third metacarpal midshaft during locomotion. By attaching three triple rosette strain gauges around the same transverse plane, and using a combined beam theory and finite element model analysis, a priori inertial loading assumptions were not required to define the strain environment of this cross-section.

METHODOLOGY

Under general halothane anesthesia, three triple element rosette strain gauges were glued to the right third metacarpal midshaft of a five year old thoroughbred. At one day post-op, the horse was run through a range of gaits and speeds on a motorized treadmill while the analog strain gauge data were sampled digitally at 200Hz. Cross-sectional areal properties and rosette locations were determined by CAT scan, and the orientation of the gauges to the long axis of the bone were assessed radiographically. Following the running protocol, the animal was again anesthetized, the gauges were removed, and the animal released to pasture.

A medium speed trot (3.6m/s) was chosen as a representative gait and speed which the animal tended toward in pasture. Digital data from 10 consecutive gait cycles, each comprised of a stance phase and a subsequent swing phase, were averaged to determine a mean gait cycle. Longitudinal normal and shear strains were calculated at each periosteal rosette site (medial, anterior, and lateral cortical surfaces) with respect to a local coordinate system aligned with its z-axis parallel to the long axis of the bone. Normal strain distributions were determined by modeling the metacarpal shaft as a prismatic beam of irregular cross-section subjected to axial loading and bending moments. Shear strains were resolved by modeling the third metacarpal as a prismatic cantilever subjected to end shearing forces and a torsional moment. Equine cortical bone was assumed to be isotropic ($E=18GPa$, $\nu=0.3$), while irregular cross-sectional geometry was approximated by a finite element mesh

consisting of 100 quadrilateral elements. Numerically applied end loading conditions were scaled until predicted strains at the gauge sites matched those measured in vivo. Normal and shear strains at each element center were used to determine SED via the Clapeyron formula ($SED=1/2\tau_{ij}\epsilon_{ij}$).

RESULTS

The distribution of normal strain implied the third metacarpal was loaded in a combination of axial compression and bending, with the neutral axis located in the anterolateral region of the cortex. Peak compressive strains reached -2400$\mu\epsilon$ and maximal tensile strains reached 800$\mu\epsilon$. Shear was a substantial component of the locomotion engendered strain milieu and was non-uniform. The distribution was resolved by a loading state of superimposed end shear and torsion that focused greatest shear in the anteromedial cortex (1500$\mu\epsilon$), while negligible shear strain was demonstrated in portions of the posterior and anteriolateral cortices. The non-uniform distribution of SED reflected the focus of peak normal and shear strains in the medial cortex (figure 1). Peak SED reached 54kPa, while at the same time 28% of the elements in the anterolateral quadrant demonstrated SED to be at least 50x smaller (1.1kPa) than this peak. Normal, shear, and SED distributions remained consistent in orientation throughout the stance phase of gait.

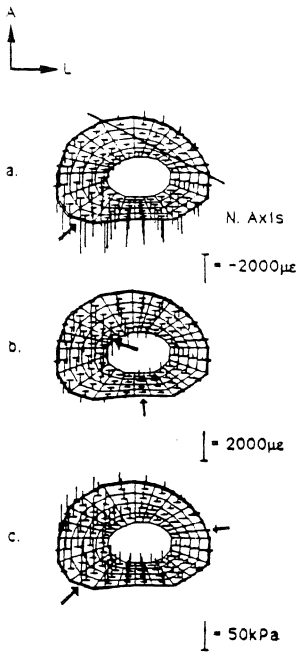


Fig. 1. Distribution of normal strain (a), shear strain (b), and SED (c) at time of peak strain (maximum strains are noted by large arrows, least strains by small arrows).

DISCUSSION

Non-uniform normal and shear strain and SED distributions reflected complex functional loading of the equine third metacarpal in a combination of bending, axial compression, end shearing and torsion. As the distribution of the strain parameters remained consistent throughout the stance phase, specific areas of the cortex were continually subjected to high magnitude strains, while other areas by comparison received only small magnitude strain input. In fact, when SED was summed over the entire gait cycle to yield a measure of total strain input to each site of the cross-section, summed SED varied by over two orders of magnitude across the cross-section. Preliminary data indicate that similar strain distributions are demonstrated at other gaits and speeds in this and other horses (8), suggesting that portions of the cortex are able to maintain their morphology despite minimal strain input. Therefore, successful maintenance of tissue would require that strain information to be spatially integrated, that sites within a given cross-section require vastly different levels of strain information, or that some aspect of the strain milieu other than peak magnitude is the principal determinant of a bone's morphology.

REFERENCES

1. O'Conner et al. (1982), J. Biom., 15:767-781. 2. Frost (1986), Intermediary Organization of the Skeleton. 3. Fyhrie & Carter (1986), J. orthop. Res., 4:304-317. 4. Cowin (1987), J. Biom., 20:1111-1120. 5. Carter et al. (1981), J. Biom., 14:63-70. 6. Rubin & Lanyon (1982), J. Expl. Biol., 101: 187-211. 7. Biewener et al. (1983), J. Zool. Lond., 201:67-82. 8. Gross et al. (1991), Trans. 37th Orthop. Res. Soc., 16:420.

This work supported by NSF EET-8658105, Army DAMD-17-90-Z-0054, and NIH AR40411.

MODAL ANALYSIS OF THE HUMAN TIBIA IN VIVO : DETERMINATION OF THE RESONANT FREQUENCIES AND MODE SHAPES.

G. Lowet, M.C. Hobatho*, M. Cornelissen, J.L. Cunningham°, G. Van der Perre.
Division of Biomechanics, K.U. Leuven, 3001 Leuven, BELGIUM.
*Inserm U305, Hotel Dieu, 31052 Toulouse, FRANCE.
°Biomedical Engineering, University of Durham, Durham, U.K.

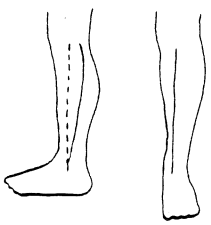
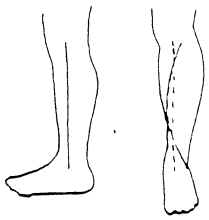
INTRODUCTION : Vibration measurements using the Impulse Frequency Response (IFR)(1) technique were performed on both tibiae of healthy persons in three different laboratories. The interest of such studies is to examine the feasibility of vibrational techniques to monitor fracture healing and to assess bone quality. There was no significant difference between the frequencies of both tibiae. In the frequency range of 0 to 1000 Hz typically three resonant frequencies were found, corresponding to a rigid body mode (I) at 125±16 Hz in the sagittal plane, a single bending mode (II) at 353±51 Hz and a double bending mode (III) at 850±62 Hz, both in the lateral plane. In some cases a resonant frequency of unidentified nature is found between I and II. A single bending mode in the sagittal plane is normally not observed with the applied measurement procedure.

REVIEW AND THEORY : In earlier works, modal analysis revealed the vibration modes of the human tibia in vitro (2) and in situ (cadaveric legs)(3). Applying the free-free conditions, two single and one double bending mode were found in the range of 0 to 1000 Hz in vitro. In situ, these three modes were found again, showing free-free conditions when the leg was positioned on elastic straps. However a fourth vibration mode was observed below the first single bending, being basically a rigid body mode with only minor deflection of the tibia itself.

PROCEDURES : Resonant frequencies of the tibias of 51 persons were measured using the IFR technique. It consists of exciting the tibia by a hammer impact and measuring its response. The force applied during the excitation is measured with a force transducer mounted at the tip of the hammer, while the response is recorded by a light-weight accelerometer, pressed against the tibia. Both signals are fed to a dual channel spectrum analyzer which calculates the transfer function, defined as the ratio of the Fourier-transform (FT) of the acceleration to the FT of the force. The maxima in the transfer function correspond to the resonant frequencies. Using modal analysis software the modal parameters, i.e. resonant frequencies, damping ratio and mode shapes, were determined, Fig. 1.In order to compare the measurements obtained in the three different centres and to study the reproducibility, a specific technical measurement protocol has been used in agreement (4). This protocol defines the accelerometer and excitation direction and position.

RESULTS AND DISCUSSION: Modal analysis revealed three vibration modes for the frequency range involved. The range of frequencies and the mode shapes are summarized in Table 1. The resonant frequencies and mode shapes obtained in vivo are similar to those obtained in situ. However, the second single bending mode was rarely observed in vivo with the actual protocol which was mainly aiming at the measurement of lateral bending modes. In the few cases where it was observed, the frequency for the second bending mode was always higher than that of the first single bending mode. The measurements were performed on relaxed persons, because a study has clearly shown an influence of muscular tension on the resonant frequencies. Below the first single bending frequency, an additional resonance of 267±39 Hz was observed occasionally. This mode is believed to be due to the skin and the mass of the accelerometer, behaving as an independant resonating system. Measurements performed in different centres show a good reproducibility of the IFR technique. As in earlier in vitro experiments a clear relationship was found between resonant frequencies and transversal as well as torsional stiffness, the above results allow to use the same technique for quality control in vivo. This technique is currently applied in a concerted action of the European Community (COMAC-BME) involving 11 different centres and clinically evaluated for monitoring fracture healing and for the assessment of osteoporosis.

Table 1 : Vibration modes in vivo.

Mode type	Rigid body (I)	Single Bending 1 (II)	Double Bending (III)
Direction	Ant-Post	Medio-Lateral	Medio-lateral
Mean ± SD (Hz)	125 ± 16	353 ± 51	850 ± 62
Min/Max (Hz)	97/169	252/474	738/971
Mode Shape			

REFERENCES:
1. Van der Perre G. et al., J. Biomech. Eng.,105:244-248,1983
2. Hobatho M.C. et al.,J. Biomech., in press 1991
3. Cornelissen M. et al., J.Biomech, 20:333-342,1987
4. Van der Perre G., Lowet G., Borgwardt A.(eds)1991, Monitoring of bone quality by vibration and wave propagation techniques, Proceedings of COMAC-BME II.2.6 1989-1990, Leuven, Belgium.

SPINE

ARTICULATIONES ZYGAPOPHYSIALES AND INTERVERTEBRAL DISK: A BIOMECHANICAL GEAR SYSTEM WITH POSITIVE DRIVE.

H. NÄGERL Department of Physics, Univ. of Göttingen.
D. KUBEIN-MEESENBURG Department of Orthodontics, Univ. of Göttingen
J. FANGHÄNEL Institue of Anatomy, Univ. of Greifswald
Germany

Beside the intervertebral disk the art. zygapophysiales connect two adjacent vertebrae. In order to be able to analyze the statics, kinematics, and dynamics of this joint complex we have to take into account the incongruity of the articulating surfaces as the essential functional constuctional feature. In a main functional plane the function of one single joint can be depicted by an open dimeric link chain (1).

In the lumbal region the lateral-convex articulating surfaces of the upper vertebra encompass the two medial-concave ones of the lower vertebra.

In the *horizontal plane* this arrangement represents a closed four-bar chain (link quadrangle). Its movable couple is the upper vertebra, its fixed support the lower one (2). Because of the positive drive (the couple shows an univariant movement) the paths of motion of all upper vertebra's points (in relation to the fixed lower vertebra) are determined by the morphology of the articulating surfaces. Along with that the location and the shape of the centrode can be derived by this morphology (fig. 1 and 2). At first approximation, the intervertebral disk does not affect the paths of this motion. It only determines the amplitude of motion. Fig. 3 shows the relation between statics and kinematics on principle in the horizontal plane.

In the *coronal-frontal plane* the interplay of the two art. zygapophysiales also engenders a link quadrangle. The lengths of its four links are selected by nature so that a plane movement parallel to the frontal plane is impossible: The coronal-frontal gear system is immovable. Therefore, a lateral bending of the trunk is only possible in context with an accompanying movement of the upper vertebra in the horizontal plane.

In the *vertical-sagittal plane* the structure of motion is determined by only one open dimeric link chain. In contrast to the two other functional planes the location of the momentary rotational axis depends on the geometry of the force system in addition to the morphology of the joints. The law of this relation is given by the *theorem of reciprocity of synarthroses* (3).

This complex interplay between muscles, joints and the intervertebral disk (and the ligaments) and the functional principle of the constrained movement (only *one* degree of freedom) will be exemplified by experiments on models in the course of this lecture. Measurements confirm the theory. The in-vivo-measurements of Gregersen and Lucas (4) structurally appear in a new and different light.

References.

(1) Kubein-Meesenburg, D., Nägerl, H. and Fanghänel, J.:
Elements of a General Theory of Joints. 1. Basic Kinematic and Static Function of Diathroses. Anat. Anz., Jena, 170, 301-308 (1990).
(2) Kubein-Meesenburg D, Nägerl H, Fanghänel J:
Elements of a General Theory of Joints. 4. Coupled Joints as simple gear systems. Anat. Anz., Jena 172 (1991) in press.

(3) Nägerl, H., D. Kubein-Messenburg and J. Fanghänel:
Elements of a General Theory of Joints. 2. Introduction into a Theory of Synarthrosis. Anat. Anz., Jena, 171 (1990) 323-333.
(4) Gregersen G.G. and D.B. Lucas:
An In Vivo Study of the Axial Rotation of the Thoracolumbar Spine. J. of Bone and joint surgery 49A, (1967), p. 247 -262.

Fig. 1: Dimeric link chain
a) The guidance of a art. zygapophysialis is given by a concavity-convexity. The contours that glide along each other possess dissimilar radii and centers of curvature.
b) Pertinent dimeric link chain: in the horizontal plane every single art. zygapophysialis can be interpreted as a diaxial link chain that links the upper and lower vertebrae up with each other.

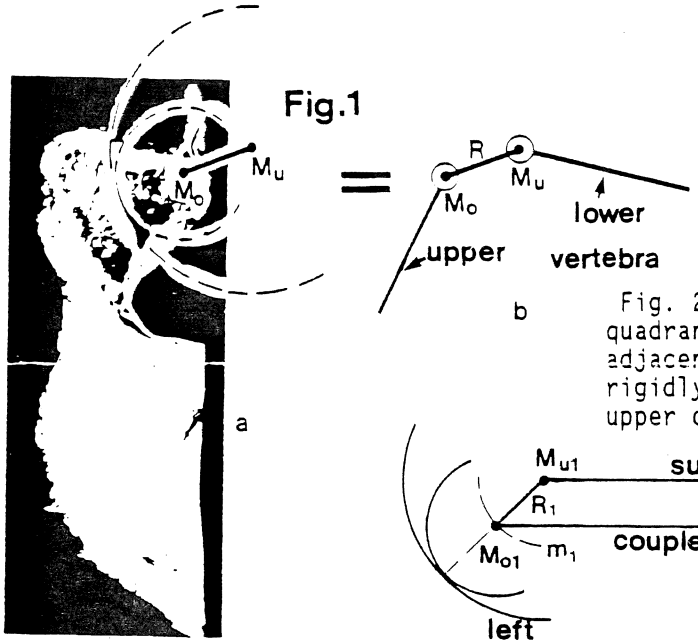


Fig. 2: Kinematically constrained link quadrangle of two art. zygapophysiales of adjacent vertebrae. The lower vertebra is rigidly attached to the fixed support, the upper one to the movable couple. The two functional extremities of the couple (M_{01} and M_{02}) run along practically circular paths (m_1, m_2)in relation to the support. Since in the course of movement the length of the couple remains constant the position of M_{01} gives the position of M_{02} and vice versa: Kinematically constrained movement.

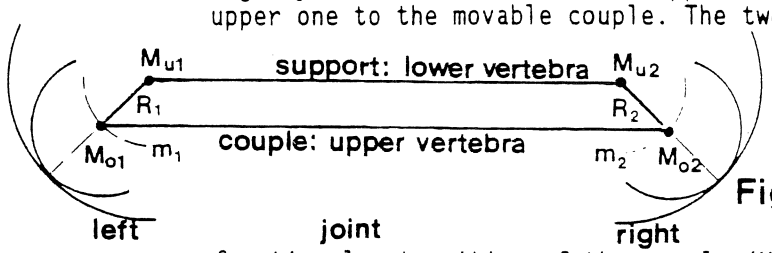


Fig. 2

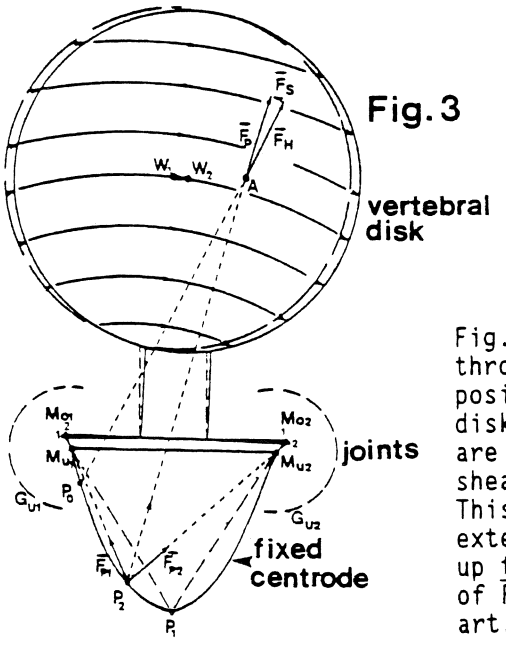


Fig. 3: A horizontal force $\bar{F}_H$, that does not run through the rotational center P_1 of the standard position, results in a shearing of the vertebral disk. Since the corresponding rotational centers are given by the fixed centrode the points of the sheared elastic body follow almost circular paths. This lateral shearing summarily engenders an external force $\bar{F}_S$ onto the upper vertebra. It adds up to $\bar{F}_H$ and yields $\bar{F}_P$. $\bar{F}_{P1}$ and $\bar{F}_{P2}$, the components of $\bar{F}_P$, merely load the articulating surfaces of the art. zygapophysiales

THE EFFECT OF A FOOTBALL HELMET ACCESSORY ON IMPACT CHARACTERISTICS AND MOMENTS OF FORCE AT THE NECK

Gary D. Heise and Richard C. Nelson, Ph.D.
Biomechanics Laboratory
The Pennsylvania State University, University Park, PA 16802

INTRODUCTION

Standard shock attenuation tests at three temperature conditions (ASTM, 1989) were performed on a football helmet with and without an outer polyurethane helmet accessory to determine if peak acceleration during impact was reduced with the accessory. Tests were also performed with an instrumented anthropometric test dummy (ATD) impacting a solid barrier set at various angles to determine if moments at the neck were different from the helmet-only condition because of the deformable polyurethane on the outside of the helmet with the introduction of the helmet accessory. Results from a forehead impact location indicated that shock attenuation characteristics were significantly improved (i.e., peak acceleration reduced) with the addition of the helmet accessory. However, all data collected were within ASTM specifications (ASTM, 1989a). Moments at the neck resulting from impacts on the crown of the head showed more inconclusive results. Peak moments in the positive direction (expected movement based on angle of impact) about the anterior-posterior axis were slightly higher when the helmet accessory was used, however some conditions displayed higher moments in the opposite direction.

REVIEW AND THEORY

Severe head and neck injuries from football impacts have become an increasing concern among researchers and physicians (Torg et al., 1990). It has been suggested that the frequency of concussive-type injuries may be reduced with advances in helmet design. In an effort to reduce the number and severity of concussive and other impact-related injuries in football, and to help extend the life of the standard hard-shell football helmet, a polyurethane pad that conforms and attaches to the outside of a standard football helmet has been designed and manufactured (Protective Sports Equipment Inc., Erie, PA). The purpose of this experiment was twofold: 1. determine if the shock attenuation characteristics of the helmet and accessory is better than the helmet alone; and 2. determine if the moments of force at the neck are increased because of the deformable nature of the accessory material.

PROCEDURES

Standard shock attenuation tests were performed in accordance with The American Society for Testing and Materials procedures (ASTM, 1989). Impact tests were performed under three different temperature incubation conditions: Ambient (21 °C), High (50 °C), and Low (-18 °C). Experimental conditions of protection included helmet only and helmet with accessory. Results are based on data from frontal impacts only (forehead position) and the average of three impacts is reported. Neck moment data were collected using a system developed by biomechanists at the University of Waterloo in Ontario (Bishop & Wells, 1990). An ATD (Hybrid III head and neck, Humanoid Systems, CA) is propelled in free flight (1.8 $m \cdot s^{-1}$) to strike a solid barrier which can be set at various angles. A six channel transducer measures three orthogonal forces and the moments of force about the atlanto-occipital junction of the dummy. All impact locations were at the crown of the head. Three angles of impact were used (90°, 70°,and 45°), and to simulate the materials impacted in game situations, a piece of artificial turf or a jersey/thigh pad combination was attached to the barrier for the latter two angle conditions. Moments about the anterior-posterior axis are reported because they were the only ones of consequence.

RESULTS AND DISCUSSION

Results from the shock attenuation tests are shown in Figure 1. For each incubation temperature condition the helmet with the accessory showed significantly lower peak acceleration values. Although every helmet and helmet-accessory condition satisfies ASTM specifications, the helmet-accessory condition clearly provides more shock attenuation. This effect is most clearly demonstrated for the cold incubation condition. Although these results are statistically significant, the practical significance in terms of reducing injury and extending helmet life remains unknown. A comprehensive field test is required to address these questions. The results obtained from the ATD concerning neck compressive forces and moments were less conclusive. With an impact angle of 90°, the compressive forces measured at the ATD were 4800 N for the helmet condition and 4300 N for the helmet-accessory condition. This is in agreement with the shock attenuation test results, however the effect appears not as great. The neck moment data for angles of impact other than 90° are shown in Figure 2. The maximum, positive moment of force about the anterior-posterior axis is shown in the figure and represents the moment at impact. Although it appears that higher moments occur for the helmet-accessory condition, in some cases the maximum moment was negative and occurred after impact. For example, this occurred at the 70° position for the helmet condition when artificial turf was impacted. A negative moment of 26 N·m was seen nearly 50 ms after the positive peak. In summary, shock attenuation characteristics of the helmet and accessory show statistically significant improvement compared to the helmet alone, yet the use of the helmet accessory showed no conclusive effect on the moments of force at the neck.

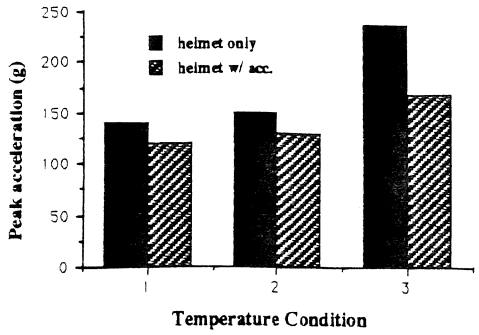


Figure 1. Mean peak acceleration data (1-ambient, 2-high, 3-low)

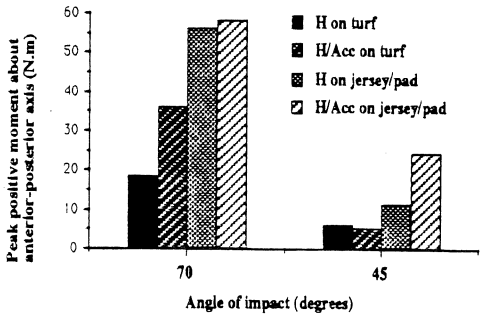


Figure 2. Peak moment data

This project is funded through the Ben Franklin Partnership Program in conjunction with Protective Sports Equipment, Inc. The authors acknowledge P.J. Bishop and Weijia Lu at the University of Waterloo for their assistance with the neck moment data collection.

REFERENCES

ASTM Standard (1989). F 429 Standard test method for shock-attenuation characteristics of protective headgear for football. Annual Book of ASTM Standards, Vol. 15.07.

ASTM Standard (1989a). F 717 Standard specification fo· football helmets. Annual Book of ASTM Standards, Vol. 15.07.

Bishop, P.J. & Wells, R.P. (1990). The inappropriateness of helmet drop tests in assessing neck protection in head-first impacts. Am. J. of Sports Med., 18, 201-205.

Torg, J.S. et al. (1990). The epidemiologic, pathologic, biomechanical, and cinematographic analysis of football-induced cervical spine truama. Am. J. of Sports Med., 18, 50-57.

SIMULATION OF BACK MOTION

Komattu, AV*; Crane, CD*; Wheeler, DL†; Miller, GJ†
Departments of Mechanical Engineering* and Orthopaedic Surgery†
University of Florida, Box J246 JHMHC, Gainesville, FL 32610

INTRODUCTION:

The objective of this work was to develop a three-dimensional (3-D) model which could accurately duplicate the motion of the back. Using this model, forces and torques acting on each spinal link during 3-D lifting tasks could then be calculated. Four marker triads consisting of 3 non-collinear reflective spheres were attached to a subject's back allowing the sections of the spine spanning the marker triads to be tracked as rigid bodies moving through space. Kinematic analysis using three different techniques were evaluated. The optimal technique incorporated a kinematic chain of six degrees of freedom between each marker triads. A closed form kinematic solution was used to determine values for the sliding and rotational freedoms at each instant in time. The resulting translational and rotational displacements were smoothed using a least squares algorithm. The smoothed data was then used to predict the instantaneous screw acting between each marker triad. The results indicate the motion of the back is effectively modeled in three dimensions using instantaneous screw motion.

PROCEDURES:

Motion data was collected by placing four reflective marker triads on the back. The movement of the markers was tracked by a video based motion analysis system (Motion Analysis, Inc.; Santa Rosa, CA) which could determine marker positions every sixtieth of a second. The plane defined by the marker triad is determined using the positional data of the spheres obtained from video based motion analysis. For each marker triad a local coordinate system is defined with respect to the ground coordinate system. The first axis is the normal to the plane formed by the marker triad. The second axis lies on this plane and is the unit vector formed by joining two of the spheres. The third axis is perpendicular to the above two axes creating a "right-handed" coordinate system.

The following three modeling techniques were implemented with varying degree of success:

(1) **Screw Theory** - This model was developed by determining the instantaneous screw upon which each of the four marker triads moved with respect to the ground coordinate system. These screws could then be subtracted to determine the instantaneous motion screws between the first and second marker triads, the second and third marker triads, and the third and fourth marker triads. Though, screw theory offers an optimal kinematic model for instantaneous back motion, this technique was overly sensitive to noise in the positional measurements.

(2) **Manipulator/Optimization** - This technique was employed by using a general six degree of freedom kinematic chain placed between marker triads. Numerical optimization was used to determine the best fit values for the link lengths, offset lengths, twist angles, and joint angles. Convergence of the optimization process was difficult due to the large number of design variables and the complexity of the objective function.

(3) **Manipulator/Closed Form/Screw Theory** - This technique implemented unique six degree of freedom kinematic chains for each segment. These chains were comprised of three links serially connected by cylindrical joints with no offset lengths and twist angles of 90°. A closed form kinematic solution [1] was used to determine values for the 3 sliding and 3 rotational freedoms at each instant in time. The resulting translational and rotational displacements were smoothed as a function of time so that the smoothed sliding distances and rotational angles could then be used to calculate the net instantaneous screw between successive marker triads. Through this process of performing a closed formed analysis followed by data smoothing and instantaneous screw calculation, an accurate three dimensional model of the back was obtained.

RESULTS AND DISCUSSION:

The models obtained using the Screw Theory and Manipulator/Optimization techniques were inadequate to define 3-D back motion due to noise sensitivity and convergence problems respectively. Therefore, further development of these techniques were not pursued. The multifaceted Manipulator/Closed Form/Screw Theory technique provided an good 3-D kinematic model for back motion. This technique allowed relative screws between each pair of marker triads to move "smoothly" as a function of time. Smooth and continuous changes in angular velocity, pitch, direction of the screw axis, and position of the screw in space were produced. The application of the screw theorem after the decoupling and smoothing of the raw motion data significantly improved the surface generated by the instantaneous screws. To aid in visualization of the motion of the spinal segments of the back and the location of the relative instantaneous screws in 3-D an IRIS 4D-310 vgx workstation (Silicon Graphics, Inc.; Mountain View, CA) has been used. The Manipulator/Closed Form/Screw Theory technique is currently being used to calculate the forces and torques acting on the spinal segments during 3-D work tasks.

REFERENCES:

[1] Duffy, J; Analysis of Mechanisms and Robot Manipulators, John Wiley, New York, 1980

ACKNOWLEDGEMENT: CDC/NIOSH grant #1-R03-OH02684-01

BIOMECHANICS OF HUMAN THORACIC SPINE LAMINECTOMY

Narayan Yoganandan, PhD, Frank Pintar, PhD,
Dennis Maiman, MD, PhD, and Gregory Bennet* MD

Department of Neurosurgery, Medical College of Wisconsin, Milwaukee, WI 53226
Department of Veterans Affairs Medical Center, Milwaukee, WI 53295
*Department of Neurosurgery, School of Medical and Biomedical Sciences, Buffalo, NY

ABSTRACT

Fresh human cadaveric thoracic columns were used to study the biomechanical alterations in the strength and stability due to laminectomy. Compression-flexion mode of loading was applied. Force, deflection, and kinematic data were gathered as a function of time. The specimens were studied under intact conditions as well as under iatrogenically altered conditions simulating two level laminectomies. The biomechanical response indicated nonlinear and sigmoidal characteristics. Mean failure forces and deformations for the intact column were 2.2 kN and 9.8 mm, respectively. For laminectomized specimens, mean failure forces were 1.2 kN with associated displacements of 9.1 mm. The stiffness and energy capacities of the laminectomized specimens were also lower compared to the intact columns. Failure deformations for both the structures were not statistically significant representing deformation sensitivity characteristics of the thoracic structure.

INTRODUCTION

It is well known in engineering mechanics that removal of a certain portion in a structure leads to its decreased load carrying capacity as well as increased localized stresses under a given external force. In columns, it may to local buckling and a reduction in the buckling load. In beam columns, results may even be more pronounced. The human thoracic spine can be considered as a beam-column as it resists both axial and eccentric forces under physiologic environments. It is prudent to expect that the excision of the lamina which is routinely performed in spinal operative procedures results in a decreased strength of the vertebrae inducing additional stresses on the column. Excision of the lamina is done in a variety of spinal treatments including herniated disc disease, spondylosis, ossification of the posterior longitudinal ligament, spinal cord tumors, and spinal stenosis. Although results from many clinical trials have been reported, biomechanical quantifications in the changes due to laminectomy in a controlled laboratory environment have not been completely addressed. The present study was therefore, conducted to determine the biomechanical alterations of the human thoracic spine due to laminectomy under compression-flexion loads.

MATERIALS AND METHODS

Fifteen fresh human cadavers were used. The mean age, height, and weight were 67 years, 172 cm, and 72 kg, respectively. All studies were conducted in a hospital environment. The subjects used in the study were determined to be free of any spinal disease based on medical history and pretest roentgenographic evaluation. Thoracolumbar columns from T11 to L1 levels were isolated and fixed in a steel ring at the superior and inferior ends with polymethyl-methacrylate. The specimens were placed on a custom designed electrohydraulic testing device via an x-y cross table. The upper end of the column was attached to the piston of the testing device so that the applied load was anterior to the specimen to induce compression-flexion forces. Retroreflective targets were inserted into the thoracolumbar column to monitor the localized spine motions. Two to four targets in each vertebral body, one target in each facet column, and one target in the posterior aspect of the spinous process were used.

Seven specimens were loaded to failure with the custom designed electrohydraulic testing device under quasistatic force application. Failure was identified as a decrease in the applied force with a corresponding increase in the compressive deflection. At this load level, the specimens were radiographed to document injury. The remaining eight specimens were studied as laminectomized (two-level laminectomy at midheight) columns. This procedure was adopted so that at the region of maximum moment the specimen was laminectomized. The laminectomized specimens were also tested to failure in the manner described above.

Biomechanical data were collected using the force gauge and a linear variable differential transformer attached to the piston using digital data acquisition procedures. The load and displacement signals were transformed to obtain the mechanical load-deflection response. The failure load, deflection, stiffness, and energy absorbing characteristics were computed. Stiffness was defined as the slope in the most linear part of the load-deflection curve. Energy was defined as the integral of the load-deflection curve up to the failure point. The biomechanical data were compared between normal and laminectomized specimens. The localized kinematic data of the retroreflective targets as a function of time were obtained using a motion analysis system. The path of each retroreflective target was stored on a video tape and later extracted digitally for further computational purposes such as relative motion of one target with respect to another target. The motion analysis system uses the principle of relative optical density for digital tracking and computation. Other biomechanical studies have successfully used the motion analysis technique for analyzing the localized kinematics of the segmented cervical spine and total column under physiologic as well as traumatic loading. Paired, student T-tests were conducted to determine the significance levels of the alterations in the localized motion of the spinal components before and after laminectomy.

RESULTS AND DISCUSSION

The biomechanical force-deflection responses demonstrated non-linear and sigmoidal characteristics typical of some biological materials. Localized motion analysis indicated that the intact columns demonstrated failure deformations of the spinal elements (e.g., vertebral body) at mid-superior portions of the spine. In contrast, laminectomized specimens exhibited failure deformations directly at the superior level of laminectomy. The mean failure forces and deformations for the intact columns were 2.2 kN (± 810) and 9.8 mm (± 2.6), respectively. At these forces, compressive fractures of the vertebral body followed by distractions of the posterior elements occurred. The mechanism of injury was consistent with the compression-flexion mode of loading. In laminectomized specimens, mean failure forces of 1.2 kN (± 282) were associated with displacements of 9.1 mm (± 3.8) representing an increase in the flexibility characteristics. Distraction of the posterior elements followed by anterior compressions occurred in these iatrogenically altered specimens. Failures routinely occurred proximal to the laminectomized level indicating instability. The mean stiffness and energy absorbing capacities of the laminectomized preparations were 202.6 N/mm and 5.02 J, respectively. In contrast, these values for the intact columns were 358.77 N/mm and 11.48 J, respectively. The decrease in the failure force ($P < 0.01$), stiffness ($P < 0.025$), and energy ($P < 0.025$) absorption characteristics for the injured columns were statistically significant. Failure deformations however, were not statistically significant. Consequently, it can be concluded that the structure irrespective of the iatrogenic alteration is deformation sensitive.

ACKNOWLEDGMENT

This research was supported in part by PHS CDC Grants R49CCR703640, R49CCR502508 and Department of Veterans Affairs Medical Center Research Funds.

A PERSONALIZED FINITE ELEMENT MODEL FOR THE STUDY OF BOSTON BRACE CORRECTION IN IDIOPATHIC SCOLIOSIS

Aubin C.-É.[1], Dansereau J.[1,2], Labelle H.[2]

1- Dept. of Mech. Eng., École Polytechnique, P.O. Box 6079, Station "A", Montréal, Québec, Canada, H3C 3A7
2- Hôpital Sainte-Justine, Montréal, Québec, Canada, H3T 1C4

INTRODUCTION: Non-invasive treatment of adolescent idiopathic scoliosis is currently made by orthosis such as the Boston brace. However, little is known about the biomechanical impact of this treatment. A biomechanical model was developed to investigate the immediate effect of the Boston brace on the spine and rib cage of adolescent scoliotic patients. Several studies[1,2] reported that costo-vertebral (CV) and costo-transverse (CT) joints play a major role in the mechanical behavior of the thorax. The finite element model presented in this paper is an improvement of the model developed by Stokes and Laible[2] and incorporates several modifications specifically concerning the geometrical and mechanical properties of CV and CT joints. Preliminary results of simulated brace forces applied on a scoliotic thorax are presented in this paper.

METHODS: The input geometry to the model was taken from stereoradiographic reconstructions[3,4] of the spine and rib cage of an idiopathic scoliotic patient (12 year old female with a lumbar curve of 37° and a thoracic curve of 32°). From this geometry, a parametric model incorporating data from published morphologic studies[5,6,7] was constructed. The nodal points were then taken from this parametric model. Each thoracic and lumbar vertebra was defined respectively by 11 and 7 nodes. Each rib (except the "floating ribs") was represented by 12 nodes (10 on the bony part and 2 on the cartilage).

The vertebrae were considered as rigid bony elements. Intercostal ligaments (modelled in a crossed pattern between adjacent ribs) and costo-vertebral ligaments were represented by truss elements. Muscle activity was not considered into the model. The intervertebral joints were modelled by different stiffness matrix elements. The sternum was represented by 14 three-nodes plate elements. The elastic and cross-sectional properties were obtained from published measurements[8,9,10]. The boundary conditions were defined in such a way that L_5 was completely constrained in translation and rotation. Brace forces used as input into the finite element model were obtained from pressure measurements made on the same scoliotic patient using new thin polymeric sensors[11].

In this preliminary study, mechanical linear behavior was assumed. The model composed of 428 nodes was analyzed by the Algor finite element package (*Algor SuperSap, Algor Interactive Systems Inc*, Pittsburgh PA). A post-processor was developed to visualize solutions obtained from the finite element model and to compare the deformed model to the reconstructed geometry of the same patient wearing her brace. Spinal and rib cage geometrical indices such as computed Cobb angles, vertebral body 3-D distance differences, apex vertebral axial rotation[12], posterior rib rotation (rib hump) and curvature (rib deformation) as well as the frontal and sagittal rib angulations were evaluated for both geometries.

RESULTS AND DISCUSSION: Figure 1 shows spinal shape differences between the deformed model and the geometry of the patient wearing her brace. Table 1 gives the numerical differences between the indices evaluated on the compared geometries. From these results it can be observed that the concordance of the two geometries supports the modelling method except sagittally on the upper part of the thorax. This can be explained by the fact that there was no constraint applied at T_1 because it has been reported in a clinical study of 26 idiopathic scoliosis patients[13] that there was a significant change of the balance (anteriorly) in the sagittal plane. However, this model shows that some other factors or mechanisms such as muscle force activity or intra abdominal pressure might participate to the stability of the whole thorax. Further analysis are necessary to completely validate the model.

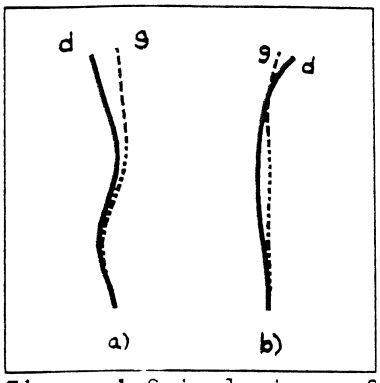


Figure 1-Spinal views of the deformed model (d) superimposed to the geometry (g) of the patient wearing her brace.
a) PA view
b) Lateral view

Table 1 - Difference in geometrical indices

Geometrical indices	Difference	
1- Lumbar Cobb angle (°)	1,3	
2- Thoracic Cobb angle (°)	8,3	
3- 3-D mean distance between vertebral body centers (mm)	14,7 ± 7,0	
4- Apex vertebral rotation (°):	T_9	L_3
- sagittal:	5,4	3,2
- axial:	2,9	6,4
- frontal:	8,1	3,6
5- Apex post. rib rot.(rib hump)(°)	0,5	
6- Apex rib post. curvature (mm^{-1})	Right: 0.0094;	Left: 0,0041
7- Apex rib angulation (°):	Right side	Left side
- frontal rib angle:	17,1	3,7
- sagittal rib angle:	7,2	3,8

REFERENCES: 1) ANDRIACCHI, T. et al., J. Biomech., 7:497, 1974. 2) STOKES, I. and LAIBLE, J.P., J. Biomech., 23:589, 1990. 3) DANSEREAU, J. and STOKES, I., J. Biomech., 21:893, 1988. 4) STOKES, I. et al., J. Orthop., Res 7:599, 1989. 5) SCOLES, P. et al, Spine, Vol.13, No.10:1082, 1988. 6) BERRY, J. et al., Spine, Vol.12, No.4:362, 1987. 7) SCHULTZ, A. et al., J. Biomech., Vol.7:311, 1974b. 8) ROBERTS, S. and CHEN, P., J. Biomech., Vol.5:191, 1972. 9) PANJABI, M. et al., J. Biomech., Vol.9:185, 1976. 10) FUNG, Biomechanical properties of living tissues, 1981. 11) DANSEREAU, J. et al., Submitted to the 15th ASB meeting, Tempe, Arizona, 1991. 12) STOKES, I. et al., Spine, Vol.11, No.3:213, 1986. 13) DANSEREAU, J. et al., 37th annual meeting of the ORS, Anaheim, CA, p.639, 1990.

AKNOWLEDGEMENTS: Research funded by CRSNG and FCAR.

EFFECTS OF PEDICLE SCREW INSTRUMENTATION AND DISK REMOVAL ON 3-D MOTION OF LUMBAR SPINAL COLUMNS SUBJECTED TO VARIOUS LOADS.

Anna G.U. Sawa, Jack M. Winters, James B. Koeneman, and Jack K. Mayfield
Bioengineering Program, Arizona State University, Tempe, AZ 85287-6006
Harrington Arthritis Research Center, Southwest Orthopaedic Institute, Phoenix, AZ 85006.

INTRODUCTION

Instrumenting lumbar spinal segments with transpedicular screws is increasing in popularity. This project was designed to study the overall and local three dimensional (3-D) motion of vertebral columns when instrumented with the Cotrel-Dubousset (CD) pedicle screw instrumentation system, both with and without disk defects. The columns were subjected to axial compressive, anterior and lateral eccentric, and torsional loads. The results showed that the CD-instrumented segments were more sensitive to the integrity of the disk in anterior bending and axial compression compared to during torsion and lateral bending. Analysis of local motion showed: (1) the main motion usually occured at the superior vertebrae; (2) there was often posterior sliding of segments above and even below the disk defect during axial compression and anterior bending tests; and (3) interpretations based only on traditional load-displacement curves can be misleading.

REVIEW & THEORY

The CD instrumentation system was initially designed for correcting scoliosis. However, the CD system is currently being used for segmental stabilization as well. The primary purpose of this study was to investigate the effects of segmental posterior CD fixation for both normal spines and spines with anterior instabilities (modeled by disk removal).

PROCEDURES

Fresh frozen (-20^{0} C) and thawed lumbar calf spines (8-10 week) were disarticulated into segments having 2, 4 and 6 vertebrae. The segments, potted with bone cement and transfixing k-wires, were tested in axial compression, anterior and lateral eccentric loading and torsion using a hydraulic test machine (Shore Western Materials Testing System). Each segment, three per indicated lengths, was tested (1) non-instrumented with intact disks (NR), (2) CD-instrumented with intact disks (FD), (3) CD-instrumented with anterior half of the mid disk and anterior longitudinal ligament removed (HD), and (4) CD-instrumented with whole mid disk and posterior ligament removed (ND). A function generator was used to produce ramp-type loads at rates of 50 N/sec and 0.5 Nm/sec. Overall compliances were determined from inverse slopes of load-displacement curves recorded with an x-y chart recorder. Vertebral motion (rotations about and translations along x-, y-, and z-axes, as well as finite screw axis parameters) was determined by recording on video cameras four reflective markers which were attached to each individual vertebrae. The motion of the markers was processed utilizing the Expert Vision system (Motion Analysis, Inc.), with 3-D kinematics of each vertebra obtained using an algorithm based on [1].

RESULTS & DISCUSSION

Based on data from the x-y charts (see Table 1), the longer segments were typically more flexible than the shorter ones in NR, FD and HD test configurations, except for torsion. Added CD-instrumentation had greater effect on overall torsional, anterior and lateral bending compliances compared to overall compressive compliances. Successive removal of the mid disk (HD and ND) resulted in increased overall compliances in all load

conditions, with torsion less significant, and had greater effects on the shorter segments, as expected (greater disk defect percentage wise for 2-segment specimens). Disk defects had the greatest affect on compliances during anterior compression-bending tests.

Motion analysis data confirmed that added instrumentation resulted in decreased overall compliances. Furthermore, the motion data verified the increase in overall compliances with successive disk removal. However, the increase in relative motion at the disk defect site was substantial only for anterior bending and axial compression tests. Analysis of motion of individual vertebrae showed that in most cases the largest relative motion occurred at the superior vertebrae, closest to the applied load and at the end of the instrumentation. In some cases, especially during lateral eccentric loading, the motion of the superior vertebrae increased with increased levels of disk defects. This suggests that perhaps the increase in overall compliances during tests modeling disk defects coincided with increased amounts of instrumentation loosening, rather than only increased motion at the disk defect site (as might be assumed based only on x-y data). Motion data showed that there were negligible amounts of coupled rotations for FD-configurations (see Table 2). However, coupled anterior bending during lateral eccentric tests increased significantly during HD- and ND-configurations. Also, motion analysis showed, as illustrated in Figure 1, that there were significant amounts of coupled posterior translations of vertebrae during anterior bending tests.

REFERENCES

[1]. Woltring, et al, J. Biomechanics, V.18, No.5, (1985), 379-389.

Acknowledgements: Funded by Southwest Orthopaedic Institute, Good Samaritan Regional and St. Luke's Medical Health Centers. Implants donated by Sofamor Co., Paris, France.

	T (deg/Nm)			AC (mm/kN)			AB (deg/Nm)			LB (deg/Nm)		
	2	4	6	2	4	6	2	4	6	2	4	6
NR	1.47	0.79	1.60	1.69	2.08	6.12	0.85	-	-	0.57	-	-
(s.d.)	1.72	0.25	0.26	0.34	0.42	0.85	0.36	-	-	0.22	-	-
FD	0.36	0.24	0.28	0.86	1.43	4.11	0.28	0.35	0.62	0.18	0.24	0.30
(s.d)	0.35	0.11	0.06	0.29	0.23	0.40	0.00	0.05	0.04	0.03	0.04	0.03
HD	0.46	0.34	0.29	1.04	1.70	4.59	0.41	0.53	0.81	0.23	0.29	0.38
(s.d.)	0.32	0.26	0.09	0.35	0.28	0.83	0.11	0.14	0.25	0.03	0.09	0.03
ND	0.48	0.41	0.30	1.75	2.33	6.84	0.88	0.87	0.97	0.36	0.34	0.47
(s.d)	0.35	0.32	0.07	0.81	0.30	3.81	0.29	0.16	0.32	0.04	0.09	0.15

Table 1. Average overall compliances during torsion (T), axial compression (AC), anterior eccentric (AB) and lateral eccentric (LB) tests for 2, 4 and 6 segment specimens non-instrumented (NR), instrumented with intact disks (FD), instrumented with half mid disk (HD), whole mid disk (ND), and all disks (AD) removed. (Based on inverse slopes of load vs. displacment curves, n=3, s.d. = sample standard deviation)

$$\begin{vmatrix} dx \\ dy \\ dz \\ \phi x \\ \phi y \\ \phi z \end{vmatrix} = \begin{vmatrix} n & n & -1.67 & -0.10 & 0.31 & -0.02 \\ n & n & -2.18 & -0.54 & -0.12 & -0.05 \\ n & n & \mathbf{-2.25} & -0.08 & 0.04 & -0.02 \\ n & n & 2.31 & \mathbf{0.22} & 0.02 & -0.11 \\ n & n & -1.07 & -0.06 & \mathbf{0.10} & -0.05 \\ n & n & -0.43 & 0.01 & 0.02 & \mathbf{0.37} \end{vmatrix} \begin{vmatrix} Fx \\ Fy \\ Fz \\ Mx \\ My \\ Mz \end{vmatrix}$$

$$\text{units:} \begin{vmatrix} \frac{mm/kN}{deg/kN} & \frac{mm/Nm}{deg/Nm} \end{vmatrix}$$

Table 2. Global motion data for average 6-segment specimen summarized in matrix form. Based on coordinate system as shown in Figure 1. Each column represents a certain loading test. (F - force, M - moment, d - translation, ϕ -rotation, n - no data, bold faced indicate main compliances, other values indicate coupled translations and rotations.)

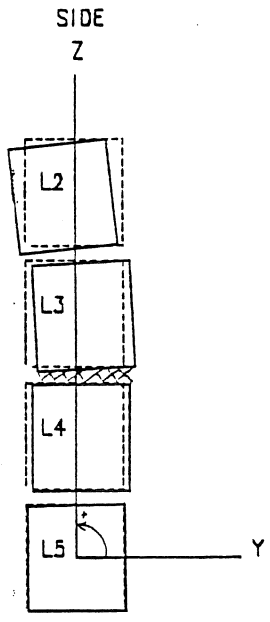


Figure 1. Example of motion of 4-segment specimen (L2L5 A) with L3-L4 disk completely removed during anterior eccentric loading (200 N applied in negative z-direction at y = -5.0 cm).

MUSCLE MECHANICS

RELATIVE CROSS-SECTIONAL AREAS OF UPPER AND LOWER EXTREMITY MUSCLES IN HUMANS

James J. Dowling, Ph.D. and Nicholas Cardone, B.P.E.
Department of Physical Education, McMaster University
Hamilton, Ontario, Canada

INTRODUCTION

The reduction of intra-subject variability of muscle cross-sectional areas was investigated using CT scans of the 20 upper and 26 lower extremities of living human subjects. The results indicated that variability could be reduced by 42% when individual muscle areas were expressed relative to the size of the functional muscle group to which they belong.

REVIEW AND THEORY

The estimation of individual muscle forces in-vivo by either EMG driven muscle models or optimization requires the scaling of the individual muscle force generating capacity. Many investigators have assumed that this capacity is proportional to the cross-sectional area (CSA) of the muscle. There is little agreement on the method of the area calculation which has resulted in wide ranges of muscle sizes and on muscle stress values (force per cross-sectional area). Brand, et al. (1986) showed that even if a stress value was agreed upon, the large intra-subject variability of muscle sizes from cadavers produced very large variability in predicted individual muscle forces. The purpose of the present investigation was to examine a method of reducing the intra-subject variability by grouping muscles into functional groups. Such a method could then be used with isometric maximal contractions to determine the force generating capacity of individual muscles without specifying an arbitrary stress value.

PROCEDURES

A diverse pool of subjects including males, females, weightlifters, non-weightlifters, adolescents, adults and elderly was used to obtain a wide variety of muscle sizes. Twenty-six Computed Tomography (CT) scans of knee extensors and 20 CT scans of elbow flexors were used for analysis. The scans were taken at the level of maximum limb girth. The CSAs of each of four knee extensors and two elbow flexors were determined via electronic planimetry of each scan. The relative cross-sectional area (RCSA) of each muscle was then calculated as a ratio of its CSA to the total CSA of the functional muscle group to which it belonged. The intra-subject variability was calculated using the coefficient of variation (standard deviation divided by the mean) and a dependent T-test was used to compare the differences in the variability of CSA with RCSA.

RESULTS AND DISCUSSION

The variability of RCSA was significantly less than CSA ($p<.01$). The variability was reduced in each of the six muscles examined in this study (see Figure 1). Many of the muscles had the variability reduced by half. The absolute values for CSA and RCSA are less meaningful because the single scans could not ensure that each muscle within the group was at its maximum bulk and perpendicular to the fibre pennation angle. For this reason, more physiological measures of CSA should be used in future and then expressed as relative sizes. When this is done, the maximum force generating capacity of an individual muscle can be calculated from a maximum isometric contraction, taking into account leverage, without the need of an arbitrary stress value and with increased reliability using the equation below.

$$F = \frac{M}{\left[MA + \sum_{i=1}^{n} \frac{R_i \cdot MA_i}{R}\right]}$$

where: M - net joint moment (N.m)
F - force of muscle (N)
MA - moment arm of muscle (m)
R - relative cross-sectional area (unitless)
n - number of other muscles in the functional group

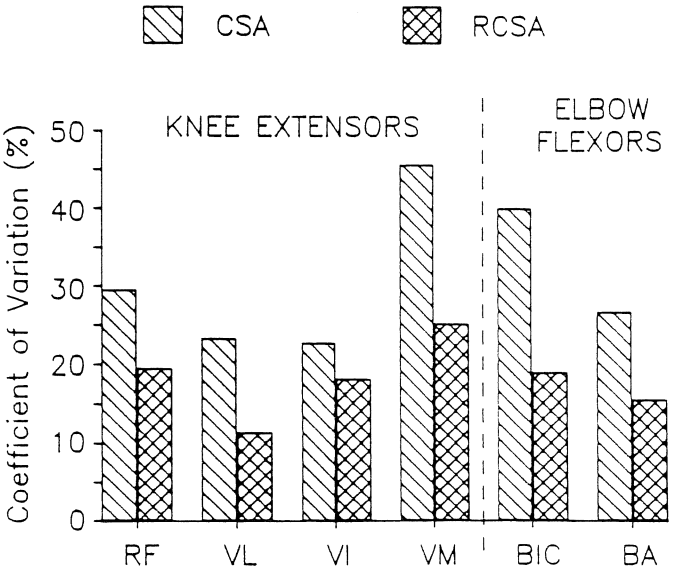


Figure 1. Coefficients of variation of the knee extensors (RF - rectus femoris, VL - vastus lateralis, VI - vastus intermedius, VM - vastus medialis) and the elbow flexors (BIC - biceps, BA - brachialis).

REFERENCES

Brand, R.A., et al. JOURNAL OF BIOMECHANICS. 19:589-596, 1986.

MORPHOMETRY OF THE PSOAS MUSCLE AS DETERMINED BY MAGNETIC RESONANCE IMAGING

J. Gavin Reid[1,2], Lori A. Livingston[1]
&
David J. Pearsall[2]

[1]School of Physical and Health Education &
[2]Department of Anatomy
Queen's University, Kingston, Ontario, Canada K7L 3N6

INTRODUCTION

Magnetic resonance images (MRI) of the human trunk were collected and analyzed in order to study the psoas muscle under *in vivo* conditions. Young, physically-active males acted as subjects. The psoas increased in size as it descended the trunk, moving anteriorly and slightly lateralward in relation to the vertebral column. Maximum cross-sectional areas for the psoas were observed at the L4/L5 level. Right-left symmetry was apparent in the aforementioned dimension. However, the length of the mediolateral moment arm was significantly ($p<.05$) greater for the right versus the left psoas from L3 to S1. This trend was not noted for the anteroposterior moment arm.

REVIEW AND THEORY

The geometry of the psoas has been largely determined from cadaveric dissections. Anthropometric variables such as the relative size and location of the muscle have been derived for use in predictive biomechanical models. However, cadaveric measurements may not accurately reflect the *in vivo* state of the muscle (Engstrom, 1990). Embalming is known to cause distortion of soft tissue and if the subjects are elderly, muscles are often atrophied due to prolonged periods of inactivity and/or disease.

The recent development of magnetic resonance imaging (MRI) and computed tomography (CT) technologies has allowed investigators to study the psoas and other trunk muscles *in vivo*. Cross-sectional areas and moment arms for the psoas have been reported by several investigators (Chaffin et al., 1990; Kumar, 1988; McGill et al., 1988; Nemeth et al., 1986; Reid et al., 1987; Tracy et al., 1989). Sample sizes varied from study to study (n=13 to n=96), as did the number of lumbar levels observed (n=1 to n=4). Men and women of varying ages were studied and four of the six studies employed subject samples with a mean age of forty years or over. The majority (but not all) of the subjects were referred to MRI or CT testing for medical reasons.

The present study was undertaken in an attempt to add to the growing database of anthropometric information on the psoas muscle. This work differs from those previously cited in that: (1) The subject population consisted of young, physically-active and asymptomatic male volunteers, and (2) Measurements were taken at nine different levels of the lumbar spine. The overall objective was to gain a more complete profile of the psoas in the lumbosacral region.

PROCEDURES

Fifteen physically-active young-adult males with a mean age of 21.5 ± 1.8 years, mean height of 177.1 ± 5.0 cm, and a mean mass of 69.8 ± 5.9 kg volunteered to participate in the study.

Data were collected via magnetic resonance imaging scans. Subjects were instructed to lay supine with the hips extended and to remain motionless for the duration of the scan. Consecutive transverse slice images of the trunk were obtained from the plane of the xiphoid

process to the symphysis pubis. Data were identified and coded at nine vertebral and intervertebral levels (L2, L2/L3, L3, L3/L4, L4, L4/L5, L5, L5/S1, S1). The psoas remained sufficiently distinct from the iliacus to be coded at the lower levels.

Outlines of the trunk, vertebral body (or intervertebral disc) and the two psoas muscles were digitized using a digitizing tablet in conjunction with an MS-DOS computer. The data were stored and consequently used to compute a number of variables.

RESULTS

The number of MRI images analyzed varied from level to level. Paired *t*-tests were used to test for left-right symmetry, while ANOVA procedures were employed to check for significant differences across vertebral levels.

Minimum values for the left and right psoas (5.8, 5.5 cm^2, respectively) observed at L2 were followed by systematic increases to maximums at L4/L5 (15.3, 16.3 cm^2) and subsequently orderly decreases to S1 (11.2, 12.3 cm^2). The cross-sectional area of the right psoas was consistently larger than that observed for the left psoas. Paired *t*-tests revealed no significant right-left differences ($p<.05$) at any level, but ANOVA results suggested that mean psoas cross-sectional area varied significantly ($p<.05$) between levels.

Mean mediolateral and anteroposterior moment arms were calculated for each of the nine segmental levels analyzed. Two trends were apparent. First, the mean value of the mediolateral moment arm consistently increased as the psoas descended from L2 (3.4 cm) to S1 (5.0 cm). Second, the anteroposterior moment arm reached miminum values (0.4 cm) from L3/L4 to L4, where the centroid of the psoas moved from a position posterior to the centroid of the vertebral column to an anterior position. Significant ($p<.05$) right versus left differences were noted for the mediolateral but not the anteroposterior moment arm from L3/L4 to L4/L5 inclusive, with the values observed for the former being greater than those observed for the latter. An ANOVA procedure revealed that mean values for the mediolateral and anteroposterior moment arms varied significantly ($p<.05$) from level to level.

DISCUSSION

The psoas data collected in this study differed from that previously reported by other researchers. This may have been the result of using a young, physically-active and asymptomatic group of subjects.

Maximum cross-sectional areas for the psoas were observed at the L4/L5 level, a finding which is in agreement with that of Tracy et al. (1989). The mean values observed at any given level were generally lesser in magnitude, however, than those cited by other investigators (McGill et al., 1988; Tracy et al., 1989). This may have been a direct result of using a proportionately leaner sample.

Psoas size appeared to be symmetrical, despite the fact that mean cross-sectional area values for the right were consistently larger than those observed for the left. Significant right-left differences were noted, however, for the mediolateral moment arm. The length of the mediolateral moment arm consistently increased as it descended the trunk. However, a similar trend was not noted for the anteroposterior moment arm.

REFERENCES

Chaffin, D.B. et al. Clin Biomech, 5, 9-16, 1990.
Engstrom, C. M.Sc. Thesis, Queen's University at Kingston, 1990.
Kumar, S. et al. Clin Biomech, 3, 137-144, 1988.
McGill, S.M. et al. J Biomech, 21, 329-341, 1988.
Nemeth, G. et al. Spine, 11, 158-160, 1986.
Reid, J.G. et al. Spine, 12, 273-275, 1987.
Tracy, M.F. et al. Spine, 14, 186-193, 1989.

THE EFFECT OF STRETCH RATE ON MUSCLE FAILURE IN VITRO

Joseph J. Crisco III, Ph.D., Richard E. Gellman, M.D., Manohar M. Panjabi, Ph.D.Peter Jokl, M.D.
Biomechanics Laboratory and Section of Sports Medicine, Department of Orthopaedics and Rehabilitation, Yale University School of Medicine, 333 Cedar Street, New Haven, Connecticut, 06510, USA

INTRODUCTION

The mechanisms of muscle strain injuries, common in athletics and in the workplace, are not well understood. Material failure of the muscle tissue is one factor. Although muscle is known to be viscoelastic, little is known about how stretch rate influences its failure. The purpose of this *in vitro* study was to compare the passive mechanical properties of whole rabbit muscle stretched to failure at two different rates. Isolated left/right pairs of tibialis anterior (n = 10) and medial gastrocnemius (n = 10) muscles were passively elongated at 0.1 mm/second and 1,000 mm/second. The load-displacement behavior to failure was recorded and the accompanying stress-strain relation was estimated. Although the medial gastrocnemius muscle was stronger than the tibialis anterior muscle, we found no difference in the failure properties of their muscle tissue. Approximately for both muscles, the average (±s.d.) failure stress increased significantly from 0.35 MPa ±0.09 MPa to 0.75 MPa ±0.2 MPa with the increased stretch rate. There was, however, no significant difference in the failure strain with the 10,000 fold increase in stretch rate. The failure strain at each rate was approximately 19% ± 4%. The site of failure consistently included the region of the myotendinous junction. A hypothesis relating the findings of this study to the observation that *in vivo* muscle strain injuries occur at higher rates of movement is also discussed.

REVIEW

Muscle strains have been classified into three types. A mild, or first degree strain, commonly called a "pulled muscle," is an overstretching of the muscle or tendon resulting in approximately 5% or less disruption of the musculotendinous unit. A moderate, or second degree strain is a tear of a greater portion, and a severe, or third degree strain is a complete rupture of the muscle.

A strain injury in its simplest form consists of the material failure of muscle. Hence, several researchers have sought to understand strain injury by simple mechanical elongation tests of isolated muscle. The site at which failure occurs in the healthy muscle-tendon unit was first studied in 1933 by McMaster, and more recently by Garrett et al. (1988). The failure properties, as influenced by age and time postmortem (Katake, 1963) and contusion injury (Jarvinen, 1975), have also been studied. The viscoelastic or time-dependent response of muscle tissue has also been investigated (Buchthal and Kaiser, 1951; Taylor et al. 1990); however, the effect of stretch rate on the failure properties of whole muscle has not been previously reported. The purpose of this study was to determine the influence of two stretch rates (quasi-static simulated by 0.1 mm/second and traumatic simulated by 1,000 mm/second) on the *in vitro* failure properties of passively stretched muscle in an animal model. The site of muscle failure was examined grossly and with scanning electron microscopy to describe the morphology at the tear site.

MATERIALS AND METHODS

Ten New Zealand white rabbits (weighing 5-6 pounds, approximately 3 months old) were sacrificed by other research facilities, and we acquired the hind legs and stored them at -20^{o} C until required for preparation and testing. After thawing the specimens in a 37°C water bath, bone-muscle-bone preparations were constructed with the tibialis anterior (TA) and medial gastrocnemius (MG) muscle of each specimen.

Each muscle specimen was stretched to failure at either a slow (0.1 millimeter per second) or a fast (1,000 millimeters per second) rate. Although the 10,000 factor difference in the stretch rate necessitated using two different experimental apparatuses, the load and displacement measurement equipment and protocol were similar. All of the statistical analyses were determined using the Student's t-test (Statview, Abacus Concepts, Inc., Berkeley California).

RESULTS AND DISCUSSION

The average and standard deviations of the energy absorbed to failure, which was calculated directly from the recorded load-displacement data, and the stress and strain at failure, based on estimates of the initial cross-sectional area, are given in Table 1. The increases in energy absorbed and stress at failure were significant (99.9%). There was no difference in the strain at failure.

Table 1. Average (n=10) and standard deviations of the failure values.

	Tibialis Anterior			Medial Gastrocnemius		
RATE (mm/s)	Energy (N*mm)	Stress (MPa)	Strain (%)	Energy (N*mm)	Stress (MPa)	Strain (%)
0.1	83 [24]	0.4 [0.1]	19 [3]	109 [31]	0.3 [0.1]	20 [5]
1,000	200 [75]	0.8 [0.2]	19 [4]	290 [128]	0.6 [0.2]	18 [5]

Dependence on Stretch Rate. We found that strength and energy absorption of passive muscle tissue increased with increasing stretch rate. Muscle has been demonstrated to behave as a viscoelastic material (Buchthal and Kaiser, 1951). However, the effect of stretch rate on the failure properties of muscle has been reported in only one other study. Contrary to our findings, Welsh et al. (1971) found no difference in the failure loads of isolated rabbit muscle stretched at rates of 0.2 mm/second and 20 mm/second. Although Garrett et al. (1988) passively pulled five different muscles of the rabbit to failure at rates of 0.17, 1.7, and 17 mm/second, they did not report any failure loads. Moreover, they reported displacement percentages to failure for only a few of their specimens, but did not report the associated stretch rates.

The other soft tissue studies of viscoelastic failure have examined ligaments (Noyes et al. 1976; Peterson and Woo, 1986; Crowninshield and Pope 1976; and Yoganandan et al. 1989). Each of these studies reported that failure stress, elastic modulus, and strain increased with increasing stretch rate, except for Yoganandan et al. (1989), who reported that the failure strain was independent of stretch rate (8.9 mm/second to 2,500 mm/second) in human cervical spine ligaments. The similar phenomena in passive muscle tissue was perhaps the most noteworthy observation of this study: the strain at failure was not different when the stretch rate was increased by a factor of 10,000.

In Contrast to the Clinical Findings. Clinical findings have reported that muscle tears occur most frequently during rapid, eccentric contractions (Brewer, 1960; Garrett, 1990), which suggests that muscle is weaker at these faster stretch rates. Yet, our experimental results and those of Taylor et al. (1990) have found that muscle is stronger and absorbs more energy when stretched at faster rates. We believe that this discrepancy can be explained as follows: We hypothesize that individual muscle fibers begin to fail at loads less than those required for complete rupture, and the viscoelastic properties of whole muscle (i.e. faster rates generate higher loads at the same displacement) are responsible for generating levels of stress sufficient to cause fiber failure at small strains, as in first degree strain injuries, but may not cause whole muscle rupture. At slow movements, the stresses and strains remain within physiological limits, because the viscoelastic effects are negligible. Although fairly simple, such an hypothesis is in agreement with both the clinical findings and the experimental results.

REFERENCES

Brewer BJ: Lect. AAOS 17:354-358, 1960
Buchthal et al.. *Biol Medd Kbh* 21:1-318, 1951
Garrett et al. *Am J Sports Med* 16:7-12, 1988
Garrett et al *Med Sci Sports Exer* 21:506-514, 1989
Jarvinen . *Acta Path Microbiol Scand* 83:269, 1975
Kabo et al. *J Biomech Eng* 104:253, 1982
Katake . *J Kyoto Pref Med Univ* 69:463 1961
McMaster. *J Bone Joint Surg* 15:705, 1933
Noyes et al.. *J Bone Joint Surg* 56A:236, 1974
Peterson et al.. *J Biomech Eng* 108:365, 1986
Taylor et al. *Am J Sports Med* 18:300, 1990
Welsh et al. *Clin Orthop* 81:171, 1971
Yoganandan et al. *Spine* 14:1102, 1989

ACKNOWLEDGEMENTS: Support was provided in part by National Institute of Health Grant AR39209 and Center for Environmental Health and Injury Control Grant R49/CCR103551.

AUTHOR INDEX

Abdul-Shafi, W.A. 72
Ahdieh, A. 64
Aissaoui, R. 188
Alberts, L.R. 72
Alexander, S. 4
Allard, P. 188
Amiel, D. 78
Anderson, D.D. 228, 230, 274
Andersson, G.B.J. 206
Andrews, D. 156
Andrews, J.G. 120, 196
Anthanasiou, K. 74
Ashman, R.B. 140
Aswad, A.D. 216
Aubin, C.E. 46, 290

Bagley, A. 234
Baker, K.J. 138
Barbieri, C.A. 228, 230
Barreto, P.M. 178
Bates, B.T. 150, 152, 224, 226
Battistini, A. 64, 268
Bechtold, J.E. 136
Beckman, S. 172
Bell, A.L. 274
Benedetti, M.G. 268
Bennet, G. 288
Berme, N. 36
Berns, G.S. 24
Bianco, P.T. 136
Binazzi, R. 64
Bloebaum, R.D. 132
Bowen, R.V. 84
Brand, R.A. 20, 138, 196
Broman, H. 50
Brown, T.D. 20, 138
Buchanan, T.S. 172
Buckwalter, J.A. 20

Caldwell, G.E. 40, 174
Caster, B.L. 150, 226
Capanna, R. 268
Cardone, N. 296
Catani, F. 64, 268
Cavanagh, P.R. 146
Chaffin, D.B. 30, 48, 206
Chandran, K.B. 248
Cinque, G. 268
Colpaert, K. 88
Comadoll, J.L. 136
Constantinides, G. 74
Constanz, B. 132
Cooke, F.W. 162
Cooke, T.D.V. 60, 168
Cooper, M.E. 212
Cooper, R.A. 212
Cornelissen, M. 278
Cornelius, W. 194
Costigan, P. 60
Cote, B. 46
Crane, C.D. 286
Crisco, J.J. 98, 196, 300
Cunningham, J.L. 278

Dansereau, J. 46, 290
Dapena, J. 8
Darling, W.G. 180
Delp, S.L. 22
Derrick, T.R. 150
de Swart, R.J. 116
DeVita, P. 110
DeWitt, J.K. 128, 254
DeZerbi, M. 64
DiAngelo, D. 76
Dobkin, B. 66
Dowling, J.J. 156, 176, 296
Dufek, J.S. 224, 226
Dujovne, A.R. 168
Dvorak, J. 98
Dzida, F.J. 74

Ebrahim, K. 194
Enoka, R. 178
Erig, M. 48

Fanghanel, J. 108, 282
Faria, I.E. 212
Fenton, M. 92
Feuerbach, J.W. 180
Fleming, S. 262
Forrester, L.W. 40
Fowler, E.G. 66
Friis, E.A. 162
Fuglevand, A.J. 178
Fukumoto, D. 262
Fyhrie, D.P. 272

Gaffney, M.B. 274
Gellman, R. 300
Giannini, S. 64, 268
Giurini, J.M. 148
Gomez, M. 78

Gottesman, D. 30
Gouw, G.J. 96
Grabiner, M.D. 28, 116
Gracovetsky, S.A. 96
Gregor, R.G. 66
Grob, D. 98
Gross, T.S. 142, 276
Gudavalli, R. 54
Gunasekaran, S. 132
Gustilo, R.B. 136
Guzelsu, N. 134

Hale, J.E. 20
Hamill, J. 152
Hannon, P. 262
Hansson, T. 50
Harbaugh, M. 164
Hart, T.J. 68
Harwood, F. 78
Hasan, S.S. 154
Hay, J.G. 120, 180
Hedden, D.M. 44
Heise, G.D. 254, 284
Hern, T. 76
Hinrichs, R.N. 128, 232, 252, 254
Hobatho, M.-C. 140, 278
Holbein, M.A. 30
Hollister, A.M. 114, 190
Hollister, S.J. 272
Holt, K.G. 152
Hooper, S.J. 162
Howell, S.M. 24
Hreljac, A.P. 32, 254
Hubbard, R. 56
Hughes, R.E. 206
Hunter, P. 110

Imbriglia, J.E. 274
Irvine, D.M.E. 228, 230

Jahnigen, D.W. 28
Jamison, J.C. 174
Jatana, S. 114, 190
Joganich, T.G. 218, 254
Jokl, P. 300
Jones, I.C. 122

Kaigle, A.M. 50
Kalenak, A. 146
Kamibayashi, L. 60
Karlsson, A. 258
Kazarian, L.E. 244
Kellam, J.F. 76
Keller, T.S. 80, 154
Kim, W. 86
Kimura, J. 272
Kitabayashi, L. 78
Koeneman, J.B. 160, 292
Kofman, J. 258
Koh, T.J. 28, 116
Komattu, A.V. 286
Korvick, D.L. 62
Kozak, K. 148
Kubein-Meesenberg, D. 108, 282
Kuo, A.D. 204
Kuo, S.C. 2

Labelle, H. 46, 290
Ladin, Z. 34, 90, 148, 256
Lavender, S.A. 206
Leardini, A. 64, 268
Li, P.Y. 90
Lindstrom, B. 258
Liu, Y.K. 238
Liu, Q. 120
Livingston, L.A. 298
Long, R. 262
Longo, J.A. 160
Lowet, G. 88, 278
Lundin, T. 28
Lupichuk, A.G. 114, 190

Magnusson, M. 50
Maiman, D.J. 52, 102, 288
Maloney, J. 210
Mann, R. 10
Marquet, P.G.J. 196
Marsh, T.P. 214, 254
Martin, P.E. 32, 218
Matyas, J. 78
Mayfield, J.K. 292
McCaw, S.T. 192
McClay, I.S. 146
McGinnis, P. 16
McLean, S.P. 254
McLeod, K.J. 276
McNitt-Gray, J. 228, 230
McTighe, T. 160
Miller, G.J. 56, 286
Miller, J.A. 196
Meglan, D. 36
Miller, D.I. 122
Moeinzadeh, M.H. 216
Moga, P.J. 48
Mohler, C.G. 20
Moore, A. 242
Mote, C.D. 112
Muffoletto, A. 74

Mungiole, M. 186
Munkasy, B.A. 232, 254
Murphy, N. 188

Nagerl, H. 108, 282
Nelson, R.C. 284
Newman, N. 96
Ngo, F. 210
Nussbaum, M.A. 48, 206

Oberg, K. 258
O'Connor, P. 56
Oda, T. 98
Oppenheim, W. 68
Oxland, T.R. 104

Panjabi, M. 98, 104, 198, 300
Pappas, A. 262
Pearsall, D.J. 44, 298
Peeraer, L. 88
Perrell, K.L. 66
Peterson, W.A. 100
Phillips, M. 210
Pichora, D.R. 166
Pijanowski, G.J. 62
Pintar, F. 52, 102, 288
Pitkin, M.R. 266
Pizzimenti, M.A. 122
Ploeg, H.L. 166, 168
Poliner, J. 92
Pope, M. 50
Portfors, C.V. 176
Prassas, S. 264
Putnam, C. 126

Rash, G. 124
Rath, K. 198
Ray, J.L. 154
Redfern, M. 30
Reid, J.G. 44, 298
Reider, C.L. 4
Rho, J.Y. 140
Reinartz, J. 52
Roozmon, P. 96
Rubin, C.T. 142, 276
Rudert, M.J. 20
Rymer, W.Z. 172

Sances, A. 102, 238
Sawa, A.G.U. 292
Schaeffer, D.J. 62
Schaffler, M.M. 272
Schaller, L. 28
Schlick, M.B. 102
Schneider, K. 68
Schoephoerster, R.T. 248
Schot, P.K. 224
Setoguchi, Y. 68
Shapiro, R. 124
Sheetz, M.P. 2
Shiavi, R. 154
Simon, S.R. 36
Singh, A.K. 114, 190
Skedros, J. 132
Skelly, W.A. 110
Smith, A.W. 38
Smith, C.M. 166, 168
Smith, S.D. 244
Snow, R.E. 84
Sommer, H.J. 146
Spengler, D.M. 154
Starkweather, K.D. 190
Ster, J.F. 212
Strauss, M.G. 210
Sullivan, W.W. 114

Thaut, M. 264
Tile, M. 76
Triano, J.J. 54

Van der Perre, G. 88, 278
Voloshin, A. 86
Vosse, A. 212
Vrahas, M. 76

Wallaeys, G. 88
Walsh, W.R. 134
Wang, Q. 222
Watson, J. 194
Wei, W.-Y. 222
Weisberger, A.M. 154
Wells, R. 242
Wheeler, D.L. 56, 286
White, S. 92
Williams, K.R. 14
Winterbottom, J. 238
Winters, J.M. 100, 186, 202, 292
Woo, S. 78
Wu, G. 34, 256
Wyss, U.P. 60, 166, 168

Yamaguchi, G.T. 128, 214
Yee, A.G. 112
Yoganandan, N. 52, 102, 238, 288
Yokoi, T. 240
Zajac, F.E. 204
Zernicke, R.F. 68
Zhu, M. 80